



The role of peroxisomes in malnutrition and metabolic disease

*In vitro and
in silico models*

José Manuel Horcas Nieto

**The role of peroxisomes in malnutrition
and metabolic disease
In vitro and in silico models**

José Manuel Horcas Nieto

This work was supported by the European Union's Horizon 2020 research and innovation programme under the Marie Skłodowska-Curie grant agreement No 812968 (PeRlCo), the Canadian Institutes of Health Research (156307), the Stichting De Cock-Hadders and Vrienden Beatrix Kinderziekenhuis.



umcg



rijksuniversiteit
 groningen



The research presented in this thesis was conducted at the Department of Pediatrics, Center for Liver and Metabolic Diseases, University Medical Center Groningen, the Netherlands. The printing of this thesis was financially supported by University of Groningen and the Graduate School of Medical Science of the University Medical Center Groningen.

Printing: Ridderprint, ridderprint.nl

Layout and design: Ridderprint | www.ridderprint.com

© Copyright 2024 Jose Manuel Horcas Nieto, Groningen, The Netherlands.

All rights reserved. No part of this thesis may be reproduced, distributed, sorted in a retrieval system, or transmitted in any form or by any means without prior permission of the author or, where applicable, the publisher holding the copyright on the published articles.



**university of
groningen**

The role of peroxisomes in malnutrition and metabolic disease

In vitro and in silico models

PhD thesis

to obtain the degree of PhD of the
University of Groningen
on the authority of the
Rector Magnificus
and in accordance with
the decision by the College of Deans.

This thesis will be defended in public on

Wednesday 8 May at 14.30 hours

by

Jose Manuel Horcas Nieto

born on 10 April 1993

Córdoba

Supervisor(s)

Prof. B.M. Bakker

Co-supervisor(s)

Dr. R.H.J. Bandsma

Assessment Committee

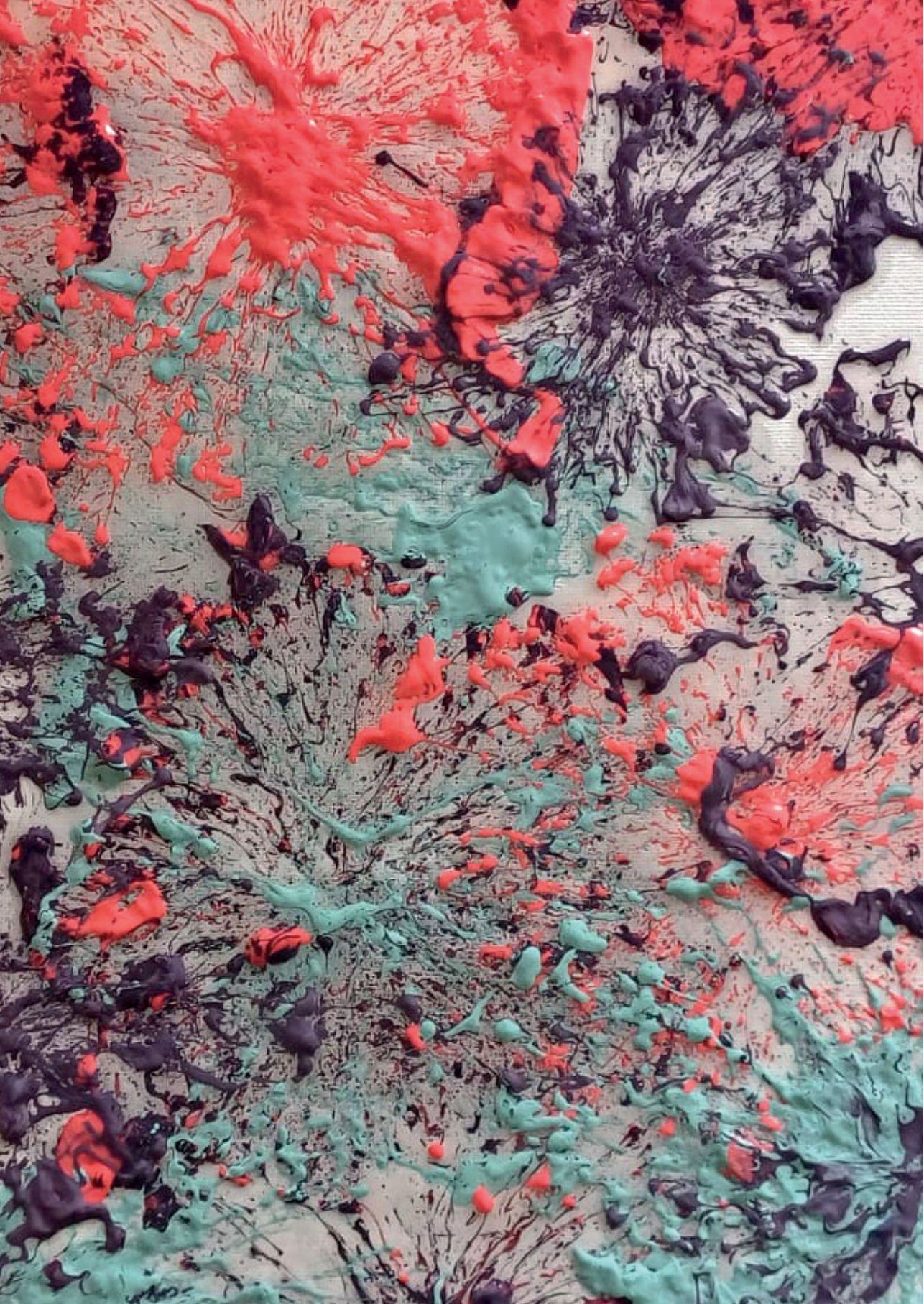
Prof. R.J.A. Wanders

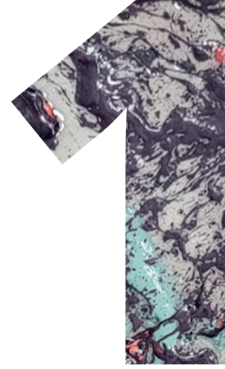
Prof. A. M. Dolga

Prof. K.N. Faber

TABLE OF CONTENTS

Chapter 1:	General Introduction	7
Chapter 2:	Organoids as a model to study intestinal and liver dysfunction in severe malnutrition	33
Chapter 3:	Towards Automatization of Organoid Analysis: A Deep Learning Approach to Localize and Quantify Organoids Images	73
Chapter 4:	Docosahexaenoic acid prevents peroxisomal and mitochondrial protein loss in a murine hepatic organoid model of severe malnutrition	89
Chapter 5:	Establishing a peroxisomal β -oxidation computational kinetic model to understand the effects of amino-acid restriction on peroxisomal β -oxidation	129
Chapter 6:	iPSC-derived liver organoids as a tool to study Medium Chain Acyl-CoA Dehydrogenase deficiency	167
Chapter 7:	General Discussion	201
Appendices		
	Summary	218
	Samenvatting	222
	Resumen para público no científico	227
	Acknowledgments	232
	Curriculum vitae	238
	List of publications	240





Chapter

General Introduction

FATTY ACID METABOLISM

Fatty acids are important molecules with multiple roles, such as structural components of cell membranes, nutrients and signaling molecules¹. They can be stored as triglycerides to be used during extended periods of fasting, illness or exercise. Fatty acid oxidation (FAO) provides a large amount of the energy requirements during periods when glucose and gluconeogenic precursors are depleted. FAO is a key metabolic process for human physiology, and its importance is highlighted by the number of inherited disorders caused by defects in the pathway².

While the majority of fatty acids are oxidized via mitochondrial β -oxidation, peroxisomes also play a key role in FAO of different substrates. Interestingly, these two organelles are able to communicate and interact with each other in the oxidation of fatty acids.

Organelles involved in metabolism of fatty acids

Mitochondria

Mitochondria are subcellular organelles in charge of the bulk of fatty-acid oxidation. These double-membrane organelles are in charge of the production of the majority of the ATP in the cell through oxidative phosphorylation³. Amongst many of the functions of mitochondria I could highlight energy metabolism, redox metabolism, calcium regulation, and signaling⁴. Regarding fatty acid metabolism, mitochondria are in charge of oxidizing long- to short-chain fatty acids to produce ATP under catabolic conditions. To do so, mitochondria can perform β -oxidation of fatty acids, a cyclic process that leads to the production of acetyl-CoA and NADH and FADH₂². These products are further metabolized in the tricarboxylic acid (TCA) cycle and oxidative phosphorylation where ATP is formed.

Mitochondria are highly dynamic organelles, which continuously experience processes of recycling and reshaping^{5,6}. They are also able to respond to their environment regulating both their structure and function. Defects in mitochondrial metabolism, namely inherited defects, DNA damage during aging and environmental factors, such as diet can be detrimental for cell survival⁷.

Peroxisomes

Peroxisomes are small (0.1–1 μ m), single-membrane subcellular organelles found in most eukaryotic cells. These organelles exert a wide range of metabolic

functions, which vary between different organisms and even between different organs in a single organism⁸. Some of the metabolic functions of peroxisomes include lipid metabolism, hydrogen peroxide metabolism, synthesis of ether lipids and bile acids, glyoxylate detoxification, and in trypanosomatids even glycolysis⁸⁹. Impairments in peroxisomal function can lead to severe diseases, highlighting the importance of these organelles. Peroxisomal disorders can be divided in peroxisomal biogenesis disorders (PBDs) and single-enzyme deficiencies.

Peroxisomal biogenesis disorders are autosomal recessive inherited disorders caused by a defect in any of the PEX genes⁸. These genes encode for proteins (peroxins) taking part in peroxisomal biogenesis. Peroxisomal biogenesis disorders affect peroxins involved in either the import of peroxisomal proteins^{10,11}, in peroxisomal division¹²⁻¹⁴ or de novo formation^{15,16}. These disorders lead to multiple metabolic dysfunctions. Single-enzyme deficiencies are caused by impairments or defects of any enzyme involved in specific peroxisomal metabolic pathways (e.g. ABCD1, ACOX1, AMACR, etc.). Unlike PBDs, single-enzyme deficiencies only affect specific metabolic functions.

One key function of peroxisomes, and the main point of interest of this thesis, is fatty acid metabolism. Peroxisomes are able to metabolize several types of fatty acids, including very long chain fatty acids (VLCFA), branched chain fatty acids (BCFA) and even medium-chain fatty acids¹⁷. Moreover, peroxisomes are also capable of oxidizing mono- and poly-unsaturated fatty acids¹⁸. To do so, peroxisomes can perform both α - and β -oxidation with a very broad range of substrates. Although peroxisomal β -oxidation is similar to the mitochondrial pathway, peroxisomes are equipped with their own set of enzymes in charge of metabolizing both straight-chain acyl-CoA to Acetyl-CoA as well as 2-methyl-branched-chain acyl-CoAs, into propionyl-CoA and Acetyl-CoA¹⁸.

The interplay between peroxisomes and mitochondria

In recent times, it has become clear that peroxisomes and mitochondria display a functional interplay, key for different metabolic processes¹⁹⁻²¹. Reactive oxygen species (ROS) are molecules formed during different cellular processes that contribute to aging processes. While essential for cell signaling, when accumulated ROS can cause oxidative damage²². As an example of the interaction between peroxisomes and mitochondria, we could highlight their combined role in ROS homeostasis²³. Another relevant example in the context of this thesis is the oxidation of fatty acids in order to maintain lipid homeostasis. While the mechanisms of interaction between these two

organelles have not been deeply characterized they involve physical contact sites, diffusion processes, and vesicular transport²⁴⁻²⁶.

Given the close interplay between the two organelles, it has been suggested that alterations in one of them (either in biogenesis, proliferation or metabolism) might potentially have an effect on the other²⁷. In the case of peroxisomes, several studies have reported that diseases affecting peroxisomal fatty acid metabolism²⁸, peroxisomal biogenesis²⁹ and peroxisomal redox activity³⁰ also had a negative effect on mitochondrial health. This phenomenon was also observed in hepatocytes of a liver-specific knockdown of PEX5. L-Pex5^{-/-} mice showed alteration of the mitochondrial inner membrane, increased oxidative stress and depletion of mitochondrial DNA³¹. On the other hand, it remains unknown if primary mitochondrial diseases also cause peroxisomal dysfunction. These findings not only support the notion of a tight interplay between both organelles, but also point towards potential compensatory mechanisms between the two organelles.

Given the importance of both mitochondria and peroxisomes in the metabolism of fatty acids, it is understandable that defects in either one of these organelles might have serious health repercussions.

Disruptions in normal fatty acid metabolism caused by nutritional and genetic disorders

Imbalances in different biochemical processes involved in fatty acid metabolism cause a vast range of human diseases. The origin of these imbalances can be either genetic (inborn errors of metabolism) or environmental factors and contextual conditions (such as nutrition and/or malnutrition). Different nutritional stressors can have an important impact on the metabolism of macronutrients.

There are multifactorial diseases which are caused by a combination of multiple genetic and dietary factors, of which none is in itself pathogenic. A common example of an acquired, multifactorial metabolic disease is Non-Alcoholic Fatty Liver Disease (NAFLD), known as one of the most prevalent chronic liver diseases. NAFLD is associated with different risk factors such as diabetes type II, obesity and metabolic syndrome^{32,33}. A contrasting example of another disease that leads to fatty liver associated with disturbances in fatty metabolism is undernutrition³⁴⁻³⁸. Interestingly, illustrating the complexity of this topic, moderately-low protein diets without malnutrition, have been shown to increase lifespan and metabolic health in mice^{39,40}.

On the other end of the spectrum, there are also monogenic diseases where a single mutation can lead to disturbances in fatty acid metabolism. These genetic diseases, which lead to a deficiency of a single enzyme of any metabolic pathway related to the metabolism of carbohydrates, fats or protein are known as inborn errors of metabolism (IEM)⁴¹. Some examples of inborn errors of metabolism affecting mitochondrial β -oxidation are deficiencies in any of the dehydrogenases involved in the first step of the pathway (SCADD, MCADD and VLCADD)⁴². IEMs often present during childhood, and they can lead to the development of life-threatening symptoms. Despite the fact that extensive research is currently being done, the fact remains that these diseases are commonly only managed palliatively as no cure is known for most of them.

This thesis focuses on two diseases affecting lipid metabolism on both ends of the spectrum: one caused by an imbalance of the diet (severe malnutrition) and the other by a genetic mutation in the ACADM gene (MCADD).

SEVERE MALNUTRITION

The first disease central to the thesis is Severe malnutrition (SM). Malnutrition refers to an imbalance or deficit in the intake of energy and nutrients required to maintain homeostasis. Malnutrition can be caused by either a deficiency or an excess of nutrients, undernutrition and overnutrition respectively⁴³. In this thesis, the term malnutrition is used to refer to undernutrition. Severe malnutrition is known as the most severe form of macronutrient deficiency. In the case of children, this can hamper optimal growth and development⁴⁴. There are different types of malnutrition, namely stunting, wasting, underweight and deficiencies of vitamins and minerals. Stunting refers to children who are too short for their age. Wasting is used to describe children who are too thin for their height. Finally, the term undernutrition engulfs both stunting and wasting. Severe malnutrition is a highly challenging global health problem: in 2023 approximately 45 million children were wasted, of whom 13.7 million were severely wasted⁴⁵. Severe malnutrition is common in low-income countries, where diets are often high in carbohydrates and contain low amounts of protein⁴⁶.

Children suffering from malnutrition present with a wide spectrum of symptoms affecting the liver and the intestine amongst other organs⁴⁷. Severely malnourished children often suffer from intestinal dysfunction, including diarrhea and increased permeability of the intestinal barrier. These factors can contribute to increased risk of dehydration and sepsis respectively⁴⁸.

Additionally, the intestine of malnourished children has been described to be severely impacted not only in function but also in structure⁴⁹. Regarding the effects of malnutrition in the liver, hepatic steatosis, hypoalbuminemia and hypoglycemia are some of the common problems observed in malnourished children^{50,51}. Hepatic steatosis in malnourished children has been linked to the observed impaired lipid metabolism.^{52,53} Moreover, the number of peroxisomes was found to be substantially decreased in the liver of malnourished children⁵⁴.

Current approaches for the study of malnutrition mostly rely on the use of animal models, including primates⁵⁵, rats⁵⁶ and more frequently, mice^{57,58} on low protein diets (LPD). These models, have shed some light onto the pathophysiology of malnutrition in the liver and the intestine and are able to recapitulate the specific phenotypes of the disease (e.g., hepatic steatosis, barrier dysfunction, etc.). Some of these studies also revealed dysfunctional mitochondria in the liver and the intestine of both mice and rats^{56,58} while peroxisomal loss in the liver was recapitulated in the rat model⁵⁶, but not yet studied in mice. While these models are physiologically relevant, and allow for a whole-body characterization of the disease, they are also limited by blood and tissue sampling and require large numbers of animals for large screenings. These limitations emphasize the need for relevant *in vitro* malnutrition models to study organ-specific phenotypes as well as intercellular communication.

The role of peroxisomes and mitochondria in severe malnutrition

An interesting feature of peroxisomes is their plasticity and their ability to respond to different stimuli and adapt to the cellular needs⁵⁹. This behavior goes in line with the response observed in malnourished children fed low protein diets. Peroxisomes have been reported to substantially decrease in number in the liver of malnourished children and rodents on low protein diets (**Figure 1**)^{54,56-58}. Moreover, mitochondria were also found to be impaired, characterized by defects in complexes I and IV *in vivo*, and reduced hepatic ATP levels. Dysfunction in both organelles might explain the accumulation of fatty acids in the liver of malnourished children leading to hepatic steatosis⁵².

In the case of the intestine of mice fed an LPD, mitochondrial abundance was reduced with a clear reduction in protein expression of complexes I and V from the electron transport chain (ETC) (**Figure 1**). Moreover, levels of reactive oxygen species were found to be increased. These results, together with decreased autophagy, were causally linked to increased permeability observed

in the intestine of the animals⁶⁰. Nothing has been published on the number and health of peroxisomes in the intestine of mice fed a low protein diet.

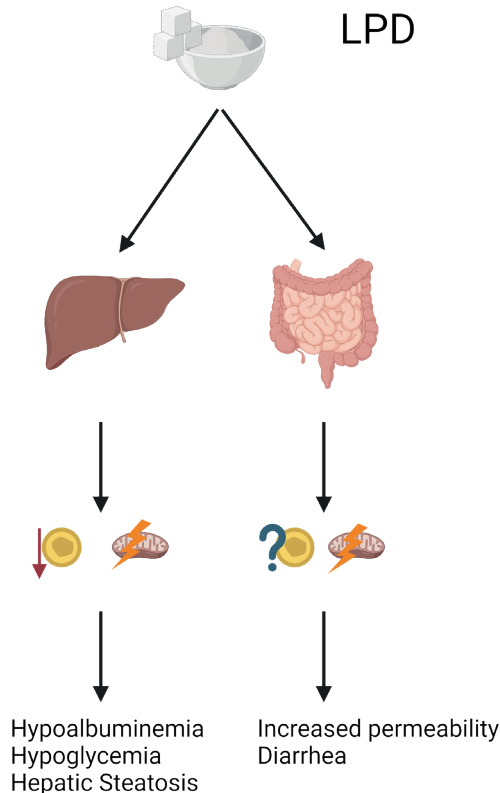


Figure 1. The effects of low protein diets and low amino acid conditions in vivo. Low protein diets lead to a loss of peroxisomes and delayed loss of mitochondria in the liver. LPD leads to dysfunctional and less abundant mitochondria in the intestine. There is no information on the number of peroxisomes in the intestine of LPD rodents or children. Created with BioRender.com

Interestingly, little is known about the actual mechanisms of peroxisomal loss in the liver of malnourished children and mice. Two main explanations have been suggested: a potential increase in autophagic degradation in order to maintain levels of precursors in the cell or a reduced biogenesis due to lack of amino acids⁵⁶.

Autophagic degradation and its role in malnutrition

Both mitochondria and peroxisomes are commonly degraded via selective autophagy^{61,62}. Autophagy is a degradation process based on the delivery of cargo, encapsulated in autophagosomes, to the lysosome, where different biological polymers are broken down by a combination of enzymes⁶³. The autophagic process starts by the formation of a structure known as the phagophore. Once the membrane of the phagophore closes around its cargo, it forms the autophagosome. This then fuses with the lysosome forming the autolysosome in which the lysosome secretes a set of enzymes able to degrade proteins, lipids and carbohydrates^{64,65}. Traditional autophagy markers, mentioned throughout this thesis, are LC3-I, LC3-II and p62. LC3-I is conjugated with phosphatidylethanolamine to form LC3-II which is then targeted to the autophagosomal membrane. Once the autophagosome fuses with the lysosome, LC3-II is degraded. Therefore, the LC3-II/LC3-I is commonly used to track the autolysosome formation. P62 is an autophagy adaptor protein which delivers polyubiquitinated cargo to the phagophore⁶⁶. This process is regulated in response to different nutritional states such as amino acid starvation, a well-known autophagy activator⁶⁷⁻⁶⁹. Since most proteins and organelles are degraded via autophagy, regulation of this process grants autophagy the ability to maintain the levels of amino acids, especially during scarcity of these nutrients⁷⁰.

The decrease in the number of peroxisomes in the liver of rats on a low protein diet has been linked to autophagic degradation⁵⁶. These results were in line with the induction of autophagy *in vitro* using amino acid deprivation⁶⁷. Moreover, peroxisomes have been described to be highly sensitive to amino acid levels and have been reported to rapidly degrade via pexophagy, selective peroxisomal autophagy, under low-amino acid concentration conditions⁷¹. Another example of peroxisomes responding to nutrient deprivation is the induction of pexophagy in yeast under nitrogen starvation conditions⁷².

A low-protein-diet study in rats showed induction of autophagy after 1 week, illustrated by elevated levels of LC3-II and reduced levels of p62. Interestingly, after 4 weeks of LPD the levels of p62 were elevated while LC3-II remained high. These results were interpreted as a potential block in autophagy after prolonged starvation⁵⁶. Some other studies in mice showed that already two weeks of LPD led to a decreased autophagy activation in mice^{57,58}. All these studies focused on the assessment of autophagy based on snapshots of LC3 and P62 at given times. However, it is important to take into consideration that autophagy is a dynamic process. While LC3-II levels are known to relate to the

number of autophagic structures in the cells, they do not quantify the actual autophagic flux⁷³.

Very few papers have been published on the role of autophagy in the intestine of LPD-fed rodents. Only one study has reported that 2 weeks of low protein diet led to a decreased autophagy in the intestine of rodents, which was thought to be the cause of the observed accumulation of dysfunctional mitochondria⁶⁰.

Peroxisomal biogenesis and PPAR- α activation

To date, no clear link between amino-acid restriction and decreased peroxisomal biogenesis has been made. One *in vivo* study in malnourished rats showed no clear effect of LPD on the expression of different peroxisins⁵⁶. Peroxisome proliferator-activated receptor (PPAR)- α is a transcriptional factor belonging to the family of nuclear receptors. It is an important regulator of energy homeostasis⁷⁴ and it controls the expression of genes involved in β -oxidation of fatty acids^{75,76}. Moreover, PPAR- α activation is known to induce proliferation of peroxisomes⁷⁷. Traditionally, PPAR- α activators, such as fibrates, have been used to treat dyslipidemia as well as to induce biogenesis of peroxisomes and mitochondria⁷⁸. While no clear effect of malnutrition on peroxisomal and mitochondrial biogenesis has been described, the effect of these compounds has been previously studied in the context of malnutrition^{56,79}. It is important to mention that some of these compounds have also been reported to cause side effects. For example, fenofibrate was able to reduce plasma triglycerides in PPAR- α null mice, as expected, but it also increased the levels of intrahepatic triglycerides⁸⁰.

Different natural ligands, such as eicosanoid derivatives and long chain polyunsaturated fatty acids (LCPUFA) have been reported to activate PPAR- α ^{76,81,82}. The ability of these natural compounds to activate PPAR- α , and thereby peroxisomal and mitochondrial biogenesis, opens the door to potential new therapies for malnutrition based on natural food supplements. In this line, several studies have already been published on the positive effects of the LCPUFA docosahexaenoic acid (DHA) on different aspects of malnutrition, such as antioxidants metabolism in rodents⁸³ and regulation of cognition in malnourished infants⁸⁴. Both of these studies highlighted the benefits of DHA supplementation in severe malnutrition.

MEDIUM CHAIN ACYL-COA DEHYDROGENASE DEFICIENCY

The second disease studied in this thesis is a monogenic disease known as Medium Chain Acyl-CoA Dehydrogenase Deficiency (MCADD). Medium-chain Acyl-CoA dehydrogenase (MCAD) is a flavoprotein containing a flavin adenine nucleotide (FAD). It catalyzes the oxidation of an acyl-CoA with the simultaneous reduction of the flavin, which then needs to be reoxidized⁸⁵. MCAD is involved in the oxidation of medium chain fatty acids in the mitochondrial β -oxidation. Prior to being metabolized, fatty acids need to be activated into their CoA ester form. The acyl-CoA esters can then be oxidized to acetyl-CoA in order to produce NADH and FADH₂. This pathway is of special importance during fasting or situations of high energy demand (cold exposure, infection, etc.) when gluconeogenic precursors are low and we depend on our fat reserves. Medium Chain Acyl-CoA Dehydrogenase Deficiency is the most common fatty acid oxidation disorder with a prevalence of 1:8000 in the Netherlands⁸⁶.

Biochemically, MCADD is characterized by the accumulation of medium-chain monocarboxylic acids and acyl-carnitines. Fatty acids of more than 12 carbons (C12) are often considered to be long while those between 10 and 6 carbons (C10-C6) are referred to as medium-chain fatty acids. Given the lack of efficient oxidation of medium-chain fatty acids, MCADD is also characterized by a high ratio C8 over C10 acylcarnitines⁸⁷⁻⁸⁹. Clinically, MCADD patients are at risk of suffering hypoketotic hypoglycemia (low levels of blood glucose and ketone bodies) which can be fatal². Interestingly, heterogeneity in symptomatology in MCADD patients is high. While some patients present with severe symptoms, other patients never develop any symptoms, even when carrying the same mutation and without surveillance⁹⁰⁻⁹².

While MCADD patients present as healthy under most conditions, they are insufficiently able to oxidize medium-chain fatty acids when they rely on fatty acid reserves such as fasting, illness or long bouts of exercise⁹³.

Current methods for the study of MCADD include animal models (rodents)^{94,95} and artificial KO cell lines. While these models have shed some light onto the pathophysiology of MCADD, both have their own limitations. Although animal models are wholistic systems that allow for a physiologically accurate picture, rodents express a long-chain acyl-CoA dehydrogenase isoform in charge of oxidizing long-chain acyl-CoAs⁹⁶. LCAD shares substrate specificity with MCAD which might alleviate the phenotype. On the other hand, KO human cell lines allow us to study the disease without expression of LCAD but are limited in terms of cell functionality and lack interaction with other organs. Moreover,

none of these systems allow researchers to address the issue of patient heterogeneity, emphasizing the need for new experimental models to study MCADD in patient derived tissue.

The role of peroxisomes in MCAD deficiency

As mentioned above, MCAD deficiency is characterized by the accumulation of substrates that are normally metabolized by the medium-chain dehydrogenase. Under non-challenging conditions other dehydrogenases are able to prevent severe phenotypes. In contrast, catabolic conditions such as fasting and recurring illness can trigger accumulation of medium-chain fatty acids in MCAD deficient patients. Peroxisomes have been reported to metabolize a wide range of substrates including medium-chain acyl-CoAs when mitochondrial import of fatty acids is inhibited⁹⁷. Interestingly, peroxisomes are equipped with all the enzymes required for the activation, import and oxidation of medium-chain fatty acids. A study reported that medium-chain acyl-CoAs can enter peroxisomes via ABCD3 (PMP70) prior to being oxidized by the peroxisomal β -oxidation. These results highlight peroxisomes as a potential route to metabolize medium-chain fatty acids in MCAD deficiency in order to prevent metabolite accumulation. Yet, no studies have reported on the role of peroxisomes in any of the mitochondrial dehydrogenase deficiencies (SCADD, MCADD or VLCADD).

NEW EXPERIMENTAL AND COMPUTATIONAL MODELS TO STUDY SEVERE MALNUTRITION AND MCADD IN VITRO AND IN SILICO

I have already introduced some of the more traditional models for the characterization and study of both severe malnutrition and MCADD. However, it is important to realize that all models are flawed and present both advantages and limitations. In the context of this thesis, I introduce two new tools for the study of the above-mentioned diseases. Here I introduce primary and iPSC-derived organoids as well as computational models to predict different metabolic outcomes.

Organoids

The development discovery of organoids in 2009⁹⁸ has entailed a change in the way we conceive the study of biology and biomedicine. Organoids are three-dimensional structures that can be derived from primary tissue as well

as from adult or pluripotent stem cells. They have the ability to proliferate in vitro, while maintaining some of the functionalities of the organ of origin⁹⁹. These structures have provided scientists with a revolutionary tool which allowed in vitro research to get one step closer to physiological relevance. While traditional 2D cell cultures rely on monolayers of one cell type, organoids allow more than one cell type to communicate with each other in a way that recapitulates the structure and functions of the tissue of origin more closely¹⁰⁰. Another advantage of organoids over 2D cultures is the possibility of deriving patient-specific organoids, allowing for more tailored research¹⁰¹. Ever since their discovery, many organoid systems have been described, recapitulating the functional and structural properties of multiple organs, including intestine⁹⁸, liver^{102,103}, stomach¹⁰⁴ and brain¹⁰⁵. Organoids have been used for many purposes, including understanding organ development, modeling of genetic diseases, drug screening, regenerative medicine and the study of organ-specific metabolism^{99,106-108}. While organoids are an excellent tool to study the effect of genetic diseases, as illustrated by an extensive number of publications¹⁰⁹, they are also highly interesting for the study of different nutritional stressors on organ metabolism¹¹⁰. Moreover, they can also be used to understand the effects of different dietary interventions on the organ of study and its metabolic regulation¹¹¹.

As mentioned above, organoids can be isolated either from primary tissue or derived from stem cells, both adult and pluripotent⁹⁹. Development of induced pluripotent stem cells (iPSCs) in 2006 by Yamanaka was regarded as a breakthrough in the field of stem cell biology¹¹². Ever since, numerous protocols describing the differentiation of iPSCs into multiple cellular lineages have been published¹¹³⁻¹¹⁶. The hepatic lineage has been induced from iPSCs using multiple protocols which are commonly based on the use of growth factors Activin A and BMP4 to induce the definitive endoderm, followed by a combination of other growth factors to further commit the cells into hepatoblasts^{113,114,117-119}. iPSC-derived hepatocytes and hepatobiliary organoids recapitulate many features of the liver such as albumin production, lipid accumulation, and urea production. In some cases, upon further differentiation towards the hepatic-lineage, these organoids are referred to as "hepatocyte-like". iPSC-derived hepatobiliary and hepatocyte-like organoids are, however, limited in their maturity level and are closer to fetal than to adult liver^{120,121}. iPSC-derived hepatobiliary organoid models have been used to study different diseases such as alcoholic liver injury¹¹⁹ or genetic diseases such as Alagille syndrome (ALGS) and Tetralogy of Fallot (TOF)¹²².

Systems medicine approach and computational models

Systems medicine is the multidisciplinary combination of different fields including biology, informatics, computational modeling and mathematics to gap the bridge between new translational research and traditional health care¹²³. This interdisciplinary methodology allows clinical investigators and physicians to team up with mathematicians and natural scientists, to tackle different medical problems in a more efficient and tailored manner¹²⁴. Their approaches commonly rely on *in vitro* and *in vivo* systems, combined with various 'omics technologies as well as different computational approaches (*in silico* systems).

Computational models are *in silico* representations of biological systems that can help us understand regulation of different biological processes. These models mathematically describe a biological system in an integrative way. Simulating their response to interventions or mutations can help us predict behaviors and outcomes of a given system under different conditions. In this thesis I will focus on computational models of metabolic pathways. One main type of metabolic computational models is a detailed kinetic model. Kinetic models for the study of metabolic pathways are based on kinetic equations describing the behavior of the enzymes of a given pathway combined with kinetic parameters commonly obtained from the literature or measured in the lab. Ordinary differential equations (ODEs) are then used to describe the dynamics of reactions in the system and how these produce and consume different metabolites. These dynamic models can predict both metabolite concentrations and fluxes over time. An interesting aspect of detailed kinetic models is the possibility to study Metabolic Control Analysis to understand the control that certain enzymes exert over metabolite concentrations or metabolic fluxes in a specific pathway^{125,126}. In order to adapt computational models to different conditions, such as different tissues or diseases, enzyme concentrations can be measured and introduced into the model. To do so, proteomics data or enzyme activity data are commonly used. There are models describing different metabolic pathways such as mitochondrial β -oxidation⁹⁵, TCA and ECT¹²⁷ and glucose metabolism¹²⁸. So far, to the best of my knowledge, no computational models describing peroxisomal β -oxidation have been published.

Another highly valuable type of computational model for the study of systems medicine is based on deep learning (DL) algorithms. These models are often referred to as 'multilayered' due to their ability to process data in different layers in which they transform the data and pass them on to the next layer until

the output layer¹²⁹. They rely on big data sets and can be used to automatize analyses and quantification of different parameters. In the context of this thesis, I will present an application of DL for the analysis of organoid number and size from brightfield microscopy images.

AIMS AND OUTLINE OF THIS THESIS

The aim of this thesis is to develop and characterize in vitro and computational translational models to study two diseases affecting fatty acid metabolism. In both diseases, peroxisomal and mitochondrial homeostasis are known or hypothesized to be disrupted. In the case of malnutrition, it has been proposed that peroxisomal loss precedes the mitochondrial phenotype⁵⁶. In the case of MCADD, peroxisomes have been hypothesized to play a compensatory role in the disease. Experimental and computational tools to study these two diseases largely overlap. Studying two different diseases, in which the interplay between mitochondria and peroxisomes is affected, will provide deeper insight into the underlying mechanisms.

In **part I**, I focus on the development and characterization of two in vitro malnutrition models from mouse primary tissue (both liver and intestine), based on growth media lacking amino acids. In **part II**, I first make use of this newly characterized malnutrition hepatic organoid model to understand the underlying causes for peroxisomal loss under low amino acid conditions. Secondly, I test different pharmacological approaches to prevent peroxisomal loss in the liver. Moreover, I also develop a detailed kinetic model of the peroxisomal β -oxidation to understand the effects of malnutrition and the different treatments on the pathway. In **part III**, I focus on the study of MCADD. To do so, I develop and characterize an MCADD in vitro model making use of patient specific iPSC-derived hepatic organoids and assess the role peroxisomes play in the disease. Finally, in **part IV** I focus on contextualizing the results presented throughout the thesis and discuss the literature on the topic. I also discuss the limitations and possibilities of these new translational models (both from the technical and the biological point of view) and highlight and potential ways to improve in the future.

Part I – Malnutrition in vitro

In **chapter 2**, I develop and characterize an organoid in vitro model to study malnutrition both in the liver and the intestine. These 3D systems replicate many of the organ-specific malnutrition phenotypes of both organs. In the case

of the liver, amino-acid deprivation leads to hypoalbuminemia and hepatic steatosis, while the effect on the intestine is characterized by increased barrier permeability. Both organs show a clear reduction in peroxisomal protein markers and dysfunctional mitochondria which are thought to be responsible for the hepatic steatosis and disruption of the intestinal barrier permeability. Moreover, as a proof of principle, I demonstrate how these in vitro models can be used as a pre-screening tool to test potential treatments to prevent both peroxisomal and mitochondrial loss. Fenofibrate and rapamycin are used to prevent peroxisomal loss and mitochondrial loss in the liver and the intestine respectively.

In chapter 3 I make use of the opportunities offered by the embedding of my PhD project in the European Perico training network, aimed at deciphering the role of peroxisomes in cellular interaction and signaling. In this chapter one of my Perico colleagues develops and implements a deep learning computational model to measure and track organoid size and growth. Together, we apply this tool to detect and measure different types of cystic organoids in brightfield microscopy images. It can be used for a wide range of purposes in different aspects of organoid research. In order to illustrate the potential of this tool we use it to measure the size of organoids under control and amino-acid deprived conditions, and we compare the results with manually annotated data from chapter 2.

Part II- Applications of the new malnutrition models

In chapter 4, I study the mechanisms underlying peroxisomal loss and potential treatments to prevent such loss. To do so, I make use of the hepatic in vitro malnutrition model described in chapter 2. Together with a colleague from the pediatrics department at the UMCG I demonstrate that amino-acid deprivation in hepatic organoids is accompanied by a clear induction of the autophagic flux, which we measure using a novel autophagic probe. Furthermore, I apply this model to identify different therapeutic compounds. Finally, I show that long-chain poly-unsaturated fatty acids (LCPUFA) are more effective than synthetic PPAR- α agonists and demonstrate that docosahexaenoic acid (DHA) prevents peroxisomal and mitochondrial loss during amino-acid deficiency.

In chapter 5, I develop a kinetic model of the peroxisomal β -oxidation based on kinetic studies described in the literature. Doing so, I review the kinetics of the enzymes involved in the pathway. Then I use the model to predict the effects of amino acid deficiency in the pathway. For that purpose, I combine targeted proteomics data from amino-acid deprived organoids and the above-

mentioned kinetic model. Moreover, I also analyze the effects of the previously described DHA supplement on the pathway to understand the role of this PPAR- α agonist.

Part III- Medium Chain Acyl-CoA Dehydrogenase Deficiency

Next, in **chapter 6** together with my colleague from the Systems Medicine group of the UMCG I develop an iPSC-derived hepatobiliary organoid model to study a particular IEM. In this case, we use fibroblasts-derived iPSCs from healthy and MCAD-deficient children and differentiate them into hepatocyte-like organoids. We show that these organoids recapitulate the biochemical MCADD phenotype and serve as valuable tool to understand pathophysiological aspects of the disease. Finally, once the MCADD organoids have been established and characterized we focus on the study of peroxisomes and the potential role they play in metabolizing medium-chain fatty acids (accumulated in the absence of MCAD) as well as on their role in coenzyme A (CoA) metabolism.

Part IV- General Discussion and future perspectives

Finally, in **chapter 7** I evaluate the progress made in the study of malnutrition and MCAD deficiency with this thesis and the advances it permitted. I focus on the potential and limitations of in vitro models and propose different solutions. I also focus on the interplay of peroxisomes and mitochondria in health and disease and the potential compensatory mechanisms from one organelle to the other. Finally, I discuss the future directions and application of translational models for metabolic research.

REFERENCES

1. De Carvalho, C. C. R. & Caramujo, M. J. The various roles of fatty acids. *Molecules* vol. 23 Preprint at <https://doi.org/10.3390/molecules23102583> (2018).
2. Houten, S. M., Violante, S., Ventura, F. V. & Wanders, R. J. A. The Biochemistry and Physiology of Mitochondrial Fatty Acid β -Oxidation and Its Genetic Disorders. *Annual Review of Physiology* vol. 78 23–44 Preprint at <https://doi.org/10.1146/annurev-physiol-021115-105045> (2016).
3. Spinelli, J. B. & Haigis, M. C. The multifaceted contributions of mitochondria to cellular metabolism. *Nature Cell Biology* vol. 20 745–754 Preprint at <https://doi.org/10.1038/s41556-018-0124-1> (2018).
4. Prosad Chakrabarty, R. & Chandel, N. S. Beyond ATP, new roles of mitochondria. *Biochem (London)* 44, 2–8 (2022).
5. Chan, D. C. Mitochondrial Dynamics and Its Involvement in Disease. (2019) doi:10.1146/annurev-pathmechdis.
6. Fenton, A. R., Jongens, T. A. & Holzbaur, E. L. F. Mitochondrial dynamics: Shaping and remodeling an organelle network. *Current Opinion in Cell Biology* vol. 68 28–36 Preprint at <https://doi.org/10.1016/j.ceb.2020.08.014> (2021).
7. Eisner, V., Picard, M. & Hajnóczky, G. Mitochondrial dynamics in adaptive and maladaptive cellular stress responses. *Nature Cell Biology* vol. 20 755–765 Preprint at <https://doi.org/10.1038/s41556-018-0133-0> (2018).
8. Wanders, R. J. A., Baes, M., Ribeiro, D., Ferdinandusse, S. & Waterham, H. R. The physiological functions of human peroxisomes. *Physiological Reviews* vol. 103 957–1024 Preprint at <https://doi.org/10.1152/physrev.00051.2021> (2023).
9. Michels, P. A. M. & Gualdrón-López, M. Biogenesis and metabolic homeostasis of trypanosomatid glycosomes: New insights and new questions. *Journal of Eukaryotic Microbiology* vol. 69 Preprint at <https://doi.org/10.1111/jeu.12897> (2022).
10. Weller, S., Gould, S. J. & Valle, D. Peroxisome Biogenesis Disorders. *Annual Review of Genomics and Human Genetics* vol. 4 165–211 Preprint at <https://doi.org/10.1146/annurev.genom.4.070802.110424> (2003).
11. Waterham, H. R., Ferdinandusse, S. & Wanders, R. J. A. Human disorders of peroxisome metabolism and biogenesis. *Biochim Biophys Acta Mol Cell Res* 1863, 922–933 (2016).
12. Schrader, M., Costello, J. L., Godinho, L. F., Azadi, A. S. & Islinger, M. Proliferation and fission of peroxisomes - An update. *Biochimica et Biophysica Acta - Molecular Cell Research* vol. 1863 971–983 Preprint at <https://doi.org/10.1016/j.bbamcr.2015.09.024> (2016).
13. Schrader, M., Kamoshita, M. & Islinger, M. Organelle interplay—peroxisome interactions in health and disease. *Journal of Inherited Metabolic Disease* vol. 43 71–89 Preprint at <https://doi.org/10.1002/jimd.12083> (2020).
14. Schrader, M., Bonekamp, N. A. & Islinger, M. Fission and proliferation of peroxisomes. *Biochimica et Biophysica Acta - Molecular Basis of Disease* vol. 1822 1343–1357 Preprint at <https://doi.org/10.1016/j.bbadis.2011.12.014> (2012).

15. Wróblewska, J. P. & van der Klei, I. J. Peroxisome maintenance depends on de novo peroxisome formation in yeast mutants defective in peroxisome fission and inheritance. *Int J Mol Sci* 20, (2019).
16. Banerjee, S. & Prinz, W. A. Early steps in the birth of four membrane-bound organelles—Peroxisomes, lipid droplets, lipoproteins, and autophagosomes. *Curr Opin Cell Biol* 84, (2023).
17. Violante, S. *et al.* Peroxisomes can oxidize medium- and long-chain fatty acids through a pathway involving ABCD3 and HSD17B4. *FASEB Journal* 33, 4355–4364 (2019).
18. Osmundsen, H., Neat, C. E. & Borrebaek, B. *Fatty acid products of peroxisomal β -oxidation.* *J Bmhum* vol. 12.
19. Schrader, M. & Yoon, Y. Mitochondria and peroxisomes: Are the ‘Big Brother’ and the ‘Little Sister’ closer than assumed? *BioEssays* vol. 29 1105–1114 Preprint at <https://doi.org/10.1002/bies.20659> (2007).
20. Fransen, M., Lismont, C. & Walton, P. The peroxisome-mitochondria connection: How and why? *International Journal of Molecular Sciences* vol. 18 Preprint at <https://doi.org/10.3390/ijms18061126> (2017).
21. Wanders, R. J. A., Waterham, H. R. & Ferdinandusse, S. Metabolic interplay between peroxisomes and other subcellular organelles including mitochondria and the endoplasmic reticulum. *Frontiers in Cell and Developmental Biology* vol. 3 Preprint at <https://doi.org/10.3389/fcell.2015.00083> (2016).
22. Shields, H. J., Traa, A. & Van Raamsdonk, J. M. Beneficial and Detrimental Effects of Reactive Oxygen Species on Lifespan: A Comprehensive Review of Comparative and Experimental Studies. *Front Cell Dev Biol* 9, (2021).
23. Fransen, M., Nordgren, M., Wang, B. & Apanasets, O. Role of peroxisomes in ROS/RNS-metabolism: Implications for human disease. *Biochimica et Biophysica Acta - Molecular Basis of Disease* vol. 1822 1363–1373 Preprint at <https://doi.org/10.1016/j.bbadis.2011.12.001> (2012).
24. Neuspiel, M. *et al.* Cargo-Selected Transport from the Mitochondria to Peroxisomes Is Mediated by Vesicular Carriers. *Current Biology* 18, 102–108 (2008).
25. Horner, S. M., Liu, H. M., Park, H. S., Briley, J. & Gale, M. Mitochondrial-associated endoplasmic reticulum membranes (MAM) form innate immune synapses and are targeted by hepatitis C virus. *Proc Natl Acad Sci U S A* 108, 14590–14595 (2011).
26. Antonenkov, V. D. & Hiltunen, J. K. Transfer of metabolites across the peroxisomal membrane. *Biochimica et Biophysica Acta - Molecular Basis of Disease* vol. 1822 1374–1386 Preprint at <https://doi.org/10.1016/j.bbadis.2011.12.011> (2012).
27. Camões, F., Bonekamp, N. A., Delille, H. K. & Schrader, M. Organelle dynamics and dysfunction: A closer link between peroxisomes and mitochondria. in *Journal of Inherited Metabolic Disease* vol. 32 163–180 (2009).
28. Fourcade, S., Ferrer, I. & Pujol, A. Oxidative stress, mitochondrial and proteostasis malfunction in adrenoleukodystrophy: A paradigm for axonal degeneration. *Free Radical Biology and Medicine* vol. 88 18–29 Preprint at <https://doi.org/10.1016/j.freeradbiomed.2015.05.041> (2015).
29. Salpietro, V. *et al.* Zellweger syndrome and secondary mitochondrial myopathy. *Eur J Pediatr* 174, 557–563 (2015).

30. Góth, L. & Nagy, T. Inherited catalase deficiency: Is it benign or a factor in various age related disorders? *Mutation Research - Reviews in Mutation Research* vol. 753 147–154 Preprint at <https://doi.org/10.1016/j.mrrev.2013.08.002> (2013).
31. Peeters, A. *et al.* Mitochondria in peroxisome-deficient hepatocytes exhibit impaired respiration, depleted DNA, and PGC-1 α independent proliferation. *Biochim Biophys Acta Mol Cell Res* 1853, 285–298 (2015).
32. Mardinoglu, A., Uhlen, M. & Borén, J. Broad Views of Non-alcoholic Fatty Liver Disease. *Cell Systems* vol. 6 7–9 Preprint at <https://doi.org/10.1016/j.cels.2018.01.004> (2018).
33. Kneeman, J. M., Misdraji, J. & Corey, K. E. Secondary causes of nonalcoholic fatty liver disease. *Therapeutic Advances in Gastroenterology* vol. 5 199–207 Preprint at <https://doi.org/10.1177/1756283X11430859> (2012).
34. Lopez-Pedrosa, J. M., Torres, M. I., Fernández, M. I., Ribes, A. & Gil, A. Nutrient Metabolism Severe Malnutrition Alters Lipid Composition and Fatty Acid Profile of Small Intestine in Newborn Piglets 1,2. *J. Nutr.* vol. 128 (1998).
35. Pezeshki, A. & Chelikani, P. K. Low Protein Diets and Energy Balance: Mechanisms of Action on Energy Intake and Expenditure. *Frontiers in Nutrition* vol. 8 Preprint at <https://doi.org/10.3389/fnut.2021.655833> (2021).
36. Thompson, D. S. *et al.* The effect of wasting and stunting during severe acute malnutrition in infancy on insulin sensitivity and insulin clearance in adult life. *J Dev Orig Health Dis* 13, 750–756 (2022).
37. Francis-Emmanuel, P. M. *et al.* Glucose metabolism in adult survivors of severe acute malnutrition. *Journal of Clinical Endocrinology and Metabolism* 99, 2233–2240 (2014).
38. Khardori, R., Bajaj, J. S., Deo, M. G. & Bansal, O. D. Insulin secretion and carbohydrate metabolism in experimental protein malnutrition. *J. Endocrinol. Invest* vol. 3 (1980).
39. Kitada, M., Ogura, Y., Monno, I. & Koya, D. The impact of dietary protein intake on longevity and metabolic health. *EBioMedicine* vol. 43 632–640 Preprint at <https://doi.org/10.1016/j.ebiom.2019.04.005> (2019).
40. Solon-Biet, S. M. *et al.* The ratio of macronutrients, not caloric intake, dictates cardiometabolic health, aging, and longevity in ad libitum-fed mice. *Cell Metab* 19, 418–430 (2014).
41. Garg, U. & Smith, L. D. Introduction to laboratory diagnosis and biomarkers in inborn error of metabolism. in *Biomarkers in Inborn Errors of Metabolism* 1–24 (Elsevier, 2017). doi:10.1016/b978-0-12-802896-4.00001-8.
42. Wanders, R. J. A., Visser, G., Ferdinandusse, S., Vaz, F. M. & Houtkooper, R. H. Mitochondrial fatty acid oxidation disorders: Laboratory diagnosis, pathogenesis, and the complicated route to treatment. *Journal of Lipid and Atherosclerosis* vol. 9 313–333 Preprint at <https://doi.org/10.12997/jla.2020.9.3.313> (2020).
43. World Health Organization. What is malnutrition? [Internet]. 2021. Available from: <https://www.who.int/news-room/fact-sheets/detail/malnutrition>.
44. Von Grebmer, K. *et al.* Synopsis: 2014 global hunger index: The challenge of hidden hunger. vol. 83 (Intl Food Policy Res Inst, 2014).

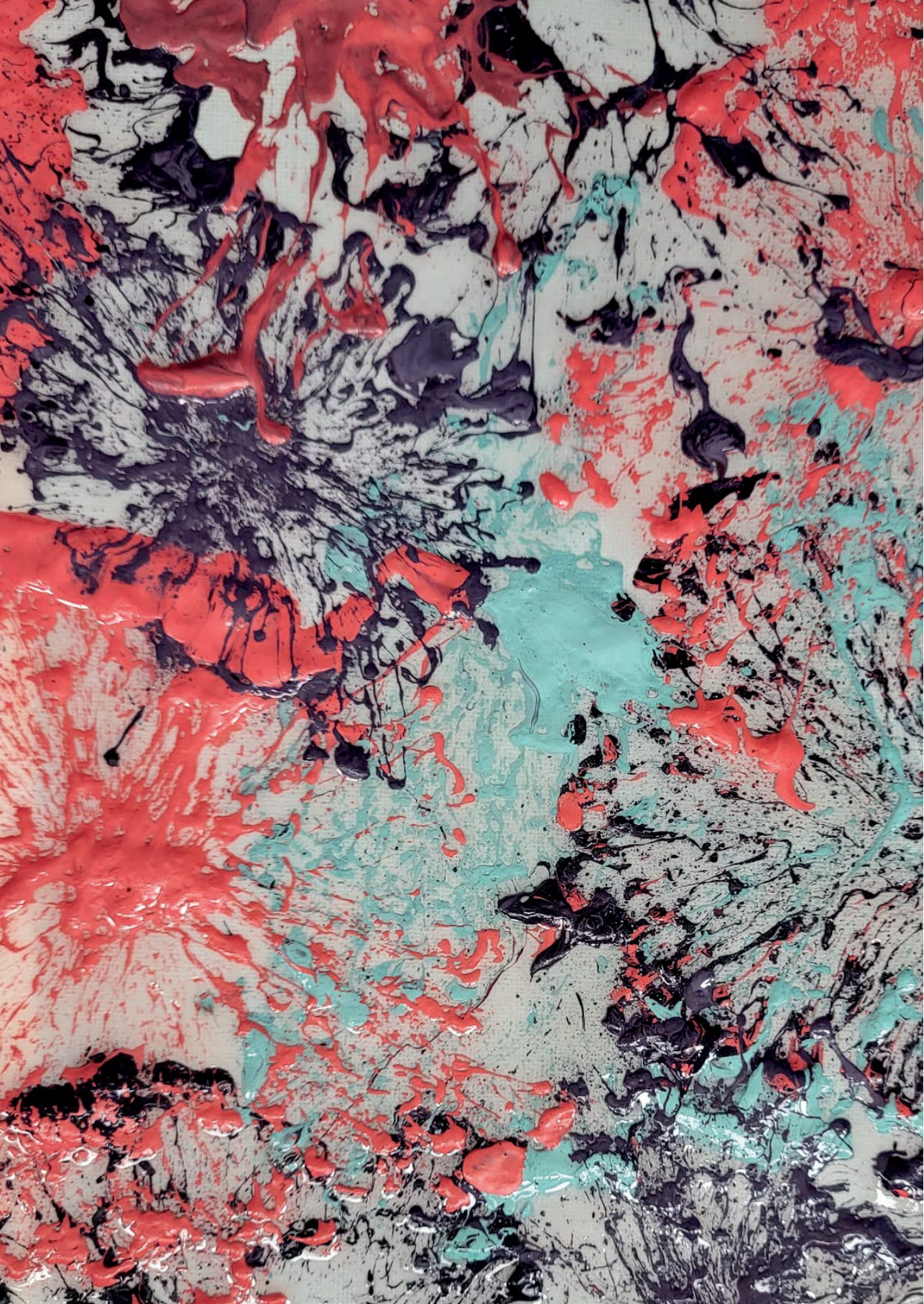
45. WHO, World Bank. United Nations Children's Fund, World Health Organization & World Bank Group. Levels and trends in child malnutrition: Key findings of the 2023 Edition of the Joint Child Malnutrition Estimates [Internet]. Geneva: WHO. 2023 Available from: <https://www.who.int/publications/i/item/9789240073791>.
46. Briend, A. Collaborating to improve the management of acute malnutrition worldwide Kwashiorkor: still an enigma-the search must go on. www.cmamforum.org (2014).
47. Bhutta, Z. A. *et al.* Severe childhood malnutrition. *Nat Rev Dis Primers* 3, (2017).
48. Grenov, B. *et al.* Diarrhea, Dehydration, and the Associated Mortality in Children with Complicated Severe Acute Malnutrition: A Prospective Cohort Study in Uganda. *Journal of Pediatrics* 210, 26-33.e3 (2019).
49. Attia, S., Feenstra, M., Swain, N., Cuesta, M. & Bandsma, R. H. J. Starved Guts: Morphologic and Functional Intestinal Changes in Malnutrition. *Journal of Pediatric Gastroenterology and Nutrition* vol. 65 491-495 Preprint at <https://doi.org/10.1097/MPG.0000000000001629> (2017).
50. Bandsma, R. H. J. *et al.* Mechanisms Behind Decreased Endogenous Glucose Production in Malnourished Children. *Pediatr Res.* (2010) doi:10.1203/PDR.0b013e3181f2b959.
51. Wharton, B. Hypoglycaemia in children with Kwashiorkor. *The Lancet* 124, 617 (1970).
52. Badaloo, A. V, Forrester, T., Reid, M. & Jahoor, F. Lipid kinetic differences between children with kwashiorkor and those with marasmus. *Am J Clin Nutr.* (2006) doi:10.1093/ajcn/83.6.1283.
53. Badaloo, A., Reid, M., Soares, D., Forrester, T. & Jahoor, F. Relation between liver fat content and the rate of VLDL apolipoprotein B-100 synthesis in children with protein-energy malnutrition. *Am J Clin Nutri.* (2005) doi:10.1093/ajcn/81.5.1126.
54. Doherty, J. F., Golden, M. H. & Brooks, S. E. Peroxisomes and the fatty liver of malnutrition: an hypothesis. *Am J Clin Nutr* 54, 674-681 (1991).
55. Enwonwu, C. O, Worthington, B. S. & Jacobson, K. L. Protein-Energy Malnutrition in Infant Non-Human Primates (*Macaca Nemestrina*) I. Correlation of Biochemical Changes with Fine Structural Alterations in the Liver. *Br. J. exp. Path* 58, 78 (1977).
56. van Zutphen, T. *et al.* Malnutrition-associated liver steatosis and ATP depletion is caused by peroxisomal and mitochondrial dysfunction. *J Hepatol* 65, 1198-1208 (2016).
57. Arvidsson Kvissberg, M. E. *et al.* Inhibition of mTOR improves malnutrition induced hepatic metabolic dysfunction. *Sci Rep* 12, (2022).
58. Hu, G. *et al.* The role of the tryptophan-NAD⁺ pathway in a mouse model of severe malnutrition induced liver dysfunction. *Nat Commun* 13, (2022).
59. Mast, F. D., Rachubinski, R. A. & Aitchison, J. D. Signaling dynamics and peroxisomes. *Current Opinion in Cell Biology* vol. 35 131-136 Preprint at <https://doi.org/10.1016/j.ceb.2015.05.002> (2015).
60. Ling, C. *et al.* Rebalancing of mitochondrial homeostasis through an NAD⁺-SIRT1 pathway preserves intestinal barrier function in severe malnutrition. *EBioMedicine* 96, (2023).
61. Glick, D., Barth, S. & Macleod, K. F. Autophagy: Cellular and molecular mechanisms. *Journal of Pathology* vol. 221 3-12 Preprint at <https://doi.org/10.1002/path.2697> (2010).
62. Mizushima, N. Snapshot: Organelle degradation. *Molecular Cell* vol. 82 1604-1604.e1 Preprint at <https://doi.org/10.1016/j.molcel.2022.03.015> (2022).

63. Mizushima, N. *et al.* A protein conjugation system essential for autophagy. *Nature* 395–398 (1998).
64. Aman, Y. *et al.* Autophagy in healthy aging and disease. *Nature Aging* vol. 1 634–650 Preprint at <https://doi.org/10.1038/s43587-021-00098-4> (2021).
65. Klionsky, D. J. *et al.* Autophagy in major human diseases. *EMBO J* 40, (2021).
66. Liu, W. J. *et al.* p62 links the autophagy pathway and the ubiquitin-proteasome system upon ubiquitinated protein degradation. *Cellular and Molecular Biology Letters* vol. 21 Preprint at <https://doi.org/10.1186/s11658-016-0031-z> (2016).
67. Chen, R. *et al.* The general amino acid control pathway regulates mTOR and autophagy during serum/glutamine starvation. *Journal of Cell Biology* 206, 173–182 (2014).
68. Tan, H. W. S., Sim, A. Y. L. & Long, Y. C. Glutamine metabolism regulates autophagy-dependent mTORC1 reactivation during amino acid starvation. *Nat Commun* 8, (2017).
69. Ghislat, G. & Knecht, E. Regulation of Autophagy by Amino Acid Starvation Involving Ca²⁺. in *Autophagy: Cancer, Other Pathologies, Inflammation, Immunity, Infection, and Aging* vol. 6 69–79 (Elsevier Inc., 2015).
70. Singh, R. & Cuervo, A. M. Autophagy in the cellular energetic balance. *Cell Metabolism* vol. 13 495–504 Preprint at <https://doi.org/10.1016/j.cmet.2011.04.004> (2011).
71. Liu, C. *et al.* Functional amino acids and autophagy: Diverse signal transduction and application. *International Journal of Molecular Sciences* vol. 22 Preprint at <https://doi.org/10.3390/ijms222111427> (2021).
72. Sakai, Y., Oku, M., van der Klei, I. J. & Kiel, J. A. K. W. Peroxisome Proliferator-Activated Receptor (PPAR): A Pharmacological Target with a Promising Future. *Pharm Res* 21, 1531–1538 (2004).
73. Yoshii, S. R. & Mizushima, N. Monitoring and measuring autophagy. *International Journal of Molecular Sciences* vol. 18 Preprint at <https://doi.org/10.3390/ijms18091865> (2017).
74. Van Raalte, D. H., Li, M., Haydn Pritchard, P. & Wasan, K. M. Peroxisome Proliferator-Activated Receptor (PPAR): A Pharmacological Target with a Promising Future. *Pharm Res* 21, 1531–1538 (2004).
75. Motojima, K., Passilly, P., Peters, J. M., Gonzalez, F. J. & Latruffe, N. Expression of Putative Fatty Acid Transporter Genes Are Regulated by Peroxisome Proliferator-activated Receptor and Activators in a Tissue-and Inducer-specific Manner*. *J Biol Chem* 273, 16710–16714 (1998).
76. Berger, J. & Moller, D. E. The Mechanisms of action of PPARs. *Annu Rev Med* 53, 409–435 (2002).
77. Lalwani, N. D. *et al.* Evaluation of Selected Hypolipidemic Agents for the Induction of Peroxisomal Enzymes and Peroxisome Proliferation in the Rat Liver. *Human Toxicol* 2, 27–48 (1983).
78. Katsiki, N. *et al.* The Role of Fibrate Treatment in Dyslipidemia: An Overview. *Curr Pharm Des* 19, 3124–3131 (2013).
79. Kersten, S. *et al.* Peroxisome proliferator-activated receptor α mediates the adaptive response to fasting. *J Clin Invest* (1999) doi:10.1172/JCI6223.

80. Yan, F. *et al.* Peroxisome proliferator-activated receptor α activation induces hepatic steatosis, suggesting an adverse effect. *PLoS One* 9, (2014).
81. Echeverría, F., Ortiz, M., Valenzuela, R. & Videla, L. A. Long-chain polyunsaturated fatty acids regulation of PPARs, signaling: Relationship to tissue development and aging. *Prostaglandins Leukotrienes and Essential Fatty Acids* vol. 114 28–34 Preprint at <https://doi.org/10.1016/j.plefa.2016.10.001> (2016).
82. Keller, H. *et al.* Fatty acids and retinoids control lipid metabolism through activation of peroxisome proliferator-activated receptor-retinoid X receptor heterodimers (peroxisome proliferator-activated receptor response element/retinoid X receptor response element/acyl-CoA oxidase gene/ nuclear hormone receptors). *Proc. Natl. Acad. Sci. USA* 90, 2160–2164 (1993).
83. Sanyoto, D. D., Asnawati, A. & Triawanti, T. Effect of DHA Supplementation on the MDA and SOD Levels in Protein Malnourished Rats. in *Journal of Physics: Conference Series* vol. 1374 (Institute of Physics Publishing, 2019).
84. Stephenson, K. *et al.* Low linoleic acid foods with added DHA given to Malawian children with severe acute malnutrition improve cognition: a randomized, triple-blinded, controlled clinical trial. *American Journal of Clinical Nutrition* 115, 1322–1333 (2022).
85. Piano, V., Palfey, B. A. & Mattevi, A. Flavins as Covalent Catalysts: New Mechanisms Emerge. *Trends in Biochemical Sciences* vol. 42 457–469 Preprint at <https://doi.org/10.1016/j.tibs.2017.02.005> (2017).
86. Jager, E. A. *et al.* A nationwide retrospective observational study of population newborn screening for medium-chain acyl-CoA dehydrogenase (MCAD) deficiency in the Netherlands. *J Inherit Metab Dis* 42, 890–897 (2019).
87. Bentler, K. *et al.* 221 newborn-screened neonates with medium-chain acyl-coenzyme A dehydrogenase deficiency: Findings from the Inborn Errors of Metabolism Collaborative. *Mol Genet Metab* 119, 75–82 (2016).
88. Bennett, M. J. Pathophysiology of fatty acid oxidation disorders. *Journal of Inherited Metabolic Disease* vol. 33 533–537 Preprint at <https://doi.org/10.1007/s10545-010-9170-y> (2010).
89. Couce, M. L. *et al.* Newborn screening for medium-chain acyl-CoA dehydrogenase deficiency: Regional experience and high incidence of carnitine deficiency. *Orphanet J Rare Dis* 8, (2013).
90. Touw, C. M. *et al.* In vitro and in vivo consequences of variant medium-chain acyl-CoA dehydrogenase genotypes. *Orphanet J Rare Dis* 8, (2013).
91. Derks, T. G. J. *et al.* The natural history of medium-chain acyl CoA dehydrogenase deficiency in the Netherlands: Clinical presentation and outcome. *Journal of Pediatrics* 148, (2006).
92. Touw, C. M. L. *et al.* Risk stratification by residual enzyme activity after newborn screening for medium-chain acyl-CoA dehydrogenase deficiency: Data from a cohort study. *Orphanet J Rare Dis* 7, (2012).
93. Heales, S. J. R. *et al.* Production and Disposal of Medium-chain Fatty Acids in Children with Medium-chain Acyl-CoA Dehydrogenase Deficiency. *J. Inher. Metab. Dis* vol. 17 (1994).

94. Tolwani, R. J. *et al.* Medium-chain acyl-CoA dehydrogenase deficiency in gene-targeted mice. *PLoS Genet* 1, 0205–0212 (2005).
95. van Eunen, K. *et al.* Biochemical Competition Makes Fatty-Acid β -Oxidation Vulnerable to Substrate Overload. *PLoS Comput Biol* 9, (2013).
96. Chegary, M. *et al.* Mitochondrial long chain fatty acid β -oxidation in man and mouse. *Biochim Biophys Acta Mol Cell Biol Lipids* 1791, 806–815 (2009).
97. Violante, S. *et al.* Peroxisomes contribute to the acylcarnitine production when the carnitine shuttle is deficient. *Biochim Biophys Acta Mol Cell Biol Lipids* 1831, 1467–1474 (2013).
98. Sato, T. *et al.* Single Lgr5 stem cells build crypt-villus structures in vitro without a mesenchymal niche. *Nature* 459, 262–265 (2009).
99. Kretzschmar, K. & Clevers, H. Organoids: Modeling Development and the Stem Cell Niche in a Dish. *Developmental Cell* vol. 38 590–600 Preprint at <https://doi.org/10.1016/j.devcel.2016.08.014> (2016).
100. Kapałczyńska, M. *et al.* 2D and 3D cell cultures – a comparison of different types of cancer cell cultures. *Archives of Medical Science* 14, 910–919 (2018).
101. Heydari, Z. *et al.* Organoids: a novel modality in disease modeling. *Bio-Design and Manufacturing* vol. 4 689–716 Preprint at <https://doi.org/10.1007/s42242-021-00150-7> (2021).
102. Huch, M. *et al.* In vitro expansion of single Lgr5 + liver stem cells induced by Wnt-driven regeneration. *Nature* 494, 247–250 (2013).
103. Huch, M. *et al.* Long-term culture of genome-stable bipotent stem cells from adult human liver. *Cell* 160, 299–312 (2015).
104. Barker, N. *et al.* Lgr5+ve Stem Cells Drive Self-Renewal in the Stomach and Build Long-Lived Gastric Units In Vitro. *Cell Stem Cell* 6, 25–36 (2010).
105. Lancaster, M. A. *et al.* Cerebral organoids model human brain development and microcephaly. *Nature* 501, 373–379 (2013).
106. Lancaster, M. A. & Knoblich, J. A. Organogenesis in a dish: Modeling development and disease using organoid technologies. *Science (1979)* 345, (2014).
107. Schutgens, F. & Clevers, H. Human Organoids: Tools for Understanding Biology and Treating Diseases. (2019) doi:10.1146/annurev-pathmechdis.
108. Hu, W. & Lazar, M. A. Modelling metabolic diseases and drug response using stem cells and organoids. *Nature Reviews Endocrinology* vol. 18 744–759 Preprint at <https://doi.org/10.1038/s41574-022-00733-z> (2022).
109. Perez-Lanzon, M., Kroemer, G. & Maiuri, M. C. Organoids for Modeling Genetic Diseases. in *International Review of Cell and Molecular Biology* vol. 337 49–81 (Elsevier Inc., 2018).
110. Kruitwagen, H. S. *et al.* Long-Term Adult Feline Liver Organoid Cultures for Disease Modeling of Hepatic Steatosis. *Stem Cell Reports* 8, 822–830 (2017).
111. Cai, T. *et al.* Effects of six common dietary nutrients on murine intestinal organoid growth. *PLoS One* 13, (2018).
112. Takahashi, K. & Yamanaka, S. Induction of Pluripotent Stem Cells from Mouse Embryonic and Adult Fibroblast Cultures by Defined Factors. *Cell* 126, 663–676 (2006).

113. Ergir, E. *et al.* Generation and maturation of human iPSC-derived 3D organotypic cardiac microtissues in long-term culture. *Sci Rep* 12, (2022).
114. Williams, L. M. *et al.* Prolonged culturing of iPSC-derived brain endothelial-like cells is associated with quiescence, downregulation of glycolysis, and resistance to disruption by an Alzheimer's brain milieu. *Fluids Barriers CNS* 19, (2022).
115. Chandrasekaran, V. *et al.* Generation and characterization of iPSC-derived renal proximal tubule-like cells with extended stability. *Sci Rep* 11, (2021).
116. Mithal, A. *et al.* Generation of mesenchyme free intestinal organoids from human induced pluripotent stem cells. *Nat Commun* 11, (2020).
117. Wu, F. *et al.* Generation of hepatobiliary organoids from human induced pluripotent stem cells. *J Hepatol* 70, 1145–1158 (2019).
118. Hannan, N. R. F., Segeritz, C. P., Touboul, T. & Vallier, L. Production of hepatocyte-like cells from human pluripotent stem cells. *Nat Protoc* 8, 430–437 (2013).
119. Wang, S. *et al.* Human ESC-derived expandable hepatic organoids enable therapeutic liver repopulation and pathophysiological modeling of alcoholic liver injury. *Cell Res* 29, 1009–1026 (2019).
120. Baxter, M. *et al.* Phenotypic and functional analyses show stem cell-derived hepatocyte-like cells better mimic fetal rather than adult hepatocytes. *J Hepatol* 62, 581–589 (2015).
121. Chang, M., Bogacheva, M. S. & Lou, Y. R. Challenges for the Applications of Human Pluripotent Stem Cell-Derived Liver Organoids. *Frontiers in Cell and Developmental Biology* vol. 9 Preprint at <https://doi.org/10.3389/fcell.2021.748576> (2021).
122. Guan, Y. *et al.* Human hepatic organoids for the analysis of human genetic diseases. *JCI Insight* 2, (2017).
123. Apweiler, R. *et al.* Whither systems medicine? *Experimental and Molecular Medicine* vol. 50 Preprint at <https://doi.org/10.1038/emm.2017.290> (2018).
124. Wolkenhauer, O., Auffray, C., Jaster, R., Steinhoff, G. & Dammann, O. The road from systems biology to systems medicine. *Pediatric Research* vol. 73 502–507 Preprint at <https://doi.org/10.1038/pr.2013.4> (2013).
125. Fell, D. A. Understanding the Control of Metabolism Cell cycle simulation View project Metabolic control analysis. vol. 2 (Portland Press, 1997).
126. Bruggeman, F. J. & Westerhoff, H. V. The nature of systems biology. *Trends in Microbiology* vol. 15 45–50 Preprint at <https://doi.org/10.1016/j.tim.2006.11.003> (2007).
127. Wu, F., Yang, F., Vinnakota, K. C. & Beard, D. A. Computer modeling of mitochondrial tricarboxylic acid cycle, oxidative phosphorylation, metabolite transport, and electrophysiology. *Journal of Biological Chemistry* 282, 24525–24537 (2007).
128. Lambeth, M. J. & Kushmerick, M. J. A computational model for glycogenolysis in skeletal muscle. *Ann Biomed Eng* 30, 808–827 (2002).
129. Wang, H. *et al.* Deep learning in systems medicine. *Briefings in Bioinformatics* vol. 22 1543–1559 Preprint at <https://doi.org/10.1093/bib/bbaa237> (2021).



Chapter



Organoids as a model to study intestinal and liver dysfunction in severe malnutrition

José M. Horcas-Nieto^{1*}, Christian J. Versloot^{1*}, Miriam Langelaar-Makkinje¹, Albert Gerding^{1,2}, Tjasso Blokzijl³, Mirjam H. Koster¹, Mirjam Baanstra⁴, Ingrid A. Martini², Robert P. Coppes⁴, Céline Bourdon⁵, Sven C.D. van Ijzendoorn⁴, Peter Kim^{5,8}, Robert H.J. Bandsma^{1,5-7§}, Barbara M. Bakker^{1§}

1. Laboratory of Pediatrics, Center for Liver, Digestive and Metabolic Diseases, University of Groningen, University Medical Center Groningen, The Netherlands; 2. Department of Laboratory Medicine, University of Groningen, University Medical Center Groningen, Groningen, The Netherlands; 3. Department of Gastroenterology and Hepatology, University of Groningen, University Medical Center Groningen, Groningen, The Netherlands; 4. Department of Biomedical Sciences of Cell & Systems, section Molecular Cell Biology, University of Groningen, University Medical Center Groningen, Groningen, The Netherlands; 5. Translational Medicine, Peter Gilgan Centre for Research and Learning, The Hospital for Sick Children, Toronto, ON, Canada; 6. Department of Nutritional Sciences, Faculty of Medicine, University of Toronto, Toronto, ON, Canada; 7. Division of Gastroenterology, Hepatology, and Nutrition, The Hospital for Sick Children, Toronto, ON, Canada; 8. Department of Biochemistry, University of Toronto, Toronto, ON, Canada.

*** These authors contributed equally to this work**

§ Corresponding authors:

Prof. dr. Barbara M Bakker

Department of Pediatrics, University of Groningen, University Medical Center Groningen
Antonius Deusinglaan 1, 9713 AV Groningen, The Netherlands Phone: +31 50 361 1542

Email: b.m.bakker01@umcg.nl

Robert Bandsma, MD, PhD

Division of Gastroenterology, Hepatology and Nutrition, The Hospital for Sick Children, 555
University Avenue, M5G 1X8, Toronto, Ontario, Canada Phone: +1 416-813-7654

Email: robert.bandsma@sickkids.ca

Published in *Biochimica et Biophysica Acta (BBA) - Molecular Basis of Disease* (2022)

<https://doi.org/10.1016/j.bbadis.2022.166635>

ABSTRACT

Hospitalized children with severe malnutrition face high mortality rates and often suffer from hepatic and intestinal dysfunction, with negative impacts on their survival. New treatments cannot be developed without understanding the underlying pathophysiology. We have established and characterized translational organoid models of severe malnutrition of the liver and the intestine. In these models, amino acid starvation recapitulates the expected organ-specific functional changes (e.g., hepatic steatosis, barrier dysfunction) accompanied by reduced mitochondrial and peroxisomal proteins, and altered intestinal tight junction proteins. Re-supplementation of amino acids or pharmacological interventions with rapamycin or fenofibrate lead to partial recovery. Restoration of protein levels aligned with signs of improved peroxisomal function in both organoids, and increased mitochondrial proteins and tight junction protein claudin-3 in intestinal organoids. We present two organoid models as novel tools to gain mechanistic insights and to act as a testing platform for potential treatments for intestinal and hepatic dysfunction in severe malnutrition.

INTRODUCTION

The recent discovery of organoids has opened exciting possibilities for studying diseases, modelling cell development and applying them as therapeutic tools¹⁻⁴. Their three dimensional and proliferative nature grants them the ability to maintain many of their organ functions, which makes them a physiologically relevant system to study diseases⁵. Organoids have been used to understand organ-specific metabolism^{6,7} and to investigate the effect of nutrients on organ homeostasis⁸. Here, we present two organoid models as tools to study the impact of severe macronutrient deficiency on organ function, the role of organelle homeostasis, and study the effects of putative therapeutic compounds.

Nutritional deficiencies compromise organ function and disrupt cellular metabolism⁹. Children with severe malnutrition present with the most severe form of macronutrient deficiency. In developing countries, low protein diets are common, as staple foods are often high in carbohydrates and relatively low in protein (e.g. maize). This together with low food diversity and high food insecurity is thought to contribute to the development of severe malnutrition¹⁰. Severely malnourished children face high mortality rates when admitted to hospital for treatment of acute, mostly infectious, illnesses (e.g. 23-46% in African hospitals)¹¹⁻¹⁴. These children often show signs of hepatic dysfunction (e.g. hypoglycaemia, bile acid dysregulation) and intestinal dysfunction (e.g. diarrhoea, increased intestinal permeability), both of which have negative impacts on their survival¹⁵⁻¹⁸. Children with severe malnutrition are extremely vulnerable and simple re-feeding protocols do not produce acceptable levels of recovery, thus the development of co-therapies are urgently needed. Clinical studies have provided some insight into the pathophysiology of the functional impairments in severe malnutrition and suggest that disrupted cellular metabolism may play a key role. Data from severely malnourished children suggests that liver fat accumulation, i.e., hepatic steatosis, is caused by impaired lipid oxidation rather than impaired secretion of lipids^{19,20}. In support, post-mortem electron microscopy images revealed hepatocytes to have dysmorphic mitochondria and a decreased number of peroxisomes, which are two of the main lipid-oxidation organelles²¹. Some studies have also reported mitochondrial morphological changes in the small intestine of severely malnourished children²²⁻²⁵, but their causal impact on intestinal dysfunction in severe malnutrition has not been demonstrated. Yet, a growing body of evidence suggests a pivotal role of mitochondria in maintaining intestinal homeostasis²⁶⁻²⁸. Further mechanistic insight is hindered by the need

of invasive sampling (e.g. biopsies) in this vulnerable patient population living in low-resource settings.

To overcome these limitations, animal models have been developed and used to start unravelling the role of organelle dysfunction induced by severe malnutrition. Data from low-protein fed rodents supports the existence of a link between loss of peroxisomes, impaired mitochondrial function and the development of hepatic steatosis in severe malnutrition^{29,30}. While a role of peroxisomes and mitochondria is also suspected in malnutrition-induced intestinal dysfunction, this has not yet been described. In vivo work is extremely valuable but does not offer the high-throughput capacity of in vitro models to analyse in-depth organelle dynamics and screen for potential interventions. In cultured cells, amino acid deprivation can lead to peroxisomal degradation²⁹ and altered mitochondrial respiration^{31,32}. However, these two-dimensional cell cultures are less suitable for extrapolating to organ function. Organoids have the advantages of cell culture – ease of sampling and control of nutrient concentrations – while maintaining broader functionality of the modelled organ^{33,34}.

The aim of this study was to develop and characterize translational organoid models of severe malnutrition of the liver and the intestine. Amino-acid deprivation in organoids compromised both hepatic function and intestinal structure and function in a similar way as found in vivo with a low-protein diet. Functional changes were accompanied by reduced mitochondrial and peroxisomal proteins, which could mostly be restored by the re-supplementation of amino acids or pharmacological interventions with rapamycin or fenofibrate. Restoration of protein levels aligned with signs of improved fatty acid oxidation in hepatic organoids and increased tight junction protein claudin-3 in intestinal organoids. We conclude that organoid models are suitable to elucidate pathophysiological processes involved in severe malnutrition and to test novel therapeutic interventions.

RESULTS

Hepatic and intestinal organoid lines were established from mouse biliary duct fragments and intestinal crypts, respectively. To mimic the effect of a low-protein diet, the organoids were cultured in a medium without any amino acids. Nevertheless, most amino acids were still detected at low levels in the medium, presumably originating from Matrigel degradation as well as from growth factors. (**Supplementary Table 1**).

Impact of amino acid starvation on structure and function of liver organoids

Liver Progenitor Organoids were matured into hepatocyte-like cells according to an established protocol³⁵. Maturation was confirmed by the reduction in expression of stem cell markers and the increase in hepatocyte differentiation markers (e. g. *Albumin*, *Hnf-4a*, *Cyp1a2* and *Cyp3a11*) in organoids grown in differentiation medium compared to progenitors, as previously described in the literature². Maturation of the organoids was also confirmed by increased albumin production, measured in the supernatant. Peroxisomal enzymes acyl-CoA oxidase 1 and catalase were significantly upregulated in the differentiated organoids, indicating the suitability of these organoids for the study of peroxisomes. (**Supplementary Figure 1**). Deprivation of amino acids up to 96 hours did not significantly affect the growth nor the morphology of mature hepatic organoids (**Figure 1a, b**). In contrast, when liver progenitor organoids received the starvation medium, organoids remained smaller than control organoids (**Supplementary Figure 2**). The different response to removal of amino acids reflects the lower proliferative state of mature hepatic organoids as indicated by lower gene expression levels of stem cells markers *Axin2* and *Lgr5* (**Supplementary Figure 1b**). Starvation of mature hepatic organoids for 48 hours substantially reduced levels of albumin released in the supernatant (**Figure 1c**) and increased fat deposition as indicated by an accumulation of intracellular triglycerides as well as an increase in lipid droplets (**Figure 1d, e**). Re-supplementation of amino acids after 48 hours of starvation completely restored albumin production and significantly decreased lipid accumulation (**Figure 1d, e**).

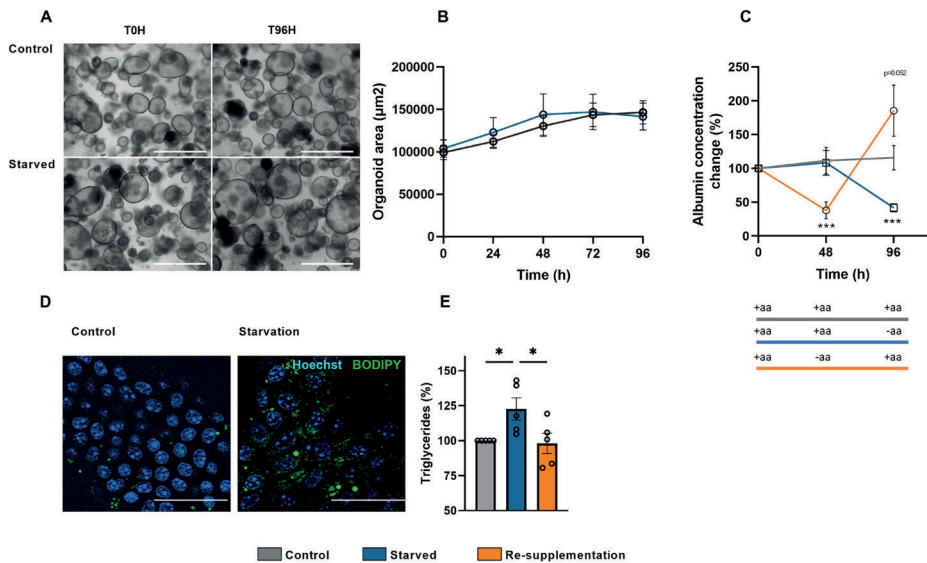


Figure 1. Amino acid starvation of mature hepatic organoids leads to functional changes without profound morphological changes. (A) Representative bright-field images of control and starved mature hepatic organoids prior (T0H) and after 96 h (T96H) amino acid starvation. Scale bar, 1 mm. (B) Size of organoids in complete culture medium (control, grey) or amino-acid free medium (starved, blue), expressed as size of an organoid at every time point of interest. Data based on 3 sets of independent experiments in which 25 randomly selected organoids were tracked. Error bars indicate SEM. (C) Albumin released in supernatant by organoids that were kept in complete medium throughout (control, grey), starved from 0h to 48h and re-supplemented with complete medium from 48h to 96h (re-supplementation, orange), or kept in complete medium and starved from 48h to 96h (starved, blue). Change in experimental conditions over time are indicated by colored bar chart. Data represents 3 biological replicates from independent experiments. Error bars indicate SEM. (* $P < 0.05$, generalized estimating equation with Tukey adjustment for post-hoc pairwise comparison). (D) Representative immunofluorescence images of control and starved mature hepatic organoids (40x magnification). BODIPY staining of fat droplets in green with Hoechst nuclei counter stain (blue). Scale bar, 50 μm . (E) Triglyceride levels in control, starved and re-supplemented organoids (as per colour legend). Data represents 5 biological replicates from independent experiments \pm SEM (* $P < 0.05$, ordinary one-way ANOVA with Tukey's post hoc test).

Impact of amino acid starvation on structure and function of small intestinal organoids

After 48 hours of amino acid starvation, intestinal organoids were significantly smaller than non-starved organoids (**Figure 2a, b** and **Supplementary Figure 4a**). In addition, amino-acid-starved organoids displayed crypt atrophy and had substantially fewer crypts than control organoids (**Figure**

2c, d and Supplementary Figure 4b). Amino-acid deprivation upregulated the expression of markers of Paneth cells (lysozyme), goblet cells (mucin-2) and enteroendocrine cells (chromogranin A), but did not affect the expression of VIL1 (enterocytes) or stem cell and proliferation markers (**Supplementary Figure 5**). FITC-dextran (4 and 10kDa) leakage into the lumen of starved organoids was increased, as indicated by increased number of FITC-dextran positive organoids as well as higher luminal fluorescence, showing that amino-acid starvation compromised the intestinal barrier function (**Figure 3a-c, Supplementary figure 5**). This is consistent with *in vivo* findings³⁶ and was supported by reduced levels of the tight-junction protein claudin-3 in amino-acid deprived intestinal organoids (**Figure 3d**). Importantly, re-supplementation of amino acids restored organoid size, crypt number, claudin-3 protein level, and expression of mucin-2 and chromogranin A, and increased stem cell markers LGR5 and Axin2 (**Figure 2a-d, Supplementary Figure 4**). Restoration of intestinal barrier function by amino-acid re-supplementation could not be properly assessed with FITC-dextran due to the high amount of content (e.g. dead cells) in the organoids lumen after 96 hours.

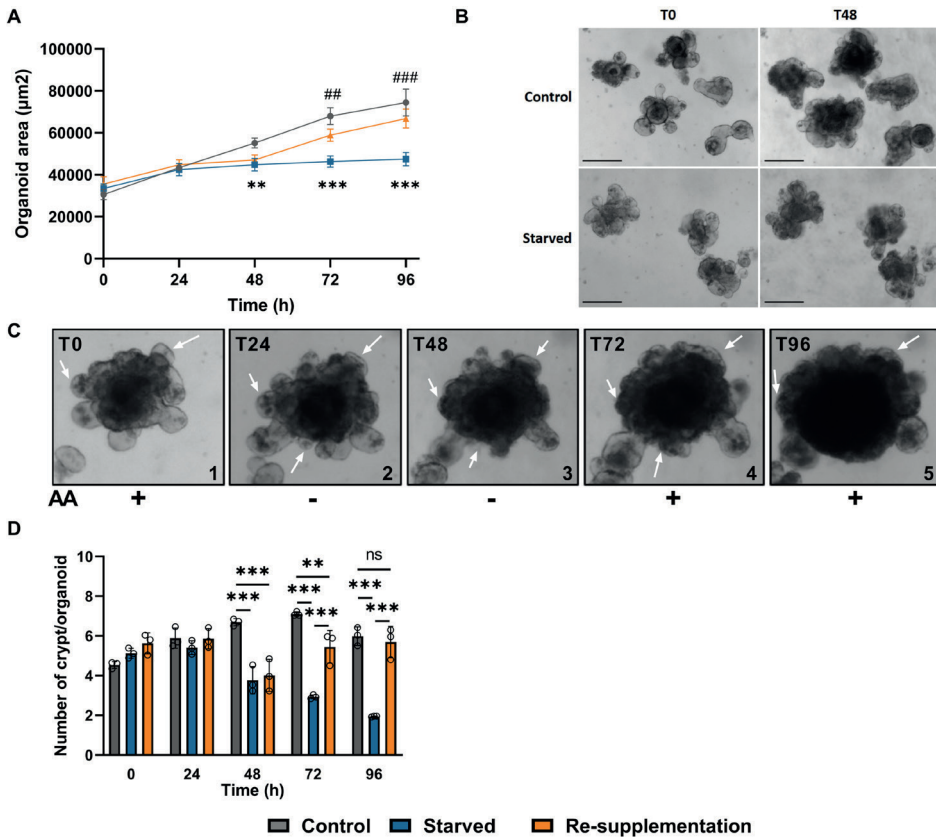


Figure 2. Amino acid deprivation induces reversible crypt atrophy, compromised growth and barrier dysfunction in intestinal organoids. **(A)** Size over time of organoids grown in complete culture medium (control, grey), amino-acid-free medium (starved, blue) or amino-acid-free medium for 48 h followed by complete culture medium for 48 h (re-supplementation, orange). Data represents the growth of 25 measured organoids in each of the 3 biological replicates from independent experiments. Error bars indicate SEM (* indicates comparison between control and starvation, # indicates comparison between starvation and re-supplementation) (*** $P < 0.001$, ** $P < 0.01$, * $P < 0.05$, ### $P < 0.001$, ## $P < 0.01$, # $P < 0.05$, generalised estimating equation with Tukey adjustment for post-hoc pairwise comparison). **(B)** Representative bright-field images of control and starved intestinal organoids at the start and after 48 h. Scale bar, 200 μm . **(C)** Representative bright-field images show an individual small intestinal organoid grown in complete culture medium for 3 days (C1), switched to amino acid free medium for 48 h (C2 and C3), and then placed in complete culture medium for 48 h (C4 and C5). Arrowheads indicate individual crypt domains. **(D)** Average number of crypts per organoid over time for control, starved and re-supplementation. Data represents the average of 25 measured organoids in each of the 3 biological replicates from three independent experiments at 5 time points. Error bars indicate SEM (** $P < 0.01$, *** $P < 0.001$, generalised estimating equation with a Poisson variance to mean relation and Tukey adjustment for post-hoc pairwise comparison).

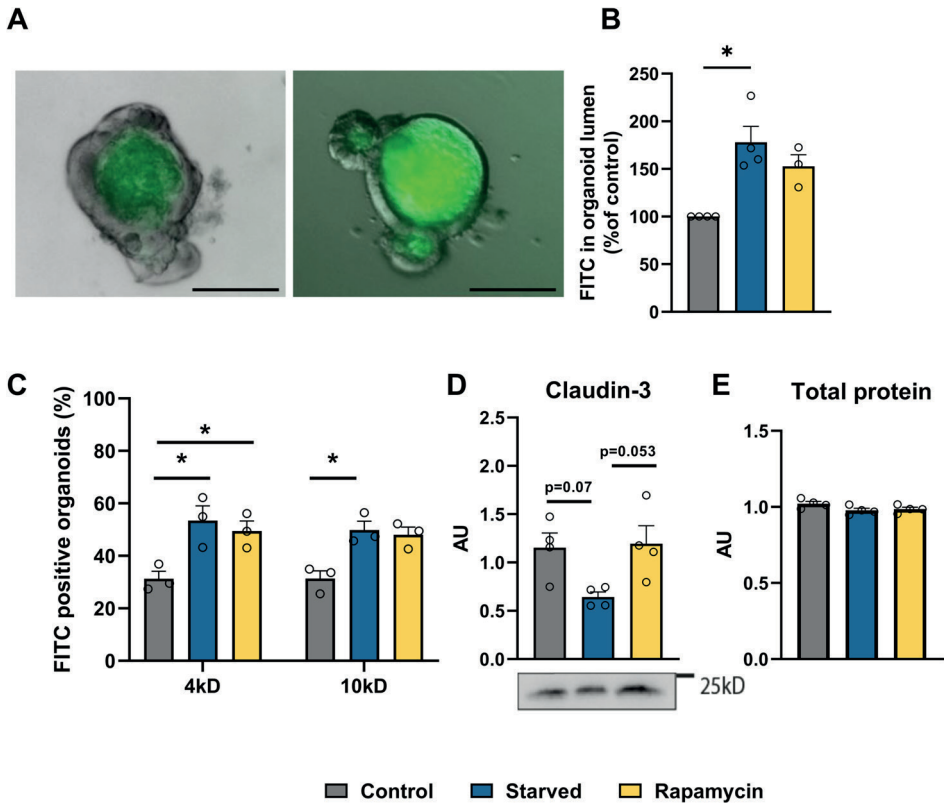


Figure 3. Amino acid deprivation induces barrier dysfunction in intestinal organoids.

(A) Representative images for 10 kDa FITC-dextran for control (left) and starved organoid (right) (10x magnification). Scale bar, 100 μ m **(B)** Average luminal FITC fluorescence for control, starved and rapamycin-administered organoids. Values are normalized to control organoids. Data represents mean of 3-4 biological replicates (from independent experiments) \pm SEM (* P <0.05, two-way ANOVA with Tukey's post hoc test). **(C)** Percentage of intestinal organoids with 4 or 10 kDa inside their lumen measured in organoids grown in complete culture medium (control), amino-acid-free medium (starved) and amino-acid-free medium supplemented with 2nM rapamycin (rapamycin). Data represents mean of 3 biological replicates (from independent experiments) \pm SEM (* P <0.05, two-way ANOVA with Tukey's post hoc test). **(D)** Immunoblot quantification and representative image of tight-junction protein claudin-3 relative to total protein (see methods) for the different conditions. Normalized to total protein. Data represents mean of 3 biological replicates (from independent experiments) \pm SEM. (* P <0.05, ** P < 0.01, Two-way ANOVA with Tukey's post-hoc test). **(E)** Relative intensity of total protein, summed over the entire lane (used for normalization to total protein, as explained in methods). Individual data points are shown for each biological replicate.

Amino-acid starvation reversibly reduces the levels of peroxisomal proteins in hepatic organoids

In vivo studies of rodents on a low-protein diet showed a decline of peroxisome numbers and altered mitochondrial morphology and function in the liver^{29,30}. Compromised oxidation of fatty acids by peroxisomes and mitochondria explains hepatic steatosis in these studies. We aimed to determine whether these findings could be recapitulated in amino-acid-deprived hepatic organoids.

Peroxisomal proliferator-activated receptor gamma coactivator 1-alpha (PGC1- α), an activator of peroxisomal and mitochondrial biogenesis³⁷, was reduced in the starved condition. Also, the protein levels of PMP-70, an ATP-binding cassette transporter and a major component of the peroxisomal membrane³⁸, was strongly reduced upon amino acid deprivation. The same was found for the peroxisomal enzymes acyl-CoA oxidase 1 (Acox-1), the first enzyme of the peroxisomal beta-oxidation and catalase, an integral part of the pathway as it scavenges the produced H_2O_2 (**Figure 4a, b**). Peroxisomal fatty acid oxidation was assessed following the metabolism of phytol, a branched-chain fatty acid precursor of phytanic acid³⁹ (**Figure 4c**). While levels of phytanic acid did not show any regulation, pristanic acid levels were significantly increased in organoids depleted of amino acids (**Figure 4d**). Pristanoyl CoA is the product of the peroxisomal alpha-oxidation, which is further metabolized in the peroxisomal beta-oxidation (**Figure 4c**). Phytanic acid is a branched-chain fatty acid and substrate for the peroxisomal α -oxidation, whereas pristanic acid is a substrate for β -oxidation. The increased pristanic acid levels may therefore indicate a reduction in peroxisomal beta-acid oxidation. Very-long chain fatty acids tetrasanoic and hexasanoic acids (C24 and C26, respectively) did not show any regulation (**Figure 4e**), in line with the absence of long-chain fatty acids from the medium.

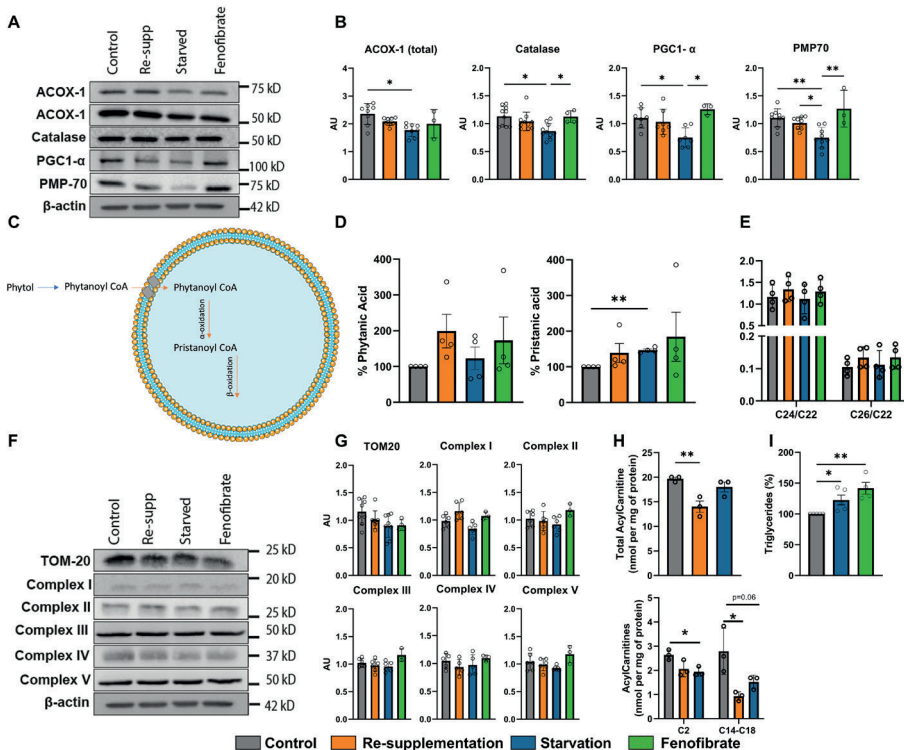


Figure 4. Impact of amino acid starvation and re-supplementation on mitochondria and peroxisomes in mature hepatic organoids **(A)** Representative immunoblot images. **(B)** Peroxisomal protein levels relative to β -actin. Quantification of data shown in **(A)** Organoids were grown in complete culture medium throughout (control, grey), amino-acid-free medium for 48 hours (starved, blue), starved from 0h to 48h and re-supplemented with complete medium from 48h to 96h (re-supplementation, orange) or in amino-acid-free medium for 48 h supplemented with 100 μ M fenofibrate (fenofibrate, green). Data represent mean \pm SEM from 7-10 biological replicates and 3 biological replicates for Fenofibrate treatment (biological replicates are obtained from independent experiments) (* P <0.05, ** P < 0.01, two-way ANOVA with Tukey's post-hoc test). **(C)** Representative scheme of the peroxisomal pathway of phytol into phytanoyl-CoA and Pristanoyl-CoA. **(D)** Percentage of phytanic acid and pristanic acid in the supernatant of organoids grown in complete culture medium (control, grey), amino-acid-free medium (48h starvation, blue), amino-acid-free medium for 48 h followed by complete culture medium for 48 h (re-supplementation, orange) or in amino-acid-free medium for 48 h supplemented with 10 μ M fenofibrate (fenofibrate, green). Data represents mean of 4 biological replicates (from independent experiments) \pm SEM (* P <0.05, ** P < 0.01. One-way ANOVA with Tukey's post-hoc test) **(E)** Ratios of very-long chain fatty acids C24/C22 and C26/C22 measured in the supernatant of organoids grown in complete culture medium (control), amino-acid-free medium (starved), amino-acid-free medium for 48 h followed by complete culture medium for 48 h (re-supplementation) or in amino-acid-free medium for 48 h supplemented with 10 μ M fenofibrate Data represents mean of 4 biological replicates (from independent experiments)

± SEM (*P<0.05, ** P< 0.01. One-way ANOVA with Tukey's post-hoc test). **(F)** Representative immunoblot images. **(G)** Mitochondrial protein levels relative to β -actin. Quantification of data shown in **(A)** Organoids were grown in complete culture medium throughout (control, grey), amino-acid-free medium for 48 hours (starved, blue), , starved from 0h to 48h and re-supplemented with complete medium from 48h to 96h (re-supplementation, orange) or in amino-acid-free medium for 48 h supplemented with 100uM fenofibrate (fenofibrate, green). Data represent mean ± SEM from 7-10 biological replicates and 3 biological replicates for Fenofibrate treatment (biological replicates are obtained from independent experiments) (*P<0.05, ** P< 0.01, two-way ANOVA with Tukey's post-hoc test). **(H)** Free carnitines and acyl-carnitines measured in supernatant of organoids grown in complete culture medium (control), amino-acid-free medium (starved), amino-acid-free medium for 48 h followed by complete culture medium for 48 h (re-supplementation). Data represents mean of 3 biological replicates (from independent experiments) ± SEM. (*P<0.05, ** P< 0.01 Ordinary one-way ANOVA). **(I)** Triglyceride levels in control, starved and fenofibrate treated organoids (as per colour legend). Data represents 4-5 biological replicates from independent experiments ± SEM (*P<0.05, ordinary one-way ANOVA with Tukey's post hoc test).

With respect to mitochondria, the levels of TOM-20 (a component of the 'translocase of outer membrane' (TOM) receptor complex) did not differ between control and amino acid starvation for 48 hours, nor did the protein complexes of the electron transport chain (**Figure 4f, g**). Total carnitine levels were unaffected after 48 hours, but significantly decreased upon reintroduction of amino acids. Long-chain acyl carnitines (C14-C18) and acetyl-carnitine (C2) were decreased after 48 hours of amino-acid starvation and not restored by reintroduction of amino acids (**Figure 4h**).

Since *in vivo* studies hinted that peroxisomal loss precedes mitochondrial events^{30,40}, we increased the duration of the amino acid starvation to 96 hours. This longer amino acid deprivation resulted in a clear reduction of mitochondrial protein markers. After 96 hours of amino acid starvation, electron transport chain complexes I to V were significantly downregulated. TOM-20 showed a weaker downward trend ($p = 0.06$) (**Figure 5a,b**). At the functional level, the longer starvation reduced ADP-stimulated respiration in the presence of palmitoyl carnitine and malate (state 3), while basal respiration remained unaffected (state 1). Uncoupled respiration (State U) showed a downward trend upon starvation, but this was not significant ($p = 0.06$) (**Figure 5c**).

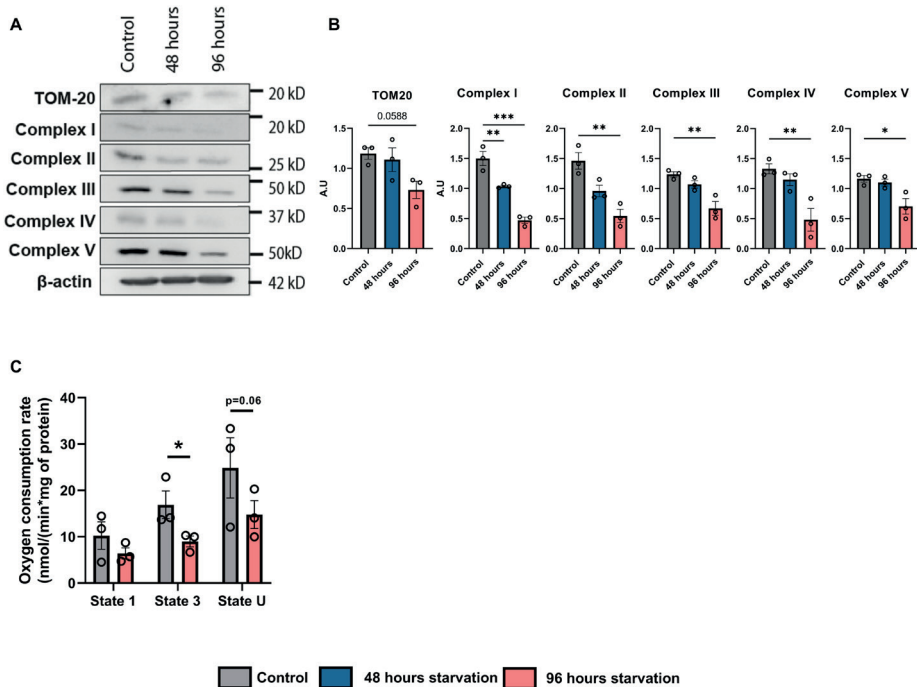


Figure 5. Mitochondrial dysfunction after prolonged amino acid starvation in mature hepatic organoids. Mature hepatic organoids were grown in complete culture medium throughout (control, grey), amino-acid-free medium for 48 hours (48 hours starvation, blue) and starved for 96h (96 hours starvation, pink). (A) Representative immunoblot images. (B) Protein levels relative to β -actin. Quantification of data shown in (A) Data represent mean \pm SEM from 3 biological replicates (biological replicates are obtained from independent experiments) (* $P < 0.05$, ** $P < 0.01$, one-way ANOVA with Tukey's post-hoc test). (C) Oxygen consumption rate in mature hepatic organoids measured as basal respiration (State 1) (ADP), State 3 (stimulated with Palmitoyl Carnitine and Malate and ADP) and uncoupled respiration (State U). Data represents the mean of 3 biological replicates (from independent experiments) \pm SEM. (* $P < 0.05$, ** $P < 0.01$ paired t test)

Re-introduction of amino acids for 48 hours following 48 hours of starvation recovered the PMP-70 levels to almost those of the control organoids. PGC1- α and catalase levels increased, but were not significantly different from either control or starved organoids (**Figure 4 a, b**). Since no regulation was observed in mitochondrial protein levels after 48 hours, re-introduction of amino acids did not have any further effect. Due to the limited lifespan of the organoids in culture, re-supplementation after 96 hours of amino acid starvation could not be done.

Amino acid deprivation reversibly reduces mitochondrial and peroxisomal content in intestinal organoids

In view of the key role of mitochondria and peroxisomes in intestinal homeostasis^{26,41}, we examined the effect of amino acid deprivation on these organelles in intestinal organoids. In contrast to hepatic organoids, amino acid starvation did not affect the protein level of PGC1- α in intestinal organoids (**Figure 6a,b**). The levels of the peroxisomal proteins PMP-70 and catalase were, however, reduced in starved intestinal organoids (**Figure 6a-b**).

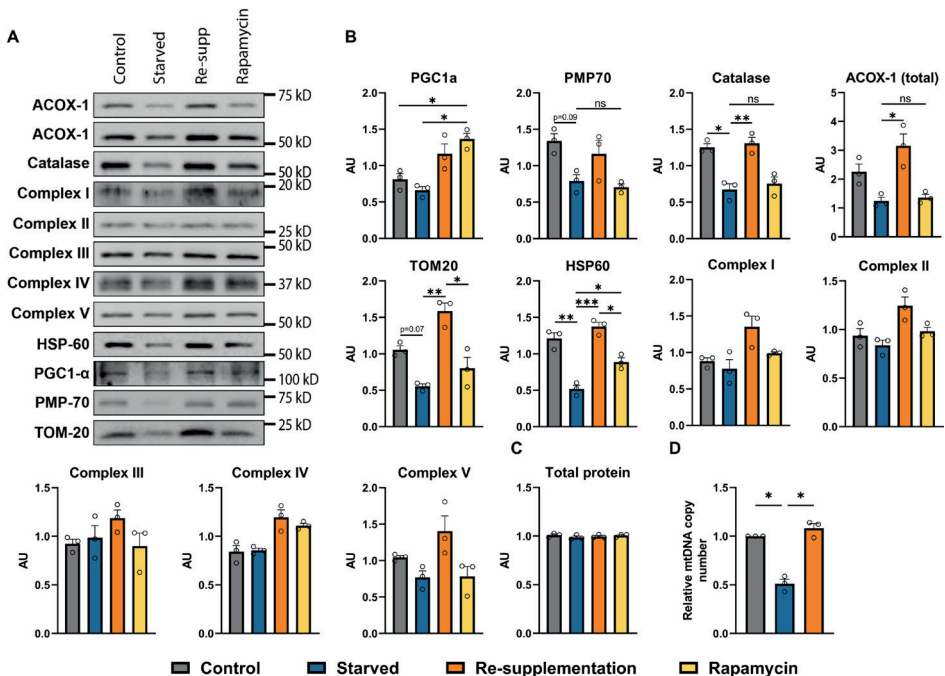


Figure 6. Impact of amino acid starvation, re-supplementation and rapamycin on mitochondria and peroxisomes in intestinal organoids. (A) Representative immunoblot images. (B) Quantification of data shown in (A). Protein levels were normalized to total protein (see methods section). Organoids were grown in complete culture medium (control), amino-acid-free medium for 48 h followed by complete culture medium for 48 h (re-supplementation) or in amino-acid-free medium for 48 h supplemented with 2nM rapamycin. Data represents mean of 3 biological replicates (from independent experiments) \pm SEM (* $P < 0.05$, ** $P < 0.01$, *** $P < 0.001$, Two-way ANOVA with Tukey's post-hoc test). (C) Relative intensity of total protein measured in each entire lane (used for total protein normalization as explained in methods). Individual data points are shown for each biological replicate. (D) Mitochondrial copy number expressed mitochondrial DNA normalized to β -globulin as reference. Data represents mean of 3 biological replicates (from independent experiments) \pm SEM. (* $P < 0.05$, ** $P < 0.01$ Ordinary one-way ANOVA).

Mitochondrial marker proteins TOM20 and Hsp60 were also downregulated by amino acid starvation (**Figure 6a-b**). Yet, the complexes of the electron transport chain were not affected by amino-acid starvation (**Figure 6a-b**). Mitochondrial copy number was also significantly decreased in starvation conditions (**Figure 6d**). Amino acid re-supplementation normalized all peroxisomal and mitochondrial characteristics, except the level of TOM20, which was even increased after re-supplementation (**Figure 6a-d**).

Interventions to preserve mitochondria and peroxisomes in starved organoids

We investigated if amino-acid-deprived organoids could be used as a model to test pharmacological interventions to preserve organ function. As a proof of principle, we tested interventions that have already been applied in animal studies. Fenofibrate, a PPAR- α agonist, was previously shown to preserve peroxisomes and mitochondrial function in the liver of rats on a low-protein diet³⁰. When administered to amino-acid starved mature hepatic organoids, fenofibrate increased levels of PGC1- α , PMP70 and catalase to values similar as the controls (**Figure 4a, b**). Acox-1, the first enzyme of the peroxisomal β -oxidation was not affected by fenofibrate, nor was its substrate pristanic acid (**Figure 5a**). No change was observed in the levels of mitochondrial proteins with fenofibrate treatment (**Figure 4a, b**). Triglycerides were not restored upon fenofibrate treatment. Instead, addition of fenofibrate in starvation medium led to a higher accumulation of intracellular TGs (**Figure 4i**).

We recently showed that rapamycin, an mTORC1 inhibitor, preserved intestinal barrier function and mitochondrial number and morphology in mice on a low protein diet (Manuscript in preparation). Likewise, in amino-acid-starved intestinal organoids, rapamycin increased the levels of mitochondrial marker protein HSP-60, although it remained lower than in control organoids (**Figure 6a,b**). In addition, protein levels of PGC1- α were increased in starved rapamycin-treated organoids to a similar level as in amino-acid-re-supplemented organoids (**Figure 6a,b**). Although PGC1- α is also known as an activator of peroxisomal biogenesis, rapamycin treatment did not affect the protein levels of peroxisomal proteins (**Figure 6a,b**). Rapamycin treatment did preserve claudin-3 protein levels in starved organoids, suggesting preserved intestinal barrier function (**Figure 3d**). However, rapamycin did not appear to decrease the FITC levels in the organoid lumen, nor the number of FITC-dextran positive organoids (**Figure 3b, c** and **Supplementary Figure 6**).

DISCUSSION

Advances in three-dimensional cultures, in particular organoids, have opened new avenues for the development of more physiological *in vitro* models of organ function and diseases¹⁻⁴. In this paper, we presented two organoid models to study pathophysiological processes and potential treatments for intestinal and hepatic dysfunction in severe malnutrition. Organ-specific manifestations of severe malnutrition were recapitulated in amino-acid-starved organoids. Concurrent mitochondrial and peroxisomal changes largely reflect *in vivo* findings and were found to be organ-specific. We showed that amino-acid-starved organoids cannot only be used to gain mechanistic insights, but also to test pharmacological interventions.

Functional impact of amino acid starvation on hepatic and intestinal organoids

Mature hepatic organoids showed no morphological or size changes upon amino-acid starvation. This could be attributed to their low proliferative state, as indicated by lower stemness markers than in hepatic progenitor organoids. Their functionality was, however, substantially impaired. Albumin production dropped upon starvation, which was expected as albumin synthesis requires amino acids as precursors and is stimulated by dietary amino acids⁴². The same was observed in low-protein fed rats³⁰ and severely malnourished children⁴³. Enlarged fat droplets, increased levels of triglycerides and elevated levels of pristanic acid point to lipid accumulation in starved hepatic organoids. Hepatic steatosis has also been commonly observed in severely malnourished children⁴⁴ and rodents on a low-protein diet^{30,45}. We did not study glucose production, even though impaired hepatic glucose production reported in severely malnourished children increases the risk of hypoglycaemia and death^{15,17}. Functional glucose production has rarely been studied in organoids since glucose 6-phosphatase (G6PC) levels are typically low *in vitro*^{46,47}. It was recently shown that organoids derived from primary hepatocytes have a higher G6PC expression³³ than organoids derived from cholangiocytes, and a normalized glycogen storage⁴⁸. This provides a perspective to study functional glucose production *in vitro*.

Intestinal organoids starved for amino acids were smaller than those in complete medium, with fewer crypts and atrophy of cryptlike domains. This could point to suppressed enterocyte proliferation, as has also been shown in intestinal organoids deprived of glutamine, methionine or valine^{49,50}. In starved organoids gene expression of stem cell and proliferation markers

was not significantly reduced, but it was nevertheless increased upon re-supplementation. This is in line with the observed re-growth of crypts. Restoration of growth and new crypt formation after amino acid re-supplementation indicates that intestinal stem cells have the capacity to recover from prolonged amino-acid starvation. Re-growth of crypts may be attributed to rapidly cycling Lgr5⁺ crypt base columnar (CBC) cells, which were previously found resilient to glutamine starvation⁴⁹. Another possibility is the mobilization of another stem cell population referred to as quiescent 'reserve' stem cells (+4 position) that are activated upon injury to restore tissue homeostasis⁵¹. Moreover, de-differentiation of progenitor cells^{52,53} as well as differentiated epithelial cells can contribute to repopulation of the stem cell niche^{54,55}. Yet, the impact of prolonged amino-acid deprivation on intestinal stem cells and on de-differentiation has not been studied. Finally, the barrier dysfunction and reduction of claudin-3 in starved intestinal organoids was in agreement with reported findings in severely malnourished children⁵⁶⁻⁵⁸ and in low-protein fed rodents³⁶.

Impact of amino acid starvation on organelle homeostasis in hepatic and intestinal organoids

We found that amino-acid starvation impacted peroxisomes earlier than mitochondria in hepatic organoids, whereas both peroxisomes and mitochondria were affected in intestinal organoids after 48 hours. The disparate impact on mitochondria plausibly reflects metabolic differences between the intestine and the liver. In the liver, mitochondria are important for fatty acid oxidation, whereas in the intestine mitochondria are essential for proper stem cell function and thereby epithelial turnover^{27,59}. In addition, nutrient requirements may be higher in the intestine due to the high turnover rate, which could lead to more severe mitochondrial changes when exposed to a similar nutritional insult.

In starved hepatic organoids we found that peroxisomal marker proteins were significantly decreased, which corresponded to reduced peroxisomal numbers in the liver of low-protein fed rodents^{29,30}. It has been shown that peroxisomes are selectively degraded upon amino acid starvation^{60,61}. Reduction of peroxisomal proteins, and particularly of Acox-1, is in line with the observed accumulation of pristanic acid in the starved organoids. Mitochondrial marker proteins and mitochondrial oxygen consumption were unaffected in 48 hours starved hepatic organoids, which was very similar in rats that were fed a low-protein diet for 1 week³⁰. However, after 4 weeks mitochondria

had an aberrant structure and compromised fatty-acid β -oxidation in these animals, which together with a decline in peroxisomal number was thought to contribute to the observed hepatic steatosis³⁰. Since it has been suggested that peroxisomal decline precedes mitochondrial decline³⁰, we decided to increase the starvation time in the organoids up to 96 hours. This delayed onset of a mitochondrial phenotype was reproduced in the organoids: after 96 hours of amino-acid starvation mitochondrial protein markers as well as functional state 3 respiration were significantly reduced. These results are consistent with findings that defects in peroxisomal biogenesis may cause mitochondrial decline^{40,62}. The decrease of acyl carnitines (already after 48 hours) preceding the reduction in oxygen consumption could be explained by the system relying on fatty acids to obtain energy after removal of amino acids.

In starved intestinal organoids both mitochondrial membrane and matrix markers were lower, reminiscent of reduced mitochondrial numbers in the intestine of mice on a low-protein diet (manuscript in preparation). The decline of peroxisomal marker proteins in intestinal organoids is a novel finding for the intestine. As mitochondria play an important role in maintaining the stem cell niche^{27,59}, reduction in mitochondrial markers proteins could contribute to the observed crypt atrophy in the organoids. Although peroxisomes are highly abundant in the small intestine⁶³, little is known about the functional significance of these organelles in this organ. In *Drosophila*, peroxisomes are required for homeostasis of intestinal epithelium⁶⁴. More recently, Du et al. reported that elevated peroxisome numbers are required for stem cell differentiation and epithelial repair in human, mouse and *drosophila* intestine⁴¹. Reduced or dysfunctional peroxisomes could result in epithelial instability⁶⁴ via redox stress, and compromise epithelial turnover⁴¹. Intestinal organoids are a versatile model to further explore the reduction of peroxisomes upon amino-acid starvation and its consequences for intestinal homeostasis.

Translation into potential treatments for severely malnourished children

We tested if targeting mitochondria and peroxisomes could preserve organ homeostasis under amino- acid deprived conditions. In starved hepatic organoids, addition of PPAR- α agonist fenofibrate partially recovered the protein expression levels of peroxisomal markers but showed no effect on pristanic acid metabolism. Fenofibrate did not recover intracellular triglyceride levels when administered during amino acid starvation. In contrast, fenofibrate treatment in low-protein fed rats significantly improved mitochondrial

β -oxidation capacity resulting in reduced hepatic fat deposition³⁰. In general, contrasting effects of fenofibrate on triglyceride have been described. For instance, in healthy mice fenofibrate reduced levels of triglycerides in serum but increased triglycerides in the liver⁶⁵. Also in HEPG2 cells, fenofibrate increased the levels of triglycerides⁶⁵. The positive effect on peroxisomal protein levels, however, offers therapeutic potential⁴⁴. Fenofibrate is usually well-tolerated during treatment of dyslipidemia, but side effects such as rhabdomyolysis are a risk in severely malnourished children⁶⁶. Further investigation is required into the mechanisms of action, into the later effects of malnutrition on the mitochondria, and into the possibilities of PPAR- α -modulating dietary components (e.g. polyunsaturated fatty acids, flavonoids) in improving hepatic function in severe malnutrition^{67,68}.

In starved intestinal organoids, rapamycin treatment preserved mitochondria and peroxisomes. This coincided with higher levels of the tight junction protein claudin-3 than in starved, untreated organoids, suggesting better maintained barrier function. Accumulating data suggests a key role for mitochondria in maintaining the intestinal barrier²⁶, but for peroxisomes this is less known. Improved mitochondrial health may be attributed to stimulated mitochondrial biogenesis, as PGC1- α protein levels were increased in rapamycin-administered starved organoids. In addition, rapamycin could improve mitochondrial homeostasis via clearance of dysfunctional mitochondria through autophagy activation⁶⁹, thereby contributing to the potentially improved barrier function. The potential positive impact of rapamycin on the intestinal barrier has therapeutic implications for severely malnourished children, because it could have potential to prevent bacterial translocation-induced clinical deterioration and death⁵⁶⁻⁵⁸.

A limitation of this study is that no human organoids were included. The choice for mouse organoids enabled us to make a direct comparison between organoids and mouse liver or intestine, particularly concerning the mitochondrial and peroxisomal phenotype. This comparison could not be made with human tissue, since invasive samples in malnourished children are scarce. A next step should be the translation to human organoids.

CONCLUSIONS

The results of this study support the notion that hepatic and intestinal organoid models can be used to further investigate underlying mechanisms of organ

dysfunction in severe malnutrition. These models are also suitable to explore therapeutic interventions.

METHODS

Isolation of intestinal crypts and biliary duct fragments and organoid culture

The use of crypts from the small intestine and ductal fragments from the liver of male C57BL/6J mice between 3 to 5 weeks of age (Jackson Laboratory, Bar Harbor, ME, USA) was approved by the Central Authority for Scientific Procedures on Animals (CCD) of the Netherlands and from the University of Groningen Ethical Committee for Animal Experiments (Animal Use Protocol Number: 171504-01-001/3).

The small intestine was dissected and divided in three sections: from proximal to distal, the duodenum, jejunum and ileum. Jejunum was used to generate organoids according to a previously described protocol¹. Intestinal organoids were kept in complete culture medium consisting of AdvDMEM/F12 plus 10mM HEPES, 1X GlutaMax and 1% Penicillin-Streptomycin (all Gibco), 1X N-2 Supplement (Invitrogen, CA, USA), 1X B-27 Supplement (Invitrogen), 1.25 mM N-Acetylcysteine (Sigma Aldrich, MO, USA), 10% Rspodin Conditioned Medium (provided by Calvin J. Kuo), 50 ng/ml EGF (Peprotech, NJ, USA) and 100 ng/ml Noggin (Peprotech). Medium was changed every 2-3 days. Intestinal organoids were passaged every 5-7 days.

Ductal fragments from livers were isolated following the protocol by Broutier et al³⁵. Biliary duct fragments were kept in culture expansion medium consisting of Advanced DMEM/F12 supplemented with 10mM HEPES, 1X GlutaMax, 1% Penicillin-Streptomycin, 1X N-2 Supplement, 1X B-27 Supplement, 10mM Nicotinamide (Sigma Aldrich), 1.25mM N-Acetylcysteine, 10% RSpodin Conditioned Medium, 30% Wnt3a CM (provided by Hans Clevers), 100 ng/ml Noggin, 50 ng/ml HGF (Peprotech), 100 ng/ml FGF-10 (Peprotech), 50 ng/ml EGF, 10nM Leu-gastrin (Sigma Aldrich). Three days after the isolation Noggin and Wnt3a CM were removed from the medium. The medium was changed every 2-3 days. Liver organoids were passaged every 6-7 days. Expansion medium promotes the proliferation of liver stem cells as well as cholangiocytes. After three days in expansion medium, organoids were transferred to hepatocyte-differentiation medium which consisted of Advanced DMEM/F12 supplemented with 10mM HEPES, 1X GlutaMax, 1% Penicillin-Streptomycin, 1X N-2 Supplement,

1X B-27 Supplement, 1 mM N-Acetylcysteine, 100 ng/ml FGF-10, 50 ng/ml EGF, 10nM Leu-gastrin, 50nM A-83-01 (Tocris, Bristol, UK) and 10uM DAPT (Sigma Aldrich). After day 13, 3µM dexamethasone (Sigma Aldrich) was added into the medium. Organoids were kept in differentiation medium until day 16.

Malnutrition in organoids using amino acid starvation and amino acid re-supplementation studies

To mimic malnutrition in organoids, a custom-made amino acid free Advanced DMEM/F12 was used (Invitrogen). Apart from this amino acid free DMEM, the formulation of the culture media was identical as described above for the respective organs.

Intestinal organoids were grown in complete culture medium for three days after passage before being placed in low amino acid culture medium for 48 hours. For the amino acid re-supplementation studies, organoids were placed in complete medium for further 48 hours after the starvation. All organoids conditions were collected at the end of day 7.

Liver progenitor organoids were grown in complete expansion medium for 3 days after passage before being placed in differentiation medium until day 12. From day 12 to day 14 they were grown in amino acid-free medium. At the end of day 14 the organoids were placed back in complete differentiation medium until the end of day 16. For simple amino acid starvation, the organoids were starved from day 14 to day 16. All the organoids conditions were collected at the end of day 16.

Therapeutic interventions

Intestinal organoids were grown in complete culture medium until three days after the passage, then placed in amino acid-free medium for 48 hours that was supplemented with rapamycin (Sigma Aldrich, MO, USA) at a final concentration of 2nM.

Hepatic organoids were grown in complete differentiation medium until day 14. From day 14 to day 16 they were grown in amino acid-free medium supplemented with fenofibrate (Sigma Aldrich) at a final concentration of either 10 or 100µM, as indicated.

Amino acid measurements

Amino acid profiles were measured by GC/MS (Agilent 9575C series GC/MSD, Agilent Technologies, Amstelveen, The Netherlands) as previously described⁷⁰.

Albumin measurement

Supernatant from the hepatic organoid cultures was collected every 24 hours starting from day 12 of the differentiation until day 16 and was stored at -20°C. The concentration of albumin in the supernatant was measured using the mouse albumin ELISA kit (Abcam, Cambridge, UK) according to the manufacturer's instructions in the Synergy H4 Hybrid Microplate Reader (BioTek Instruments Inc., VT, USA).

RNA isolation, reverse transcription and quantitative real-time qPCR

Total RNA was extracted from organoids using the commercially available RNeasy Mini Kit (Qiagen, Hilden, Germany) according to the manufacturer's instructions. RNA quality and quantity was determined with NanoDrop (NanoDrop Technologies, Wilmington, DE, USA). Reverse transcription was completed with the M-MLV Reverse Transcriptase (200 U/μL) (Invitrogen) according to the manufacturer's instructions. qPCR reactions were performed using FastStart Universal SYBR Green Master (Rox) (Sigma Aldrich) in 384 well format in duplicate with 20 ng total cDNA per well in a QuantStudio 7 Flex (Thermo Fisher Scientific). All primers sequences (Integrated DNA technologies Inc., Coralville, IA, USA) are listed in **Supplementary Table 2**. Peptidylprolyl isomerase A (cycophilin A)(PPIA) served as endogenous control, as expression was stable between experimental groups and was used for normalization. Relative expression was calculated using the $\Delta\Delta C(t)$ method relative to the control organoids.

Triglyceride measurement

Organoids were collected in 1X TBS in MiliQ water. Fat was extracted using chloroform-methanol in a 2:1 ratio. Quantitative determination of hepatic triglycerides was done with the DiaSys Triglyceride FS kit (Holzheim, Germany, Cat #157109910971). Results were normalized to protein content.

BODIPY Staining

Hepatic organoids were fixed in 4% PFA for 1 hour at 37°C. Permeabilization and staining were done simultaneously in CLMS buffer (PBS, 3% BSA, 10mM glycine) containing 0.1% saponine, 15µM BODIPY (Thermo Fisher Scientific) and 5µM Hoechst (Thermo Fisher Scientific) for 1 hour at room temperature. The organoids were washed with PBS and images were acquired with an AxioObserver Z1 compound microscope, 40X objective and AxioCam Mrm3 CCD camera.

Permeability measurement (FITC)

Permeability of intestinal organoids was assessed using fluorescence markers. Organoids were incubated with FITC-dextran 4kDa or 10kDa (TdB consultancy, Uppsala, Sweden) at a final concentration of 1.25µM in their respective Ad.DMEM/F12 for 30 minutes at room temperature. Organoids were washed 5-10 times with PBS to remove non-specific binding. The degree of accumulation in the lumen of 15 organoids chosen at random served as a measure for permeability. Organoids were imaged with an AxioObserver Z1 compound microscope, 2.5x or 10x objective and AxioCam MRm3 CCD camera. ZEN 3.1 blue was used to measure the fluorescence in the organoid lumen. To correct for differences in background fluorescence, the intensity was measured in three different areas around the organoid. The mean intensity measured in three squares around the organoid was subtracted from the luminal fluorescence.

Immunoblotting

For Western blotting, the protocol was based on a previously published paper⁷¹. Organoids were collected using the respective cold Advanced DMEM/F12 (with or w/o amino acids) and kept on ice for 10 minutes to ensure Matrigel dissolvment. Organoids were centrifuged at 200-290G for 5 minutes followed by one wash with cold PBS. Organoids were again centrifuged and resuspended in 200uL of radio immunoprecipitation assay buffer (1%IGEPAL CA-630, 0.1% SDS, and 0.5% sodium deoxycholate in PBS) supplemented with Complete Protease Inhibitor Cocktail (Cat. No. 1186145001; Sigma-Aldrich), Phosphatase Inhibitor Cocktail 2 (Cat. No. P5726; Sigma Aldrich) and Cocktail 3 (Cat. No. P0044; Sigma Aldrich). Organoid lysates were sonicated using Sonics Vibra cell VCX130 (Sonics & Materials inc, Newtown, USA) using a 50% amplitude four times for 10 seconds. Protein concentration was measured using Pierce BCA Protein Assay Kit (ThermoScientific, Rockford, IL, USA). All samples

were adjusted to the lowest protein concentration value. Lysates were then processed as previously described⁷¹.

High resolution respirometry

Hepatic organoids were collected in Ad.DMEM/F12 at 4°C and kept on ice for 10 minutes to properly disrupt the Matrigel. After centrifugation at 200g for 5 minutes at 4°C, supernatant was removed and organoids were washed with MiR05 buffer followed by another centrifugation step. Organoids were then resuspended in 600uL of MiR05 buffer (110mM sucrose, 60mM potassium lactobionate, 20mM taurine, 20mM HEPES, 0.5mM EGTA, 10mM KH₂PO₄, 3mM MgCl₂, 1mg/ml bovine serum albumin, pH 7.1).

The rate of oxygen consumption of the organoids was measured using a two-channel high-resolution Oroboros Oxygraph-2 k (Oroboros, Innsbruck, Austria) at 37°C. Firstly, organoids were provided with 1mM ADP. Maximal ADP-stimulated respiration was achieved by addition of the oxidable substrates Palmitoyl Carnitine (25uM) plus Malate (2mM) to stimulate the fatty acid β -oxidation (State 3). Next, basal respiration (state 4) was determined using Oligomycin to block ATP synthase. Finally, 0.5mM FCCP was added in order to study the oxygen consumption during uncoupled respiration (State U). Oxygen consumption rates were normalized for protein content.

Mitochondrial copy number

Organoids were collected in basal AdvDMEM/F12 and lysed in lysis buffer (100 mM Tris-HCL pH8.5, 5 mM EDTA, 0.2% SDS, 200 mM NaCl and 20 mg/ml proteinase K) for 2 hours prior to the addition of RNase A. Isopropanol was used to precipitate the DNA, and the pellet was washed with 70% ethanol. After centrifugation at max. speed at 4°C, the pellet was resuspended in TE buffer and DNA yields were measured. qPCR reactions were performed using FastStart Universal SYBR Green Master (Rox) (Sigma Aldrich) in 384 well format in duplicate with 10 ng (for the intestinal samples) and 20ng (for the hepatic samples) total DNA per well in a QuantStudio 7 Flex. Mitochondrial DNA was measured using home-made primers (Supplementary Table 2) and normalized to the values of nuclear β -globulin as reference.

Branched chain fatty acid and very long chain fatty acid measurements

Mature hepatic organoids were incubated with 25 μ M phytol (Sigma Aldrich) for 48 hours prior to quenching in ice-cold methanol. Methanol was evaporated at 37°C under a steady stream of N₂ for 40 minutes. Next, the pellet was reconstituted in PBS. Samples were hydrolysed in two steps. First, an acid hydrolysis step was performed to release the fatty acids from the different moieties they are bound to without affecting phytanic acid. This was followed by a basic hydrolysis to convert esterified fatty acids into free fatty acids. Pentafluorobenzyl bromide (PFB-Br) was added for the derivatization. The PFB derivatives were analysed on the GC/MS (Agilent 7890/5975 inert XL GCMS System, Agilent Technologies, Amstelveen, The Netherlands) in negative chemical ionization mode (NCI). Results were normalized for protein content.

Acylcarnitines measurements

Mature hepatic organoids were incubated with 1mM L-carnitine (Sigma Aldrich) for 24 hours prior to collection in TBS. Intracellular acylcarnitines were measured following the previously published protocol⁷⁰

Imaging of the liver and intestinal organoids and processing of the images

Organoid cultures were followed over time with an AxioObserver Z1 compound microscope (Carl Zeiss), 2.5x and 5x objectives and an AxioCam MRm3 CCD camera (Carl Zeiss). Raw images were processed using the ZEN 3.1 blue edition software. The number and size of organoids were assessed in the whole well. A set of 25 organoids were manually counted in each well, tracked over time and measured throughout the different time points.

Availability of data and materials

The datasets used and/or analysed during the current study are available from the corresponding author on reasonable request.

FUNDING

This work was supported by the European Union's Horizon 2020 research and innovation programme under the Marie Skłodowska-Curie grant agreement No

812968; the Canadian Institutes of Health Research (156307); and the Stichting De Cock-Hadders.

SUPPLEMENTAL INFORMATION

Supplemental information includes five figures and three tables.

STATISTICAL ANALYSIS

All results are expressed as mean \pm standard error of the mean (SEM) as indicated. Biological replicates are considered as independent experiments. Group differences were assessed with repeated measures ANOVA for multiple day organoids size measurements or an ordinary one or two-way ANOVA with Tukey's post hoc multiple comparisons analyses. Statistical analysis was performed with GraphPad Prism Software Version 9.02 (Graphpad Software, San Diego, California USA). Statistical significance was given as *** P value < 0.001 , ** P value < 0.01 and * P value < 0.5 ; NS or no indication means no significant changes.

ACKNOWLEDGEMENTS

We would like to thank Karen van Eunen, Niels Kloosterhuis and Marieke Smit for their technical support with intestinal organoids and animal work. We would also like to acknowledge Hans Clevers, Tomohiro Mizutani, Jeroen Korving and Klaas Nico Faber for their advice on culturing of organoids

REFERENCES

1. Sato, T. *et al.* Single Lgr5 stem cells build crypt-villus structures in vitro without a mesenchymal niche. *Nature* 459, 262–265 (2009).
2. Huch, M. *et al.* In vitro expansion of single Lgr5+ liver stem cells induced by Wnt-driven regeneration. *Nature* 494, 247–250 (2013).
3. Huch, M. & Koo, B.-K. Modeling mouse and human development using organoid cultures. *Development* 142, 3113–3125 (2015).
4. Dutta, D., Heo, I. & Clevers, H. Disease Modeling in Stem Cell-Derived 3D Organoid Systems. *Trends Mol Med* 23, 393–410 (2017).
5. Clevers, H. Modeling Development and Disease with Organoids. *Cell* 165, 1586–1597 (2016).
6. Okkelman, I. A., Neto, N., Papkovsky, D. B., Monaghan, M. G. & Dmitriev, R. I. A deeper understanding of intestinal organoid metabolism revealed by combining fluorescence lifetime imaging microscopy (FLIM) and extracellular flux analyses. *Redox Biol* 30, 101420 (2020).
7. Kruitwagen, H. S. *et al.* Long-Term Adult Feline Liver Organoid Cultures for Disease Modeling of Hepatic Steatosis. *Stem Cell Reports* 8, 822–830 (2017).
8. Cai, T. *et al.* Effects of six common dietary nutrients on murine intestinal organoid growth. *PLoS One* 13, e0191517 (2018).
9. Chen, Y., Michalak, M. & Agellon, L. B. Importance of Nutrients and Nutrient Metabolism on Human Health. *Yale J Biol Med* 91, 95–103 (2018).
10. André Briend PhD, M. D. Kwashiorkor: still an enigma – the search must go on. (2014).
11. Attia, S. *et al.* Mortality in children with complicated severe acute malnutrition is related to intestinal and systemic inflammation: an observational cohort study. *American Journal of Clinical Nutrition* 104, 1441–1449 (2016).
12. Kerac, M. *et al.* Follow-up of post-discharge growth and mortality after treatment for severe acute malnutrition (FuSAM study): a prospective cohort study. *PLoS One* 9, e96030 (2014).
13. Munthali, T., Jacobs, C., Sitali, L., Dambe, R. & Michelo, C. Mortality and morbidity patterns in under-five children with severe acute malnutrition (SAM) in Zambia: a five-year retrospective review of hospital-based records (2009–2013). *Arch Public Health* 73, 23 (2015).
14. Ubesie, A. C., Ibeziako, N. S., Ndiokwelu, C. I., Uzoka, C. M. & Nwafor, C. A. Under-five protein energy malnutrition admitted at the University of Nigeria Teaching Hospital, Enugu: a 10 year retrospective review. *Nutr J* 11, 43 (2012).
15. Wharton, B. Hypoglycaemia in children with kwashiorkor. *Lancet* 1, 171–173 (1970).
16. Nduhukire, T., Atwine, D., Rachel, L. & Byonanebye, J. E. Predictors of in-hospital mortality among under-five children with severe acute malnutrition in South-Western Uganda. *PLoS One* 15, e0234343 (2020).
17. Bandsma, R. H. J. *et al.* Mechanisms behind decreased endogenous glucose production in malnourished children. *Pediatr Res* 68, 423–428 (2010).

18. Grenov, B. *et al.* Diarrhea, Dehydration, and the Associated Mortality in Children with Complicated Severe Acute Malnutrition: A Prospective Cohort Study in Uganda. *J Pediatr* 210, 26–33 (2019).
19. Badaloo, A. V, Forrester, T., Reid, M. & Jahoor, F. Lipid kinetic differences between children with kwashiorkor and those with marasmus. *Am J Clin Nutr* 83, 1283–1288 (2006).
20. Badaloo, A., Reid, M., Soares, D., Forrester, T. & Jahoor, F. Relation between liver fat content and the rate of VLDL apolipoprotein B-100 synthesis in children with protein-energy malnutrition. *Am J Clin Nutr* 81, 1126–1132 (2005).
21. Brooks, S. E., Goldon, M. H. & Taylor, E. Hepatic ultrastructure in children with protein-energy malnutrition. *West Indian Med J* 41, 139–145 (1992).
22. Shiner, M., Redmond, A. O. & Hansen, J. D. The jejunal mucosa in protein-energy malnutrition. A clinical, histological, and ultrastructural study. *Exp Mol Pathol* 19, 61–78 (1973).
23. Campos, J. V *et al.* Jejunal mucosa in marasmic children. Clinical, pathological, and fine structural evaluation of the effect of protein-energy malnutrition and environmental contamination. *Am J Clin Nutr* 32, 1575–1591 (1979).
24. Brunser, O., Castillo, C. & Araya, M. Fine structure of the small intestinal mucosa in infantile marasmic malnutrition. *Gastroenterology* 70, 495–507 (1976).
25. Theron, J. J., Wittmann, W. & Prinsloo, J. G. The fine structure of the jejunum in kwashiorkor. *Exp Mol Pathol* 14, 184–199 (1971).
26. Rath, E., Moschetta, A. & Haller, D. Mitochondrial function - gatekeeper of intestinal epithelial cell homeostasis. *Nat Rev Gastroenterol Hepatol* 15, 497–516 (2018).
27. Ludikhuize, M. C. *et al.* Mitochondria Define Intestinal Stem Cell Differentiation Downstream of a FOXO/Notch Axis. *Cell Metab* 32, 889–900.e7 (2020).
28. Lopes, F. *et al.* ER-stress mobilization of death-associated protein kinase-1-dependent xenophagy counteracts mitochondria stress-induced epithelial barrier dysfunction. *J Biol Chem* 293, 3073–3087 (2018).
29. Sargent, G. *et al.* PEX2 is the E3 ubiquitin ligase required for pexophagy during starvation. *J Cell Biol* 214, 677–690 (2016).
30. van Zutphen, T. *et al.* Malnutrition-associated liver steatosis and ATP depletion is caused by peroxisomal and mitochondrial dysfunction. *J Hepatol* 65, 1198–1208 (2016).
31. Johnson, M. A. *et al.* Amino acid starvation has opposite effects on mitochondrial and cytosolic protein synthesis. *PLoS One* 9, e93597 (2014).
32. Fabris, G., Dumortier, O., Pisani, D. F., Gautier, N. & Van Obberghen, E. Amino acid-induced regulation of hepatocyte growth: possible role of Drosha. *Cell Death Dis* 10, 566 (2019).
33. Hu, H. *et al.* Long-Term Expansion of Functional Mouse and Human Hepatocytes as 3D Organoids. *Cell* 175, 1591–1606.e19 (2018).
34. Zachos, N. C. *et al.* Human Enteroids/Colonoids and Intestinal Organoids Functionally Recapitulate Normal Intestinal Physiology and Pathophysiology. *J Biol Chem* 291, 3759–3766 (2016).

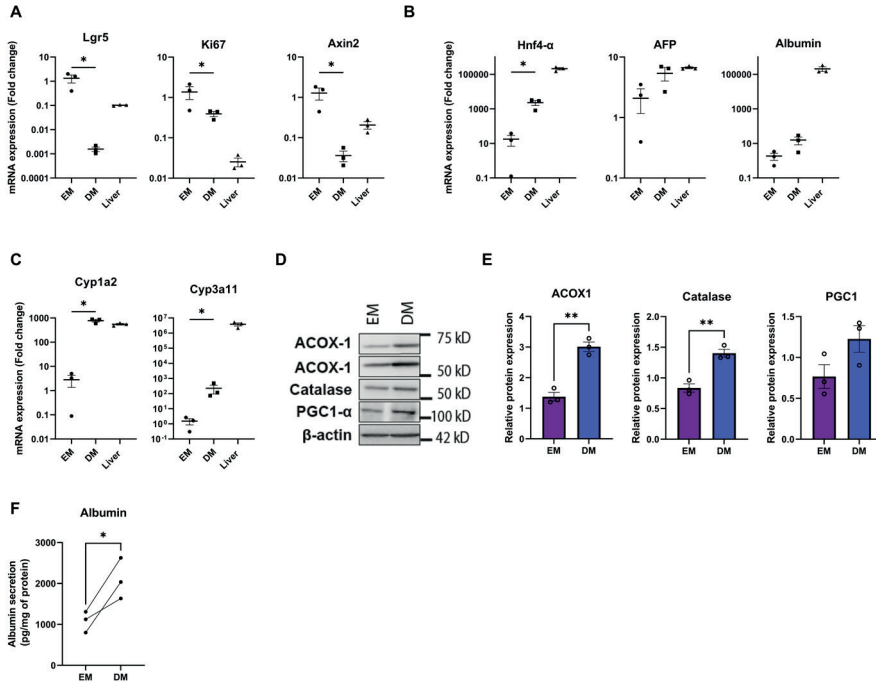
35. Broutier, L. *et al.* Culture and establishment of self-renewing human and mouse adult liver and pancreas 3D organoids and their genetic manipulation. *Nat Protoc* 11, 1724–1743 (2016).
36. Brown, E. M. *et al.* Diet and specific microbial exposure trigger features of environmental enteropathy in a novel murine model. *Nat Commun* 6, 7806 (2015).
37. Huang, T.-Y. *et al.* Overexpression of PGC-1 α increases peroxisomal activity and mitochondrial fatty acid oxidation in human primary myotubes. *Am J Physiol Endocrinol Metab* 312, E253–E263 (2017).
38. Imanaka, T., Aihara, K., Suzuki, Y., Yokota, S. & Osumi, T. The 70-kDa peroxisomal membrane protein (PMP70), an ATP-binding cassette transporter. *Cell Biochem Biophys* 32, 131–138 (2000).
39. Wanders, R. J. A., Komen, J. & Ferdinandusse, S. Phytanic acid metabolism in health and disease. *Biochim Biophys Acta* 1811, 498–507 (2011).
40. Braverman, N. E., D'Agostino, M. D. & MacLean, G. E. Peroxisome biogenesis disorders: Biological, clinical and pathophysiological perspectives. *Dev Disabil Res Rev* 17, 187–196 (2013).
41. Du, G. *et al.* Peroxisome Elevation Induces Stem Cell Differentiation and Intestinal Epithelial Repair. *Dev Cell* 53, 169–184.e11 (2020).
42. Wada, Y., Takeda, Y. & Kuwahata, M. Potential Role of Amino Acid/Protein Nutrition and Exercise in Serum Albumin Redox State. *Nutrients* 10, (2017).
43. Morlese, J. F. *et al.* Albumin kinetics in edematous and nonedematous protein-energy malnourished children. *Am J Clin Nutr* 64, 952–959 (1996).
44. Williams, C. D. A nutritional disease of childhood associated with a maize diet. *Arch Dis Child* 8, 423–433 (1933).
45. Hu, G. *et al.* The role of the tryptophan-nicotinamide pathway in a model of severe malnutrition induced liver dysfunction. *Submitted* (2021).
46. Cassim, S., Raymond, V.-A., Lapierre, P. & Bilodeau, M. From in vivo to in vitro: Major metabolic alterations take place in hepatocytes during and following isolation. *PLoS One* 12, e0190366 (2017).
47. Nagarajan, S. R. *et al.* Lipid and glucose metabolism in hepatocyte cell lines and primary mouse hepatocytes: a comprehensive resource for in vitro studies of hepatic metabolism. *Am J Physiol Endocrinol Metab* 316, E578–E589 (2019).
48. Peng, W. C. *et al.* Inflammatory Cytokine TNF α Promotes the Long-Term Expansion of Primary Hepatocytes in 3D Culture. *Cell* 175, 1607–1619.e15 (2018).
49. Moore, S. R. *et al.* Glutamine and alanyl-glutamine promote crypt expansion and mTOR signaling in murine enteroids. *Am J Physiol Gastrointest Liver Physiol* 308, G831–9 (2015).
50. Saito, Y. *et al.* Effect of essential amino acids on enteroids: Methionine deprivation suppresses proliferation and affects differentiation in enteroid stem cells. *Biochem Biophys Res Commun* 488, 171–176 (2017).
51. Richmond, C. A., Shah, M. S., Carlone, D. L. & Breault, D. T. An enduring role for quiescent stem cells. *Developmental dynamics* 245, 718–726 (2016).
52. Buczacki, S. J. A. *et al.* Intestinal label-retaining cells are secretory precursors expressing Lgr5. *Nature* 495, 65–69 (2013).

53. van Es, J. H. *et al.* Dll1+ secretory progenitor cells revert to stem cells upon crypt damage. *Nat Cell Biol* 14, 1099–1104 (2012).
54. Tetteh, P. W. *et al.* Replacement of Lost Lgr5-Positive Stem Cells through Plasticity of Their Enterocyte-Lineage Daughters. *Cell Stem Cell* 18, 203–213 (2016).
55. Jadhav, U. *et al.* Dynamic Reorganization of Chromatin Accessibility Signatures during Dedifferentiation of Secretory Precursors into Lgr5+ Intestinal Stem Cells. *Cell Stem Cell* 21, 65–77.e5 (2017).
56. Amadi, B. *et al.* Impaired Barrier Function and Autoantibody Generation in Malnutrition Enteropathy in Zambia. *EBioMedicine* 22, 191–199 (2017).
57. Farràs, M. *et al.* Characterizing the metabolic phenotype of intestinal villus blunting in Zambian children with severe acute malnutrition and persistent diarrhea. *PLoS One* 13, e0192092 (2018).
58. Boaz, R. T., Joseph, A. J., Kang, G. & Bose, A. Intestinal permeability in normally nourished and malnourished children with and without diarrhea. *Indian Pediatr* 50, 152–153 (2013).
59. Khaloian, S. *et al.* Mitochondrial impairment drives intestinal stem cell transition into dysfunctional Paneth cells predicting Crohn's disease recurrence. *Gut* 69, 1939–1951 (2020).
60. Hara-Kuge, S. & Fujiki, Y. The peroxin Pex14p is involved in LC3-dependent degradation of mammalian peroxisomes. *Exp Cell Res* 314, 3531–3541 (2008).
61. Jiang, L., Hara-Kuge, S., Yamashita, S.-I. & Fujiki, Y. Peroxin Pex14p is the key component for coordinated autophagic degradation of mammalian peroxisomes by direct binding to LC3-II. *Genes Cells* 20, 36–49 (2015).
62. Peeters, A. *et al.* Mitochondria in peroxisome-deficient hepatocytes exhibit impaired respiration, depleted DNA, and PGC-1 α independent proliferation. *Biochim Biophys Acta* 1853, 285–298 (2015).
63. Roels, F. *et al.* Different types of peroxisomes in human duodenal epithelium. *Gut* 32, 858–865 (1991).
64. Di Cara, F., Bülow, M. H., Simmonds, A. J. & Rachubinski, R. A. Dysfunctional peroxisomes compromise gut structure and host defense by increased cell death and Tor-dependent autophagy. *Mol Biol Cell* 29, 2766–2783 (2018).
65. Yan, F. *et al.* Peroxisome proliferator-activated receptor α activation induces hepatic steatosis, suggesting an adverse effect. *PLoS One* 9, (2014).
66. Kiskac, M. *et al.* A case of rhabdomyolysis complicated with acute renal failure after resumption of fenofibrate therapy: a first report. *Indian J Pharmacol* 45, 305–306 (2013).
67. Rigano, D., Sirignano, C. & Tagliatela-Scafati, O. The potential of natural products for targeting PPAR α . *Acta Pharm Sin B* 7, 427–438 (2017).
68. Keller, H. *et al.* Fatty acids and retinoids control lipid metabolism through activation of peroxisome proliferator-activated receptor-retinoid X receptor heterodimers. *Proc Natl Acad Sci U S A* 90, 2160–2164 (1993).
69. Bartolomé, A. *et al.* MTORC1 Regulates both General Autophagy and Mitophagy Induction after Oxidative Phosphorylation Uncoupling. *Mol Cell Biol* 37, (2017).

70. Evers, B. *et al.* Simultaneous Quantification of the Concentration and Carbon Isotopologue Distribution of Polar Metabolites in a Single Analysis by Gas Chromatography and Mass Spectrometry. *Anal Chem* 93, 8248–8256 (2021).
71. Heberle, A. M. *et al.* The PI3K and MAPK/p38 pathways control stress granule assembly in a hierarchical manner. *Life Sci Alliance* 2, (2019).

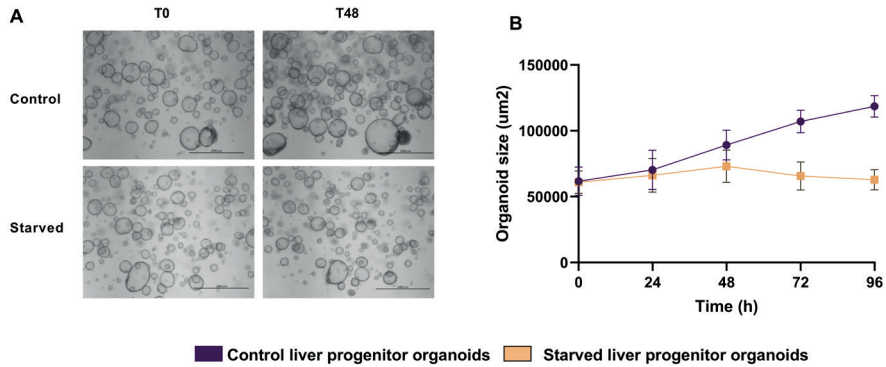
SUPPLEMENTARY FILES

Supplementary Figure 1. Differentiation of Murine Liver Organoids into Hepatocyte-like cells.



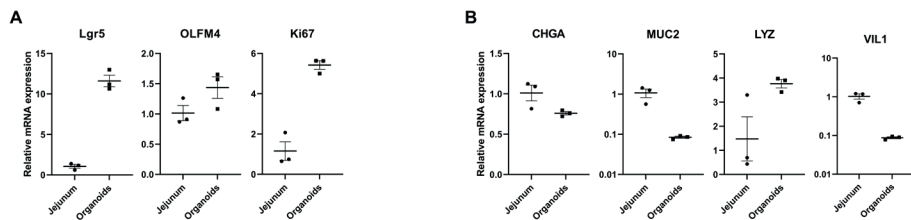
Relative gene expression of stem cells markers (**A**) and early and mature hepatocyte markers (**B**) measured in liver progenitor organoids and differentiated mature hepatic organoids as well as liver homogenate. Liver progenitor organoids expressed stem cell markers (e.g. LGR5, AXIN2) while differentiated mature hepatic organoids expressed early and mature hepatocyte markers (e.g. HNF4A, CYP1A2). Data represents 3 biological replicates from independent experiments. * $p < 0.05$, Mann-Whitney U test. (**D**) Representative immunoblot images (**E**) Immunoblot quantification of peroxisomal proteins ACOX1, Catalase and PGC1- α measured in the progenitors and differentiated organoids. Data represents 3 biological replicates from independent experiments. * $p < 0.05$, Unpaired t test. (**F**) Hepatocyte function test of liver organoids cultures in EM and DM shown as albumin secretion in the medium. Data represents 3 biological replicates from independent experiments. * $p < 0.05$, Paired t test.

Supplementary Figure 2. Organoid size and growth rate of liver progenitor organoids cultured in control and amino-acid-free medium.



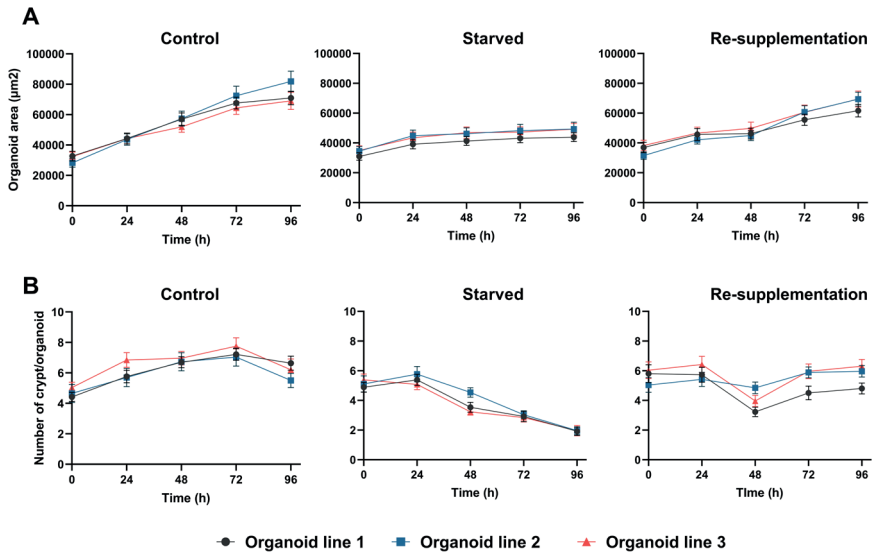
(A) Representative images of liver progenitor organoids that were grown in complete culture medium (control) or amino-acid-free medium (starved) for 96 hours. Scale bar, 1000 µm. (B) Size of organoids in complete culture medium (control) or amino-acid free medium (starved), expressed as size of an organoid at every time point of interest. Data based on 3 sets of experiments in which 25 randomly selected organoids were tracked). Error bars indicate the SEM (*P<0.05, **P<0.01, *** P<0.001, unpaired t test at individual time points).

Supplementary Figure 3. Characterization of murine intestinal organoids.



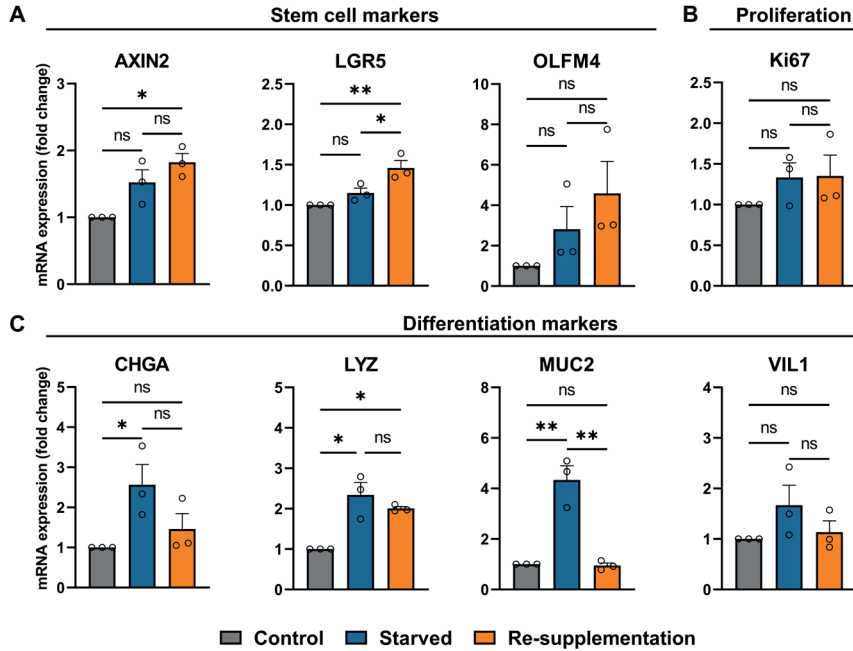
Relative gene expression of stem cells and proliferation markers (A) and mature epithelial markers (B) measured in mouse jejunum and intestinal organoids. (A) Stem cell and proliferation markers include: LGR5, OLFM4 (olfactomedin 4), and Ki67. Mature epithelial markers include: CHGA (Chromogranin A) as a marker for enteroendocrine cells ; MUC2 (Mucin 2), as a marker for goblet cells ; VIL1 (Villin 1), as a marker for enterocytes and LYZ (Lysozyme) as a marker for Paneth cells.

Supplementary Figure 4. Organoid size and number of crypts per organoid



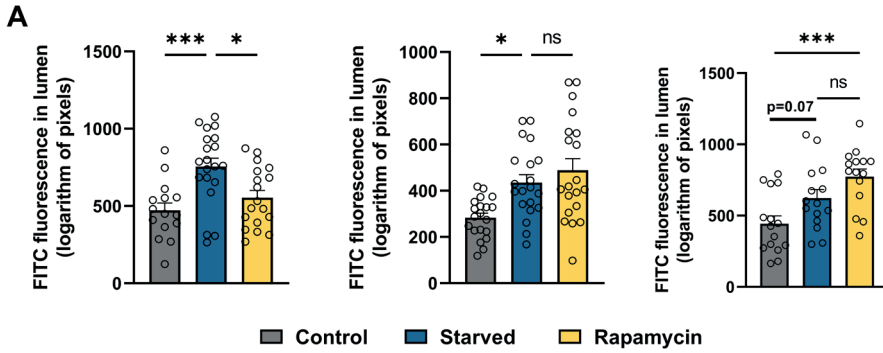
Organoids were grown in complete culture medium (control), amino-acid-free medium (starved), amino-acid-free medium for 48 h followed by complete culture medium for 48 h (re-supplementation). **(A)** The size of 26 organoids was measured every 24 hours for each experimental condition in 3 different organoid lines. **(B)** In addition, the number of crypts per organoid were assessed in the organoids that were measured in (A).

Supplementary Figure 5. Relative gene expression markers for stem cells, proliferation and differentiation in intestinal organoids.



Relative gene expression of stem cells markers (A), proliferation markers (B) and markers of differentiation (C) measured in intestinal organoids grown in complete culture medium (control), amino-acid-free medium (starved) or amino-acid-free medium for 48 h followed by complete culture medium for 48 h (re-supplementation). Data represents 3 biological replicates (independent experiments) (* $P < 0.05$, ** $P < 0.01$, Two-way ANOVA with Tukey's post hoc test). AXIN2, axis inhibition protein 2, LGR5, Leucine Rich Repeat Containing G Protein-Coupled Receptor 5, OLFM4, olfactomedin 4 CHGA, chromogranin A; LYZ, lysozyme; MUC2, mucin-2; VIL1, villin 1.

Supplementary Figure 6. FITC fluorescence in the lumen of intestinal organoids.



FITC fluorescence was measured in the lumen of intestinal organoids that were grown in complete culture medium (control), amino-acid-free medium (starved) and amino-acid-free medium supplemented with 2nM rapamycin (rapamycin). Graphs represent three different organoid lines. Data points are individual organoids random selected by a random generator and the error bars indicate the SEM. (* $P < 0.05$, *** $P < 0.001$, two-way ANOVA with Tukey's post hoc test).

Supplementary Table 1. Amino acid concentrations measured in the medium of mature hepatic organoids.

Amino acid	Concentration (μM)	
	Control medium	Amino-acid-starvation medium
Alanine	1405 \pm 110	86 + 19
Asparagine	32 \pm 8	7.0 \pm 0.2
Glutamic Acid	136 \pm 169	166 \pm 233
Glutamine	480 \pm 164	10 \pm 1
Glycine	144 \pm 3	5 \pm 0.1
Isoleucine	328 \pm 11	8 \pm 2
Leucine	327 \pm 9	10 \pm 2
Lysine	284 \pm 26	16 \pm 4
Phenylalanine	188 \pm 10	10 \pm 2
Proline	162 \pm 22	41 \pm 5
Serine	147 \pm 9	2 \pm 0
Tyrosine	151 \pm 10	14 \pm 1
Valine	410 \pm 3	18 \pm 4

Amino acid concentrations were measured in medium that had been in the well with organoids for 48 hours. Data is expressed as mean \pm SD and represents 3 biological replicates (from independent experiments) for control medium and 2 biological replicates for amino-acid-starvation medium measured in hepatic organoid cultures.

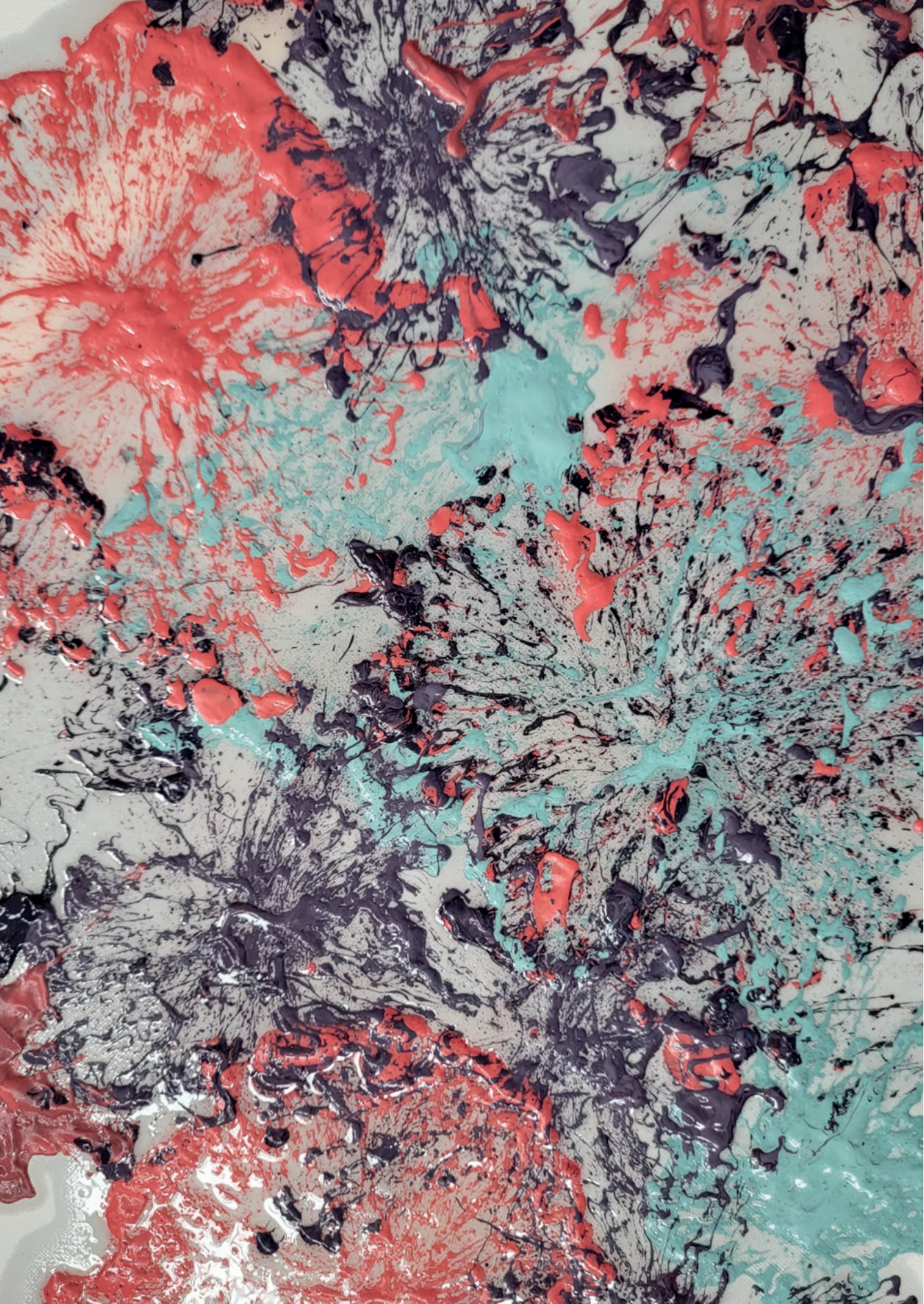
Supplementary Table 2. List of primer sequences used in RT-qPCR

Gene Name	Forward and reverse primer sequence (5'- 3')
PPIA	Fwd: TTCCTCCTTTACAGAATTATTCCA Rev: CCGCCAGTGCCATTATGG
LGR5	Fwd: GGAAATGCTTTGACACACATTC Rev: GGAAGTCATCAAGGTTATTATAA
AXIN2	Fwd: TAAGCAGCCGTTCCGCGATG Rev: TTCTTCCAGTTCCTCTCAG
Ki67	Fwd: ATCATTGACCGCTCCTTTAGGT Rev: GCTCGCCTTGATGGTTCCCT
HNF4-a	Fwd: GCTAAGGCGTGGGTAGGG Rev: AGGCTGTTGGATGAATTGAGG
AFP	Fwd: CCAGGAAGTCTGTTTCACAGAAG Rev: CAAAAGGCTCACACCAAAGAG
CYP1a2	Fwd: TTCAGTCCCTCCTTACAGCC Rev: TCCAAGGCAGAATACGGTGAC
CYP3a11	Fwd: TGGTCAAACGCCTCTCCTTGCTG Rev: ACTGGGCCAAAATCCCGCCG
TBX3	Fwd: GAGGCCAAGGAACTTTGGGA Rev: AGGGAACATTCGCCTTCCTG
Catalase	Fwd: AGCGACCAGATGAAGCAGTG Rev: TCCGCTCTCTGCAAAGTGTG
ACOX1	Fwd: TAACTCCTCACTCGAAGCCA Rev: AGTTCATGACCCATCTCTGTC
Albumin	Fwd: GCGCAGATGACAGGGCGGAA Rev: GTGCCGTAGCATGCGGGAGG
VIL1	Fwd: GCTTGCCACAACCTCCTAAGAT Rev: TCAGTTTAGTCATGGTGGACGA
MUC2	Fwd: TGTGGAACCGGAAGATG Rev: GACCACAGGTATGTTCTGGA
CHGRA	Fwd: CGATCCAGAAAGATGATGGTC Rev: CGGAAGCCTCTGTCTTTCC
OLFM4	Fwd: AGAAATCGTGGCTCTGAAG Rev: GTTACCACACCACCATGAC
LYZ1	Fwd: AGACCGAAGCACCGACTATG Rev: CGGTTTTGACATTGTGTTCCG
Mito	Fwd: CCCAGCTACTACCATCATTCAAGT Rev: GATGGTTTGGGAGATTGGTTGATGT
β -globulin	Fwd: AAGGTGAACGCCGATGAAGT Rev: ATCAAAGTACCCTGGGTCC

Fwd, forward primer; Rev, reverse primer.

Supplementary Table 3. List of primary antibodies used in immunoblotting.

Name	Company	Category number	Dilution
ACOX1	Abcam	Ab184032	1:1000
B-actin	Sigma-Aldrich	A5441	1:1000
Catalase	Santa Cruz	SC-271803	1:1000
Claudin-3	Thermo Fisher Scientific	54481	1:2000
Claudin-3	Life Technologies	341700	1:1000
HSP60	Cell Signaling	4870S	1:1000
PGC1 α	Abcam	54481	1:1000
PMP70	Sigma-Aldrich	P0497	1:1000
TOM20	Cell Signaling	D8T4N	1:1000
Total OXPHOS	Abcam	110413	1:1000



Chapter



Towards Automatization of Organoid Analysis: A Deep Learning Approach to Localize and Quantify Organoids Images

Asmaa Haja^{1,§*}, José M. Horcas-Nieto^{2,*}, Barbara M. Bakker², Lambert Schomaker¹

1. Bernoulli Institute, University of Groningen, The Netherlands; 2. Laboratory of Pediatrics, Center for Liver, Digestive and Metabolic Diseases, University Medical Center Groningen, The Netherlands

*** These authors contributed equally to this work.**

§ Corresponding author:

Asmaa Haja

Bernoulli Institute, University of Groningen, The Netherlands

Email: a.haja@rug.nl

Published in Computer Methods and Programs in Biomedicine Update (2023)

<https://doi.org/10.1016/j.cmpbup.2023.100101>

ABSTRACT

The interest in the use of organoids in the biomedical field has increased exponentially in the past years. Organoids, or three-dimensional “mini-organs”, have the ability to proliferate and self-organize in vitro, while display varying morphologies. When in culture, these structures can overlap with each other making the quantification and morphological characterization a challenging task. Quick and reliable analysis of organoids images could help in precisely modeling disease phenotypes as well as provide information of organ development. Therefore, automatization of the quantification and measurements is an important step towards an easier, faster, and less biased workflow.

In order to accomplish this, a free e-Science service (OrganelX) has been developed for localization and quantification of organoid size based on deep learning methods. The ability of the system was tested on murine liver organoids, and the data are made publicly available. The OrganelX e-Science free service is available at <https://organelx.hpc.rug.nl/organoid/>

INTRODUCTION

New advances in the biomedical field have presented us with the need for new technical and analytical approaches. The field of organoids has experienced a massive upsurge in the past 15 years. Organoids are three dimensional mini-structures that in culture recapitulate some features and functions of the organ of origin. Ever since organoids were first described in 2009¹, the field has continued to expand rapidly. After that, many different types of organoids, recapitulating different organs, have been described²⁻⁶. These three-dimensional structures have become widely popular due to their ability to self-organize and proliferate while maintaining multiple biological functions⁷. Organoids can be used for multiple purposes, ranging from developmental studies to diseases modeling, as well as, drug screening^{7,8}.

Since it is the three-dimensional environment that allows cells to organize and behave in a more physiologically relevant manner, it is understandable how important morphology and size are⁷. It is common for researchers to track organoid morphology and size as these are the first signs of health and disease. This is often done for multiple purposes: either for developmental reasons/optimization of the culture conditions^{9,10}, or in the context of different diseases¹¹.

Another interesting approach to studying organoid health is tracking organoids' size in time¹². This is done in order to determine the growth and expansion rate of the culture in time. This proliferative status of the organoids can provide relevant information regarding developmental state of the organ, regeneration, response to pharmacological interventions.

However, it is important to highlight that due to the way these structures are cultured, high variability in size is often observed between organoids in the same dome (**Figure 1B** and **1C**). One of the main reasons for this is the way they are distributed in the hydrogel domes. Since these domes are three-dimensional structures (**Figure 1A**), not all organoids have access to the same amount of nutrients in the medium. Often, this causes organoids around the edges of the hydrogel to have easier access to nutrients, reaching bigger sizes than those organoids contained in the middle of the dome (**Figure 1B** and **1C**). Another complexity arising from this type of culture is the proliferative state of the cells that leads to different organoids expanding and collapsing at different rates.

Because of this high variability between organoids in the same dome, researchers need to quantify large numbers of organoids per well in order

to get an accurate description of what is happening in the culture. Counting and measuring the size of multiple organoids per dome is a manual process that can take several hours depending on the density of the cultures. These measurements are highly influenced by factors such as tiredness, personal interpretation, etc. This can lead to low reproducibility between measurements. Brightfield images of the cultures provide a good opportunity to get a broader impression of the health/state of the culture. These organoids can then be manually counted and measured using different softwares. To do so, scientists need to manually select the area of the organoid of interest and trace it in order to get an approximation to the size. Organoid cultures can vary in density, showing as little as a few organoids to as many as a hundred. Another difficulty of tracking organoid's growth in time, is the need to image the cultures repeatedly (i.e. every 24 hours) and finding the same organoid at every time point in order to track its growth rate. Overall, this task is highly time-consuming and has a very high person-dependent variability.

OrgaQuant¹³ is an open-source implementation that addresses this issue. However, this tool does not perform a pixel-wise segmentation of organoids. Instead, it uses a bounding box to detect an organoid. Thus, the area of an organoids cannot be computed accurately. Additionally, OrgaQuant does not allow for user interventions, and does not relate organoids from different stack images of a Z-stack image. Another group¹⁴ has also published annotated organoid images, in which each organoid is surrounded by a bounding box created by experts. However, these data can only be accessed upon contacting the authors. Due to the use of bounding boxes, the correct area of each organoid cannot be computed. This is important since the growth characteristics are crucial for organoid research. Even though they trained a deep neural network to detect and track organoids, this model is not publicly available. In order to overcome these problems, we have extended the OrganelX e-Science service¹⁵ to segment and analyze organoids culture. This system allows researchers to upload their brightfield images in order to quantify the number of organoids present in the image as well as to measure their area. The system allows researchers to calculate the average area of multiple organoids of a culture or only of those of interest. It also offers the possibility to select multiple organoids of interest in different Z-stacks of the dome (**Figure 1A**). Moreover, the system indicates the organoids that are found in different stacks. Another application would be to track organoids in time using images acquired at different time points.

The contributions of this work are presented as follows: (1) Design of a deep-learning algorithm and processing pipeline dedicated to organoid-image

analysis; (2) Development of an e-Science service that detects, segments, and analyses organoids images; (3) Testing the system on a use case to evaluate the area and growth analysis; and (4) Providing public data for the use case.

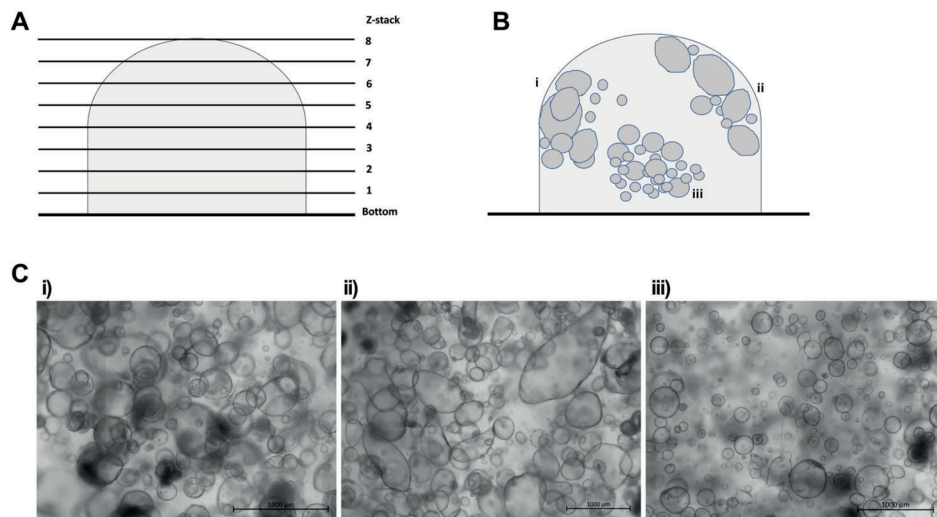


Fig. 1. Organoids display high variability in size and morphology in culture. (A) Representative sketch of a hydrogel dome. Line bars represent the different Z-stacks of the dome. (B) Representative Sketch of the distribution of organoids in a hydrogel dome. i) Organoids accumulate in one area overlapping. ii) Organoids around the edge of the hydrogel dome develop to bigger sizes and more complex morphologies. iii) Organoids in the middle of the dome display smaller sizes and more spherical morphologies. (C) Representative brightfield images exemplifying the different distributions and morphologies described in B.

METHOD AND IMPLEMENTATION

Murine liver progenitor organoids culture

Ductal fragments from male C57BL/6J mice between 3 to 5 weeks of age (Jackson Laboratory, Bar Harbor, ME, USA) were isolated following the published protocol by Broutier et al¹⁶. Ethical approval was obtained from the Central Authority for Scientific Procedures on Animals (CCD) of the Netherlands and from the University of Groningen Ethical Committee for Animal Experiments (Animal Use Protocol Number: 171504-01-001/3). These fragments were kept in expansion medium consisting of Advanced DMEM/F12 supplemented with 10mM HEPES, 1% (v/v) GlutaMax, 1% (v/v) Penicillin-Streptomycin (all Gibco), 1% B-27 Supplement (Invitrogen) 1% N-2 Supplement (Invitrogen), 10mM Nicotinamide (Sigma Aldrich), 1.25mM N-Acetylcysteine

(Sigma Aldrich), 10% RSpondin Conditioned Medium (provided by Calvin J. Kuo), 30% Wnt3a CM (provided by Hans Clevers), 100 ng/ml Noggin (PeproTech) 50 ng/ml HGF (PeproTech), 100 ng/ml FGF-10 (PeproTech), 50 ng/ml EGF (PeproTech), 10nM Leu-gastrin. Three days after the isolation Noggin and Wnt3a CM were removed from the medium. The medium was changed every 2-3 days. Liver progenitor organoids were passaged every 6-7 days. Insult-exposed organoids were grown in the same medium but in the presence of no amino acids.

Organoid imaging

Organoid cultures were followed over time with an AxioObserver Z1 compound microscope (Carl Zeiss), 2.5x and 5x objectives and an AxioCam MRm3 CCD camera (Carl Zeiss) in brightfield. Raw images were processed using the ZEN 3.1 blue edition software. The whole well was imaged by selecting 9 tiles that were later on stitched together. On average 20 different Z-stacks were imaged in order to ensure all organoids in the Matrigel dome were detected. The number and size of organoids were assessed in the whole well. For the first case study, 95 organoids (previously measured by OrganelX) were manually counted. For the second case study, and tracking in time of the organoids, a set of 25 organoids were randomly selected and measured. Images, of the same cultures, were acquired every 24 h and the same 25 organoids were measured at every time point. For manual measurement of the organoids, ZEN3.1 (blue edition) from Carl Zeiss Microscopy GmbH was used. The outline of the organoids was traced using the draw spline tool and the area was calculated by the software.

The OrganelX e-Science service

For the purpose of studying organoids in culture the free e-Science webpage* offers different functionalities. The service offered by the website begins after uploading a CZI file by the user. A CZI file, which is suitable for microscope image data and captured by the Carl Zeiss microscope, contains tile images for each stack as well as image stacks. It is to be mentioned that the system will be further developed to include different types of images files. In addition to the CZI file, the user needs to provide a short experiment ID and sample ID. This is beneficial for future comparisons between experiments and samples in experiment. The user will be redirected to a page that tracks the request's progress and presents the final results in an interactive way.

Organoids in each image stack are automatically detected and segmented using Mask-RCNN¹⁷. Mask-RCNN is a state-of-the-art instance segmentation

framework based on convolutional neural network that outputs a mask channel consisting of a pixel-wise prediction of organoids' location. As training this framework from scratch is a non-trivial task, we employ and adjust a pre-trained model¹⁸. It is relevant to mention that the computation time for each uploaded CZI file varies and depends on the number of stacks, images sizes, and the number of found organoids in each image stack. With this in mind, an optional step is offered for the user to provide an email address so that a notification will be sent to the email address when the computation is completed. Each of the segmented organoids will get an unique number (ID).

* <https://organelx.hpc.rug.nl/organoid/>

Upon completing this step, an automated analysis step begins for grouping and assigning identical organoids of different stacks. Organoids of different stacks are called identical when their mask center-point is within a certain distance and the Interaction of Union¹⁹ value of their bounding boxes is within a certain range.

Once all internal computations are finished, the results will be presented on the page to which the user is redirected, or an electronic notification is sent, if an email address has been provided. The number of the successfully detected and segmented organoids for all stack images will be given. The user can interactively perform the following operations:

- Select a stack image and preview the organoids that are detected by MASK-RCNN for that specific stack image. The corresponding number of detected organoids for this stack will be specified.
- Select multiple organoids of interest. As a result, the area of each selected organoid will be shown. Additionally, the minimum, maximum, average, and total areas will be marked. The area of each organoid depends on the unit scale given by the CZI file. A radio button is provided to determine whether to select identical organoids of all stack or to only consider organoids of the chosen stack.
- Extract and download a summary zip file containing:
 1. PNG images of all stacks including the selected and unselected organoids.
 2. CSV file of the identical organoids represented by unique ID and corresponding name.
 3. Excel file, in which each sheet includes information of the selected organoids (ID, bounding box coordinates, mask border, and the area) for each stack image.

It should be noted that multiple compute requests can be simultaneously handled. The size of the CZI file should be smaller than 1.5GB. The width and height of the stack images can be in any size. However, the bigger the image size is the more computational time would be needed. For each request separately, all above-mentioned computations will be computed and represented in the redirected page within a maximum of 12 hours after uploading the CZI file. Currently, the results will be deleted after a week of the submitted request.

VALIDATION AND RESULTS

To validate the accuracy of OrganelX along with its interactive tool we defined and compared two scenarios.

Segmentation and area calculation for one stack image

For a randomly chosen stack image, we manually annotated 95 organoids and compared their cross-sectional area against the computed area by OrganelX. It is to be mentioned that the segmentation of one stack image using OrganelX was completed in a few minutes while the time for the manual segmentation for the same stack was around 1h. Furthermore, while manual counting allowed us to segment 95 organoids, OrganelX was able to count twice as many organoids. **Figure 2A** shows the chosen stack image in addition to the manually segmented organoids in red. The black and blue points in **Figure 2B** denote the cross-sectional area of those manually and OrganelX segmented organoids, respectively. The results demonstrate that the overall computed areas are nearly identical with a minor difference for some organoids. To demonstrate the accuracy of this result in a number, the average of the absolute differences between manual and OrganelX segmented area was calculated, and divided by the total manual segmented area. An inaccuracy of less than 0.001% was obtained.

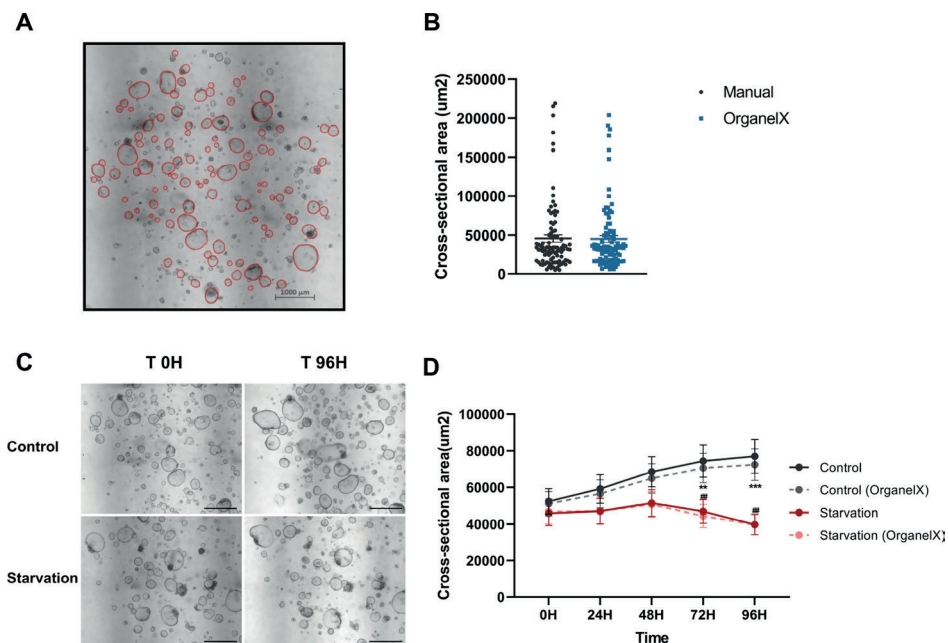


Fig. 2. Evaluation results. (A) Representative bright field image of a liver progenitor organoid culture at day 3 after passaging with medium to small structures. 95 organoids have been selected and manually measured (indicated by red contour). Scale bar, 1000 μm (B) Size of 95 individual organoids measured manually compared to the same organoids measured by OrganelX. (C) Representative bright-field images of liver progenitor organoids imaged at time point 0 H and 96 H. The upper row shows control organoids in complete condition medium and the bottom row shows organoids in a medium depleted of amino acids (Starvation). The scale bars present 1000 μm (D) Cross-sectional area of 25 random organoids tracked in time, measured every 24 H. The black and solid line represents control conditions measured manually. The grey and dotted line represents control conditions measured by OrganelX. The red and solid line represents starvation conditions measured manually. The light red and dotted line represents starvation conditions measured by OrganelX. Error bars indicate the SEM. (* $P < 0.05$, ** $P < 0.01$, *** $P < 0.001$, unpaired t test at individual time points for comparison between Control and Starvation conditions of the manually selected organoids. (# $P < 0.05$, ## $P < 0.01$, ### $P < 0.001$, unpaired t test at individual time points for comparison between Control and Starvation conditions of organoids measured by OrganelX). (For interpretation of the references to color in this figure legend, the reader is referred to the web version of this article.)

Segmentation and growth area over time

Once the ability of the system to replicate manually annotated data was assessed, its ability to track organoids in time was evaluated.

In this case study, liver progenitor organoids have been grown in either complete medium (referred to as control) or in medium lacking all amino

acids (referred to as starvation), which are essential for growth. This work is based on a previous study in which we demonstrated that long periods of amino-acid depletion lead to reduced growth of liver progenitor organoids²⁰. Organoids in starvation medium, although coming from the same initial culture as the control ones, have impaired growth and smaller size due to the insult introduced at time point 0 H. To illustrate the results, these organoids have been tracked over time by imaging them every 24 H. In order to study the growth rate, 25 organoids for each medium were randomly selected and their cross-sectional areas were measured every 24 hours using brightfield images. **Figure 2C** demonstrates the growth at time point 0 and after 96 hours for organoids in control and starvation medium.

Figure 2D demonstrates the area of those selected organoids over the experiment time. As it can be seen, the area of the organoids measured by OrganelX is very similar to those manually segmented especially for those in starvation medium. Only small differences of the areas are reported for those in the control medium after 48 hours. This is due to the fact that organoids are growing, their sizes increase over time, and OrganelX fails to quantify the size of such large organoids. This dissimilarity highlights the importance of continuously training OrganelX in order to optimize its response to bigger organoids.

Publicly available data

The e-Science website offers the tested data to be publicly available. **Table 1** demonstrates the number of stacks in each file (S), the total number of detected organoids in the dome (O), as well as the average of all areas of the detected organoids in the dome (A) for the controlled and starvation medium. While OrganelX is able to measure more organoids than manual annotation, researchers have the option to select the organoids they are interested in. In this case, Table 1 also presents the organoids selected by a researcher (OMS) for a random selected stack (MS), in which small dying structures were not selected. The total average of those selected organoids is shown in the (AMS) column.

Time	Control						Starvation					
	(S)	(O)	(A)	(MS)	(OMS)	(AMS)	(S)	(O)	(A)	(MS)	(OMS)	(AMS)
0 H	16	295	20951.03	9	134	37325.41	16	219	19353.19	10	82	39574.40
24 H	24	292	21617.07	6	84	51460.78	24	222	20319.44	5	68	46615.94
48 H	27	302	24782.65	5	93	58830.05	27	221	22521.13	6	73	51887.36
72 H	20	298	25058.80	6	98	56627.89	20	226	20824.84	6	79	44464.50*
96 H	26	295	24240.08	3	100	51565.53	26	171	18044.25	3	64	35669.64**

Table 1. The number of stacks in each CZI file (S), the total number of detected organoids in the dome (O), the average of the total detected organoids area in the dome in (A), a manual selected stack (MS), the number of manually selected organoids in the MS stack (OMS), and the average of the total selected organoids area in the MS stack in (AMS). * $P < 0.05$, ** $P < 0.01$, *** $P < 0.001$, unpaired t test at individual time points for comparison between Control and Starvation conditions of the manually selected organoids.

DISCUSSION AND CONCLUSION

This paper introduces an extension to the OrganelX e-Science website that automatically detects and segments organoids upon uploading a CZI file containing different stack images. It also offers functionalities such as selecting organoids of interest, computing their area, and counting the number of organoids in each stack image. The performance of the website was evaluated using two scenarios, in which OrganelX has shown the ability to accurately segment organoids. Regardless of the small variability in individual sizes, OrganelX is able to track down in time the size of multiple organoids with similar outcome as manual measurements. Moreover, OrganelX offers the possibility to easily increase the sample size (e.i. from 25 organoids up to hundreds) in order to produce a more descriptive result. 10 Segmented CZI files with more than 30,000 detected structures were made publicly available. Most organoids of up to 10000 μm^2 of area can be easily detected by OrganelX. As depicted on Figure 2B, OrganelX is also able to measure organoids between 150000 μm^2 and 200000 μm^2 . The upper limit of detection lies somewhere between 200000 μm^2 and 250000 μm^2 . It is to be noticed that for this quantification, each individual stack image has been regarded as an independent image. OrganelX has only been tested on murine liver organoids, which present a common cystic morphology. However, it is possible

to also measure any other types of organoids. As long as these organoids have an approximately spherical morphology they should be detected. The method has not yet been tested on non-cystic morphologies such as murine intestinal organoids. For the future, OrganelX will be trained to work with different morphologies.

DECLARATION OF COMPETING INTEREST

The authors declare that they have no known competing financial interests or personal relationships that could have appeared to influence the work reported in this paper.

ACKNOWLEDGEMENTS

We thank the Center for Information Technology of the University of Groningen for their support and for providing access to the Peregrine high performance computing cluster. The e-Science server would not have been possible without the support and nurturing of Ger Strikwerda.

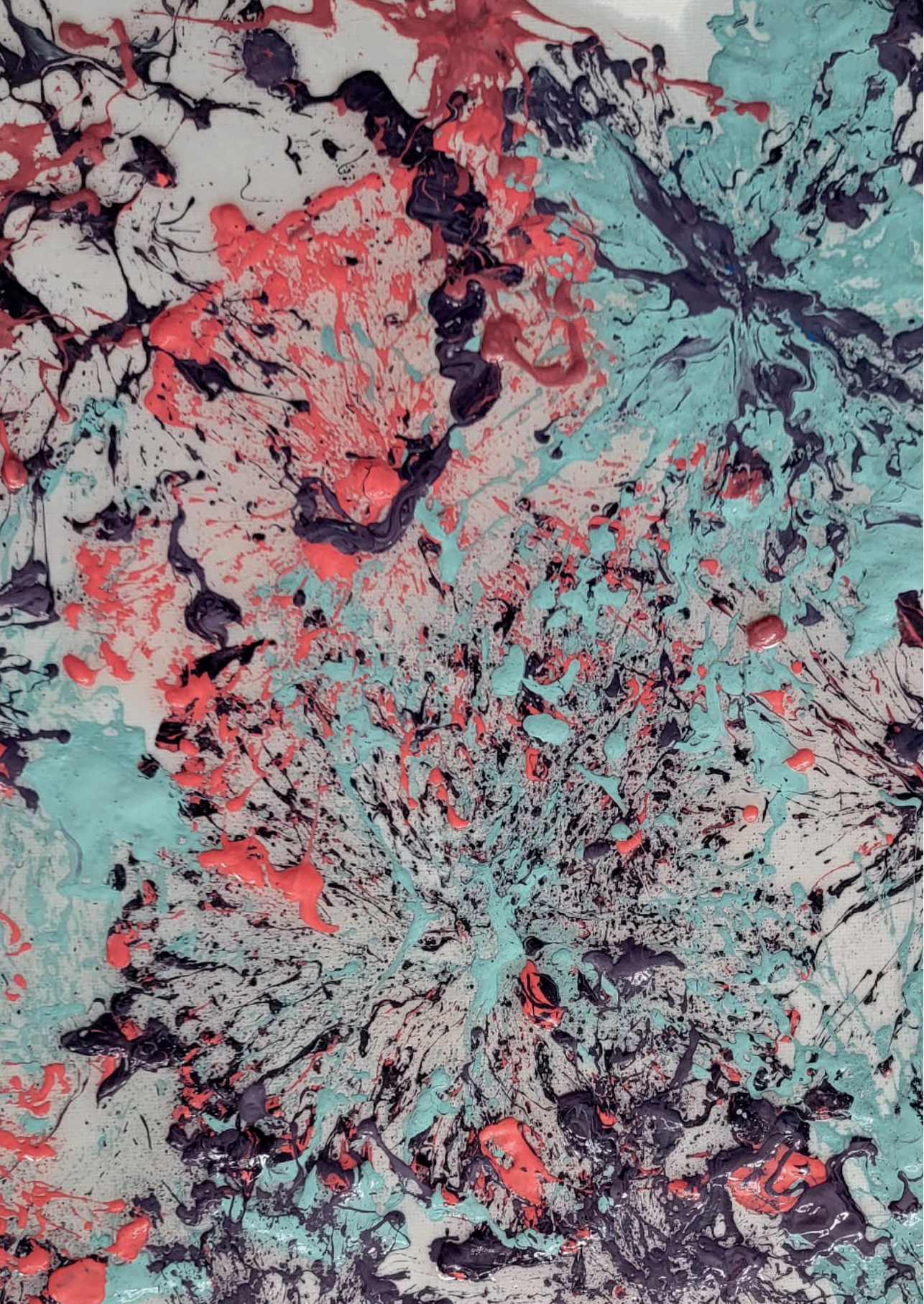
FUNDING

This project has received funding from the European Union's Horizon 2020 research and innovation programme under the Marie Skłodowska-Curie grant agreement No 81296.

REFERENCES

1. Sato, T. et al. Single Lgr5 stem cells build crypt-villus structures in vitro without a mesenchymal niche. *Nature* 459, 262–265 (2009).
2. Huch, M. et al. In vitro expansion of single Lgr5 + liver stem cells induced by Wnt-driven regeneration. *Nature* 494, 247–250 (2013).
3. Lancaster, M. A. et al. Cerebral organoids model human brain development and microcephaly. *Nature* 501, 373–379 (2013).
4. Takasato, M. et al. Kidney organoids from human iPS cells contain multiple lineages and model human nephrogenesis. *Nature* 526, 564–568 (2015).
5. Jin, L. et al. In vitro multilineage differentiation and self-renewal of single pancreatic colony-forming cells from adult C57Bl/6 mice. *Stem Cells Dev* 23, 899–909 (2014).
6. Barker, N. et al. Lgr5+ve Stem Cells Drive Self-Renewal in the Stomach and Build Long-Lived Gastric Units In Vitro. *Cell Stem Cell* 6, 25–36 (2010).
7. Lancaster, M. A. & Knoblich, J. A. Organogenesis in a dish: Modeling development and disease using organoid technologies. *Science* (1979) 345, (2014).
8. Schutgens, F. & Clevers, H. Human Organoids: Tools for Understanding Biology and Treating Diseases. (2019) doi:10.1146/annurev-pathmechdis.
9. Boonekamp, K. E. et al. Long-term expansion and differentiation of adult murine epidermal stem cells in 3D organoid cultures. *Proc Natl Acad Sci U S A* 116, 14630–14638 (2019).
10. Levin, G. et al. R-Spondin 1 (RSPO1) Increases Mouse Intestinal Organoid Unit Size and Survival in vitro and Improves Tissue-Engineered Small Intestine Formation in vivo. *Front Bioeng Biotechnol* 8, (2020).
11. Wrenn, E. D., Moore, B. M., Greenwood, E., McBirney, M. & Cheung, K. J. Optimal, Large-Scale Propagation of Mouse Mammary Tumor Organoids. *J Mammary Gland Biol Neoplasia* 25, 337–350 (2020).
12. DiStefano, T. et al. Accelerated and Improved Differentiation of Retinal Organoids from Pluripotent Stem Cells in Rotating-Wall Vessel Bioreactors. *Stem Cell Reports* 10, 300–313 (2018).
13. Kassis, T., Hernandez-Gordillo, V., Langer, R. & Griffith, L. G. OrgaQuant: Human Intestinal Organoid Localization and Quantification Using Deep Convolutional Neural Networks. *Sci Rep* 9, (2019).
14. Bian, X. et al. A deep learning model for detection and tracking in high-throughput images of organoid. *Comput Biol Med* 134, (2021).
15. Haja, A. & Schomaker, L. R. B. A Fully Automated End-to-End Process for Fluorescence Microscopy Images of Yeast Cells: From Segmentation to Detection and Classification. in *Lecture Notes in Electrical Engineering* vol. 784 LNEE 37–46 (Springer Science and Business Media Deutschland GmbH, 2022).
16. Broutier, L. et al. Culture and establishment of self-renewing human and mouse adult liver and pancreas 3D organoids and their genetic manipulation. *Nat Protoc* 11, 1724–1743 (2016).
17. He, K., Gkioxari, G., Dollár, P. & Girshick, R. Mask R-CNN. (2017).

18. Lu, A. X., Zarin, T., Hsu, I. S. & Moses, A. M. YeastSpotter: Accurate and parameter-free web segmentation for microscopy images of yeast cells. *Bioinformatics* 35, 4525–4527 (2019).
19. Rezaatofghi, H. et al. Generalized Intersection over Union: A Metric and A Loss for Bounding Box Regression.
20. Horcas-Nieto, J. M. et al. Organoids as a model to study intestinal and liver dysfunction in severe malnutrition. *Biochim Biophys Acta Mol Basis Dis* 1869, (2023).



Chapter



Docosahexaenoic acid prevents peroxisomal and mitochondrial protein loss in a murine hepatic organoid model of severe malnutrition

José M. Horcas-Nieto¹, W. Alfredo Rios-Ocampo¹, Miriam Langelaar-Makkinje¹, Rinse de Boer², Albert Gerding^{1,3}, Serhii Chornyj⁴, Ingrid A. Martini³, Justina C. Wolters^{1,5}, Ronald J. A. Wanders⁴, Hans R. Waterham⁴, Ida J. Van der Klei², Robert H.J. Bandsma^{1,6,7,8}, Johan W. Jonker¹, Barbara M. Bakker^{1S}

1. Laboratory of Pediatrics, Center for Liver, Digestive and Metabolic Diseases, University of Groningen, University Medical Center Groningen, The Netherlands; 2. Molecular Cell Biology, Groningen Biomolecular Sciences and Biotechnology Institute, University of Groningen, Groningen, The Netherlands; 3. Department of Laboratory Medicine, University of Groningen, University Medical Center Groningen, Groningen, The Netherlands; 4. Laboratory Genetic Metabolic Diseases, Amsterdam UMC Location AMC, University of Amsterdam, Amsterdam, Netherlands; 5. Interfaculty Mass Spectrometry Center, University of Groningen, University Medical Center Groningen, The Netherlands; 6. Translational Medicine Program, Peter Gilgan Centre for Research and Learning, The Hospital for Sick Children, Toronto, ON, Canada; 7. Department of Nutritional Sciences, Faculty of Medicine, University of Toronto, Toronto, ON, Canada; 8. Division of Gastroenterology, Hepatology, and Nutrition, The Hospital for Sick Children, Toronto, ON, Canada

§ Corresponding author:

Prof. dr. Barbara M Bakker

Department of Pediatrics, University of Groningen, University Medical Center Groningen
Antonius Deusinglaan 1, 9713 AV Groningen, The Netherlands Phone: +31 50 361 1542

Email: b.m.bakker01@umcg.nl

Manuscript in preparation

ABSTRACT

Introduction

Acute and chronic exposure to low amino acid conditions have been shown to lead to a reduction in hepatic peroxisomal and mitochondrial content. There is limited understanding of the underlying mechanisms behind this loss, but data suggests degradation through autophagy. Both organelles play a key role in fatty acid metabolism, which may explain why dysfunction in either one of them might lead to hepatic steatosis.

Methods

Using a previously established murine hepatic organoid model of severe malnutrition, we characterized the effects of prolonged amino-acid restriction on peroxisomal and mitochondrial protein levels and on autophagic flux. To do so, we developed concatemers of ¹³C-labelled peptide standards for quantification of over 50 different peroxisomal proteins. To assess the autophagic flux, we transduced hepatic organoids with a GFP-LC3-RFP-LC3ΔG probe. Finally, the effect of PPAR-α activation on peroxisomal loss was determined with various agonists.

Results

Prolonged (96 h) amino-acid restriction led to a more severe loss of peroxisomes than a 48 h restriction, and with a substantial induction of autophagic flux. This was accompanied by accumulation of intracellular triglycerides, loss of mitochondrial and peroxisomal proteins, and loss of peroxisomal functionality. While PPAR-α agonists WY-14643 and linoleic acid (LA) had no effect, docosahexaenoic acid (DHA) supplementation partly prevented peroxisomal and mitochondrial loss under amino-acid restricted conditions and partly inhibited autophagy.

Discussion

The potential of DHA to prevent loss of peroxisomes and mitochondrial functions in low protein diets and severe malnutrition warrants further causal and translational testing in preclinical models and clinical trials, including its use as nutritional supplement.

INTRODUCTION

Recent studies have identified the loss of peroxisomes and mitochondrial dysfunction as key consequences of low protein diets in rodents¹⁻³, leading to metabolic aberrations, similarly as was previously observed in malnourished children⁴. These results were recapitulated in vitro using hepatic organoids grown in a low amino acid environment⁵. Although these models have shed some light on the interplay of mitochondria and peroxisomes in malnutrition, little is known about the pathophysiology behind the loss of both organelles. Degradation of organelles in low amino acid concentrations has been previously linked to an increase in autophagic turnover⁶, which was also observed in malnourished rodents¹. Organelles such as peroxisomes and mitochondria are frequently degraded via selective autophagy^{7,8}. Autophagy helps to remove and degrade misfolded proteins or damaged organelles. Moreover, autophagy also helps maintaining adequate cellular levels of amino acids as precursors for biosynthesis or as fuels, when there is a shortage of these nutrients⁹. Prolonged autophagy and loss of peroxisomes and mitochondria, however, may affect their essential functions in lipid metabolism.

Staple foods high in carbohydrates, lack of access to varied diets, and food insecurity are common in developing countries. These factors, and specifically low protein diets, often lead to severe malnutrition in young children¹⁰, characterized by an imbalance in energy and nutrient intake in relation to the body's requirements. Malnutrition is regarded as one of the most severe deficiencies of macronutrients and it affects metabolic homeostasis, thus hampering healthy development of children. Severe acute malnutrition (SAM) is known as the most life-threatening type of malnutrition¹¹. Children with severe malnutrition commonly develop symptoms of hepatic dysfunction including hypoglycaemia, hypoalbuminemia and hepatic steatosis^{12,13}. Impaired lipid oxidation has also been observed in malnourished children, and is thought to be the main cause of hepatic steatosis^{14,15}. Post-mortem electron microscopy images showed a decreased number of peroxisomes and compromised mitochondria in the liver of malnourished children⁴. In agreement with the key role of these organelles in lipid metabolism, this is accompanied by the development of hepatic steatosis and increased oxidative stress in malnourished children.

Current management protocols often do not lead to rapid metabolic recovery¹⁶ and mortality remains high in acutely ill children with severe malnutrition¹⁷, which makes the need for new treatment approaches of high importance. Peroxisome proliferator-activated receptor (PPAR)- α is a transcriptional

factor within the family of nuclear receptors known to induce proliferation of peroxisomes and highly expressed in tissues involved in fatty acid metabolism, such as the liver¹⁸. Activation of PPAR- α increases the expression of genes involved in peroxisomal and mitochondrial β -oxidation, thereby upregulating the uptake, activation and oxidation of fatty acids¹⁹⁻²². Therefore, PPAR- α activation might recover peroxisomal number and mitochondrial health by upregulation of β -oxidation genes, as observed in malnourished rats supplemented with fenofibrate¹, and thereby reduce fat accumulation, at least in rodents. Some of the most commonly described PPAR- α ligands are synthetic compounds, such as fibrates. In addition, naturally occurring compounds, including long-chain polyunsaturated fatty acids (LCPUFA), have also been reported to be PPAR- α agonists²³. Promising results in improvement of cognition of severely malnourished children highlight the latter compounds as interesting dietary supplements²⁴.

Discovery of the organoid technology in 2009²⁵ has transformed the field of biomedicine, providing scientists with physiologically relevant in vitro disease models. Organoids are proliferative 3D structures, derived from primary tissue, adult stem cells or pluripotent stem cells. These structures contain different cell types and mimic the functions of the organ of origin²⁶. Organoids are valuable tools for the study of organ development, disease modelling and drug screening^{27,28}. They have also been shown to be a relevant system to study nutrient metabolism^{29,30} and metabolic diseases³¹. We have previously used organoids to model severe malnutrition using long-term exposure to low amino-acid levels. Although no amino acids were added to the medium, all amino acids were found in low concentrations, probably coming from degradation of the Matrigel or the cytokines and growth factors present in the medium⁵. The latter study recapitulated liver-specific phenotypes of malnutrition, including peroxisomal loss and mitochondrial dysfunction.

The aim of the present study was to use the previously established murine hepatic malnutrition in vitro model⁵ to gain more insight into the mechanisms of peroxisomal loss under different durations of exposure to low-amino acid conditions and assess the role of autophagy therein. Moreover three different PPAR- α agonists, including a synthetic ligand (WY-14643) and two long-chain polyunsaturated fatty acids (linoleic acid and docosahexaenoic acid), were tested to determine their ability to prevent peroxisomal loss. We used a GFP/RFP autophagic flux reporter system to quantify the effect of amino acid restriction and PPAR- α activation on autophagic flux. We conclude that the natural lipid docosahexaenoic acid (DHA) is a promising compound to explore

as pharmacological treatment for the protection of peroxisomal matrix and mitochondrial proteins in malnutrition.

RESULTS

Liver progenitor organoids generated from mice were differentiated into hepatocyte-like organoids and used for the study of amino-acid restriction, as previously described⁵.

Prolonged amino-acid deprivation leads to severe peroxisomal loss in mature hepatic organoids

To investigate the effect of the duration of amino-acid restriction on peroxisomal loss, hepatic organoids were exposed to amino-acid free medium for 48 or 96 h. Clearly, 96 h of amino acid restriction led to a more severe and significant decline in the levels of the peroxisomal marker proteins than 48 h (**Figure 1a and 1b**). Levels of PMP70, an ATP binding cassette transporter of fatty acids into the peroxisome, and one of the most abundant peroxisomal membrane proteins, were strongly reduced after amino acid starvation. Acyl-CoA oxidase 1 (ACOX1), the first enzyme of the peroxisomal β -oxidation, and catalase, the enzyme metabolising the hydrogen peroxide produced by ACOX1 and multiple other oxidases, were also significantly reduced after 48 or 96 h of amino-acid restriction compared to control cells (**Figure 1a and 1b**).

To obtain a more comprehensive insight into the different peroxisomal proteins affected by amino acid deprivation, we quantified several peroxisomal proteins by targeted proteomics³⁰. For the proteomic analysis, we designed and used as internal standards a panel of ¹³C-labelled peptides with the QconCAT technology³². These standards target 57 murine peroxisomal proteins as well as their human orthologues. Up to 28 peroxisomal proteins (depending on the experimental condition and amount of organoids), 4 of which have dual localization, were sufficiently abundant to be detected and quantified in the hepatic organoids. These included metabolite transporters, as well as enzymes of the β -oxidation and α -oxidation (**Supplementary Table 1**). Overall, a time-dependent reduction of these peroxisomal proteins was observed in response to amino-acid deprivation (**Figure 1c**).

Immunofluorescence analysis using antibodies against PMP70 revealed a reduced number of green punctae in the starved organoids, indicating a reduced number of peroxisomes, but only after 96 hours of amino-acid

deprivation (**Figure 1d and e**). In electron micrographs, double-membrane bound electron-dense structures, with peroxisome-like structures inside, appeared in the organoids depleted of amino acids for either 48 or 96 hours (**Figure 1f**). These structures probably represent autophagosomes or autolysosomes, suggesting autophagy is occurring, most likely also including degradation of peroxisomes. These results are in agreement with previous observations in amino-acid deprived cell cultures³³.

We then wondered if amino acid restriction also affected the biogenesis of peroxisomes. Peroxins (PEX) are proteins involved in various aspects of peroxisome biogenesis. Gene expression of these peroxins was assessed by qPCR. PEX3, PEX6 and PEX19 are essential peroxins for the assembly of peroxisomal membranes. Targeting and insertion of membrane proteins involved PEX19 as a cytosolic receptor protein, PEX3 works as a membrane anchoring site for cargo-loaded PEX19 and PEX16 as possible receptor for PEX3³⁴. The mRNA level of *PEX3* was significantly upregulated in amino-acid deprived organoids, while *PEX19* showed a downwards trend and *PEX16* remained unchanged. For the import of proteins into the peroxisome, PEX5 and PEX7 recognize cargo with Peroxisome Targeting Sequence 1 and 2 (PTS-1 and 2), respectively. Interestingly, mRNA level of *PEX7* was significantly downregulated, while *PEX5* was upregulated in amino-acid deprived organoids. The mRNA levels of *PEX1* and *PEX6*, peroxins involved in the protein import, remained unchanged. The mRNA level of *PEX11*, involved in peroxisomal fission³⁵, was increased upon amino acid removal (**Figure 1g**). These results indicate that amino-acid deprivation in hepatic organoids differently affects expression of mRNAs encoding peroxisomal biogenesis proteins.

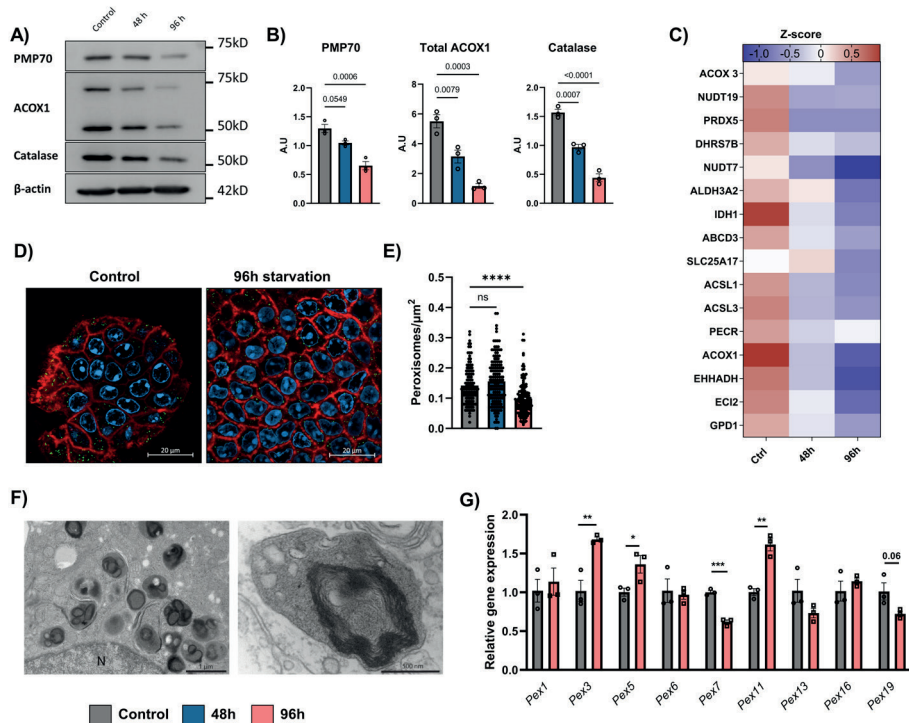


Figure 1. Longer amino-acid restriction lead to more severe loss of peroxisomal proteins and induces the formation of autophagosome-like structures. (A) Representative immunoblot images. (B) Protein levels relative to β-actin. Quantification of data shown in A and replicates thereof. For ACOX1 quantification, antibody intensities of both bands were summed. Organoids were grown in complete medium (control) or in amino-acid restricted medium for 48h or 96h. Data represent mean ± SEM from 3 biological replicates obtained from independent experiments (* $P < 0.05$, ** $P < 0.01$, ordinary one-way ANOVA with Tukey's post-hoc test). (C) Heatmap representing targeted proteomics data from control conditions, 48 h of amino-acid restriction and 96 h of amino-acid restriction. Data represents 4 biological replicates. (D) Representative single Airyscan slice immunofluorescence images. On the left side control organoids and on the right organoids after 96 hours in low amino acid conditions. Peroxisomes stained for PMP70 in green, with DAPI nuclei counter stain (blue) and phalloidin (red). Scale bar, 10 μm. (E) Quantification of number of peroxisomes per μm² per cell based on PMP70 staining in D from 3 biological replicates (* $P < 0.05$, ** $P < 0.01$, *** $P < 0.001$ ordinary one-way ANOVA). (F) Electron microscopy images upon 48 and 96 hour amino-acid restricted organoids showing double-membrane electron-dense structures. N; nucleus. (G) Relative gene expression of peroxins in organoids in control condition or in amino-acid restricted for 96 hours. Data represent mean ± SEM from 3 biological replicates (* $P < 0.05$, ** $P < 0.01$, unpaired t-test).

Amino-acid restriction increases autophagic flux in mature hepatocyte-like organoids

The previously reported reduction of mitochondrial proteins⁵, together with reduction of peroxisomal proteins and the appearance of structures resembling autophagosomes, suggests altered autophagy in the amino-acid deprived cultures. Increased appearance of autophagosomes might result either from a stabilization of autophagosomes due to an impairment in the last steps of the autophagic process, or from an increase in the formation of autophagosomes, coinciding with an elevated autophagic flux.

To functionally quantify the autophagic flux in the organoids, we established a system based on expression of the GFP-LC3-RFP-LC3ΔG probe, as reported by Kaizuka et al.³⁶ Upon autophagy activation, ATG4 cleaves the probe into equal amounts of GFP-LC3 and RFP-LC3ΔG. GFP-LC3 is then degraded in a normal way, while RFP-LC3ΔG is stable, and therefore not degraded, and works as an internal standard. Liver progenitor organoids were transduced to express the autophagic flux probe as described on **Figure 2a**. Two days post-transduction, stable progenitors were harvested and the cells were sorted to get an enriched population of double positives for the expression of both GFP and RFP (**Figure 2b,c**).

Figure 2b shows the gating strategy used for the enrichment of double positive cells. From the whole population (gate A) we excluded duplets and cellular aggregates (gate B); the enriched population is depicted in gate C (**Figure 2b**). As expected³⁶, amino-acid deprivation activated the autophagy flux in the organoids, as can be inferred from a reduced GFP/RFP ratio (**Figure 2d, e**).

While after 48 hours of amino-acid restriction there was only a mild downward trend of the GFP/RFP ratio (**Figure 2d upper panel, e**), after 96 hours the GFP/RFP ratio was substantially and significantly reduced, indicating a clear time-dependent activation of autophagy (**Figure 2d lower panel, e**). Surprisingly, the autophagy inhibitor bafilomycin A1 caused only minor increase of the GFP/RFP ratio in 48 h starved organoids, without any effect after 96 h (**Figure 2d, e**). Interestingly, while amino-acid restriction-induced autophagy could not be prevented with chloroquine, chemically-induced autophagy (using rapamycin) could be prevented by chloroquine co-treatment (**Supplementary Figure 1**). This may indicate that prolonged amino-acid-restriction induced autophagy is not sensitive to classical autophagy inhibitors such as Bafilomycin A1 (**Figure 2d lower panel, e**) and chloroquine (**Supplementary Figure 1**).

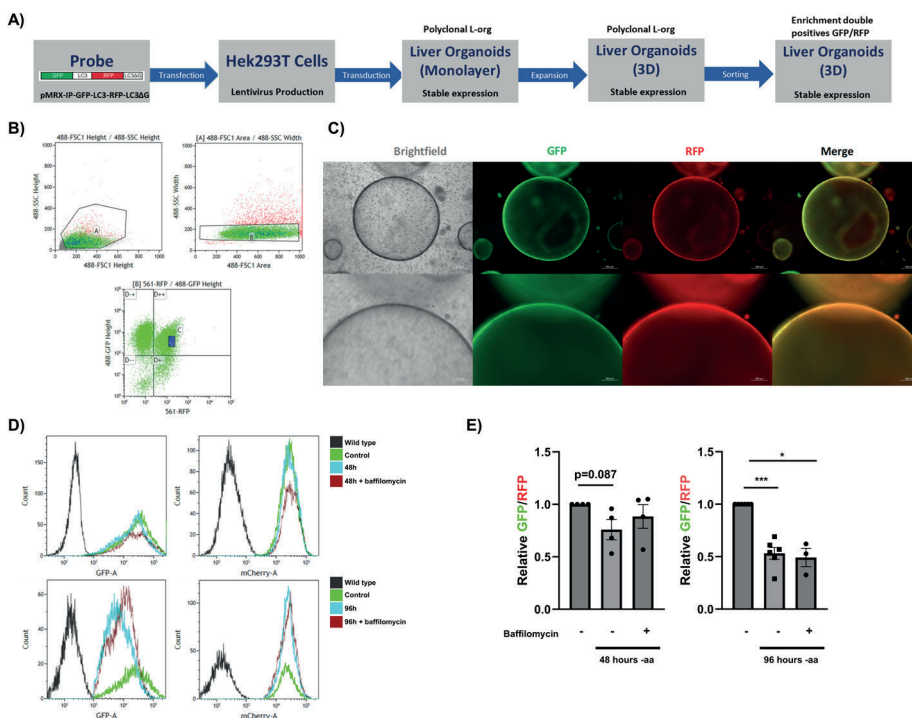


Figure 2. Amino-acid restriction induces activation of autophagic flux in pMRX-IP-GFP-LC3-RFP-LC3ΔG liver organoids. (A) Scheme of generation of pMRX-IP-GFP-LC3-RFP-LC3ΔG organoids. (B) Gating strategy for organoid sorting. First graph indicates the whole population. Second graph depicts the gating for single cells excluding aggregates. Third graph illustrates the separating based on GFP and RFP expression. (C) Representative brightfield and IF images of pMRX-IP-GFP-LC3-RFP-LC3ΔG liver organoids. Scale bar 100 μm. (D) Representative cytograms depicting the GFP and RFP intensities measured in the cells under different conditions. Wild type organoids (grey), organoids expressing pMRX-IP-GFP-LC3-RFP-LC3ΔG grown in complete amino acid medium (green), in amino acid restricted medium (blue), or in amino-acid restricted medium with bafilomycin A1 (maroon). Analysis was performed after 48 h (upper two graphs) or 96 h (bottom two graphs). (E) Left graph represents GFP/RFP fluorescence intensities ratio in organoids under control condition or in amino-acid restricted medium 48 h (left) or 96 h (right) and treated or untreated with 100nM bafilomycin. Data represent mean ± SEM from at least 3 biological replicates. Right graph shows GFP/RFP fluorescence intensities ratio in organoids under control conditions or in amino-acid restricted medium for 96 hours, and treated or untreated with bafilomycin. Data represent mean ± SEM from at least 3 biological replicates (*P < 0.05, **P < 0.01, one sample t test)

Screening PPAR- α agonist for the prevention of peroxisomal loss in hepatic organoids

Peroxisome proliferator-activated receptor α (PPAR- α) is a nuclear receptor that works as a ligand-regulated transcriptional factor. PPAR- α is activated by a wide range of ligands, of which synthetic fibrates are most widely described³⁷. It can, however, also be activated by natural ligands such as various fatty acids and eicosanoid derivatives²¹.

Here, we assessed the effect of three PPAR- α agonists on peroxisomal proliferation and fatty acid metabolism in amino-acid restricted organoids. We tested one synthetic compound (WY-14643) and two polyunsaturated fatty acids: linoleic acid (18:2 ω 6 fatty acid) and docosahexaenoic acid (DHA, C26: ω 3). Linoleic acid (LA) did not rescue any of the peroxisomal protein markers PMP70, ACOX1, or catalase (**Figure 3a,b**), whereas PPAR- α agonist WY-14643 had only a minor rescuing effect on ACOX1. ACOX1, is synthesized as 75 kDa polypeptide, which upon import into the peroxisome is proteolytically cleaved into two smaller peptides, 21 kDa and 55 kDa³⁸. Supplementation of the highest dose (200 μ M) of WY-14643 prevented the loss of the uncleaved, 75 kDa protein, while the smaller (53 kDa) was almost significant. (**Figure 3c,d**). In contrast, the natural compound DHA prevented the loss of catalase and the 55 kDa form of ACOX1 in dose dependent manner, with a complete rescue to control levels at the highest dose. DHA did not affect levels of PMP70 nor of the uncleaved form of ACOX1 (75 kDa) (**Figure 3e, f**). Since LA and WY-14643 did not show any protection against peroxisomal loss, the effect of DHA might be mediated via a PPAR- α -independent mechanism.

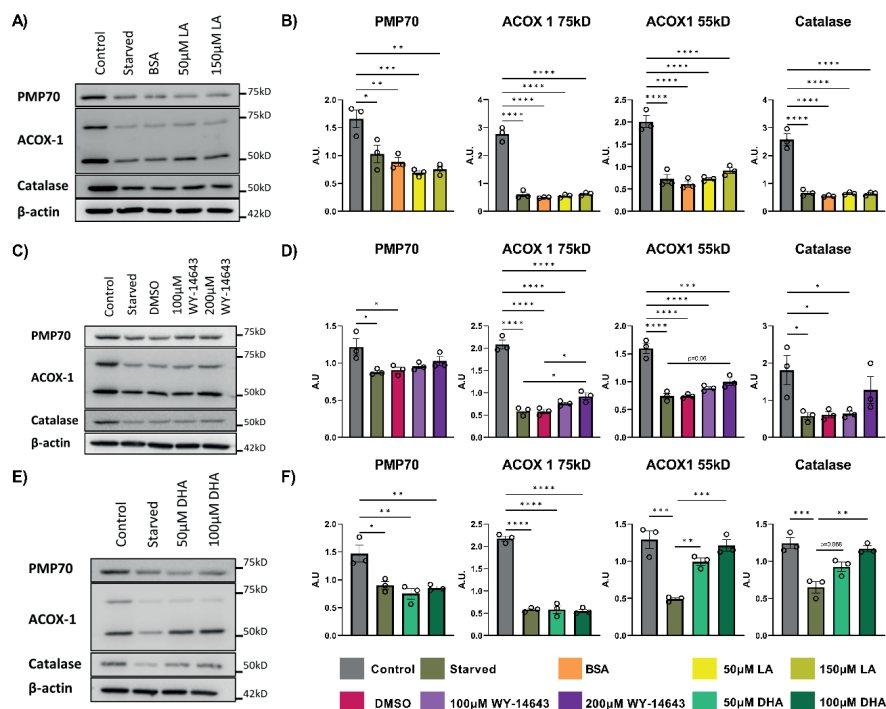


Figure 3. Effects of the different PPAR- α agonists on peroxisomal protein levels in amino-acid restriction conditions. Organoids were grown in complete medium (Control) or in restriction medium for 96 hours (Starved), restriction medium with vehicle (DMSO) or (BSA), and in the presence of two different concentrations of LA (50 μ M and 150 μ M), WY-14643 (100 μ M and 200 μ M) or DHA (50 μ M and 100 μ M) (A, C, E) Representative immunoblot images (B,D,F) Peroxisomal protein levels relative to β -actin. Quantification of data shown in A, C, and E, respectively, and replicates thereof. Data represent mean \pm SEM from 3 biological replicates (biological replicates are obtained from independent experiments) (* P < 0.05, ** P < 0.01, ordinary one-way ANOVA with Tukey's post-hoc test).

Effect of DHA on mitochondrial and peroxisomal proteome

Since DHA had the largest rescuing effect on peroxisomal marker proteins, we set out to analyse the effect of this compound more comprehensively, using quantitative, targeted proteomics. Next to the above described peroxisomal protein panel, also previously validated panels of proteins involved in mitochondrial metabolism³², and glucose and glycogen metabolism³⁹ were analysed. The results replicated the overall reduction of peroxisomal proteins upon amino-acid deprivation (Fig. 4a), and additionally showed a clear reduction of proteins involved in mitochondrial fatty-acid β -oxidation, TCA cycle and oxidative phosphorylation (Fig. 4b). The highest dose of DHA

supplementation prevented this loss of peroxisomal and mitochondrial proteins (**Fig. 4a** and **b**). Enzymes involved in glycolysis, gluconeogenesis and glycogen metabolism showed a milder downregulation upon amino acid removal, some of which were normalised by DHA (**Supplementary Figure 4**).

Effects of DHA supplementation on peroxisomal function and health

Since DHA supplementation recovered peroxisomal and mitochondrial proteins, including enzymes involved in fatty acid oxidation (FAO), we hypothesized that it could also decrease the levels of intracellular triglycerides (TG). In line with our earlier observations⁵ amino-acid restriction led to a mildly elevated TG level in the hepatic organoids. Contrarily to what was expected, DHA supplementation did not reduce the TG level. However, given that the organoids were stimulated with a fatty acid, we cannot rule out an increase in β -oxidation. The higher concentration of DHA even led to a further accumulation of intracellular triglycerides when compared to the restriction conditions (**Figure 4c**). This could be caused by incorporation of DHA into phospholipids, inducing other fatty acids to be used to TG synthesis or even by direct incorporation of DHA into TG.

To continue assessing peroxisomal functionality, we studied the ability of peroxisomes to metabolize phytanoyl-CoA in control and starved organoids as we previously reported⁵. Phytanic acid is a branched-chain fatty acid that is primarily oxidized by the peroxisomal α -oxidation, yielding pristanic acid as a product, which subsequently undergoes peroxisomal β -oxidation^{40,4} (**Figure 4d**). Mature hepatic organoids were incubated with 25 μ M of phytol. Amino-acid restricted organoids had substantially lower levels of phytanic and pristanic acid than control organoids, suggesting that peroxisomal fatty-acid oxidation is affected. Since pristanic acid is an intermediate metabolite in the pathway, however, the effect on the flux of peroxisomal fatty oxidation is unclear. Moreover, DHA supplementation did not affect the levels of phytanic or pristanic acid at any concentration (**Figure 4e**).

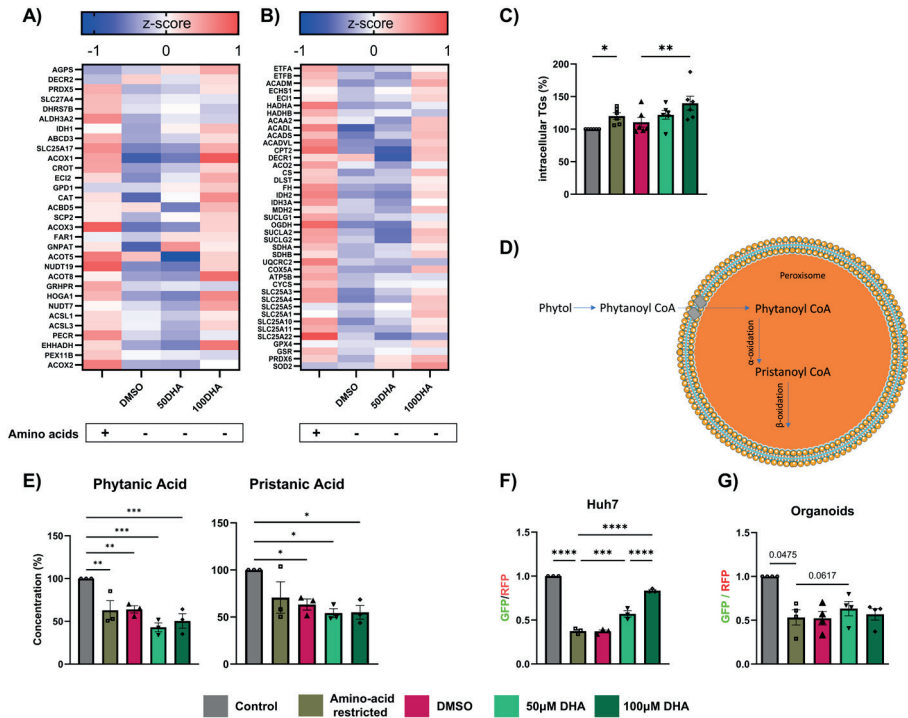


Figure 4. DHA supplementation prevents the loss of multiple peroxisomal and mitochondrial proteins and prevents autophagy in amino-acid restricted (96 h) organoids. Organoids were grown in complete medium (Control) or in amino-acid restriction medium for 96 h (Starved) with DMSO or DHA (50 μ M and 100 μ M) (A) Heat map of peroxisomal proteins detected including several metabolic pathways and transporters quantified using targeted proteomics. (B) Heat map of mitochondrial proteins detected including fatty acid oxidation, TCA cycle, ETC and reactive oxygen species detoxification quantified using targeted proteomics. Z-scores were used to normalize the data and protein abbreviations are used according to Uniprot. (In red high Z-score indicating upregulated proteins and in blue low Z-score indicating downregulated proteins). (C) Triglycerides levels in control, starved (96 hours) and starved treated with DMSO (vehicle) and 50 and 100 μ M of DHA (as per color legend). Data represents 6 biological replicates from independent experiments \pm SEM (* P < 0.05, ordinary one-way ANOVA with Tukey's post hoc test). (D) Scheme of the metabolism of phytol into phytanoyl-CoA and pristanoyl-CoA in the peroxisome. (E) Concentration of phytanic and pristanic acid in the supernatant of organoids. Data represents 3 biological replicates \pm SEM (* P < 0.05, ** P < 0.01, RM One-way ANOVA with Tukey's post-hoc test). (F) GFP/RFP fluorescence intensities ratio in Huh7 cells in control conditions and 48 h of amino-acid restriction treated and untreated with DMSO or DHA (50 and 100 μ M). Data represent mean \pm SEM from 3 biological replicates (* P < 0.05, ** P < 0.01 One-way ANOVA with Tukey's post-hoc test). (G) GFP/RFP fluorescence intensities ratio in organoids expressing pMRX-IP-GFP-LC3-RFP-LC3 Δ G. Data represent mean \pm SEM from 3 biological replicates (* P < 0.05, ** P < 0.01 One-way ANOVA with Tukey's post-hoc test).

Effects of DHA on peroxisomal biogenesis and autophagy

Given that DHA supplementation increased the overall pattern of peroxisomal and mitochondrial proteins, we investigated the effect of DHA on both peroxisomal biogenesis and autophagic degradation. DHA nor any of the other compounds tested showed any effect on the peroxins involved in peroxisomal biogenesis (**Supplementary figure 2**). In a first test on Huh7 cells transduced with the pMRX-IP-GFP-LC3-RFP-LC3ΔG construct, 48 hours of amino-acid restriction induced autophagic flux, similarly to what was observed in the hepatic organoids. Autophagic flux decreased to control levels after DHA treatment in a dose-dependent manner (**Figure 4f**), but was not affected by the other PPAR-α agonists, WY-14643 or LA (**Supplementary Figure 3**). These results are in agreement with what was previously observed in oxidative stress-induced autophagy and TNF-α-induced autophagy^{41,42}. In the GFP-LC3-RFP-LC3Δ hepatic organoids, the activation of autophagic flux by 96 h of amino-acid deprivation was replicated, but it was not rescued by DHA (**Figure 4g**). The effect of DHA on autophagy, at least in the Huh7 cell line, goes in line with the observed prevention of peroxisomal and mitochondrial protein loss. The results suggest, however, that in the organoids the rescue of peroxisomal and mitochondrial proteins by DHA might occur via an autophagy-independent mechanism.

DISCUSSION

In this study we have demonstrated that prolonged amino acid restriction leads to peroxisomal loss with increased autophagic degradation and alterations in peroxisomal biogenesis in a murine hepatic organoid model. To assess autophagic flux we have implemented the use of the novel GFP-LC3-RFP-LC3ΔG probe in the hepatic organoids. Using targeted proteomics, we then demonstrated that DHA supplementation prevented the loss of both peroxisomal and mitochondrial proteins in the context of amino acid restriction.

Mechanisms of peroxisomal loss in amino acid restriction and potential therapeutic interventions

Amino-acid deficiency has been previously linked with peroxisomal loss⁴³, however, the mechanisms behind this process in malnutrition still remain unclear. While the main cause of peroxisomal loss in amino-acid starvation has been described to be pexophagy⁴³, these studies focused on the effect of

complete amino-acid starvations. However, little is known about the longer-term effects of exposure to low amino-acid levels in contrast to complete and shorter starvations. Moreover, there is little information available on the effect of amino-acid restriction on peroxisomal biogenesis.

In this study, hepatic organoids were grown in amino acid restricted medium but not in complete starvation conditions. Organoids were still exposed to low levels of amino acids coming from the Matrigel, in which the organoids are cultured, or potentially from the degradation of growth factors present in the medium as specified in previous literature⁵. These conditions mimic low protein diets (LPD) like in *in vivo* conditions better.

Several groups have demonstrated that autophagy is altered in rodents in response to low protein diets at a very young age¹⁻³. The results reported here are in agreement with those observed in rats on a 1 week low protein diet. However, when rodents were subjected to a prolonged LPD, autophagy was hampered, both in liver and intestine. In the liver of rats fed a low protein diet for 1 week, LC3II was increased while P62 was downregulated, suggesting autophagy to be increased. In contrast, exposure to LPD for 4 weeks led to an increase in p62, which was interpreted as a block in autophagy¹. Similarly, studies using mice on LPD for 2 weeks reported a reduction of autophagy. However, while in both cases the protein levels of LC3-II were downregulated, one of the studies also reported a downregulation of the LC3II/I² while the other did not³. Given the nature of *in vivo* work, all of these studies assessed autophagy by western blotting and only a snapshot of the pathway was provided at a given time point.

Here we demonstrated that organoids are a dynamic and accessible tool to study autophagic flux in the context of amino acid restriction. To do so, we implemented the use of a dynamic probe (GFP-LC3-RFP-LC3ΔG)³⁶, developed for the study of autophagy in live cells. We reported that 96 h amino acid restriction led to an induction of autophagy, as also observed in rats on LPD for a short time and in other *in vitro* models under amino acid starvation³³.

With respect to peroxisomal biogenesis, rodents fed a low protein diet for 4 weeks did not show any regulation in gene expression of peroxins involved in peroxisomal biogenesis¹. In the present study, we have demonstrated that amino acid restriction has an impact on the expression of genes involved in peroxisomal biogenesis. Since some genes were upregulated and others downregulated we could not draw any clear conclusions. However, further characterization of this differential regulation might help identify the functional impact. Conspicuously, both catalase and ACOX1 are imported

into the peroxisome via PTS1, which then binds to PEX5. Nonetheless, PEX5 is clearly upregulated in the amino-acid deprived conditions, which does not go in line with the decrease in both catalase and ACOX1. This might indicate a compensatory mechanism in order to promote peroxisomal import in conditions with lower number of peroxisomes.

Different therapeutics, including peroxisomal and mitochondrial biogenesis activators as well as autophagy regulators, have been tested in order to prevent peroxisomal and mitochondrial loss and hepatic dysfunction in the context of malnutrition. Activation of PPAR- α activates peroxisomal and mitochondrial biogenesis as well as genes encoding enzymes involved in peroxisomal and mitochondrial fatty acid oxidation^{22,44,45}. In order to prevent peroxisomal and mitochondrial loss in the context of malnutrition, PPAR- α agonist fenofibrate has been previously tested both in vitro and in vivo^{1,5}. Fenofibrate supplementation recovered the levels of peroxisomal protein marker PMP70 and lowered hepatic triglycerides while increasing the levels of ATP in a LPD rat model¹. Fibrates have been widely used for the treatment of dyslipidemia and to induce the biogenesis of peroxisomes and mitochondria ameliorating the hepatic phenotype⁴⁶. Fibrates however cause some side effects. When PPAR- α *null* mice were administered fenofibrate, the levels of serum triglycerides were decreased, but intrahepatic TGs were significantly increased⁴⁷. These results suggest that these compounds might not be ideal candidates to treat malnourished children.

In the case of malnourished children, treatment with dietary supplements is attractive as a simple and safe approach when compared to synthetic compounds such as fibrates. Conveniently, polyunsaturated fatty acids have also been reported to be potent PPAR activators⁴⁸. These compounds can be found in foods and can be easily supplemented on ready-to-use foods (RTUF) already used in refeeding protocols for malnourished children.

Docosahexaenoic acid is a potential candidate to prevent peroxisomal loss in in vivo conditions

Docosahexaenoic acid is an ω -3 LCPUFA commonly found in seafood, seaweed and breast milk. It can also be synthesized from α -linolenic acid (ALA)⁴⁹. DHA plays an important role in many metabolic processes, and can be found in the bloodstream, lipid stores and cell membranes. Adequate levels of DHA in infants have been linked with optimal development⁵⁰. Moreover, low levels of DHA were found in breast milk from mothers from malnourished children and

it was suggested that DHA levels in malnourished children highly depend on the DHA intake from breast milk⁵¹.

The effects of DHA supplementation have been previously tested in the context of malnutrition. For instance, supplementation in malnourished rats led to a decrease in the production of malondialdehyde (MDA) in blood, a lipid peroxidation marker that reports oxidative stress. It also increased the levels of superoxide dismutase⁵², together suggesting that DHA supplementation may reduce oxidative stress. A clinical study in malnourished Malawian children showed that RUTF supplemented with DHA led to an increase in the Malawi Developmental Assessment Tool (MDAT) score. This could be attributed to its clear cognitive benefit and increase in levels of 1-palmitoyl-2-eicosapentaenoyl-sn-glycero-3-phosphocholine, an ω 3 fatty acid that is important for regulation of cognition⁵³. In line with this, breast-milk LCPUFA levels were linked to neural maturation of breastfed infants^{54,55}. These reports in combination emphasize the potential of DHA as a beneficial supplement for the treatment of malnourished children.

To the best of our knowledge, there are no reports on the effect of DHA on the peroxisomal and mitochondrial content in the liver of malnourished children. Moreover, the fact that WY-14463 and LA showed no effect on peroxisomal recovery suggests that the effects of DHA might not be PPAR- α related. In fibroblasts from patients carrying defects in peroxisomal β -oxidation, DHA supplementation induced peroxisomal elongation via oligomerization of PEX11 β and peroxisomal division via DLP1, thus boosting peroxisomal content⁵⁶. This mechanism might potentially explain the higher levels of peroxisomal proteins in DHA treated organoids in our study.

It needs to be investigated whether DHA prevents peroxisomal loss in vivo during exposure to an LPD. When combining all information, both the effect of LDP and of DHA seem context dependent. The LPD induced autophagy in a short-term experiment¹. DHA blocked autophagy activation in Huh7 cells, had no effect on autophagy in amino-acid deprived hepatic organoids (this study), and was previously reported to activate autophagy in the presence of amino acids, via mTORC⁵⁷. One study reported that DHA inhibited oxidative stressed-induced autophagy via the AMPK-dependent signaling pathway⁴², while another showed a decrease in autophagy markers in TNF- α -induced autophagy⁴¹. This suggests that DHA may act via multiple routes in a context dependent manner. That PPAR- α activators (WY-14463 and LA) had no effect on the Huh7 (**Supplementary Figure 3**), may be explained by the generally low effect of PPAR- α activators on human cells in contrast to rodent cells⁵⁸.

In a broader perspective it will be interesting to test co-supplementation with vitamin B3 (nicotinamide or nicotinamide ribose), which was previously found to rescue mitochondrial function in the liver of LPD-treated mice². A combination of nutritional supplements might synergistically improve mitochondrial and peroxisomal function as well as organ function.

Conclusions

In conclusion, we found that docosahexaenoic acid prevents the loss of some peroxisomal and mitochondrial proteins in a hepatic organoid model of malnutrition. Our results warrant testing of DHA as a potential dietary supplement in a more physiologically relevant animal model of severe malnutrition.

METHODS

Isolation of biliary ducts and organoid culture

Hepatic organoids lines were established using mouse biliary ducts isolated from the liver of male C57BL/6J mice between 3 and 5 weeks of age (Jackson Laboratory, Bar Harbor, ME, USA) following the previously reported protocol⁵⁹.

Ductal fragments were placed in isolation medium (IM) consisting of Advanced DMEM/F12 (Gibco), supplemented with 10 mM HEPES, 1x GlutaMax, 1% Penicillin-Streptomycin (all Gibco), 1x N2-Supplement (Invitrogen), 1X B27-Supplement without vitamin A (Invitrogen), 10 mM Nicotinamide (Sigma Aldrich), 1.25 mM N-AcetylCysteine (Sigma Aldrich), 10% Rspodin-1 condition medium (kindly provided by Calvin J. Kuo), 30% Wnt3a conditioned medium (kindly provided by Hans Clevers), 100 ng/ml Noggin, 50 ng/ml HGF, 100 ng/ml FGF-10, 50 ng/ml EGF (all Peprotech), 10 nM Leu-gastrin (Sigma Aldrich) and 10 μ M Y 27632 dihydrochloride (Axon Medchem). Three days after isolation, Wnt3a CM and Noggin were removed from the medium. Y 27632 dihydrochloride was removed 4 days after isolation. Medium without Wnt3a-CM and Noggin was used to keep the organoids in culture and referred to as expansion medium (EM).

Medium was changed every 2-3 days and they were passaged every 7-9 days in a split ratio 1:6 – 1:9 on average.

In order to differentiate the organoids into more mature hepatocyte-like organoids, after passage they were kept in EM medium for 3 days and then

changed into differentiation medium (DM) containing: Advanced DMEM/F12 (Gibco), supplemented with 10 mM HEPES, 1x GlutaMax, 1% Penicillin-Streptomycin, 1x N2-Supplement, 1X B27-Supplement without vitamin A, 10 mM Nicotinamide, 1 mM N-AcetylCysteine, 100 ng/ml FGF-10, 50 ng/ml EGF, 10 nM Leu-gastrin, 50 nM A-83-01 (Axon Medchem) and 10 μ M DAPT (Sigma). Between day 13 and 16, the medium was supplemented with 3 μ M dexamethasone (Sigma Aldrich). These protocols were based on published literature⁵⁹.

Malnutrition in organoids using amino acid free medium

In order to mimic the effects of a low protein diet, mature hepatic organoids were cultured in a custom-made amino acid-free medium as previously reported⁵.

Organoids were kept in complete DM until day 12, when they were changed into restriction differentiation medium that contained all the same supplements but was completely depleted of all amino acids. Organoids were kept in starvation for 96 h until the end of day 16 when they were collected for further studies. In the case of the shorter (48 h) amino acid restrictions, organoids were kept in complete DM until day 14, when they were changed into restriction medium and collected at the end of day 16.

Fluorescence microscopy

Hepatic organoids were fixed with 1% formaldehyde in 0.1M PBS pH 7.4 for 15 min. Organoids were blocked and permeabilized in 0.1 M PBS with 20mM glycine, + 3% (w/v) BSA (9048-46-8; Fisher Scientific) and 0.1% (w/v) saponin (47036-50G-F; Sigma-Aldrich) pH 7.4 for 60 min at RT. Organoids were incubated with antibodies against PMP70 (Sigma: P0497) 1:400 in the same buffer. Subsequently organoids were washed in PBS three times and incubated with donkey anti-rabbit IgG (H+L) Alexa Fluor 488 (A21206; Thermo Fisher Scientific, Invitrogen) at 1:800 dilution. For actin labeling, phalloidin Alexa Fluor 546 was used (A22283; Thermo Fisher Scientific) at 1:200 dilution in parallel with the labeling with secondary antibodies. Organoids were imaged in PBS containing DAPI. All steps were performed in a glass bottom 96 wells plate. Airyscan images were captured with a confocal microscope (LSM800; Carl Zeiss) equipped with a 32-channel gallium arsenide phosphide photomultiplier tube (GaAsP-PMT), Zen 2009 software (Carl Zeiss), and a 40 \times 1.20 NA objective (Carl Zeiss). Peroxisome numbers per cell were quantified using Fiji. For each cell the grey values are adapted to visualize and quantify the separate peroxisomes because of the difference in staining intensities between the edge and the

middle part of the organoids. For each cell the number of peroxisomes per square micron is calculated from three biological replicates.

Electron microscopy

Hepatic organoids were incubated in DMEM on ice to dissolve the Matrigel. Organoids were washed in 0.1M sodium cacodylate (103256; Millipore) pH 7.2 and fixed for 75 min with 2% glutaraldehyde (G7661; Sigma-Aldrich) in sodium cacodylate. Organoids were post fixed with 1% osmium tetroxide (19134; Electron Microscopy Sciences) and 1% ferrocyanide in sodium cacodylate for 60 min. Samples were *en bloc* stained O/N with 0.5% uranyl acetate, dehydrated in series of ethanol and embedded in epon. 80 nm thin sections were collected on carbon evaporated formvar copper grids and analyzed with a CM12 transmission electron microscope (Philips) running at 100 kV.

Therapeutic interventions with different PPAR- α agonists

Mature hepatic organoids were cultured in complete DM until day 12. The organoids were then placed in amino acid free DM supplemented with different PPAR-alpha agonists at different concentrations. WY-14643 (Axon Medchem) was tested at two different concentrations 100 and 200 μ M based on literature reports⁶⁰⁻⁶². Docosahexaenoic acid (DHA) (Sigma Aldrich) was tested at two different concentrations 50 and 100 μ M^{63,64}. Linoleic Acid (Sigma Aldrich) was tested at two different concentrations 50 and 150 μ M^{65,66}. The vehicles DMSO and fatty acid-free BSA were tested in the same volume as that of the higher concentration of the compounds used.

Transfection of Hek293T cells for production of γ -retroviral particles.

Hek293T packaging cells were seeded in a 10 cm standard tissue culture dish to reach a confluency of 80%. Transfection of cells was performed using 7.0 μ g of Retroviral transfer plasmid pMRX-IP/GFP-LC3-RFP-LC3 Δ G (kindly provided by Noboru Mizushima, Department of Biochemistry and Molecular Biology, University of Tokyo, Tokyo, Japan; Addgene plasmid #84572; (<http://n2t.net/addgene:84572>; RRID:Addgene_84572)³⁶, 7.5 μ g pGag/Pol, 2.5 μ g pVSV-G packaging vectors and 1 μ g pAdvantage expression enhancer. The plasmid mix was added to PEI (Polysciences Inc. Cat N: 23966-2) transfection reagent prepared in Opti-MEMTM Reduced Serum Medium (Gibco, Cat N: 31985062) at 1:5 ratio (plasmid DNA Mix:PEI). The final mix was added to Hek293T cells dropwise. Media from viral particles producing-cells (10mL) was collected

after 24 h and 48 h and filtered through a 0.45 μm SFCA filter (Corning, Cat N: 431220). Finally, 0.5 μL of polybrene (4mg/mL stock concentration) (SIGMA, Cat N: H9268-5G) per mL of media was added to enhance retroviral transduction. For transduction of target cells, 1 mL or 2 mL (depending on experiment design) of retroviral supernatant was used. Then, target cells were incubated for at least 24 hours at 37°C and 5% CO₂.

Establishment of LC3B-GFP-RFP-LC3 Δ G liver organoids

Organoids were collected in Advanced DMEM/F12 and kept on ice for 10 minutes to disrupt the Matrigel. Organoids were then centrifuged at 290G for 5 minutes and reconstituted in 1mL of pre-warmed Trypsin for 5 minutes. Then, mechanical disruption of the organoids was used to dissociate them into single cells. 10 mL of advanced DMEM/F12 were added and the organoids were centrifuged again to remove the trypsin. Cells were counted and approximately 4×10^5 cells were placed in 500 μL of expansion medium supplemented with 10 μM Y 27632 dihydrochloride. Equal volume of viral medium, produced as described in the previous section, was added and placed into a 24 well plate well (pre-coated with Matrigel). The cells were kept in the incubator at 37°C for 48 h. Cells were then trypsinized and collected. After removal of the trypsin, the cells were reconstituted in advanced DMEM/F12 and Matrigel (1:3) and plated in domes. Expansion medium was supplemented with 10 μM Y 27632 dihydrochloride. After 24 h, the medium was changed to selection medium (EM containing Puromycin 1:500)

FACS sorting of stable mouse liver organoids expressing the autophagic flux probe

In order to isolate single clonal progenitors of liver organoids that properly express the autophagic flux probe GFP-LC3-RFP-LC3 Δ G (double positive cells) and exclude GFP-LC3 Δ G cells caused by homologous recombination during the transfection and transduction procedures reported by Kaizuka et al., 2016³⁶ we sorted the polyclonal stable liver organoids and performed an enrichment of GFP-RFP double positive cells. In brief, polyclonal liver organoids were harvested and individualized as previously mentioned. Cells were kept on ice in FACS buffer containing 1X HBSS (Gibco), 2% FCS (Gibco), 2% BSA, 1% Penicillin-Streptomycin (P/S). Cell sorting was performed using the MoFlo Astrios EQ Cell Sorter (Beckman Coulter, Life sciences) with a 100 μm nozzle and the 488 nm and 561 nm lasers. Sort rate was set up to 25.000 events/sec and approximately 1.000.000 double positive events were recorded and

harvested in a FACS tube containing 2 mL of expansion medium supplemented with 10 μ M Y 27632 dihydrochloride and 2 μ g/mL puromycin selection treatment followed by a centrifugation step at 290G for 5 minutes; then the pellet was reconstituted in 1 mL of pre-warmed expansion medium supplemented with puromycin (2 μ g/mL). Cells were counted and viability was determined by trypan blue staining (higher than 90%). Approximately 5000 sorted cells were reconstituted in advanced DMEM/F12 and Matrigel (1:3 ratio) and plated in domes in 24 well plates. The organoids were maintained in 500 μ L expansion medium supplemented with 10 μ M Y 27632 dihydrochloride and 2 μ g/mL puromycin selection treatment and kept in the incubator at 37°C and 5% CO₂. Enough liver progenitors were seeded and expanded for either performing experiments or storage in liquid nitrogen. Two days after sorting the formation of new liver organoids was confirmed as well as the expression of GFP and RFP were determined by fluorescence microscopy.

Generation of stable HuH7 cells expressing the autophagic flux probe

Wild-type HuH7 cells were seeded in control medium containing DMEM supplemented with 1% P/S and 10% FCS in a 6 well plate a day before transduction and kept in the incubator at 37°C and 5% CO₂. Cells were transduced with 2 mL of retroviral supernatant and incubated for 48 h. Next day and 48h after transduction cells were checked for positive GFP and RFP expression by fluorescence microscopy. After 48 h post-transduction, cells were harvested and expanded for two consecutive passages. The transduced-HuH7 cells were maintained in DMEM-GlutaMAX (Gibco, NL) media supplemented with 10% FCS, 1% P/S and 2 μ g/mL puromycin. The cells generated in this step were considered polyclonal stable HuH7 cells expressing the autophagic flux probe GFP-LC3-RFP-LC3 Δ G, in short cells were called Poly-HuH7-3 Δ G. In order to produce single monoclonal HuH7 cells that properly express the autophagic flux probe GFP-LC3-RFP-LC3 Δ G (double-positive cells) and exclude homologous recombination during the transfection and transduction procedures reported by Kaizuka et al., 2016³⁶ we sorted the polyclonal cells. In short, polyclonal HuH7 cells were harvested and kept on ice in FACS buffer containing 1X HBSS, 2% FCS, 2% BSA, 1% P/S. Cell sorting was performed using the MoFlo Astrios EQ Cell Sorter (Beckman Coulter, Life sciences) with a 100 μ m nozzle equipped with the 488 nm and 561 nm lasers. Sort rate was set up to 25.000 events/sec and individual sort mode was used. Single double-positive (GFP/RFP) cells were dripped in 96-well plates previously filled with 200 μ L of standard cultured media supplemented with 2 μ g/mL puromycin. A total of 3 96-well

plates were filled with single double-positive cells to increase the chance of colonies growing. Sorted cells in 96-well plates were followed for the formation of single colonies with homogeneous shape for not longer than 12 days; wells with more than one colony were discarded. Seven colonies were followed and expanded under selection media with puromycin (2 $\mu\text{g}/\text{mL}$) and storage for further characterization.

Measuring of autophagic flux by FACS

Stable monoclonal-HuH7-3 ΔG cells or enriched-LivOrg-3 ΔG were grown in either control conditions (Ad. DMEM containing 1% P/S and 10% FCS) or in amino-acid restricted medium (a custom-made amino acid-free medium containing 1% P/S and 10% FCS). Organoids were treated with 150 nM of rapamycin to chemically induce autophagy. Bafilomycin A1 was used at 100 nM and Chloroquine at 50 μM . Cells were harvested using Accutase (Sigma, Cat N A9664-500ML) and individualized according with the methodology previously described. Cells were kept on ice in FACS buffer containing 1X HBSS, 2% FCS, 2% BSA. Cells were analyzed with the BD LSR-II cytometer (BD, Biosciences) equipped with a 488 nm laser and 561 nm laser. Samples were acquired using DIVA 8.0 software and at least 10.000 events for each sample were acquired. Data was saved as FCS 3.0 or 3.1 files and compensation was not required in any case. Data was processed with Kaluza software (Beckman Coulter). For calculating the autophagic activity, the GFP and RFP mean fluorescence intensity (MFI) (Geometric mean) was used to calculate the GFP/RFP ratio which reversely correlates with autophagic activity.

Immunoblotting

The protocol used for Western blotting was based on a previously published paper⁶⁷. Ice cold Ad.DMEM/F12 (with or without amino acids) was used to collect organoids, and these were kept on ice for 10 minutes. Organoids were then centrifuged at 290G for 5 minutes and washed with PBS once. After a second centrifugation, they were reconstituted in 200 μL of radio immunoprecipitation assay buffer (1% IGEPAL CA-630, 0.1% SDS, and 0.5% sodium deoxycholate in PBS) supplemented with Complete Protease Inhibitor Cocktail (Cat. No. 1186145001; Sigma-Aldrich), Phosphatase Inhibitor Cocktail 2 (Cat. No. P5726; Sigma Aldrich) and Cocktail 3 (Cat. No. P0044; Sigma Aldrich). Organoids were then sonicated using a 30% amplitude four times for 10 seconds using Sonics Vibra cell VCX130 (Sonics & Materials inc.). Protein concentrations were measured using Pierce BCA Protein Assay Kit (Thermo Scientific) and all the

samples were adjusted to the lowest concentration of all the samples. The lysates were further processed in the same way as previously described. Signals were normalized to a loading control (β -actin) as indicated. The list of antibodies used can be found in **Supplementary Table 2**.

RNA isolation, reverse transcription and real time qPCR

Total RNA was extracted from the organoids using the commercially available RNase easy Kit (Qiagen) as described by the manufacturer. The purity and quantity of the RNA was assessed using NanoDrop (NanoDrop Technologies). For the reverse transcription M-MLV Reverse Transcriptase (200 U/ μ l) (Invitrogen) was used as established by the manufacturer. qPCR was performed in 384 well format in duplicates (10 ng per well) using FastStart Universal SYBR Green Master (Rox) (Sigma Aldrich). qPCR was performed using QuantStudio 7 Flex (Thermo Fischer Scientific). All primer (Integrated DNA technologies Inc.) sequences are listed in **Supplementary Table 3**.

Fat isolation and quantification of triglycerides

Organoids were collected in ice-cold Ad.DMEM/F12 (with or without amino acids) and left in ice for 10 minutes to disrupt the Matrigel. The organoids were pelleted and washed with PBS. They were then reconstituted in ice-cold 1X TBS. Fat was isolated using chloroform: methanol in a 2:1 ratio and levels of intracellular triglycerides were quantitatively determined using the DiaSys Triglyceride FS kit. All the results were normalized to protein content.

Quantitative targeted proteomics

Quantitative targeted proteomics were performed following the published protocol by Wolters et al³². Organoids were collected in ice-cold Ad. DMEM/ F12 (with or without amino acids) and incubated in ice for 10 minutes to disrupt Matrigel. The organoids were then centrifuged at 290G and the pellets were washed with cold PBS to ensure Matrigel removal. Pellets were then reconstituted in lysis buffer (0.1% v/v NP40, 0.4 M NaCl, 10 mM Tris-HCl and 1 mM EDTA, pH 8.0) supplemented with Complete Protease Inhibitor Cocktail (Cat. No. 1186145001; Sigma-Aldrich), Phosphatase Inhibitor Cocktail 2 (Cat. No. P5726; Sigma Aldrich) and Cocktail 3 (Cat. No. P0044; Sigma Aldrich). Organoids were then sonicated using a 30% amplitude for four times for 10 seconds using Sonics Vibra cell VCX130 (Sonics & Materials inc.). Protein concentrations were measured using Pierce BCA Protein Assay Kit (Thermo Scientific) and all the samples were adjusted to the lowest concentration of all the samples.

Isotopically-labelled concatemer derived standard peptides were selected for the targets of interest (QconCAT technology, PolyQuant GmbH). In-gel digestion, LC-MS and analysis were performed as previously described by Wolters et al³². The list of peptides used for targeted proteomics of peroxisomal proteins can be found in **Supplementary Table 1**.

Branched chain fatty acids measurements

Organoids were incubated with 25 μ M phytol (Sigma Aldrich) for 48 h prior to quenching with ice-cold methanol. Methanol was then evaporated under a constant stream of N₂. The remaining pellet was reconstituted in PBS and using a 30% amplitude for four times for 10 seconds using Sonics Vibra cell VCX130 (Sonics & Materials inc.). Samples were further processed as previously described⁵.

Statistical Analysis

Results are expressed as mean \pm standard error of the mean (SEM). Biological replicates are considered as independent experiments using independent organoid lines. Analyses were performed using GraphPad Prism Software Version 9.02 (Graphpad Software). Statistical significance between comparisons is provided in figure's legends. no indication means no significant changes (ns).

FUNDING

This project has received funding from the European Union's Horizon 2020 research and innovation programme under the Marie Skłodowska-Curie grant agreement No 812968, and by the Netherlands Organisation for Health Research and Development under grant number 435005013.

ACKNOWLEDGEMENTS

We would like to thank Niels Kloosterhuis and Marieke Smit for their technical support with animal work. We would like to thank Nicolette Huijkman for the lentivirus production and establishment of stable cell lines. We would also like to thank Tjaša Košir for her advice on the choice of PEX transcript and interpretation.

REFERENCES

1. van Zutphen T, Ciapaite J, Bloks VW, et al. Malnutrition-associated liver steatosis and ATP depletion is caused by peroxisomal and mitochondrial dysfunction. *J Hepatol.* 2016;65(6):1198-1208. doi:10.1016/j.jhep.2016.05.046
2. Hu G, Ling C, Chi L, et al. The role of the tryptophan-NAD⁺ pathway in a mouse model of severe malnutrition induced liver dysfunction. *Nat Commun.* 2022;13(1). doi:10.1038/s41467-022-35317-y
3. Arvidsson Kvissberg ME, Hu G, Chi L, et al. Inhibition of mTOR improves malnutrition induced hepatic metabolic dysfunction. *Sci Rep.* 2022;12(1). doi:10.1038/s41598-022-24428-7
4. Doherty JF, Golden MH, Brooks SE. Peroxisomes and the fatty liver of malnutrition: an hypothesis. *Am J Clin Nutr.* 1991;54:674-681. doi:10.1093/ajcn/54.4.674
5. Horcas-Nieto JM, Versloot CJ, Langelaar-Makkinje M, et al. Organoids as a model to study intestinal and liver dysfunction in severe malnutrition. *Biochim Biophys Acta Mol Basis Dis.* 2023;1869(3). doi:10.1016/j.bbadis.2022.166635
6. Liu C, Ji L, Hu J, et al. Functional amino acids and autophagy: Diverse signal transduction and application. *Int J Mol Sci.* 2021;22(21). doi:10.3390/ijms222111427
7. Glick D, Barth S, Macleod KF. Autophagy: Cellular and molecular mechanisms. *Journal of Pathology.* 2010;221(1):3-12. doi:10.1002/path.2697
8. Mizushima N. SnapShot: Organelle degradation. *Mol Cell.* 2022;82(8):1604-1604.e1. doi:10.1016/j.molcel.2022.03.015
9. Singh R, Cuervo AM. Autophagy in the cellular energetic balance. *Cell Metab.* 2011;13(5):495-504. doi:10.1016/j.cmet.2011.04.004
10. Briend A. Collaborating to Improve the Management of Acute Malnutrition Worldwide Kwashiorkor: Still an Enigma-the Search Must Go On.; 2014. www.cmamforum.org
11. World Health Organization Geneva MANAGEMENT OF SEVERE MALNUTRITION: A MANUAL FOR PHYSICIANS AND OTHER SENIOR HEALTH WORKERS.
12. Bandsma RHJ, Mendel M, Spoelstra MN, et al. Mechanisms Behind Decreased Endogenous Glucose Production in Malnourished Children. *Pediatr Res.* Published online 2010. doi:10.1203/PDR.0b013e3181f2b959
13. Wharton B. Hypoglycaemia in children with Kwashiorkor. *The Lancet.* 1967;295(7639):171-173. doi:10.1016/s0140-6736(70)90408-3
14. Badaloo A V, Forrester T, Reid M, Jahoor F. Lipid kinetic differences between children with kwashiorkor and those with marasmus. *Am J Clin Nutr.* Published online 2006. doi:10.1093/ajcn/83.6.1283
15. Badaloo A, Reid M, Soares D, Forrester T, Jahoor F. Relation between liver fat content and the rate of VLDL apolipoprotein B-100 synthesis in children with protein-energy malnutrition. *Am J Clin Nutri.* Published online 2005. doi:10.1093/ajcn/81.5.1126
16. di Giovanni V, Bourdon C, Wang DX, et al. Metabolomic changes in serum of children with different clinical diagnoses of malnutrition. *Journal of Nutrition.* 2016;146(12):2436-2444. doi:10.3945/jn.116.239145

17. Diallo AH, Sayeem Bin Shahid ASM, Khan AF, et al. Childhood mortality during and after acute illness in Africa and south Asia: a prospective cohort study. *Lancet Glob Health*. 2022;10(5):e673-e684. doi:10.1016/S2214-109X(22)00118-8
18. Lalwani ND, Reddy MK, Qureshi SA, et al. Evaluation of Selected Hypolipidemic Agents for the Induction of Peroxisomal Enzymes and Peroxisome Proliferation in the Rat Liver. *Human Toxicol*. 1983;2:27-48. doi:10.1177/096032718300200103
19. Motojima K, Passilly P, Peters JM, Gonzalez FJ, Latruffe N. Expression of Putative Fatty Acid Transporter Genes Are Regulated by Peroxisome Proliferator-activated Receptor and Activators in a Tissue-and Inducer-specific Manner*. *J Biol Chem*. 1998;273(27):16710-16714. doi:10.1074/jbc.273.27.16710
20. Tugwood JD, Issemann I, Anderson RG, Bundell KR, McPheat WL, Green S. The mouse peroxisome proliferator activated receptor recognizes a response element in the 5' flanking sequence of the rat acyl CoA oxidase gene. *EMBO Journal*. 1992;11(2):433-439. doi:10.1002/j.1460-2075.1992.tb05072.x
21. Berger J, Moller DE. The Mechanisms of action of PPARs. *Annu Rev Med*. 2002;53:409-435. doi:10.1146/annurev.med.53.082901.104018
22. Van Raalte DH, Li M, Haydn Pritchard P, Wasan KM. Peroxisome Proliferator-Activated Receptor (PPAR): A Pharmacological Target with a Promising Future. *Pharm Res*. 2004;21:1531-1538. doi:10.1023/b:pham.0000041444.06122.8d
23. Echeverría F, Ortiz M, Valenzuela R, Videla LA. Long-chain polyunsaturated fatty acids regulation of PPARs, signaling: Relationship to tissue development and aging. *Prostaglandins Leukot Essent Fatty Acids*. 2016;114:28-34. doi:10.1016/j.plefa.2016.10.001
24. Rahmawaty S, Meyer BJ. Stunting is a recognized problem: Evidence for the potential benefits of ω -3 long-chain polyunsaturated fatty acids. *Nutrition*. 2020;73. doi:10.1016/j.nut.2019.110564
25. Sato T, Vries RG, Snippert HJ, et al. Single Lgr5 stem cells build crypt-villus structures in vitro without a mesenchymal niche. *Nature*. 2009;459(7244):262-265. doi:10.1038/nature07935
26. Kretzschmar K, Clevers H. Organoids: Modeling Development and the Stem Cell Niche in a Dish. *Dev Cell*. 2016;38(6):590-600. doi:10.1016/j.devcel.2016.08.014
27. Lancaster MA, Knoblich JA. Organogenesis in a dish: Modeling development and disease using organoid technologies. *Science (1979)*. 2014;345(6194). doi:10.1126/science.1247125
28. Schutgens F, Clevers H. Human Organoids: Tools for Understanding Biology and Treating Diseases. Published online 2019. doi:10.1146/annurev-pathmechdis
29. Zietek T, Giesbertz P, Ewers M, et al. Organoids to Study Intestinal Nutrient Transport, Drug Uptake and Metabolism – Update to the Human Model and Expansion of Applications. *Front Bioeng Biotechnol*. 2020;8. doi:10.3389/fbioe.2020.577656
30. Mun SJ, Lee J, Chung KS, Son MY, Son MJ. Effect of microbial short-chain fatty acids on cyp3a4-mediated metabolic activation of human pluripotent stem cell-derived liver organoids. *Cells*. 2021;10(1):1-13. doi:10.3390/cells10010126
31. Hu W, Lazar MA. Modelling metabolic diseases and drug response using stem cells and organoids. *Nat Rev Endocrinol*. 2022;18(12):744-759. doi:10.1038/s41574-022-00733-z

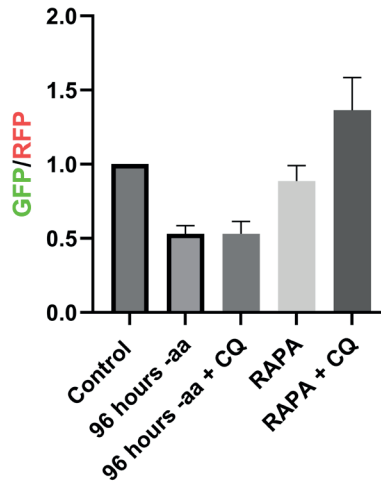
32. Wolters JC, Ciapaite J, Van Eunen K, et al. Translational Targeted Proteomics Profiling of Mitochondrial Energy Metabolic Pathways in Mouse and Human Samples. *J Proteome Res.* 2016;15(9):3204-3213. doi:10.1021/acs.jproteome.6b00419
33. Sutton MN, Huang GY, Zhou J, et al. Amino acid deprivation-induced autophagy requires upregulation of DIRAS3 through reduction of E2F1 and E2F4 transcriptional repression. *Cancers (Basel).* 2019;11(5). doi:10.3390/cancers11050603
34. Farré J, Mahalingam SS, Proietto M, Subramani S. Peroxisome biogenesis, membrane contact sites, and quality control. *EMBO Rep.* 2019;20(1). doi:10.15252/embr.201846864
35. Kobayashi S, Tanaka A, Fujiki Y. Fis1, DLP1, and Pex11p coordinately regulate peroxisome morphogenesis. *Exp Cell Res.* 2007;313(8):1675-1686. doi:10.1016/j.yexcr.2007.02.028
36. Kaizuka T, Morishita H, Hama Y, et al. An Autophagic Flux Probe that Releases an Internal Control. *Mol Cell.* 2016;64(4):835-849. doi:10.1016/j.molcel.2016.09.037
37. Grygiel-Górniak B. Peroxisome proliferator-activated receptors and their ligands: Nutritional and clinical implications - A review. *Nutr J.* 2014;13(1). doi:10.1186/1475-2891-13-17
38. Osumi T, Hashimoto T, Ui N. *Purification and Properties of Acyl-CoA Oxidase from Rat Liver 1.* Vol 87.; 1980. <https://academic.oup.com/jb/article-abstract/87/6/1735/2186664>
39. Vieira-Lara MA, Dommerholt MB, Zhang W, et al. Age-related susceptibility to insulin resistance arises from a combination of CPT1B decline and lipid overload. *BMC Biol.* 2021;19(1). doi:10.1186/s12915-021-01082-5
40. Wanders RJA, Komen J, Ferdinandusse S. Phytanic acid metabolism in health and disease. *Biochim Biophys Acta Mol Cell Biol Lipids.* 2011;1811(9):498-507. doi:10.1016/j.bbalip.2011.06.006
41. Pacheco FJ, Almaguel FG, Evans W, et al. Docosahexanoic acid antagonizes TNF- α -induced necroptosis by attenuating oxidative stress, ceramide production, lysosomal dysfunction, and autophagic features. *Inflammation Research.* 2014;63(10):859-871. doi:10.1007/s00011-014-0760-2
42. Tatsumi Y, Kato A, Niimi N, et al. Docosahexaenoic Acid Suppresses Oxidative Stress-Induced Autophagy and Cell Death via the AMPK-Dependent Signaling Pathway in Immortalized Fischer Rat Schwann Cells 1. *Int J Mol Sci.* 2022;23(8). doi:10.3390/ijms23084405
43. Sargent G, Zutphen T van, Shatseva T, et al. PEX2 is the E3 ubiquitin ligase required for pexophagy during starvation. *Journal of Cell Biology.* 2016;214(6). doi:10.1083/jcb.201511034
44. Kersten S, Seydoux J, Peters JM, Gonzales FJ, Desvergne B, Wahli W. Peroxisome proliferator-activated receptor α mediates the adaptive response to fasting. *J Clin Invest.* Published online 1999. doi:10.1172/JCI6223
45. Contreras A V., Torres N, Tovar AR. PPAR- α as a key nutritional and environmental sensor for metabolic adaptation. *Advances in Nutrition.* 2013;4(4):439-452. doi:10.3945/an.113.003798
46. Katsiki N, Nikolic D, Montalto G, Banach M, Mikhailidis DP, Rizzo M. The Role of Fibrate Treatment in Dyslipidemia: An Overview. *Curr Pharm Des.* 2013;19:3124-3131. doi:10.2174/1381612811319170020

47. Yan F, Wang Q, Xu C, et al. Peroxisome proliferator-activated receptor α activation induces hepatic steatosis, suggesting an adverse effect. *PLoS One*. 2014;9(6). doi:10.1371/journal.pone.0099245
48. Keller H, Dreyert C, Medint J, Mahfoudi A, Ozato: K, Wahli W. Fatty acids and retinoids control lipid metabolism through activation of peroxisome proliferator-activated receptor-retinoid X receptor heterodimers (peroxisome proliferator-activated receptor response element/retinoid X receptor response element/acyl-CoA oxidase gene/nuclear hormone receptors). *Proc Natl Acad Sci USA*. 1993;90:2160-2164. doi:10.1073/pnas.90.6.2160
49. Burdge GC, Calder PC. Conversion of α -linolenic acid to longer-chain polyunsaturated fatty acids in human adults. *Reprod Nutr Dev*. 2005;45(5):581-597. doi:10.1051/rnd:2005047
50. Calder PC. Docosahexaenoic acid. *Ann Nutr Metab*. 2016;69(1):8-21. doi:10.1159/000448262
51. Smit EN, Oelen EA, Seerat E, Muskiet FAJ, Boersma ER. Breast milk docosahexaenoic acid (DHA) correlates with DHA status of malnourished infants. *Arch Dis Child*. 2000;82(6):493-494. doi:10.1136/ad.82.6.493
52. Sanyoto DD, Asnawati A, Triawanti T. Effect of DHA Supplementation on the MDA and SOD Levels in Protein Malnourished Rats. In: *Journal of Physics: Conference Series*. Vol 1374. Institute of Physics Publishing; 2019. doi:10.1088/1742-6596/1374/1/012036
53. Stephenson K, Callaghan-Gillespie M, Maleta K, et al. Low linoleic acid foods with added DHA given to Malawian children with severe acute malnutrition improve cognition: a randomized, triple-blinded, controlled clinical trial. *American Journal of Clinical Nutrition*. 2022;115(5):1322-1333. doi:10.1093/ajcn/nqab363
54. Jensen CL, Lapillonne A. Docosahexaenoic acid and lactation. *Prostaglandins Leukot Essent Fatty Acids*. 2009;81(2-3):175-178. doi:10.1016/j.plefa.2009.05.006
55. Thomas Brenna J, Varamini B, Jensen RG, Diersen-Schade DA, Boettcher JA, Arterburn LM. Docosahexaenoic and arachidonic acid concentrations in human breast milk worldwide. *Am J Clin Nutr*. 2007;85:1457-1464. doi:10.1093/ajcn/85.6.1457
56. Itoyama A, Honsho M, Abe Y, Moser A, Yoshida Y, Fujiki Y. Docosahexaenoic acid mediates peroxisomal elongation, a prerequisite for peroxisome division. *J Cell Sci*. 2012;125(3):589-602. doi:10.1242/jcs.087452
57. Jing K, Song KS, Shin S, et al. Docosahexaenoic acid induces autophagy through p53/AMPK/mTOR signaling and promotes apoptosis in human cancer cells harboring wild-type p53. *Autophagy*. 2011;7(11):1348-1358. doi:10.4161/auto.7.11.16658
58. Broutier L, Andersson-Rolf A, Hindley CJ, et al. Culture and establishment of self-renewing human and mouse adult liver and pancreas 3D organoids and their genetic manipulation. *Nat Protoc*. 2016;11(9):1724-1743. doi:10.1038/nprot.2016.097
59. Shin MH, Lee SR, Kim MK, Shin CY, Lee DH, Chung JH. Activation of peroxisome proliferator-activated receptor alpha improves aged and UV-irradiated skin by catalase induction. *PLoS One*. 2016;11(9). doi:10.1371/journal.pone.0162628
60. Hwang YP, Won SS, Jin SW, et al. WY-14643 regulates CYP11B1 expression through peroxisome proliferator-activated receptor α -mediated signaling in human breast cancer cells. *Int J Mol Sci*. 2019;20(23). doi:10.3390/ijms20235928

61. Wang R, Zhao J, Jin J, et al. WY-14643 attenuates lipid deposition via activation of the PPAR α /CPT1A axis by targeting Gly335 to inhibit cell proliferation and migration in ccRCC. *Lipids Health Dis.* 2022;21(1). doi:10.1186/s12944-022-01726-7
62. Enguita M, Razquin N, Pamplona R, Quiroga J, Prieto J, Fortes P. The cirrhotic liver is depleted of docosahexaenoic acid (DHA), a key modulator of NF- κ B and TGF β pathways in hepatic stellate cells. *Cell Death Dis.* 2019;10(1). doi:10.1038/s41419-018-1243-0
63. Luo W, Li L, Xu W, Zhang J, Xu J. Toxic effects of docosahexaenoic acid treatment in the rat liver BRL-3A cell. *Toxics.* 2021;9(5). doi:10.3390/toxics9050112
64. Tang KS. Protective effect of arachidonic acid and linoleic acid on 1-methyl-4-phenylpyridinium-induced toxicity in PC12 cells. *Lipids Health Dis.* 2014;13(1). doi:10.1186/1476-511X-13-197
65. Butler M, Huzel N, Barnabé N, Gray T, Bajno L. Linoleic acid improves the robustness of cells in agitated cultures. *Cytotechnology.* 1999;30(1-3):27-36. doi:10.1023/a:1008048126055
66. Heberle AM, Navas PR, Langelaar-Makkinje M, et al. The PI3K and MAPK/p38 pathways control stress granule assembly in a hierarchical manner. *Life Sci Alliance.* 2019;2(2). doi:10.26508/lsa.201800257

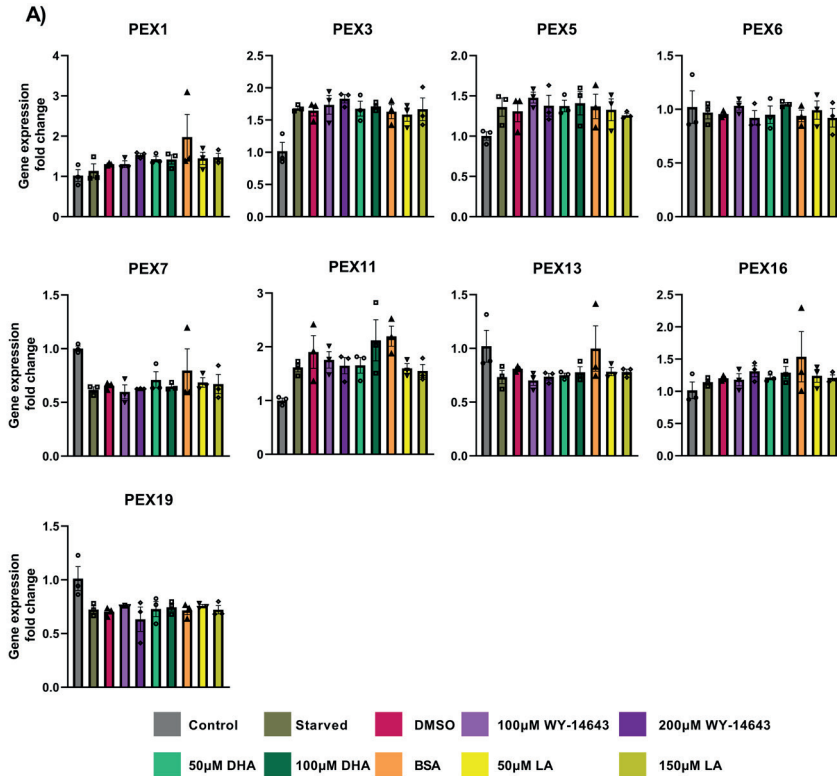
SUPPLEMENTARY FILES

Supplementary Figure 1. Effect of chloroquine on autophagy flux in hepatic organoids.



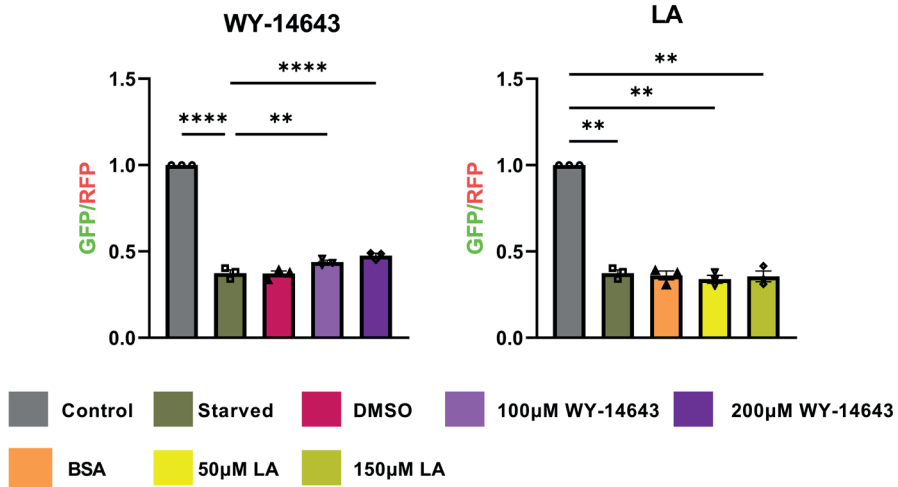
GFP/RFP fluorescence ratio in organoids in control conditions (Control) and 96 h of amino acid starvation treated and untreated with 50 μ M Chloroquine. Organoids were also treated with 150nM Rapamycin with and without Chloroquine. Data represent mean \pm SEM from 2 biological replicates.

Supplementary Figure 2. Effect of PPAR- α agonists on peroxisomal biogenesis.



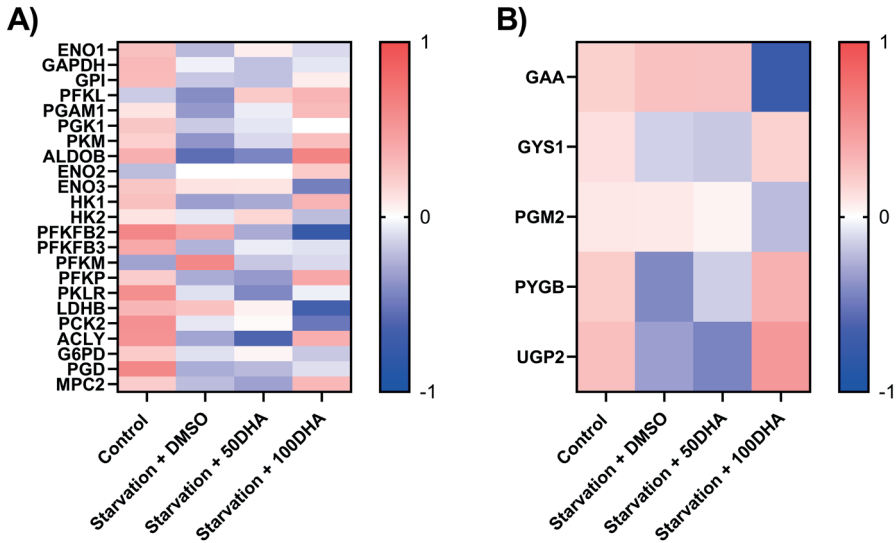
(A) Relative gene expression of different peroxisomal biogenesis markers. Organoids were grown in complete culture medium (Control) or in starvation medium for 96 h (Starved), starvation medium with vehicle (DMSO) and (BSA) and in the presence of two different concentrations of WY-14643 (100 μ M and 200 μ M), DHA (50 μ M and 100 μ M) and LA (50 μ M and 150 μ M). Data represent mean \pm SEM from 3 biological replicates (biological replicates are obtained from independent experiments).

Supplementary Figure 3. Effect of PPAR- α agonists on autophagic flux



(A) GFP/RFP fluorescence intensities ratio in Huh7 cells in control conditions and 48 h of amino acid starvation treated and untreated with DMSO (vehicle) or WY-14643 (100 μ M or 200 μ M). Data represent mean \pm SEM from 3 biological replicates (* P < 0.05, ** P < 0.01, **** P < 0.001 RM One-way ANOVA) **(B)** GFP/RFP fluorescence ratio in Huh7 cells in control conditions and 48 h of amino acid starvation treated and untreated with BSA (vehicle) or Linoleic acid (50 μ M or 150 μ M). Data represent mean \pm SEM from 3 biological replicates (* P < 0.05, ** P < 0.01 RM One-way ANOVA)

Supplementary figure 4. Effect of DHA on glycolysis, gluconeogenesis and pentose phosphate pathway.



Organoids were grown in complete culture medium (Control) or in starvation medium for 96 hours with vehicle (DMSO) and or DHA (50 μ M and 100 μ M). (A) Heatmap of enzymes involved in glycolysis, gluconeogenesis and PPP (Z-score normalized per protein). (B) Heatmap of enzymes involved in glycogen metabolism (z-score normalized per protein).

Supplementary Table 1. List of all proteins included in the peroxisomal targeted proteomics and the peptide sequence.

M denotes the peptide is mouse and HM for both mouse and human

Protein	Peptide sequence
FA2H_M	LFHSDLIEAFSK
FA2H_HM	SGFGISTK
HACL1_HM	LNWILHFGLPPR
HACL1_HM	SEEQVSGAK
ACOX3_M	GGYISGEQTGR
ACOX3_M	TVDFLEAYPGILGQK
AGPS_M	GISDPLTVFEHTAAAAR
AGPS_HM	YGSVAFPNFEQGVACLK
FAR1_HM	ALAEYVVQEGAK
FAR1_HM	APAFLYDIYLR
GNPAT_HM	LYWAVFSEYVK
GNPAT_HM	VCVNEEQIK
ACOT5_M	DIIDILNVPLEAPDQK
ACOT5_M	GPGVGLLGISK
ACOT6_M	GPNIIGLIGVSK
ACOT6_M	GQFPPIIDLYGSIGGLCEHR
CRAT_HM	ALQPIVSEEEWAHTK
CRAT_HM	QDFVDLQGQLR
HAO2_HM	EDAELAVK
HAO2_M	GIIVSNHGGR
DECR2_M	GQVLQLHAGAAK
DECR2_HM	HLAVEWGPQNIR
NUDT12_HM	AIAHQLIK
NUDT12_M	HIANLLANAK
NUDT19_M	FGLGPEPPR
NUDT19_M	FLPGAHVFPGGVLDAADSSPDWVR
CYP4F18_M	CCTQDIVLPDGVISR
PRDX5_M	THLPGFVEQAGALK
PRDX5_HM	VNLAELEFK
ABCD1_HM	ETGLLALHSAALVSR
ABCD1_HM	TFLSVYVAR
ABCD2_HM	GASPIGPTLLAGLVVYATAK
ABCD2_HM	IIVNVEEIAFYR
PEX11A_HM	LCLTLANLNR

PEX11A_M	NFCDILIPLNQLGIYK
PXMP2_M	AVSSGILSALGNLLAQTIK
PXMP2_M	LLEVSGLLR
SLC16A7_HM	AVTVFFK
SLC16A7_M	LLDITGEYK
SLC27A4_HM	ILSFVYPIR
SLC27A4_HM	QLDEYSSSVANFLQAR
PHYH_M	GTLKPHDYPK
PHYH_M	IQDFQEDELFR
DHRS7B_M	HATQAFFDCLR
DHRS7B_M	TLAPGLFFR
FAR2_HM	NVWFFIVSFCYK
FAR2_HM	SILITGATGFLGK
ACOT12_M	FIENATPDGLK
ACOT12_M	SVVLPSVPSSPQYIR
ACOT3_M	ASLNSLVGGPVIWGGEP
ACOT3_M	DIVDLLNPLEGPDQK
ACOT3_M	SLIPVER
ACOT4_M	IVNEAVIWGGEVK
ACOT4_M	SELYTQIASDR
ACOT8_HM	SVSEDEVHVHSLHCYFVR
ACOT8_M	VVNPPTLTLQLALEPK
GRHPR_HM	FLYTGR
GRHPR_M	VFVTGPLPAEGR
HOGA1_M	APLQELSPTEEEALR
HOGA1_HM	DSGGDVTR
NUDT7_M	FSVLVPLLAR
NUDT7_M	LAVLVALIILEQSPAFK
ALDH3A2_M	YLAPTILTDVDPNSK
ALDH3A2_M	YSFDTFSHQRPCLLK
IDH1_HM	GWPLYLSTK
IDH1_HM	TVEAEAAHGTVTR
LDHB_HM	DYSVTANSK
LDHB_HM	IVVVTAGVR
ABCD3_HM	IANPDQLLTQDVEK
ABCD3_HM	VLGELWPLFGGR
ACBD4_HM	ACPGPLSSLTLSVR
ACBD4_HM	QFQAAVSVIQNLPK
PEX11G_HM	GVLWAGR
PEX11G_HM	LFDDLAMFVYTK

SLC25A17_HM	EEGLLAPYR
SLC25A17_HM	GIIDAFHQIIR
TMEM135_HM	ENFQLGAFLGSFVSIYK
TMEM135_HM	HYEDNCISYCIK
ACSL1_HM	DGWLHTGDIGK
ACSL1_M	VLQPTIFPVVPR
ACSL3_HM	NLFILAYNYK
ACSL3_HM	VLSEAAISASLEK
PECR_M	LTAAVDELK
PECR_M	NQVAVVTGGGTGIGK
ACOX1_M	SFLVGSAAQSLSK
ACOX1_HM	WWPGGLGK
EHHADH_HM	CLYSLINEAFK
EHHADH_M	VVGVPVALDLITSGR
CROT_HM	HLLGLLLIK
CROT_HM	SGGGGNFVLSTSLVGCLR
AGXT_M	LLLGPGPSNLAPR
AGXT_M	QGIQYVFQTR
HAO1_HM	AIFVTVDTPYLGNR
HAO1_HM	QLDGVDPATIDVLP EIVEAVEGK
ECH1_M	AVVVGAGK
ECI2_M	ASQQDFENALNQVK
ECI2_HM	WDAWNALGSLPK
CYP4F3_M	ALSDEDIR
CYP4F3_M	IFHPAFIKPVVLAPALVAPK
GPD1_HM	ITVVQEVDTEICGALK
GPD1_HM	LISEVIGER
CAT_HM	FYTEDGNWDLVGNNTPIFFIR
CAT_M	GAGAFGYFEVTHDITR
ACBD5_M	GSLNEQIALVLIR
ACBD5_HM	QATEGPCK
PEX11B_HM	FCITVSHLNR
PEX11B_HM	NACDLFIPLDK

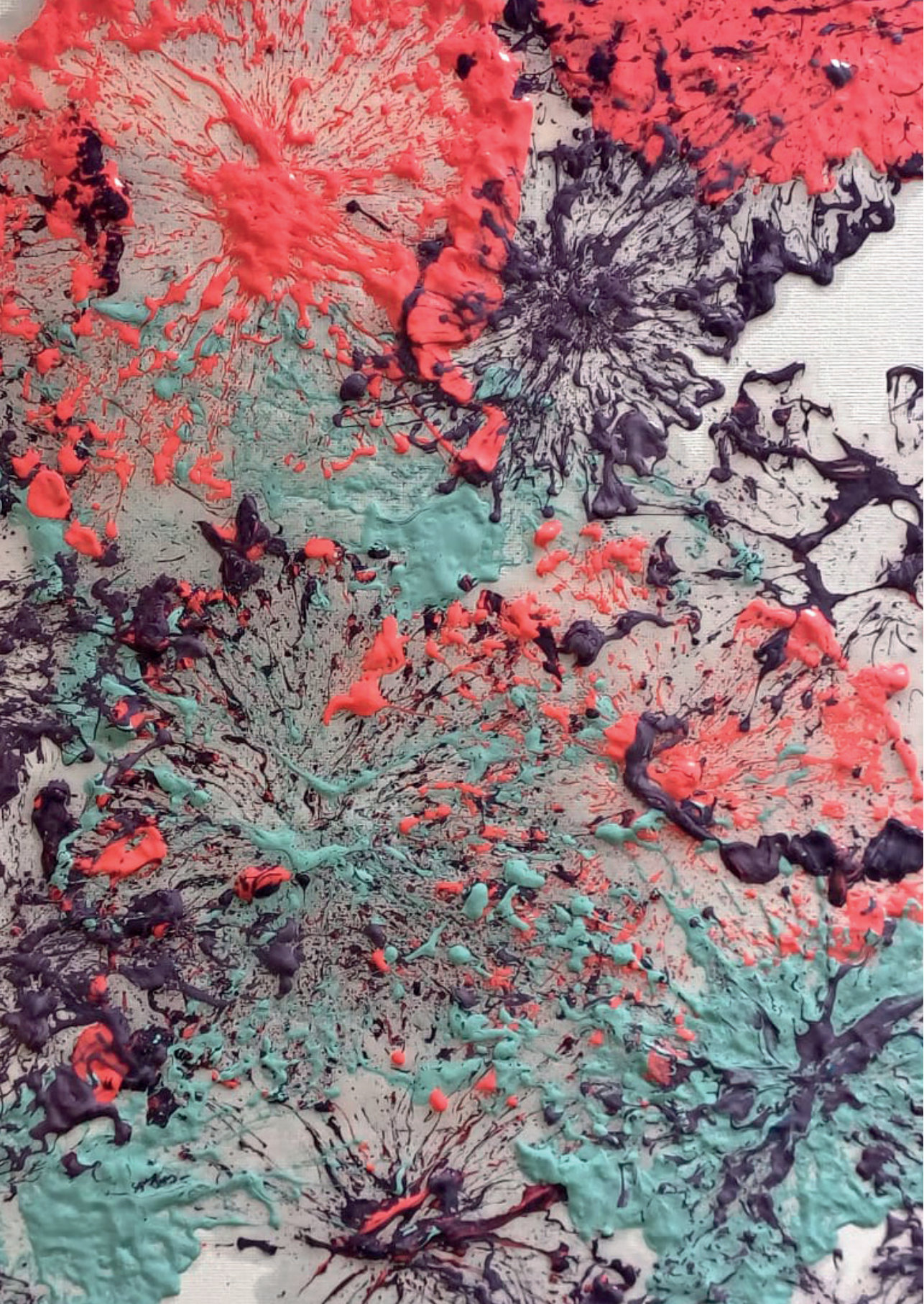
Supplementary Table 2. List of primary antibodies.

Name	Company	Catalogue number
ACOX1	Abcam	Ab184032
β -actin	Sigma-Aldrich	A5441
PMP70	Sigma-Aldrich	P0497
Catalase	Santa Cruz	SC-271803

Supplementary Table 3. List of primer sequences used in RT-qPCR

Gene Name	Forward and reverse primer sequence (5'- 3')
PPIA	Fwd: TTCCTCCTTTCACAGAATTATTCCA Rev: CCGCCAGTGCCATTATGG
PEX1	Fwd: AAGGAAGAGCGTATTAAGCTGGA Rev: TCGATTCCGCACTCTGTTCT
PEX5	Fwd: GCTGAGGAGTATCTGGAGCAGT Rev: CCTTGGACACAAAGTCACTGGC
PEX7	Fwd: CCGAGTTCTCTCCGTACCTG Rev: ACGTCAAACAAGCCGTCATTC
PEX11 α	Fwd: GACGCCTTCATCCGAGTCG Rev: CGGCCTCTTTGTCAGCTTTAGA
PEX13	Fwd: AACCAACACTTACAAGAGTGCC Rev: CCGTAGGCTCCATATCCAGAAG
PEX16	Fwd: AGGTCGCTTCTCCGATTCAC Rev: TGAGAGCAATGACGAGCCAAC
PEX3	Fwd: GCTCGGCGACAGTACCATTTT Rev: CGAGTTGAGCTGCTGCATTAAG
PEX6	Fwd: GGCAAGTTGAGATCCTGGAAGG Rev: GGTGGTATCAGCCAGAAAGGCA
PEX19	Fwd: CTA CT CAGAGGGCTCGCTTTGA Rev: CCGACAGATTGAGAGCATCCAG

Fwd, forward primer; Rev, reverse primer.



Chapter



Establishing a peroxisomal β -oxidation computational kinetic model to understand the effects of amino-acid restriction on peroxisomal β -oxidation

José M. Horcas-Nieto¹, J. C. W. Odendaal¹, Barbara M. Bakker¹§

1. Laboratory of Pediatrics, Center for Liver, Digestive and Metabolic Diseases, University of Groningen, University Medical Center Groningen, The Netherlands;

§ Corresponding authors:

Prof. dr. Barbara M Bakker

Department of Pediatrics, University of Groningen, University Medical Center Groningen
Antonius Deusinglaan 1, 9713 AV Groningen, The Netherlands Phone: +31 50 361 1542

Email: b.m.bakker01@umcg.nl

Manuscript in preparation

ABSTRACT

Peroxisomes play a key role in fatty acid metabolism and are crucial for oxidation of very-long-chain fatty acids, branched-chain fatty acids and bile-acid intermediates. The importance of peroxisomes is highlighted by the number of diseases caused by disruptions of peroxisomal biogenesis and metabolism. Computational models of metabolism are used to simulate metabolite concentrations and fluxes in response to e.g. pathogenic mutations, gene-expression regulation or nutritional or pharmacological interventions. No computational kinetic model has yet been described for the peroxisomal β -oxidation. Here, we first reviewed the kinetic properties of the enzymes involved in the peroxisomal β -oxidation of straight-chain fatty acids. To acquire a deeper understanding of the pathway, we developed a detailed kinetic computation model. The model is composed of reversible kinetic equations and kinetic parameters, obtained from the literature, that describe the behavior of the enzymes. To obtain a full kinetic dataset, it was necessary to combine data from mouse, rat and human enzymes. The model predicts the concentrations of the different metabolites and the fluxes through the enzymes at steady state. Metabolic control analysis revealed acyl-CoA oxidase 1 (ACOX1) to be the enzyme with the highest flux control coefficient of the pathway (0.58). This partially supports the prevailing hypothesis that ACOX1 is a rate-limiting enzyme of the pathway, although we show that it is not the only one. 3-Ketoacyl-CoA thiolase 1 (ACAA1) was found to be the second enzyme with control in the pathway, with a flux control coefficient of 0.42. The rest of enzymes did not exert any control. Integration of proteomics data from hepatic organoids allowed to build context-specific models. Simulations of these models predicted that amino-acid restriction led to a reduction in the metabolic flux of the pathway, which could be rescued by supplementation of docosahexaenoic acid (DHA). Interestingly, differential regulation was observed between the different intermediate metabolites of the pathway in response to amino-acid restriction and rescue by DHA.

This study describes -to the best of our knowledge- the first detailed kinetic model of the peroxisomal β -oxidation of straight-chain fatty acids. It can be a powerful tool to investigate different metabolic diseases in which the enzymes in the pathway are implicated, as well as therapeutic approaches or nutritional interventions.

INTRODUCTION

Peroxisomes are small organelles, found in practically all eukaryotic cells and highly abundant in the liver of mammals¹. These single-membrane organelles present a wide range of functions, including hydrogen peroxide and lipid metabolism². Given the importance of peroxisomes, impairments in these organelles lead to metabolic disorders³. Similar to mitochondria, peroxisomes can metabolize fatty acids to generate ATP, in a process known as β -oxidation. While mitochondria are in charge of metabolizing the majority of fatty acids, including those with long, medium and short acyl chains, peroxisomes metabolize a wider range of substrates². These less studied organelles metabolize very-long and long-chain fatty acids (VL/LCFA), as well as dicarboxylic fatty acids, 2-methyl-branched-chain fatty acids, and CoA esters of eicosanoids and bile acid intermediates⁴. Peroxisomes have even been described to metabolize medium-chain fatty acids, illustrating their versatility and overlapping function with mitochondria⁵.

Peroxisomal β -oxidation is essential for the shortening of fatty acids that are poor substrates for mitochondria. It has been suggested that the peroxisomal β -oxidation has a preference for monounsaturated fatty acids when compared to their respective saturated forms^{6,7}. Peroxisomal β -oxidation also has the ability to oxidize polyunsaturated fatty acids (PUFAs)^{8,9}. Peroxisomes contain two systems of enzymes to perform the β -oxidation of fatty acids. The first set of enzymes, which are induced by PPAR- α activation, is in charge of metabolizing straight-chain acyl-CoAs to produce acetyl-CoA. The PPAR- α non-inducible system can metabolize 2-methyl-branched-chain acyl-CoAs into propionyl-CoA¹⁰. This should not be confused with fatty-acid α -oxidation, which oxidizes 3-methyl-branched acyl-CoA species¹¹. In both cases, the peroxisomal β -oxidation consists of four reactions: 1) oxidation of the acyl-CoA into a 2-enoyl-CoA by introduction of a double bond between C2 and C3, 2) hydration to form a 3-hydroxyacyl-CoA, 3) a dehydrogenation to form 3-oxoacyl-CoA and 4) a thiolytic cleavage that produces a shortened acyl-CoA and acetyl-CoA or propionyl-CoA depending on the starting substrate¹². Prior to the metabolization of the fatty acids, these need to be activated into their CoA form.

Detailed kinetic models are highly useful computational tools used to decipher the functioning of biological processes. Kinetic models permit researchers to predict metabolite concentrations as well as fluxes over time of a given pathway. Since they are based on detailed enzyme kinetic parameters, model simulations can be used to predict the impact of specific mutations,

regulation of enzyme concentrations, and nutritional and pharmacological interventions^{13,14}. While several kinetic models have been constructed and experimentally validated for mitochondrial metabolism¹⁵⁻¹⁷, no kinetic model of peroxisomal fatty-acid metabolism has been reported yet. One of the biggest challenges for the establishment of a peroxisomal β -oxidation model is the relatively limited availability of reliable kinetic parameters for the enzymes involved in the pathway. Most of the kinetic studies date back to the early 90s and lack information on oxidation of very-long-chain substrates due to experimental limitations caused by the extremely low solubility of these compounds¹⁸. Another limiting factor is the lack of kinetic information on peroxisomal transporters.

The aim of this study is to review the kinetics that are available for the different enzymes and transporters involved in the peroxisomal β -oxidation and use this knowledge to build a first kinetic model of the pathway in liver cells. Subsequently, we present a case study in which we use the model to predict the effect of amino-acid restriction on the pathway flux and metabolite concentrations. To do so, proteomics data from *in vitro* studies were integrated into the model, thereby generating a context-specific model.

RESULTS AND DISCUSSION

Review of kinetics of enzymes involved in the peroxisomal β -oxidation

We first present a detailed review of the kinetics of the different enzymes and transporters involved in the β -oxidation of straight-chain acyl-CoAs in the peroxisome. The activation of fatty acids by acyl-CoA synthetases¹⁹ is outside the scope of this work. We have evaluated different studies based on their relevance for *in vivo* conditions. The papers selected, and hereby discussed, were chosen based on their physiological relevance. Enzymatic assays measured at supraphysiological conditions (pH, temperature, H_2O_2 concentration, etc.) were not considered. In cases when one study did not provide sufficient kinetic data, two or more studies were combined. Since there is no complete dataset for any single organism, we included information obtained from mouse, rat and human liver, and when relevant also from other tissues or organisms.

Once a saturated acyl-CoA is inside the peroxisome, it is oxidized by ACOX1 into a 2-trans-enoyl CoA. This reaction is coupled to the oxidation of molecular

oxygen into hydrogen peroxide, which is then converted back into molecular oxygen by catalase. The resulting 2-trans-enoyl-CoA is further hydrated, dehydrogenated and thiolysed to give a C_{n-2} -acyl-CoA and an acetyl-CoA by the bifunctional enzyme (DBP and LBP) and the peroxisomal 3-ketoacyl-CoA thiolase 1 (ACAA1) and Sterol Carrier Protein X (SCP2), respectively. The resulting C_{n-2} -acyl-CoA can be further oxidized in the next β -oxidation cycle, or reversibly converted into an acyl-carnitine by the carnitine acetyltransferase (CRAT) or the carnitine octanoyltransferase (CROT). These carnitine esters can be exported out of the peroxisome (Figure 1).

Transport of Acyl-CoAs into the peroxisomes

Prior to their processing inside the peroxisomes, fatty acyl-CoAs are imported into the organelle. ATP binding cassette (ABC) transporters are membrane-bound proteins, found in many organelles, catalyzing the transport of lipids, amino acids, and peptides and driven by the hydrolysis of ATP. Within the superfamily of ATP-binding cassette transporters there is a subfamily known as “subfamily D”. Three of these ABCD transporters have been identified in the peroxisome: adrenoleukodystrophy protein (ALDP or ABCD1), ALDP-related protein (ALDRP or ABCD2), and the 70kDa peroxisomal membrane protein (PMP70 or ABCD3)^{20,21}.

ABCD1 and ABCD2 have overlapping specificities for their substrates²¹. ABCD1 is responsible for the transport of saturated and unsaturated LCFA-CoAs and VLCFA-CoAs into the peroxisome. While there is a clear overlap in substrate specificity between ABCD1 and ABCD2, there are different substrates to which they exhibit their preferences. ABCD2 has a higher specificity for C22:0-CoA and poly-unsaturated fatty acids C22:6-CoA and C24:6-CoA^{20,22}. PMP70 (ABCD3) is one of the most abundant membrane proteins in peroxisomes and it transports the broadest range of substrates. ABCD3 transports saturated and unsaturated LCFA, such as C10:0-CoA, C12:0-CoA and C16:0-CoA, C18:1-CoA, C18:2-CoA, C20:5-CoA and C22:6-CoA²³ as well as phytanoyl and pristanoyl-CoA and dicarboxylic acids²⁴. Moreover, mice depleted of ABCD3 showed accumulation of C27-bile acids in liver, intestine and bile²⁵.

There is a clear lack of kinetic information on the peroxisomal ABCD transporters. To date, we have not found any studies describing the kinetic properties of the import of fatty acids into the peroxisome. Measuring transporter kinetics is a laborious process highly affected by lipid membrane dynamics and difficult isolation procedures.

Acyl-CoA oxidase 1

Acyl-CoA oxidase 1, the first enzyme of the peroxisomal β -oxidation pathway is commonly referred to as the rate limiting step^{26,27}. This statement is based on studies reporting that the K_m values of the enzyme for certain substrates such as lauroyl-, myristoyl-, palmitoyl- and stearoyl-CoA²⁷ are almost the same as the ones observed for the whole pathway²⁸. Moreover, the variations in V_{max} reported by Hovik²⁸ in the whole pathway were described to be very similar to those reported for ACOX1²⁷. These results, together with a similar pattern in substrate inhibition, have been used to define ACOX1 as the rate-limiting step of the pathway. Formal proof of this statement would require Metabolic Control Analysis²⁹.

Rat liver peroxisomes have at least three acyl-CoA oxidases. ACOX1 shows activity towards straight-chain acyl-CoAs, including mono- and dicarboxylic fatty acids. ACOX2 metabolizes bile acid intermediates. Finally, ACOX3, traditionally known as pristanoyl-CoA oxidase, is involved in the oxidation of 2-methyl-branched-chain fatty acids³⁰. Interestingly, human peroxisomes only have ACOX1 and a second branched-chain acyl-CoA oxidase, which oxidizes 2-methyl-branched-chain acyl-CoAs as well as straight-chain acyl-CoAs (dicarboxylic VLCFA). Given the complexity of the system, and the lack of kinetic parameters except for ACOX1, we focus on the oxidation of straight-chain acyl-CoAs performed by ACOX1 here¹⁰.

Acyl-CoA Oxidase 1 is synthesized as a polypeptide, which is proteolytically cleaved into the two smaller (functional) peptides upon import into the peroxisome²⁷. The enzyme introduces a double bond between C2 and C3 of the acyl-CoA substrate, thus converting it into a 2-enoyl-CoA. ACOX1 is a flavoprotein that contains an FAD group. This FAD group is reduced into $FADH_2$ upon the oxidation of an acyl-CoA into a 2-enoyl CoA. The electrons are then donated to molecular oxygen, which in turn is reduced to hydrogen peroxide. This reaction is different from that catalyzed by the first enzyme of mitochondrial β -oxidation (acyl-CoA dehydrogenase), which ultimately donates the electrons to the electron transport chain to produce ATP³¹.

Crystallography studies of ACOX1 demonstrated that the structure of the enzyme is similar to that of the medium-chain acyl-CoA dehydrogenase (MCAD)³², particularly, at its active site. Although both enzymes contain an FAD molecule, the flavin ring is very protected in MCAD, which makes it unreachable to molecular oxygen. In the case of ACOX1 this ring is in a large cavity, where it is accessible to molecular oxygen. Interestingly, the binding site between MCAD and the electron transport flavoprotein, which donates the electrons

to the electron transport chain, is located on a face of the flavin ring normally shielded in ACOX1³². These two factors can potentially explain why the FADH₂ in acyl-CoA oxidases donates the electrons directly to molecular oxygen and not the ETC.

Several groups have characterized ACOX1 and measured its kinetic properties, either using the isolated enzyme or peroxisomal fractions^{9,27}. Most groups found K_m values for acyl-CoAs with 14-18 carbon atoms (C14-C18) to be very similar between them and lower than those found for shorter substrates (C8 to C4). These results emphasize the preference of ACOX1 for longer chain fatty acids. V_{max} values were relatively similar for most chain lengths ranging from C8 to C16, values were relatively similar for most chain lengths ranging from C8 to C16, with the highest value for C16³³. Different groups also reported similar values of the K_m for oxygen^{9,27}. No information about the K_m for H₂O₂ was found. However, given that the enzyme is virtually irreversible, product inhibition by H₂O₂ is probably negligible. The enzyme was reported to be inhibited by CoA by Hovik et al³⁴, in line with previous observations in which CoA inhibited β -oxidation of acyl-CoA esters³⁴. Acetyl-CoA was also reported to be an inhibitor of the enzyme, yet no K_i values were reported³⁴. Interestingly, the enzyme was also inhibited by 3-ketohexadecanoyl-CoA. This inhibition was thought to be relevant for regulation of the pathway as the K_m of the downstream ACAA1 enzyme for 3-ketohexadecanoyl-CoA was found to be several times higher than the K_i of ACOX1 for the same compound²⁷. The authors did not specify the putative impact of such regulation. We may speculate, however, that a strong feedback inhibition of ACOX1 by 3-ketohexadecanoyl-CoA would prevent overloading the pathway, well before ACAA1 is saturated.

Catalase

Hydrogen peroxide, produced by peroxisomal oxidases including ACOX1, is a reactive oxygen species that can lead to cellular damage at high concentrations³⁵. Catalase is an important enzyme in the peroxisome, in charge of degrading hydrogen peroxide back into molecular oxygen and water³⁶. High levels of H₂O₂ in the peroxisome can modify the last enzyme of the peroxisomal β -oxidation (3-ketoacyl-CoA thiolase) as well as its substrate acetoacetyl-CoA³⁷. Therefore, the presence of catalase is of clear importance in the peroxisome in order to avoid H₂O₂ accumulation.

Kinetic properties of catalase from different organisms, including bovine liver, human erythrocytes and many bacterial strains, have been extensively studied³⁸. Several groups have isolated and characterized catalase, and

reported very different results depending on the methods and assays employed. While catalase has been reported not to follow Michaelis-Menten kinetics throughout the entire range of substrates^{38,39}, it has also been reported to do so when the concentration of H_2O_2 is kept below 200 mM. At higher concentrations, hydrogen peroxide inactivates the enzyme, which has been suggested to alter apparent K_m and V_{max} values. Most kinetic assays of catalase performed in the early days, where done in the presence of supraphysiological concentrations H_2O_2 (up to molar range), which might have affected the results⁴⁰. Apparent K_m values vary between 40 to almost 600 mM³⁹, while the apparent k_{cat} ranges between 55,000 to over 800,000 s^{-1} ³⁹. Moreover, the K_{eq} and the second order rate of the reaction have also been reported to be very high⁴¹. While high variability between values is observed, all the measured V_{max} and K_m are extremely high, reflecting the high turnover of the enzyme and the fact that hydrogen peroxide is shortly-lived in the peroxisome⁴².

Bifunctional Protein

The second and third reactions of the peroxisomal β -oxidation are catalyzed by a bifunctional enzyme, which performs first a hydration reaction converting the 2-enoyl-CoA into a 3-hydroxyacyl-CoA, and then a dehydrogenation of which the final product is a 3-ketoacyl-CoA. There are two isoenzymes, usually referred to as L- and D- bifunctional protein (LBP and DBP), but sometimes as peroxisomal multifunctional enzyme type I and II (MFE-I and MFE-II)^{43,44}.³⁹

Most peroxisomal substrates are metabolized by the D-bifunctional protein (DBP), while the L-form metabolizes preferentially dicarboxylic acids⁴⁵. Specifically, the D-functional protein metabolizes very-long-chain enoyl-CoAs, branched chain fatty acids and bile acid intermediates^{44,46}. The enzyme donates the electrons to NAD^+ in order to produce NADH. Jiang et al^{44,47}, purified both DBP and LBP from human liver and studied their characteristics. They showed that while both enzymes were present in similar amounts and had similar specific activities for their respective substrates, the D-form had a higher activity towards longer carbon-chain substrates than the L-form. DBP showed its maximal activity towards decanoyl-CoA and dodecanoyl-CoA.

Peroxisomal 3-ketoacyl-CoA thiolase 1 (ACAA1)

The fourth and last step of the peroxisomal β -oxidation is catalyzed by different thiolase isoenzymes. These enzymes catalyze the thiolytic cleavage of 3-ketoacyl-CoAs, which yields an acyl-CoA that is shortened by two carbons plus acetyl-CoA. Mouse and rat peroxisomes contain three different 3-ketoacyl-CoA thiolases, namely thiolase A, thiolase B, and SCP-2/3-ketoacyl-CoA thiolase

(SCPx). Human peroxisomes contain two thiolases: the peroxisomal 3-ketoacyl-CoA thiolase (ACAA1) and the Sterol Carrier Protein x (SCP2)².

Here, we focus on the role of 3-ketoacyl-CoA thiolase (ACAA1) in the metabolism of straight-chain fatty acids. Cleland et al⁴⁸ proposed that peroxisomal 3-ketoacyl-CoA thiolase followed a ping-pong mechanism. This was later confirmed by Miyazawa et al⁴⁹. In 1981 Miyazawa et al. isolated the enzyme from rat liver and compared its kinetic properties to the mitochondrial thiolases⁴⁹. Interestingly, at this point only one peroxisomal 3-ketoacyl-CoA thiolase was reported and it was not specified whether it was A or B. They reported low K_m values for the longer-chain substrates and the highest velocity with 3-keto-octanoyl-CoA as the substrate. In later studies, the measured activities and substrate specificities of the 3-ketoacyl-CoA thiolases A and B from livers of rats treated with clofibrate were the same⁵⁰.

Even though the reaction catalyzed by peroxisomal 3-ketoacyl-CoA thiolase is in principle reversible, the thiolysis reaction is thermodynamically favoured over the condensation reaction^{51,47}. The enzyme can be inhibited by both CoA and acetyl-CoA. Substrate inhibition by CoA is, however, only observed at concentrations higher than 100 μ M.⁴⁹

Carnitine acetyltransferase and carnitine octanoyltransferase

Once the acyl-CoAs have been shortened, they can either enter into a new cycle of β -oxidation or be converted to their cognate carnitine ester by one of two enzymes, namely carnitine acetyltransferase (CRAT) or carnitine octanoyltransferase (CROT). Acylcarnitines are exported out of the peroxisomes and transported into mitochondria via the carnitine acylcarnitine carrier⁵².

In 1983, Miyazawa et al purified and characterized both carnitine octanoyltransferase and carnitine acetyltransferase from rat liver^{53,54}. When assaying CROT, they reported higher K_m values for shorter chain-lengths (C2-C6) compared to the low and constant values for substrates between C8 and C18. However, Farrel et al.⁵⁵ reported that the apparent K_m values for the murine enzyme were not constant: these values were smaller for substrates between C4 and C12 and larger for C14, C16 and C18. Both groups reported CROT to exhibit its maximum activity towards hexanoyl-CoA, while the maximum activity of CRAT was observed towards butyryl-CoA⁵⁵, highlighting the difference in chain-length specificity between the two enzymes. CRAT exhibited very similar values for the assayed acyl-CoAs (C2-C8) with a higher value for C12. Farrel et al. also reported that the chain length of the acyl-CoA influenced the K_m for L-carnitine. This is highly important in vivo, given the

presence of different acyl-CoAs (of different chain length) in the cell under different physiological conditions⁵⁵. We did not find any absolute values for the V_{\max} of CRAT.

Integrating kinetic data into a computational kinetic model of the peroxisomal β -oxidation

To assess the physiological relevance of the kinetic parameters collected in studies with purified enzymes and peroxisomal fractions, we integrated the data into a computational model of the peroxisomal β -oxidation of straight-chain acyl-CoAs. To predict the regulation of the peroxisomal β -oxidation flux and metabolite concentrations in mouse liver organoids under different physiological conditions, we adjusted the V_{\max} values based on proteomics obtained from these organoids.

Building a computational model

The computational model for the peroxisomal β -oxidation contains the enzymes depicted in **Figure 1**. Because of the limited kinetic information available, the first version of the model is restricted to oxidation of saturated straight-chain fatty acids containing an even number of carbons, starting from C18. It does not take transport into consideration yet.

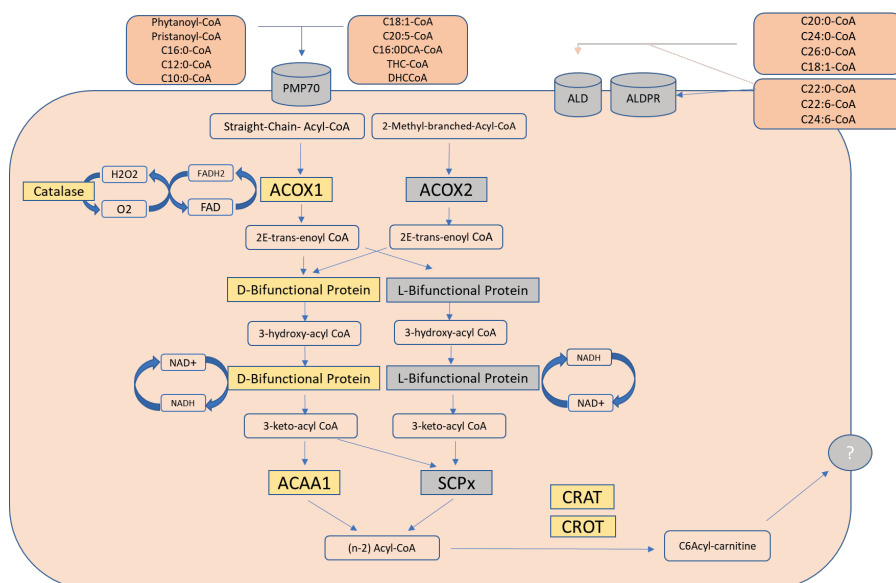


Figure 1. Scheme of the enzymes included in the computational model. In yellow the enzymes that are part of the ‘traditional’ PPAR-inducible β -oxidation, which is modeled in this paper. In grey the enzymes not yet included in the model. Import and export are not considered in the model.

Kinetic parameters implemented in the model were chosen from a selection of the papers cited above, based on a ranking according to their physiological relevance (**Supplementary text 1**). To obtain a complete parameter set, kinetic constants were combined from rat, mouse and human.

Two substrate-two product reversible Michaelis-Menten kinetics (convenience kinetics⁵⁶) were used as the starting point, unless stated differently. For example, the rate of ACOX1 was calculated according to **Equation 1**, which is based on the rate equation of ACADM previously published which takes into account substrate competition¹⁵.

$$v_{ACOX1_{C_n} \text{ AcylCoA}} = \frac{Sf_{ACOX1_{C_n} \text{ AcylCoA}} * Vmax_{ACOX1} * \left(\frac{[C_n \text{ AcylCoA}]}{Km_{C_n} \text{ AcylCoA}} \right) * \left(\frac{[O_2]}{Km_{O_2}} \right) - \left(\frac{[C_n \text{ EnoylCoA}]}{Km_{C_n} \text{ EnoylCoA}} \right) * \left(\frac{[H_2O_2]}{Km_{H_2O_2} * K_{eq}} \right)}{\left(\left(1 + \sum_{n=18}^{n=18} \left(\frac{[C_n \text{ AcylCoA}]}{Km_{C_n} \text{ AcylCoA}} + \frac{[C_n \text{ EnoylCoA}]}{Km_{C_n} \text{ EnoylCoA}} \right) \right) * \left(1 + \left(\frac{[O_2]}{Km_{O_2}} \right) + \left(\frac{[H_2O_2]}{Km_{H_2O_2}} \right) \right) \right)}$$

Equation 1. Rate equation for Acyl-CoA Oxidase 1. Rate equation is based on convenience kinetics⁵⁶.

The computational model consists of 6 enzymes with their corresponding rate equations, 24 ordinary differential equations (ODE) for variable metabolite concentrations, and additionally 7 boundary fixed metabolite concentrations (for a detailed equations see **Supplementary Text 1**). ODEs describe the change of different metabolites in time as a result of the enzyme rates (production and consumption). Model simulations allow to predict time courses of all the different variable metabolite concentrations in the pathway, including acyl-CoAs, enoyl-CoAs, ketoacyl-CoAs and acylcarnitines of the different chain lengths (C18 to C8). Subsequently, concentrations of the different metabolites as well as the enzyme fluxes are calculated at the steady state.

Assumptions and conversion factors

V_{\max} values are given in μmol of product per minute per milligram of peroxisomal protein. For the calculation of V_{\max} values, the following scenarios were encountered. (i) When the activity was measured in purified enzyme, the V_{\max} was corrected by the concentration of the enzyme in a human liver⁴⁷ and then converted to peroxisomal protein, using that 1.92% of the liver protein content is peroxisomal protein⁵⁷. (ii) When the activity of the enzyme was measured in the peroxisomal fraction and expressed per peroxisomal protein, no further calculations were needed.

We assume a peroxisomal volume of approximately $1.8 \cdot 10^{-6} \text{ L} \cdot \text{mg of protein}^{-1}$ (equal to that of mitochondria⁵⁸).

The structure of the active site of ACOX1 is essentially the same as that of MCAD³². This leads to a very similar binding of the substrate in both enzyme and a similar oxidation mechanism and FAD reduction. Because of this, and the lack of information on K_m values for the products of ACOX1 we have used the of MCAD for the different enoyl-CoAs¹⁵.

As mentioned in the results section of this paper, catalase only follows MM kinetics if the H_2O_2 concentration remains below a certain level, due to product inhibition. Given the high concentrations of H_2O_2 needed to reach this inhibition, we assume that the enzyme does follow MM kinetics. Moreover, because of its high K_{eq} , the reaction was modelled as irreversible. Given the disparity in values in V_{\max} , we selected different papers about the isolated enzyme and averaged all the V_{\max} values. Moreover, we also took the value measured in human liver tissue extract and compared.

Equilibrium constant values (K_{eq}) were obtained, unless otherwise specified, from eQuilibrator (pH 7.5, pMg 3.0 and Ionic strength 0.25M).

Table 1 shows the concentrations of the different metabolites at steady state.

Metabolite	Concentration (μM)
C18 AcylCoA	150.0
C18 EnoylCoA	100.4
C18 KetoacylCoA	1.0
C16 AcylCoA	117.8
C16 AcylCarnitine	841.5
C16 EnoylCoA	9.2
C16 KetoacylCoA	0.1
C14 AcylCoA	107.1
C14 AcylCarnitine	765.0
C14 EnoylCoA	4.3
C14 KetoacylCoa	0.04
C12 AcylCoA	347.5
C12 AcylCarnitine	2481.8
C12 EnoylCoA	3.7
C12 KetoacylCoA	0.03
C10 AcylCoA	191.6
C10 AcylCarnitine	1368.8
C10 EnoylCoA	6.8
C10 KetoacylCoA	0.06
C8 AcylCoA	649.1
C8 AcylCarnitine	4636.5
C8 EnoylCoA	8.2
C8 KetoacylCoA	0.08
C6 AcylCoA	4.9
H ₂ O ₂	9.5

Table 2 shows the fluxes through the different enzymes in the presence of the different chain-length substrates.

Enzyme	Flux ($\mu\text{mol}\cdot\text{min}^{-1}\cdot\text{mgProt}^{-1}$)
ACOX1 for C18, C16, C14, C12, C10 and C8	$1.6\cdot 10^{-4}$
DBP for C18, C16, C14, C12, C10 and C8	$1.6\cdot 10^{-4}$
ACAA1 for C18, C16, C14, C12, C10 and C8	$1.6\cdot 10^{-4}$
CROT for C16, C14, C12, C10 and C8	0
CRAT for C16, C14, C12, C10 and C8	0
CROT for C6	$-6.4\cdot 10^{-6}$
CRAT for C6	$-1.5\cdot 10^{-4}$
Catalase	$9.6\cdot 10^{-4}$

Table 1 shows the concentrations of the metabolites at steady state. The concentration of acyl-CoA and acyl-carnitine species is clearly higher than those of the enoyl-CoAs and ketoacyl-CoAs for all the chain lengths. Moreover, the ketoacyl-CoA species are the least abundant ones, probably due to the high equilibrium constant of ACAA1 ($2.5 \cdot 10^5$).

Table 2 shows the fluxes through the different enzymes at steady state. The flux of the pathway is lower than that described in the literature²⁸. Moreover, the flux is significantly lower than the V_{\max} of ACOX1. In part this can be explained by the fact that we include six rounds of β -oxidation with substrates ranging from C18 through C8. Thus, only one sixth of the total ACOX1 pool is available for each round. In contrast, in experimental settings, the time is often relatively short, hence only one or two rounds of β -oxidation are observed. Further reduction of the flux relative to the V_{\max} of ACOX1 may be caused by almost complete saturation of the enzyme in the model by the high concentration of C18-acylCoA. This would leave little catalytic capacity for subsequent rounds. This is reminiscent of the vulnerability towards substrate overloading that was previously reported for a mitochondrial kinetic model⁵⁹. For future studies, we aim to incorporate the import and export of products and substrates, and/or reduce the concentration of C18-acylCoA, to assess if peroxisomal β -oxidation is also sensitive towards overloading.

Metabolic Control Analysis

To analyze how the pathway would respond to regulation of enzyme concentrations, we applied the theoretical framework of Metabolic Control Analysis²⁹. Here, the Flux Control Coefficient (FCC) of a specific enzyme i (C_i^J) expresses the relative change of the flux J in response to a small increase in rate v_i of this enzyme. The FCC of an enzyme i on the steady-state flux J is mathematically defined as:

$$C_i^J = \frac{d \ln J / d \ln p}{\partial \ln v_i / \partial \ln p}$$

Here p is a parameter that selectively affects v_i . An FCC close to 0 indicates that the enzyme has little to no effect on the pathway's flux, while an FCC close to 1 indicates a high control over the rate. The summation of all the control coefficients of the enzymes involved in the pathway equals to 1²⁹. In order to numerically calculate the FCC of the different enzymes, the V_{\max} s were individually changed ($\pm 0.1\%$ of their maximal velocity) and the change of flux of the pathway was computed (**Figure 2a**)

ACOX1 was found to be the enzyme with the highest FCC (0.58). In essence, this is in agreement with the hypothesis proposed before, that ACOX1 is the rate limiting enzyme of the peroxisomal β -oxidation²⁸. However, this proposal was only based on the similarity between the ACOX1 kinetics and the flux, not on a formal analysis of flux control. This modelling result now supports the hypothesis. At the same time, the fact that the FCC is lower than 1, suggests that ACOX1 may share flux control with another enzyme. Indeed, ACAA1 also exerted a high control on the pathway's flux. Control by ACAA1 has not been described before. Nevertheless, it is in line with studies on mitochondrial β -oxidation, where both experimental and computational analysis showed that the mitochondrial ketoacyl-CoA thiolase (MCKAT) took over some control under specific conditions^{59,60}. The concentration of the C18-acylCoA substrate (10 μ M versus 150 μ M) had only a minor effect on the distribution of flux control (**Figure 2a**).

Typically, flux control tends to decrease if an enzyme is activated. Indeed, when increasing the V_{\max} of ACOX1 by a factor of five, a shift in control towards ACAA1 was observed (**Figure 2b**). This indicates that the distribution of flux control may be regulated by gene expression and enzyme content. It also underlines the relevance of reliable kinetic parameters.

As mentioned in the literature review part of this paper, very disparate parameters were found for the V_{\max} of Catalase^{38,61,62}. It has been reported that the K_m and the V_{\max} of catalase are extremely high. Since we could not find kinetic parameters for catalase isolated from human or rodent liver, we used the average of different parameters for catalases isolated from different origins. These values were extremely high, with a calculated V_{\max} higher than 46000 $\mu\text{mol} \cdot \text{min}^{-1} \cdot \text{mg PeroxisomalProt}^{-1}$ and a K_m of 93000 μM ³⁸.

Interestingly, another study⁶³ measured the V_{\max} of catalase in human liver tissue and reported it to be 0.18 $\mu\text{mol} \cdot \text{min}^{-1} \cdot \text{mg liver Prot}^{-1}$. Upon conversion to peroxisomal protein (see calculations above), this becomes 9.375 $\mu\text{mol} \cdot \text{min}^{-1} \cdot \text{mg peroxisomal Prot}^{-1}$, hence much lower than the above-mentioned values. However, the control coefficient distribution remained the same with the higher and the lower V_{\max} values. The flux of the pathway only changed minimally. Given that the lower value was closer to those of the rest of the enzymes, all the predictions were performed using this V_{\max} value.

Finally, we also modeled the catalase rate with the reported second order rate constant $k = 7.9 \cdot 10^6 \text{ M}^{-1} \text{ s}^{-1}$ ⁴¹. To do so, the rate of the enzyme was defined by:

$$v = k \cdot [\text{Catalase}] \cdot [\text{H}_2\text{O}_2]$$

In this case, the results for the FCC obtained were the same as those obtained with a high V_{\max} for catalase. Results are summarized in **Supplementary File 2**. In summary, it is likely that the catalytic capacity of catalase is so high that it does not exert any flux control under most conditions.

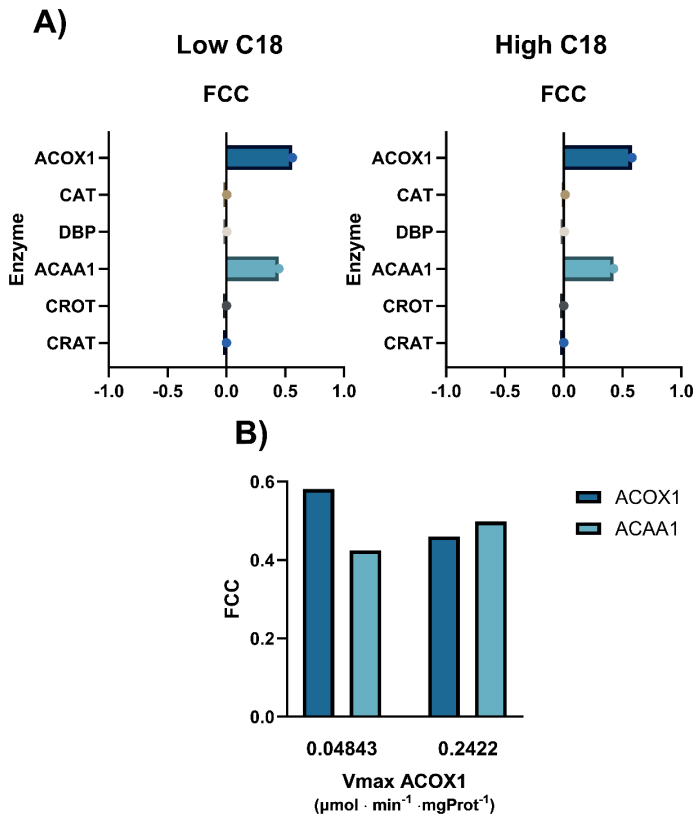


Figure 2. Metabolic control analysis. (A) Flux control coefficients in the model in the presence of low (10 μM) and high (150 μM) C18-acylCoA. Enzymes are displayed in descending order based on their order in the pathway. (B) Changes in the FCC of both ACOX1 and ACAA1 when increasing the V_{\max} of ACOX1 by 5 and 10 times. The analysis was done at 150 μM C18-acylCoA

Case Study: Amino acid restriction leads to a reduction in ACOX1 and Catalase activity

Long periods of exposure to low amino-acid levels have been demonstrated to lead to a reduction in peroxisomal number both in vivo and in vitro studies⁶⁴⁻⁶⁶.

Moreover, this also led to a reduction in peroxisomal functionality in murine hepatic organoids as measured by the metabolism of phytanic acid⁶⁶. However, the results could not be directly linked to a decreased flux of the β -oxidation of fatty acids. To assess the potential of the above-presented model, we have combined it with targeted proteomics data from a previously published malnutrition in vitro model (**chapter 4**). Murine hepatic organoids were exposed to amino-acid restricted media for 96 hours, which led to a decrease in the levels of peroxisomal proteins measured by targeted proteomics (**Chapter 4**). Moreover, the organoids showed an accumulation of triglycerides (TGs), both after 48 and 96 hours, which was hypothesized to be caused by defects in the metabolism of fatty acids due to the impairments in both mitochondria and peroxisomes (**Chapter 4**)⁶⁶. To understand the effect of amino-acid restriction on the peroxisomal β -oxidation flux, we integrated the proteomics data in the model. To this end the V_{max} values of the enzymes were decomposed in the corresponding K_{cat} value and enzyme concentration $[E]$:

$$V_{max} = k_{cat} \cdot [E]$$

While all the enzymes included in the model were present in the targeted proteomic panel, not all enzymes were present in high enough concentrations to be detected. Here we integrated the enzyme concentrations that were detected (**Chapter 4**), namely ACOX1, catalase and CROT.

The overall flux of the pathway was predicted to decrease substantially and significantly upon amino-acid restriction. While the absolute values are different for the different biological replicates involved in the experiments, the overall trends are the same (**Figure 3a**). Interestingly, neither the acyl-CoA nor the acyl-carnitine profile changed in the amino-acid restricted conditions (**Supplementary Figure 1**) while the levels of enoyl-CoAs and ketoacyl-CoAs were decreased for all the chain lengths (**Figure 3b** and **c**, and **Supplementary File 1**). These results suggest that while the flux of the pathway is downregulated, homeostasis of acyl-CoAs and acyl-carnitines is maintained.

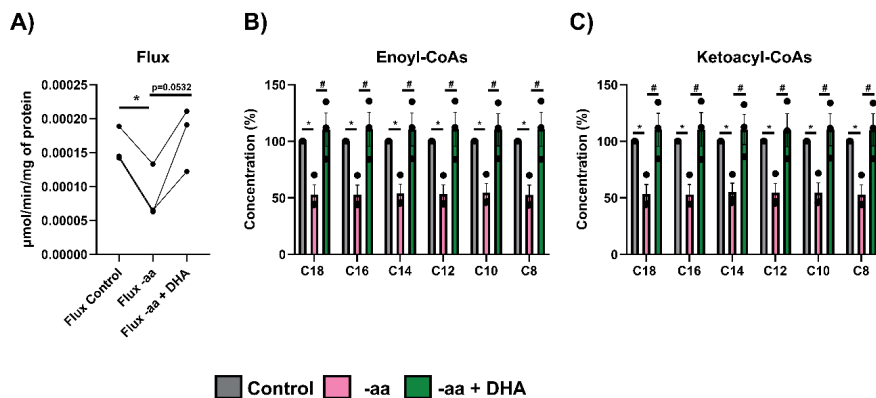


Figure 3. The effects of amino-acid restriction on the peroxisomal β -oxidation. (A) Overall pathway flux in $\mu\text{mol} \cdot \text{min}^{-1} \cdot \text{mg}$ of peroxisomal protein both in control and amino-acid restriction and amino-acid restriction supplemented with 100 μM DHA restricted conditions. (B) Enoyl-CoA and (C) Ketoacyl-CoA profiles in control and amino-acid restriction and amino-acid restriction supplemented with 100 μM DHA. Data represents simulations for 3 biological replicates (* indicates comparisons between control and -aa, # indicates comparisons between -aa and -aa + DHA, no indication means not significant) (* $P < 0.05$, ** $P < 0.01$, # $P < 0.05$ paired two-tailed t-test).

We also simulated the effect of supplementing the amino-acid restricted organoids with docosahexaenoic acid (DHA). As we previously reported (**Chapter 4**), DHA supplementation to amino-acid restricted organoids prevented the loss of multiple peroxisomal and mitochondrial proteins in a dose-dependent manner, while it did not prevent the accumulation of TGs. When supplementing DHA, the flux of the pathway was significantly increased when compared to that of the amino-acid restricted organoids, and reached levels similar to those of the controls (**Figure 3d**). Moreover, the decrease in all enoyl and ketoacyl-CoA species was also prevented (**Figure 3e** and **f**), while no changes in the values of acyl-CoAs or acyl-carnitines were observed (**Supplementary Figure 1**).

CONCLUSIONS AND OUTLOOK

In this paper we presented a review on different enzymes involved in the peroxisomal β -oxidation of straight-chain fatty acids and used the data to generate (to the best of our knowledge) the first computational kinetic model

of the peroxisomal β -oxidation. The model predicts metabolite concentrations and pathway fluxes under different conditions. This study also highlights the potential to integrate proteomics data obtained into a kinetic model to understand metabolic regulation in peroxisomal diseases.

Future studies are required to extend the model with the metabolism of branched-chain fatty acids. Detailed kinetic studies will be needed to incorporate the import and export of fatty acids into the peroxisome.

METHODS

Computational methods

The computational model was coded in Python. It consists of 24 ordinary differential equations and 6 rate equations for a total of 6 enzymes. Steady state fluxes and concentrations were calculated with the `odeint` function and by setting all the time derivatives to zero. The (fixed) C18-acylCoA concentration was 150 μM , unless stated differently. A detailed description of the model and equations can be found in **Supplementary Text 1**.

The model script can be found in https://colab.research.google.com/drive/1-raOWdS341mwhoR4kVe1_vayT0AEyyp. Access can be granted upon request.

Experimental methods

All the experimental procedures using murine liver organoids are described in **chapter 4**.

Statistical Analysis

Results are expressed as mean \pm standard error of the mean (SEM). Biological replicates are considered as independent experiments, since they were done with independent organoid lines. Analyses were performed using GraphPad Prism Software Version 9.02 (Graphpad Software). Statistical significance between comparisons is provided in figure legends. No indication means no significant changes (ns).

FUNDING

This project has received funding from the European Union's Horizon 2020 research and innovation program under the Marie Skłodowska-Curie grant agreement No 812968.

ACKNOWLEDGEMENTS

We would like to thank Prof. Ronald Wanders for his help and insights into peroxisomal biochemistry and Karen van Eunen for advice on the computational modeling.

REFERENCES

1. De Duve, Christian. & Baudhuin, Pierre. Peroxisomes (Microbodies and Related Particles). *Physiol Rev.* 46, 323–357 (1966).
2. Wanders, R. J. A. & Waterham, H. R. Biochemistry of mammalian peroxisomes revisited. *Annual Review of Biochemistry* vol. 75 295–332 Preprint at <https://doi.org/10.1146/annurev.biochem.74.082803.133329> (2006).
3. Schrader, M., Costello, J., Godinho, L. F. & Islinger, M. Peroxisome-mitochondria interplay and disease. *Journal of Inherited Metabolic Disease* vol. 38 681–702 Preprint at <https://doi.org/10.1007/s10545-015-9819-7> (2015).
4. Wanders, R. J. A., Baes, M., Ribeiro, D., Ferdinandusse, S. & Waterham, H. R. The physiological functions of human peroxisomes. *Physiological Reviews* vol. 103 957–1024 Preprint at <https://doi.org/10.1152/physrev.00051.2021> (2023).
5. Violante, S. *et al.* Peroxisomes can oxidize medium- and long-chain fatty acids through a pathway involving ABCD3 and HSD17B4. *FASEB Journal* 33, 4355–4364 (2019).
6. Osmundsen, H., Neat, C. E. & Borrebaek, B. *Fatty acid products of peroxisomal β -oxidation.* *J Bmhum* vol. 12.
7. Neat, C. E., Thomassent, M. S. & Osmundsen, H. Effects of high-fat diets on hepatic fatty acid oxidation in the rat Isolation of rat liver peroxisomes by vertical-rotor centrifugation by using a self-generated, iso-osmotic, Percoli gradient. *Biochem. J* vol. 196 (1981).
8. Hiltunen, J. K., Karki, T., Hassinen, I. E. & Osmundsen, H. β -Oxidation of polyunsaturated fatty acids by rat liver peroxisomes. A role for 2,4-dienoyl-coenzyme A reductase in peroxisomal β -oxidation. *Journal of Biological Chemistry* 261, 16484–16493 (1986).
9. Hovik, R. & Osmundsen, H. Peroxisomal β -oxidation of long-chain fatty acids possessing different extents of unsaturation. *Biochem. J* vol. 247 (1987).

10. Vanhove, G. F. *et al.* The CoA Esters of 2-Methyl-branched Chain Fatty Acids and of the Bile Acid Intermediates Di- and Trihydroxycoprostanic Acids Are Oxidized by One Single Peroxisomal Branched Chain Acyl-CoA Oxidase in Human Liver and Kidney. *Journal of Biological Chemistry* 268, 10335–10344 (1993).
11. Croes, K., Van Veldhoven, P. P., Mannaerts, G. P. & Casteels, M. α -Oxidation of 3-Methyl-branched Fatty Acids: A Revised Pathway Confined to Peroxisomes. *Lipids* 34, (1999).
12. Reddy, J. K. & Hashimoto, T. Peroxisomal β -oxidation and peroxisome proliferator-activated receptor α : An Adaptive Metabolic System. www.annualreviews.org (2001).
13. Liberti, M. V. *et al.* A Predictive Model for Selective Targeting of the Warburg Effect through GAPDH Inhibition with a Natural Product. *Cell Metab* 26, 648–659.e8 (2017).
14. Haanstra, J. R. *et al.* Targeting pathogen metabolism without collateral damage to the host. *Sci Rep* 7, (2017).
15. van Eunen, K. *et al.* Biochemical Competition Makes Fatty-Acid β -Oxidation Vulnerable to Substrate Overload. *PLoS Comput Biol* 9, (2013).
16. Wu, F., Yang, F., Vinnakota, K. C. & Beard, D. A. Computer modeling of mitochondrial tricarboxylic acid cycle, oxidative phosphorylation, metabolite transport, and electrophysiology. *Journal of Biological Chemistry* 282, 24525–24537 (2007).
17. Odendaal, C. *et al.* Personalised modelling of clinical heterogeneity between medium-chain acyl-CoA dehydrogenase patients. *BMC Biol* 21, 184 (2023).
18. Kamp, F., Zakim, D., Zhang, F., Noy, N. & James Hamilton, and A. *Fatty Acid Flip-Flop in Phospholipid Bilayers is Extremely Fast*. *Biochemistry* vol. 34 <https://pubs.acs.org/sharingguidelines> (1192).
19. Watkins, P. A. & Ellis, J. M. Peroxisomal acyl-CoA synthetases. *Biochim Biophys Acta Mol Basis Dis* 1822, 1411–1420 (2012).
20. Chorny, S., Ijlst, L., van Roermund, C. W. T., Wanders, R. J. A. & Waterham, H. R. Peroxisomal Metabolite and Cofactor Transport in Humans. *Frontiers in Cell and Developmental Biology* vol. 8 Preprint at <https://doi.org/10.3389/fcell.2020.613892> (2021).
21. Morita, M. & Imanaka, T. Peroxisomal ABC transporters: Structure, function and role in disease. *Biochimica et Biophysica Acta - Molecular Basis of Disease* vol. 1822 1387–1396 Preprint at <https://doi.org/10.1016/j.bbadis.2012.02.009> (2012).
22. Genin, E. C. *et al.* Substrate specificity overlap and interaction between adrenoleukodystrophy protein (ALDP/ABCD1) and adrenoleukodystrophy-related protein (ALDRP/ABCD2). *Journal of Biological Chemistry* 286, 8075–8084 (2011).
23. Imanaka, T. *et al.* Characterization of the 70-kDa peroxisomal membrane protein, an ATP binding cassette transporter. *Journal of Biological Chemistry* 274, 11968–11976 (1999).
24. van Roermund, C. W. T., Ijlst, L., Wagemans, T., Wanders, R. J. A. & Waterham, H. R. A role for the human peroxisomal half-transporter ABCD3 in the oxidation of dicarboxylic acids. *Biochim Biophys Acta Mol Cell Biol Lipids* 1841, 563–568 (2014).
25. Ferdinandusse, S. *et al.* A novel bile acid biosynthesis defect due to a deficiency of peroxisomal ABCD3. *Hum Mol Genet* 24, 361–370 (2015).

26. Bronfman, M., Inestrosa, N. C., Nervi, F. O & Leighton, F. Acyl-CoA synthetase and the peroxisomal enzymes of β -oxidation in human liver Quantitative analysis of their subcellular localization. *Biochem. J* vol. 224 (1984).
27. Osumi, T., Hashimoto, T. & Ui, N. Purification and Properties of Acyl-CoA Oxidase from Rat Liver 1. *J Biochem* 87, 1735–1746 (1980).
28. Hovik, R. & Osmundsen, H. Peroxisomal β -oxidation of long-chain fatty acids possessing different extents of unsaturation. *Biochem. J* 247, 531–535 (1987).
29. Fell, D. A. Metabolic Control Analysis: a survey of its theoretical and experimental development. *Biochem. J* 286, 313–330 (1992).
30. Van Veldhoven, P. P. et al. Identification and Purification of a Peroxisomal Branched Chain Fatty Acyl-CoA Oxidase*. *The Journal of Biological Chemistry* vol. 266 (1991).
31. Henriques, B. J., Katrine Jentoft Olsen, R., Gomes, C. M. & Bross, P. Electron transfer flavoprotein and its role in mitochondrial energy metabolism in health and disease. *Gene* 776, (2021).
32. Nakajima, Y. et al. Three-Dimensional Structure of the Flavoenzyme Acyl-CoA Oxidase-II from Rat Liver, the Peroxisomal Counterpart of Mitochondrial Acyl-CoA Dehydrogenase 1. *J. Biochem* vol. 131 <https://academic.oup.com/jb/article-abstract/131/3/365/814628> (2002).
33. Suzuki, H., Yamada, J., Watanabe, T. & Suga, T. Compartmentation of dicarboxylic acid β -oxidation in rat liver: importance of peroxisomes in the metabolism of dicarboxylic acids. *Biochim Biophys Acta Gen Subj* 990, 25–30 (1989).
34. Hovik, R. & Osmundsen, H. Factors which affect the activity of purified rat liver acyl-CoA oxidase.
35. Heo, S., Kim, S. & Kang, D. The role of hydrogen peroxide and peroxiredoxins throughout the cell cycle. *Antioxidants* vol. 9 Preprint at <https://doi.org/10.3390/antiox9040280> (2020).
36. Nandi, A., Yan, L.-J., Kumar Jana, C. & Das, N. Role of Catalase in Oxidative Stress-and Age-Associated Degenerative Diseases. (2019).
37. Hashimoto, F. & Hayashi, H. Significance of catalase in peroxisomal fatty acyl-CoA / β -oxidation. *Biochimica et Biophysica Acta* vol. 921 (1987).
38. Switala, J. & Loewen, P. C. Diversity of properties among catalases. *Arch Biochem Biophys* 145–154 (2022) doi:10.1016/S0003-9861(02)00049-8.
39. Zamocky, M., Furtmüller, P. G. & Obinger, C. Evolution of catalases from bacteria to humans. *Antioxid Redox Signal* 10, 1527–1547 (2008).
40. Ogura, Y. Catalase Activity at High Concentration of Hydrogen Peroxide. *Arch. Biochem. Biophys.* 57, 288–300 (1955).
41. Ogura, Y. & Yamazaki, I. Steady-State Kinetics of the Catalase Reaction in the Presence of Cyanide. *J. Biochem* 94, 403–408 (1983).
42. Kehrer, J. P. & Robertson, J. D. 1.14 Free Radicals and Reactive Oxygen Species. in *Comprehensive Toxicology (Second Edition)* (ed. Chalerne A. McQueen) vol. 1 277–307 (Elsevier, 2010).
43. Dieuaide-noubhani, M., Novikov, D., van Veldhoven, P. P. & Mannaerts, G. P. Identification and characterization of the 2-enoyl-CoA hydratases involved in peroxisomal β -oxidation in rat liver. *Biochem. J* vol. 321 (1997).

44. Jiang, L. L., Miyazawa, S. & Hashimoto, T. Purification and Properties of Rat D-3-Hydroxyacyl-CoA Dehydratase: D-3-Hydroxyacyl-CoA Dehydratase/D-3-Hydroxyacyl-CoA Dehydrogenase Bifunctional Protein 1 di(2-ethylhexyl)phthalate; bifunctional protein, enoyl-CoA hydratase/3-hydroxyacyl-CoA dehydrogenase bi-functional protein; trifunctional protein, enoyl-CoA hydratase/3-hydroxyacyl-CoA dehydrogenase/3-ketoacyl-CoA thiolase trifunctional protein. Downloaded from. *J. Biochem* vol. 120 <http://jlb.oxfordjournals.org/> (1996).
45. Houten, S. M. *et al.* Peroxisomal L-bifunctional enzyme (Ehhadh) is essential for the production of medium-chain dicarboxylic acids. *J Lipid Res* 53, 1296–1303 (2012).
46. Dieuaide-noubhani, M., Novikov, D., van Veldhoven, P. P. & Mannaerts, G. P. Identification and characterization of the 2-enoyl-CoA hydratases involved in peroxisomal β -oxidation in rat liver. *Biochem. J* vol. 321 (1997).
47. Jiang, L. L., Kurosawa, T., Sato, M., Suzuki, Y. & Hashimoto, T. Physiological Role of D-3-Hydroxyacyl-CoA Dehydratase/ D-3-Hydroxyacyl-CoA Dehydrogenase Bifunctional Protein 1. *J. Biochem* vol. 121 <http://jlb.oxfordjournals.org/> (1997).
48. Cleland, W. W. The kinetics of enzyme-catalyzed reactions with two or more substrates or products. *Biochimica et Biophysica Acta (BBA) - Specialized Section on Enzymological Subjects* 67, 104–137 (1963).
49. Miyazawa, S., Furuta, S., Osumi, T., Hashimoto, T. & Up, N. *Properties of Peroxisomal 3-Ketoacyl-CoA Thiolase from Rat Liver 1*. vol. 90 (1981).
50. Antonenkov, V. D., Van Veldhoven, P. P., Waelkens, E. & Mannaerts, G. P. Comparison of the stability and substrate specificity of purified peroxisomal 3-oxoacyl-CoA thiolases A and B from rat liver. *Biochim Biophys Acta* 1737, 136–141 (1999).
51. Antonenkov, V. D., Van Veldhoven, P. P., Waelkens, E. & Mannaerts, G. P. Substrate specificities of 3-oxoacyl-CoA thiolase a and sterol carrier protein 2/3-oxoacyl-coa thiolase purified from normal rat liver peroxisomes. Sterol carrier protein 2/3-oxoacyl-CoA thiolase is involved in the metabolism of 2-methyl-branched fatty acids and bile acid intermediates. *Journal of Biological Chemistry* 272, 26023–26031 (1997).
52. Jakobs, B. S. & Wanders, R. J. A. Fatty acid β -oxidation in peroxisomes and mitochondria: The first, unequivocal evidence for the involvement of carnitine in shuttling propionyl-CoA from peroxisomes to mitochondria. *Biochem Biophys Res Commun* 213, 1035–1041 (1995).
53. Miyazawa, S., Ozasa, H., Osumi, T. & Hashimoto, T. Purification and Properties of Carnitine Octanoyltransferase and Carnitine Palmitoyltransferase from Rat Liver 1. *J. Biochem* 94, 529–542 (1983).
54. Miyazawa, S., Ozasa, H., Furuta, S., Osumi, T. & Hashimoto, T. Purification and Properties of Carnitine Acetyltransferase from Rat Liver. *J. Biochem* 93, 439–451 (1983).
55. Farrell, S. O., Fiol, C. J., Reddy, J. K. & Bieber, L. L. Properties of purified carnitine acyltransferases of mouse liver peroxisomes. *Journal of Biological Chemistry* 259, 13089–13095 (1984).
56. Liebermeister, W. & Klipp, E. Bringing metabolic networks to life: Convenience rate law and thermodynamic constraints. *Theor Biol Med Model* 3, (2006).
57. Hartl, F.-U., Just, W. W., Kijster, A. & Schimassek, H. Improved Isolation and Purification of Rat Liver Peroxisomes by Combined Rate Zonal and Equilibrium Density Centrifugation. *Arch Biochem Biophys* 237, 124–134 (1985).

58. Adrian, R., Gear, L. & Bednarek, J. M. Direct Counting and Sizing of Mitochondria in Solution. *J Cell Biol* 54, 325–345 (1972).
59. Martines, A. C. M. F., van Eunen, K., Reijngoud, D. J. & Bakker, B. M. The promiscuous enzyme medium-chain 3-keto-acyl-CoA thiolase triggers a vicious cycle in fatty-acid beta-oxidation. *PLoS Comput Biol* 13, (2017).
60. Eaton, S. Control of mitochondrial β -oxidation flux. *Prog Lipid Res* 41, 197–239 (2001).
61. Terzenbach, D. P. & Blaut, M. Purification and Characterization of a catalase from the nonsulfur phototrophic bacterium *Rhodospira rubra* ATH 2.4.1 and its role in the oxidative stress response. *Arch Microbiol* 503–508 (1998) doi:10.1007/s002030050603.
62. Shima, S. *et al.* Purification, characterization, and primary structure of a monofunctional catalase from *Methanosarcina barkeri*. *Arch Microbiol* 317–323 (1999) doi:10.1007/s002030050716.
63. Krisans, S. K., Ericsson, J., Edwards, P. A. & Keller, G.-A. Farnesyl-diphosphate Synthase Is Localized in Peroxisomes*. *Journal of Biological Chemistry* 269, 14165–14169 (1994).
64. van Zutphen, T. *et al.* Malnutrition-associated liver steatosis and ATP depletion is caused by peroxisomal and mitochondrial dysfunction. *J Hepatol* 65, 1198–1208 (2016).
65. Sargent, G. *et al.* PEX2 is the E3 ubiquitin ligase required for pexophagy during starvation. *Journal of Cell Biology* 214, (2016).
66. Horcas-Nieto, J. M. *et al.* Organoids as a model to study intestinal and liver dysfunction in severe malnutrition. *Biochim Biophys Acta Mol Basis Dis* 1869, (2023).

SUPPLEMENTARY FILES

Supplementary text 1

Ordinary differential equations

The peroxisomal β -oxidation model here presented consists of a set of ordinary differential equations (ODEs) that describe the change of the metabolites in the pathway as a function of time. The model is composed of 24 ODEs. To compute the steady state these are set equal to zero.

Most of the enzymes in the model catalyze accept CoA esters of multiple chain-lengths as a substrate, with the exception of catalase. The ODE describing the time dependence of a metabolite concentration balances all the rates of the reactions that produce the metabolite minus the rates of the reactions that consume it. Metabolite concentrations are in μM , time in min, and rates in $\mu\text{mol}/\text{min}/\text{mg}$ peroxisomal protein. To relate concentrations in μM to rates in $\mu\text{mol}/\text{min}/\text{mg}$ peroxisomal protein, in the ODEs a correction is made for the volume of the peroxisome. Both CROT and CRAT are described in the direction of the acyl-CoA formation from acyl-carnitines, and all other reactions in the direction of fatty-acid breakdown. The ODEs are defined as follows:

$$\begin{aligned} \frac{dC18EnoylCoA}{dt} &= \frac{v_{ACOX1C18} - v_{DBPC18}}{V_{PEX}} \\ \frac{dC18KetoacylCoA}{dt} &= \frac{v_{DBPC18} - v_{ACAA1C18}}{V_{PEX}} \\ \frac{dC16AcylCoA}{dt} &= \frac{v_{ACAA1C18} + v_{CROT_{C16}} - v_{ACOX1C16}}{V_{PEX}} \\ \frac{dC16AcylCarnitine}{dt} &= \frac{-v_{CROT_{C16}}}{V_{PEX}} \\ \frac{dC16EnoylCoA}{dt} &= \frac{v_{ACOX1C16} - v_{DBPC16}}{V_{PEX}} \\ \frac{dC16KetoacylCoA}{dt} &= \frac{v_{DBPC16} - v_{ACAA1C16}}{V_{PEX}} \\ \frac{dC14AcylCoA}{dt} &= \frac{v_{ACAA1C16} + v_{CROT_{C14}} - v_{ACOX1C14}}{V_{PEX}} \\ \frac{dC14AcylCarnitine}{dt} &= \frac{-v_{CROT_{C14}}}{V_{PEX}} \\ \frac{dC14EnoylCoA}{dt} &= \frac{v_{ACOX1C14} - v_{DBPC14}}{V_{PEX}} \\ \frac{dC14KetoacylCoA}{dt} &= \frac{v_{DBPC14} - v_{ACAA1C14}}{V_{PEX}} \\ \frac{dC12AcylCoA}{dt} &= \frac{v_{ACAA1C14} + v_{CROT_{C12}} - v_{ACOX1C12}}{V_{PEX}} \\ \frac{dC12AcylCarnitine}{dt} &= \frac{-v_{CROT_{C12}}}{V_{PEX}} \end{aligned}$$

$$\begin{aligned} \frac{dC12EnoylCoA}{dt} &= \frac{v_{ACOX1C12} - v_{DBPC12}}{V_{PEX}} \\ \frac{dC12KetoacylCoA}{dt} &= \frac{v_{DBPC12} - v_{ACAA1C12}}{V_{PEX}} \\ \frac{dC10AcylCoA}{dt} &= \frac{v_{ACAA1C12} + v_{CROT_{C10}} + v_{CRAT_{C10}} - v_{ACOX1C10}}{V_{PEX}} \\ \frac{dC10AcylCarnitine}{dt} &= \frac{-v_{CROT_{C10}} - v_{CRAT_{C10}}}{V_{PEX}} \\ \frac{dC10EnoylCoA}{dt} &= \frac{v_{ACOX1C10} - v_{DBPC10}}{V_{PEX}} \\ \frac{dC10KetoacylCoA}{dt} &= \frac{v_{DBPC10} - v_{ACAA1C10}}{V_{PEX}} \\ \frac{dC8AcylCoA}{dt} &= \frac{v_{ACAA1C10} + v_{CROT_{C8}} + v_{CRAT_{C8}} - v_{ACOX1C8}}{V_{PEX}} \\ \frac{dC8AcylCarnitine}{dt} &= \frac{-v_{CROT_{C8}} - v_{CRAT_{C8}}}{V_{PEX}} \\ \frac{dC8EnoylCoA}{dt} &= \frac{v_{ACOX1C8} - v_{DBPC8}}{V_{PEX}} \\ \frac{dC8KetoacylCoA}{dt} &= \frac{v_{DBPC8} - v_{ACAA1C8}}{V_{PEX}} \\ \frac{dC6AcylCoA}{dt} &= \frac{v_{ACAA1C8} + v_{CROT_{C6}} + v_{CRAT_{C6}}}{V_{PEX}} \\ \frac{dH_2O_2}{dt} &= \frac{(v_{ACOX1C18} + v_{ACOX1C16} + v_{ACOX1C14} + v_{ACOX1C12} + v_{ACOX1C10} + v_{ACOX1C8}) - v_{Cat}}{V_{PEX}} \end{aligned}$$

Fixed boundary metabolites and conserved moieties

NAD

NADH

FreeCoA

AcetylCoA

Carnitine

$O_2 = O_2 \text{ Initial} + H_2O_2$

Kinetic rate equations

In this section we present the rate equations that describe the conversion of multiple substrates by different enzymes. The majority of the reactions are modelled as reversible Michaelis-Menten equations, based on convenience kinetics¹, with competitive inhibition by all alternative substrates and products, as it was done previously for the mitochondrial β -oxidation. The only exception

is the reaction catalyzed by catalase, which is modelled as irreversible Michaelis-Menten, because of its extremely high equilibrium constant (K_{eq}). In the case of CROT and CRAT, the reaction is described in the direction of the formation of acyl-CoA (reverse reaction), as the V_{max} in the literature was measured in this direction. The rates of all the enzymes are given in $\mu\text{mol} \cdot \text{min}^{-1} \cdot \text{mg}$ peroxisomal Protein $^{-1}$.

List of rate equations:

ACOX1

For n = 8, 10, 12, 14, 16, 18:

$$V_{ACOX1 c_n} = \frac{sf_{ACOX1 c_n} \cdot Vmax_{ACOX1} \cdot \frac{C_{AcylCoA} \cdot O_2}{K_{mACOX1} C_{AcylCoA} K_{mACOX1 O_2}} - \frac{C_{EnoylCoA} \cdot H_2O_2}{K_{mACOX1} C_{AcylCoA} K_{mACOX1 O_2} K_{eqACOX1}}}{\left(1 + \sum_{n=8}^{18} \left(\frac{C_{AcylCoA}}{K_{mACOX1} C_{AcylCoA}} + \frac{C_{EnoylCoA}}{K_{mACOX1} C_{EnoylCoA}} \right) \right) \cdot \left(1 + \frac{H_2O_2}{K_{mACOX1} H_2O_2} + \frac{O_2}{K_{mACOX1} O_2} \right) \cdot \left(1 + \frac{CoA}{K_{ACOX1} CoA} \right) \cdot \left(1 + \frac{C_{KetoacylCoA}}{K_{ACOX1} KetoacylCoA} \right)}$$

DBP

For n = 8, 10, 12, 14, 16, 18:

$$V_{DBP c_n} = \frac{sf_{DBP c_n} \cdot Vmax_{DBP} \cdot \frac{C_{EnoylCoA} \cdot (NAD)}{K_{mDBP} C_{EnoylCoA} K_{mDBP} NAD} - \frac{C_{KetoacylCoA} \cdot NADH}{K_{mDBP} C_{EnoylCoA} K_{mDBP} NAD \cdot K_{eqDPB}}}{\left(1 + \sum_{n=8}^{18} \left(\frac{C_{EnoylCoA}}{K_{mDBP} C_{EnoylCoA}} + \frac{C_{KetoacylCoA}}{K_{mDBP} C_{KetoacylCoA}} \right) \right) \cdot \left(1 + \frac{(NAD)}{K_{mDBP} NAD} + \frac{NADH}{K_{mDBP} NADH} \right)}$$

ACAA1

For n = 8, 10, 12, 14, 16, 18:

$$V_{ACAA1 c_n} = \frac{sf_{ACAA1 c_n} \cdot Vmax_{ACAA1} \cdot \left(\frac{C_{KetoacylCoA} \cdot CoA}{K_{mACAA1} C_{KetoacylCoA} K_{mACAA1} CoA} - \frac{C_{AcylCoA} \cdot NADH}{K_{mACAA1} C_{KetoacylCoA} K_{mACAA1} CoA K_{eqACAA1}} \right)}{\left(1 + \sum_{n=8}^{18} \left(\frac{C_{KetoacylCoA}}{K_{mACAA1} C_{KetoacylCoA}} + \frac{C_{AcylCoA}}{K_{mACAA1} C_{AcylCoA}} \right) + \frac{AcetylCoA}{K_{mACAA1} AcetylCoA} \right) \cdot \left(1 + \frac{CoA}{K_{mACAA1} CoA} + \frac{NADHAcetylCoA}{K_{mACAA1} AcetylCoA} \right)}$$

CROT = described in the direction of the Acyl-CoA (reverse reaction)

For n = 6, 8, 10, 12, 14, 16

$$V_{CROT c_n} = \frac{sf_{CROT c_n} \cdot Vmax_{CROT} \cdot \left(\frac{C_{AcylGarnitine} \cdot CoA}{K_{mCROT} C_{AcylGarnitine} K_{mCROT} C_n CoA} - \frac{C_{AcylCoA} \cdot Carnitine}{K_{mCROT} C_{AcylGarnitine} K_{mCROT} C_n CoA K_{eqCROT}} \right)}{\left(1 + \sum_{n=6}^{16} \left(\frac{C_{AcylGarnitine}}{K_{mCROT} C_{AcylGarnitine}} + \frac{C_{AcylCoA}}{K_{mCROT} C_{AcylCoA}} \right) \right) \cdot \left(1 + \frac{CoA}{K_{mCROT} C_n CoA} + \frac{Carnitine}{K_{mCROT} Carnitine} \right)}$$

CRAT = described in the direction of the Acyl-CoA (reverse reaction)

For n = 6, 8, 10,

$$V_{\text{CRAT } C_n} = \frac{sf_{\text{CRAT } C_n} \cdot v_{\text{max}_{\text{CRAT}}} \cdot \left(\frac{C_r \text{AcylGarnitine} \cdot \text{CoA}}{K_m \text{CRAT } C_r \text{AcylGarnitine} \cdot K_m \text{CRAT } C_n \text{CoA}} - \frac{C_r \text{AcylCoA} \cdot \text{Carnitine}}{K_m \text{CRAT } C_r \text{AcylGarnitine} \cdot K_m \text{CRAT } C_n \text{CoA} \cdot K_{\text{eq}_{\text{CRAT}}}} \right)}{\left(1 + \sum_{n=8}^{10} \frac{C_r \text{AcylGarnitine}}{K_m \text{CRAT } C_r \text{AcylGarnitine}} + \frac{C_r \text{AcylCoA}}{K_m \text{CRAT } C_r \text{AcylCoA}} \right) \cdot \left(1 + \frac{\text{CoA}}{K_m \text{CRAT } C_n \text{CoA}} + \frac{\text{Carnitine}}{K_m \text{CRAT } \text{Carnitine}} \right)}$$

CAT

First order

$$V_{\text{cat}} = \frac{v_{\text{max}_{\text{cat}}} \cdot \text{H}_2\text{O}_2}{K_m \text{cat} \text{H}_2\text{O}_2 + \text{H}_2\text{O}_2}$$

Second order rate

$$V_{\text{cat}} = K \cdot [\text{catalase}] \cdot \text{H}_2\text{O}_2$$

Kinetic parameters

Parameter	Value		Value corrected		Ref
ACOX1					
V_{\max_ACOX1}	3.130	$\mu\text{mol}/\text{min}/\text{mg protein}$	0.04843	$\mu\text{mol}/\text{min}/\text{mg peroxisomal protein}$	2
sf_C18_ACOX1	0.65	/			2
sf_C16_ACOX1	1	/			2
sf_C14_ACOX1	1.1	/			2
sf_C12_ACOX1	0.38	/			2
sf_C10_ACOX1	1.06	/			2
$Km_C18_AcylCoa_ACOX1$	9.6	μM			2
$Km_C16_AcylCoa_ACOX1$	11.6	μM			2
$Km_C10_AcylCoa_ACOX1$	20	μM			2
$Km_C8_AcylCoa_ACOX1$	58.8	μM			2
$Km_C18_EnoylCoa_ACOX1$	1.08	μM			3
$Km_C16_EnoylCoa_ACOX1$	1.08	μM			3
$Km_C14_EnoylCoa_ACOX1$	1.08	μM			3
$Km_C12_EnoylCoa_ACOX1$	1.08	μM			3
$Km_C10_EnoylCoa_ACOX1$	1.08	μM			3
$Km_C8_EnoylCoa_ACOX1$	1.08	μM			3
Km_O2_ACOX1	5	μM			3
Km_H2O2_ACOX1	10	μM			/
K_{eq_ACOX1}	$6.8 \cdot 10^{12}$	/			eQ
Ki_Coa_ACOX1	63.3	μM			4
$Ki_C16ketoacyl-Coa$	0.47	μM			2
DBP					
V_{\max_DBP}	2.5	$\mu\text{mol}/\text{min}/\text{mg protein}$	0.338	$\mu\text{mol}/\text{min}/\text{mg peroxisomal protein}$	5
sf_C18_DBP	0.44	/			6
sf_C16_DBP	0.82	/			6
sf_C14_DBP	1	/			6
sf_C12_DBP	0.96	/			6
sf_C10_DBP	0.87	/			6
sf_C8_DBP	0.62	/			6

<i>K_m</i> _C18_EnoylCoa_DBP	10	μM	6
<i>K_m</i> _C16_EnoylCoa_DBP	10	μM	6
<i>K_m</i> _C14_EnoylCoa_DBP	10	μM	6
<i>K_m</i> _C12_EnoylCoa_DBP	10	μM	6
<i>K_m</i> _C10_EnoylCoa_DBP	10	μM	6
<i>K_m</i> _C8_EnoylCoa_DBP	10	μM	6
<i>K_m</i> _C18_KetoacylCoa_DBP	1.4	μM	3
<i>K_m</i> _C16_KetoacylCoa_DBP	1.4	μM	3
<i>K_m</i> _C14_KetoacylCoa_DBP	1.4	μM	3
<i>K_m</i> _C12_KetoacylCoa_DBP	1.6	μM	3
<i>K_m</i> _C10_KetoacylCoa_DBP	2.3	μM	3
<i>K_m</i> _C8_KetoacylCoa_DBP	4.1	μM	3
<i>K_m</i> _NAD_DBP	58	μM	3
<i>K_m</i> _NADH_DBP	5.4	μM	3
<i>K_{eq}</i> _DBP	1·10 ⁻³		eQ

ACAA1

<i>V_{max}</i> _ACAA1	144	μmol/min/ mg protein	6.7	μmol/min/mg peroxisomal protein	6
<i>sf</i> _C18_ACAA1	0.08	/			7
<i>sf</i> _C16_ACAA1	0.17	/			7
<i>sf</i> _C14_ACAA1	0.49	/			7
<i>sf</i> _C12_ACAA1	0.69	/			7
<i>sf</i> _C10_ACAA1	1	/			7
<i>sf</i> _C8_ACAA1	0.86	/			7
<i>K_m</i> _C18_KetoacylCoa_ACAA1	10	μM			7
<i>K_m</i> _C16_KetoacylCoa_ACAA1	1.9	μM			7
<i>K_m</i> _C14_KetoacylCoa_ACAA1	2.45	μM			7
<i>K_m</i> _C12_KetoacylCoa_ACAA1	3	μM			7
<i>K_m</i> _C10_KetoacylCoa_ACAA1	8	μM			7
<i>K_m</i> _C8_KetoacylCoa_ACAA1	8.6	μM			7
<i>K_m</i> _C16_AcylCoa_ACAA1	13.83	μM			3

$K_{m-C14_AcylCoa_ACAA1}$	13.83	μM	3
$K_{m-C12_AcylCoa_ACAA1}$	13.83	μM	3
$K_{m-C10_AcylCoa_ACAA1}$	13.83	μM	3
$K_{m-C8_AcylCoa_ACAA1}$	13.83	μM	3
$K_{m-C16_AcylCoa_ACAA1}$	13.83	μM	3
$K_{m-AcetylCoa_ACAA1}$	30	μM	3
K_{m-CoA_ACAA1}	16	μM	7
K_{eq_ACAA1}	$2.49 \cdot 10^5$		EQ,7

CROT

V_{max_CROT}	0.117		$\mu\text{mol}/\text{min}/\text{mg}$ peroxisomal protein	8
sf_C18_CROT	0	/		9
sf_C16_CROT	0.25	/		9
sf_C14_CROT	0.51	/		9
sf_C12_CROT	0.125	/		9
sf_C10_CROT	0.62	/		9
sf_C8_CROT	0.85	/		9
Sf_C6_CROT	1	/		9
$K_{m-C16_AcylCoa_CROT}$	5.2	μM		8
$K_{m-C14_AcylCoa_CROT}$	5.3	μM		8
$K_{m-C12_AcylCoa_CROT}$	8.3	μM		8
$K_{m-C10_AcylCoa_CROT}$	10	μM		8
$K_{m-C8_AcylCoa_CROT}$	6.5	μM		8
$K_{m-C6_AcylCoa_CROT}$	23	μM		8
$K_{m-C16_AcylCarnitine_CROT}$	13	μM		8
$K_{m-C14_AcylCarnitine_CROT}$	4.6	μM		8
$K_{m-C12_AcylCarnitine_CROT}$	5	μM		8
$K_{m-C10_AcylCarnitine_CROT}$	20	μM		8
$K_{m-C8_AcylCarnitine_CROT}$	48	μM		8
$K_{m-C6_AcylCarnitine_CROT}$	220	μM		8
$K_{m-carnitine C16_CROT}$	38	μM		8
$K_{m-carnitine C14_CROT}$	64	μM		8
$K_{m-carnitine C12_CROT}$	61	μM		8
$K_{m-carnitine C10_CROT}$	68	μM		8

$K_{m_carnitine\ C8_CROT}$	112	μM		8
$K_{m_carnitine\ C6_CROT}$	94	μM		8
$K_{m_CoA\ C16_CROT}$	5	μM		8
$K_{m_CoA\ C14_CROT}$	11	μM		8
$K_{m_CoA\ C12_CROT}$	8.1	μM		8
$K_{m_CoA\ C10_CROT}$	8.3	μM		8
$K_{m_CoA\ C8_CROT}$	57	μM		8
$K_{m_CoA\ C6_CROT}$	52	μM		8
K_{eq_CROT}	0.3			eQ

CRAT

V_{max_CRAT}	0.117			$\mu\text{mol}/\text{min}/\text{mg}$ peroxisomal protein	8
sf_C10_CRAT	0.66	/			9
sf_C8_CRAT	0.83	/			9
sf_C6_CRAT	1	/			9
$K_{m_C10_AcylCoa_CRAT}$	28.7	μM			9
$K_{m_C8_AcylCoa_CRAT}$	19.1	μM			9
$K_{m_C6_AcylCoa_CRAT}$	20	μM			9
$K_{m_C10_AcylCarnitine_CRAT}$	519	μM			9
$K_{m_C8_AcylCarnitine_CRAT}$	395	μM			9
$K_{m_C6_AcylCarnitine_CRAT}$	344	μM			9
$K_{m_carnitine\ C10}$	519	μM			9
$K_{m_carnitine\ C8}$	395	μM			9
$K_{m_carnitine\ C6}$	344	μM			9
K_{m_CoA}	39.1	μM			8
K_{eq_CRAT}	0.3				eQ

CAT

V_{max_CAT}			4600	$\mu\text{mol}/\text{min}/\text{mg}$ peroxisomal protein	10-12
	0.18	$\mu\text{mol}/\text{min}/$ mg liver protein	9.375	$\mu\text{mol}/\text{min}/\text{mg}$ peroxisomal protein	13
V_{max_CAT}					
$K_{m_H2O2_cat}$	93	mM	93000	μM	12

Volume of peroxisome	$1.8 \cdot 10^{-6}$	L:mgProtein	3
NAD	250	μM	3
NADH	25	μM	3
AcetylCoA	700	μM	3
FreeCoA	700	μM	14
Carnitine	2000	μM	7
Oxygen	260	μM	/

Assumptions and calculations

The K_m of ACOX1 for H_2O_2 was estimated to be higher than that of oxygen as the enzyme runs in the forward direction and it is not expected to have high affinity for the product. No K_m value was found in the literature. The value 10 is theoretical and not expected to affect the reaction, given the high K_{eq} .

The V_{max} of CRAT used was the same as found for CROT as no studies reporting the absolute value were found.

K_{m_CoA} of CRAT was estimated by averaging the values of K_m for Coa in the presence of C6, C8 and C10 of CROT.

The V_{max} of Catalase was calculated by averaging the V_{max} of different papers isolated from different organisms. The average obtained was 46249.99, therefore we approximated it to 46000.

The concentration of oxygen was estimated to be the solubility of oxygen in water at 37 °C.

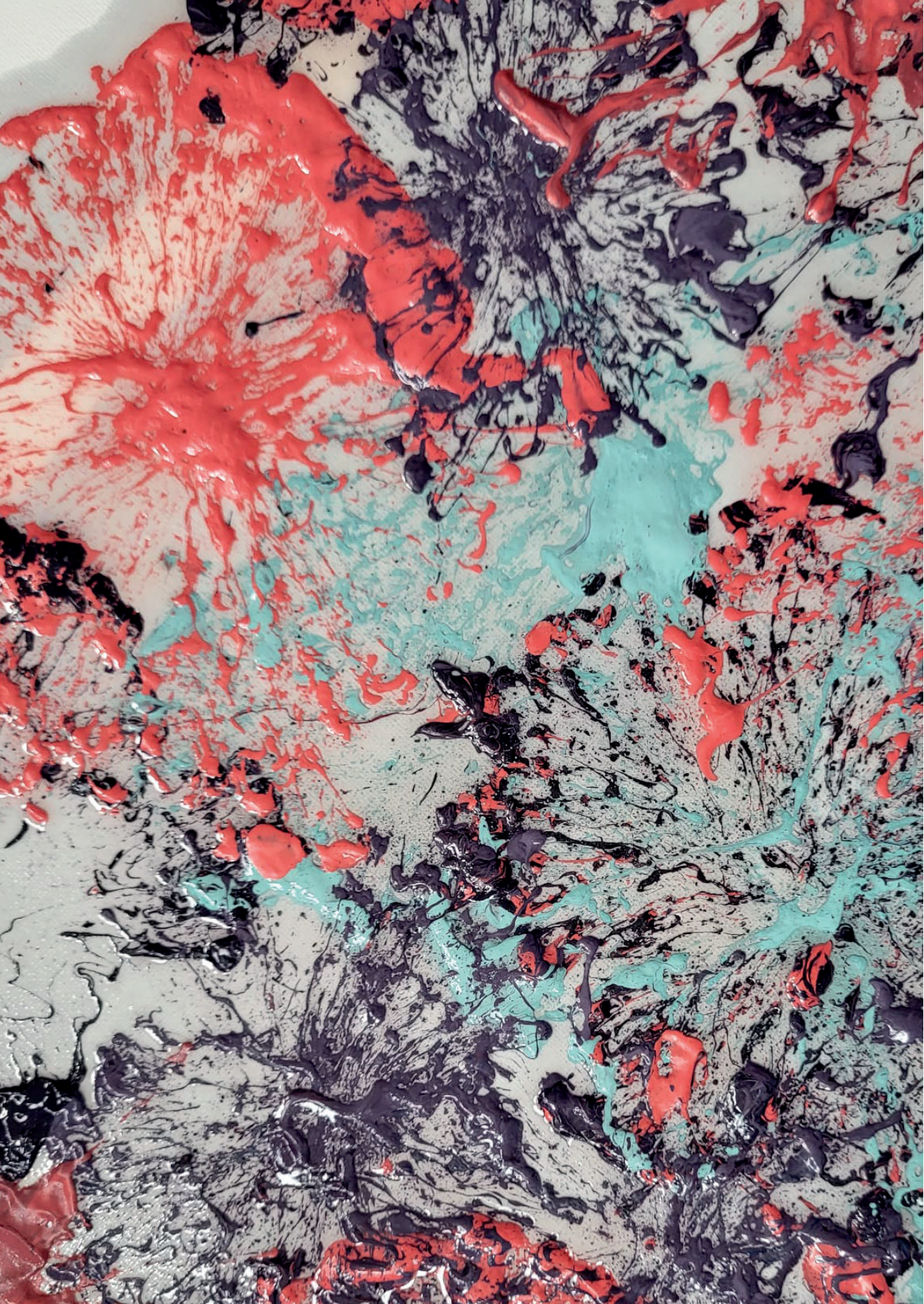
When expressed per peroxisomal protein this volumes was assumed to be similar to that of mitochondria. This assumption is not so strange as it seems, since the volume per protein is similar for mitochondria and cytosol (value X versus value Y), suggesting that its order of magnitude is not very different for different cellular compartments.

Supplementary references

1. Liebermeister W, Klipp E. Bringing metabolic networks to life: Convenience rate law and thermodynamic constraints. *Theor Biol Med Model.* 2006;3. doi:10.1186/1742-4682-3-41
2. Osumi T, Hashimoto T, Ui N. Purification and Properties of Acyl-CoA Oxidase from Rat Liver 1. *J Biochem.* 1980;87:1735-1746. doi:10.1093/oxfordjournals.jbchem.a132918.
3. van Eunen K, Simons SMJ, Gerding A, et al. Biochemical Competition Makes Fatty-Acid β -Oxidation Vulnerable to Substrate Overload. *PLoS Comput Biol.* 2013;9(8). doi:10.1371/journal.pcbi.1003186
4. Hovik R, Osmundsen H. Factors Which Affect the Activity of Purified Rat Liver Acyl-CoA Oxidase.
5. Furuta S, Miyazawa S, Osumi T, Hashimoto T, Ui N. Properties of Mitochondrial and Peroxisomal Enoyl-CoA Hydratases from Rat Liver 1. *Biochem.* 1980;88(4):1059-1070. doi:10.1093/oxfordjournals.jbchem.a133057
6. Miyazawa S, Furuta S, Osumi T, Hashimoto T, Up N. Properties of Peroxisomal 3-Ketoacyl-CoA Thiolase from Rat Liver 1. Vol 90.; 1981.
7. Odendaal C, Jager EA, Martines ACMF, et al. Personalised modelling of clinical heterogeneity between medium-chain acyl-CoA dehydrogenase patients. *BMC Biol.* 2023;21(1):184. doi:10.1186/s12915-023-01652-9
8. Miyazawa S, Ozasa H, Osumi T, Hashimoto T. Purification and Properties of Camitine Octanoyltransferase and Camitine Palmitoyltransferase from Rat Liver 1. *J Biochem.* 1983;94(2):529-542.
9. Farrell SO, Fiol CJ, Reddy JK, Bieber LL. Properties of purified carnitine acyltransferases of mouse liver peroxisomes. *Journal of Biological Chemistry.* 1984;259(21):13089-13095. doi:10.1016/s0021-9258(18)90661-7
10. Terzenbach DP, Blaut M. Purification and Characterization of a catalase from the nonsulfur phototrophic bacterium *Rhodospirillum rubrum* strain ATH 2.4.1 and its role in the oxidative stress response. *Arch Microbiol.* 1998;(1069):503-508. doi:10.1007/s002030050603
11. Shima S, Netrusov A, Sordel M, Wicke M, Hartmann GC, Thauer RK. Purification, characterization, and primary structure of a monofunctional catalase from *Methanosarcina barkeri*. *Arch Microbiol.* 1999;(171):317-323. doi:10.1007/s002030050716
12. Switala J, Loewen PC. Diversity of properties among catalases. *Arch Biochem Biophys.* 2022;(401):145-154. doi:10.1016/S0003-9861(02)00049-8.
13. Krisans SK, Ericsson NJ, Edwardsn PA, Keller GA. Farnesyl-diphosphate Synthase Is Localized in Peroxisomes*. *Journal of Biological Chemistry.* 1994;269(19):14165-14169. doi:10.1016/S0021-9258(17)36769-8
14. Horie S, Isobe M, Suga T. Changes in CoA Pools in Hepatic Peroxisomes of the Rat under Various Conditions. *J Biochem.* 1986;99(5):1345-1352. doi:10.1093/oxfordjournals.jbchem.a135602

Supplementary Table 2. Metabolites at steady state in control, amino-acid restriction and amino-acid restriction supplemented with 100 μ M DHA.

	L009		100DHA		L011		%		100DHA		L014		%		100DHA	
	Control	DMSO	Control	DMSO	Control	DMSO	Control	DMSO	Control	DMSO	Control	DMSO	Control	DMSO	Control	DMSO
C18 acylcoa	150	150	100	150	100	150	100	150	100	150	100	150	100	150	100	150
C18 ketoacylcoa	90.669	40.507	44.67568849	76.434	84.3000364	88.065	39.076	43.873575	120.206	134.9643519	118.68	83.414	70.2847946	132.895	111.9776	100
C18 ketoacylcoa	0.899	0.403	44.82758621	0.759	84.4274127	0.883	0.389	44.08436	1.188	134.5413364	1.173	0.827	70.5029838	1.312	111.85	100
C16 acylcoa	117.812	117.812	100.0009488	117.812	100	117.812	117.812	100	117.812	100	117.812	117.812	100	117.812	100	100
C16 acylcarnitine	841.518	841.518	100	841.518	100	841.518	841.518	100	841.518	100	841.518	841.518	100	841.518	100	100
C16 ketoacylcoa	8.293	3.693	44.53153262	6.979	84.15531171	8.143	3.963	43.744629	11.041	135.5555556	10.936	7.623	69.94861442	12.229	112.2133	100
C16 ketoacylcoa	0.081	0.036	44.44444444	0.068	83.95061728	0.079	0.035	44.303797	0.107	135.443058	0.105	0.074	70.47619048	0.118	112.381	100
C14 acylcoa	107.102	107.102	100	107.102	100	107.102	107.102	100	107.102	100	107.102	107.102	100	107.102	100	100
C14 acylcarnitine	765.016	765.016	100	765.016	100	765.016	765.016	100	765.016	100	765.016	765.016	100	765.016	100	100
C14 ketoacylcoa	3.889	1.785	45.89868861	3.285	84.464901517	3.82	1.726	45.183246	5.159	135.052356	5.093	3.58	70.29258841	5.713	112.1736	100
C14 ketoacylcoa	0.037	0.018	48.64864865	0.032	86.4848648649	0.037	0.017	45.945946	0.049	132.4324324	0.048	0.034	70.83333333	0.054	112.5	100
C12 acylcoa	347.451	347.451	100	347.451	100	347.451	347.451	100	347.451	100	347.451	347.451	100	347.451	100	100
C12 acylcarnitine	2481.79	2481.79	100	2481.79	100	2481.79	2481.79	100	2481.79	100	2481.79	2481.79	100	2481.79	100	100
C12 ketoacylcoa	3.343	1.509	45.13909662	2.816	84.23571642	3.283	1.458	44.4106	4.452	135.6076759	4.394	3.074	69.95903505	4.935	112.3122	100
C12 ketoacylcoa	0.032	0.015	46.875	0.027	84.375	0.031	0.014	45.16129	0.042	135.483871	0.042	0.03	71.42857143	0.046	109.5238	100
C10 acylcoa	191.627	191.627	100	191.627	100	191.627	191.627	100	191.627	100	191.627	191.627	100	191.627	100	100
C10 acylcarnitine	1368.767	1368.767	100	1368.767	100	1368.767	1368.767	100	1368.767	100	1368.767	1368.767	100	1368.767	100	100
C10 ketoacylcoa	6.145	2.869	46.68836452	5.211	84.80065094	6.04	2.776	45.960265	8.097	134.0562914	7.995	5.668	70.89430894	8.94	111.8199	100
C10 ketoacylcoa	0.06	0.028	46.66666667	0.051	85	0.059	0.027	45.762712	0.079	133.8983051	0.078	0.056	71.9487179	0.087	111.5385	100
C8 acylcoa	649.117	649.117	100	649.117	100	649.117	649.117	100	649.117	100	649.117	649.117	100	649.117	100	100
C8 acylcarnitine	4636.549	4636.549	100	4636.549	100	4636.549	4636.549	100	4636.549	100	4636.549	4636.549	100	4636.549	100	100
C8 ketoacylcoa	7.345	3.256	44.32947583	6.179	84.1252528	7.213	3.14	43.532511	9.779	135.5746569	9.653	6.75	69.92644774	10.831	112.7035	100
C8 ketoacylcoa	0.072	0.032	44.44444444	0.061	84.7222222	0.071	0.031	43.661972	0.095	133.8028169	0.094	0.066	70.21276596	0.105	111.7021	100
C6 acylcoa	4.46	1.999	44.8705278	3.703	83.0260683	4.29	1.958	45.641036	5.981	139.4172494	5.872	4.136	70.4359673	6.511	110.8822	100
H2O2	10.308008	4.769578	46.27060825	5.551723	53.85838974	6.907884	5.301351	76.743486	11.623568	168.2958197	11.953225	8.753823	73.23949943	12.11016	101.2005	100
Flux	0.000144661	6.50E-05	44.92888872	0.000122158	84.4445505	0.000142	6.27E-05	44.116939	1.91E-04	134.448117	0.000188709	1.33E-04	70.58360633	2.11E-04	111.7872	100



Chapter



iPSC-derived liver organoids as a tool to study Medium Chain Acyl-CoA Dehydrogenase deficiency

José. M Horcas-Nieto^{1*}, Ligia A Kiyuna^{1*}, Miriam Langelaar-Makkinje¹, Albert Gerding^{1,2}, Mathilde J. C. Broekhuis³ Flavio Bonanini⁴, Madhulika Singh⁵, Dorota Kurek⁴, Amy C. Harms⁵, Thomas Hankemeier⁵, Floris Foijer³, Barbara M. Bakker^{1§}

1 Laboratory of Paediatrics, University of Groningen, University Medical Centre Groningen, Groningen, the Netherlands; 2 Department of Laboratory Medicine, University of Groningen, University Medical Center Groningen, Groningen, The Netherlands; 3. European Research Institute for the Biology of Ageing, University of Groningen, University Medical Center Groningen, Groningen, The Netherlands; 4. Mimetas, Leiden, The Netherlands; 5. Metabolomics and Analytics Centre, Leiden Academic Centre for Drug Research, Leiden University, The Netherlands

*** These authors contributed equally to this work**

§ Corresponding author:

Prof. dr. Barbara M Bakker

Department of Pediatrics, University of Groningen, University Medical Center Groningen
Antonius Antonius Deusinglaan 1, 9713 AV Groningen, The Netherlands, Building 3226.
Postbus 196, 9700 AD Groningen, The Netherlands (Internal ZIP Code EA12) Phone: +31 50 361 1542

Email: b.m.bakker01@umcg.nl

Submitted

ABSTRACT

Background

Medium chain acyl-CoA dehydrogenase deficiency (MCADD) is an inherited metabolic disease, characterized by a mutation in the *ACADM* gene. Interestingly, even with the same mutation, patients often present with very heterogeneous symptoms, ranging from fully asymptomatic to life-threatening hypoketotic hypoglycemia. The mechanisms underlying this heterogeneity remain unclear. Therefore, there is a need for in vitro models of MCADD that recapitulate the clinical phenotype as a tool to study the pathophysiology of the disease.

Methods

Fibroblasts of control and symptomatic MCADD patients with the c.985A>G (p.K329E) were reprogrammed into induced pluripotent stem cells (iPSCs). iPSC were then differentiated into hepatic expandable organoids (EHOs), further matured to Mat-EHOs, and functionally characterized.

Results

EHOs and Mat-EHOs performed typical hepatic metabolic functions, such as albumin and urea production. The organoids metabolized fatty acids, as confirmed by acyl-carnitine profiling and high-resolution respirometry. MCAD protein was fully ablated in MCADD organoids, in agreement with the instability of the mutated MCAD protein. MCADD organoids accumulated medium-chain acyl-carnitines, with a strongly elevated C8/C10 ratio, characteristic clinical phenotype of the disease. Notably, C2 and C14 acyl-carnitines were found decreased in MCADD Mat-EHOs. Finally, MCADD organoids exhibited differential expression of genes involved in mitochondrial β -oxidation and peroxisomal coenzyme A metabolism, particularly upregulation of *NUDT7*.

Discussion

iPSC-derived organoids of MCADD patients recapitulated the major clinical phenotype of the disease. Mat-EHOs expressed relevant pathways involved in putative compensatory mechanisms, notably CoA metabolism. The upregulation of *NUDT7* expression may play a role in preventing excessive accumulation of dicarboxylic acids in MCADD. This patient-specific-hepatic organoid system is a promising platform to study the phenotypic heterogeneity between MCADD patients.

INTRODUCTION

Medium-chain acyl-CoA dehydrogenase (MCAD) is one of the flavoenzymes that catalyze the first step of mitochondrial β -oxidation of fatty acids. It oxidizes medium-chain acyl-CoA into 2-enoyl-CoA. MCAD deficiency (MCADD) is an autosomal recessive disease and the most common fatty acid oxidation disorder (FAOD) with a prevalence of 1/8,300 in the Netherlands¹. Interestingly, people homozygous for an *ACADM* mutation can present various clinical phenotypes. While some patients remain asymptomatic throughout life, some experience life-threatening hypoketotic hypoglycemia when exposed to catabolic stress (e.g. fasting and intercurrent illness)²⁻⁴. After diagnosis, the most common treatment relies on avoidance of fasting and an emergency regimen^{5,6}. While the mutation c.985A>G (p.K329E) is estimated to account for more than 90% of pathogenic alleles, the implementation of MCADD in newborn screening has revealed several *ACADM* variants of unknown significance⁷. The clinical risk associated with individual variants and the mechanisms underlying metabolic decompensation remain unclear^{7,8}. Patients with residual MCAD activity, equal or above 10%, have been referred to as mild and often remain asymptomatic¹. However, within the group that is homozygous for the classical c.985A>G (p.K329E) mutation, patients may present with a wide range of symptoms and disease severity, suggesting a limited genotype-phenotype correlation. Therefore, it is likely that genetic variation beyond the *ACADM* gene, the environment, and epigenetics play a major role in the development of a metabolic crisis⁹.

Preclinical, mechanistic studies of the pathophysiology underlying MCADD have traditionally relied on the use of animal models¹⁰⁻¹². However, rodents are equipped with an extra dehydrogenase, long-chain acyl-CoA dehydrogenase (LCAD), which shows overlapping substrate specificity with MCAD¹³ and may therefore mask the phenotype. Additionally, a full *ACADM* deletion cannot elucidate the effect of individual point mutations in the *ACADM* gene. This makes human and patient-derived in vitro models an attractive alternative for the study of MCADD. Organoids are 3D multicellular structures that proliferate in vitro, while recapitulating several functions of the organ of origin. They can be obtained from primary tissue as well as from pluripotent and adult stem cells¹⁴. Liver organoids recapitulate several hepatic functions such as albumin production, bile acid production, and CYP3A4 activity¹⁵. Since they were first described¹⁶, organoids have been used for an increasing number of applications including the study of differentiation, organ development¹⁷, and (metabolic) disease¹⁸, as well as drug screening¹⁹. For primary tissue, highly invasive liver

biopsies are required. In contrast, hepatobiliary organoids can also be derived from induced pluripotent stem cells (iPSCs)²⁰⁻²³. The latter can be obtained from fibroblasts, lymphoblasts, or even urine cells, providing an expandable source of hepatic cells through a minimally invasive procedure²⁴. Several protocols have been developed for differentiating iPSCs into hepatobiliary organoids. Although these organoids remain closer to fetal than to adult tissue²⁵⁻²⁷, they represent an important organ-specific system to understand not only the disease mechanism but also patient-specific phenotypes and symptomatology.

Patient-specific iPSC-derived MCADD hepatobiliary organoids could serve (i) to study the effect of different mutations in the *ACADM* gene itself and (ii) to study compensatory mechanisms that may depend on genetic variation outside the *ACADM* gene. To realize this goal, it is important that organoids recapitulate the major disease phenotype. Moreover, pathways that have been hypothesized to play a compensatory role in asymptomatic patients, should be active in the organoids. Putative compensatory enzymes and pathways include short-chain acyl-CoA dehydrogenase²⁸, peroxisomal β -oxidation²⁹ and coenzyme A metabolism²⁸. Whereas the MCAD enzyme is localized in the mitochondria, peroxisomes are single membrane organelles equipped with their own β -oxidation pathway. They are involved in many metabolic processes and highly abundant in liver cells. They are renowned for their ability to oxidize branched-chain and very-long-chain fatty acids³⁰, yet they are also capable of oxidizing medium-chain fatty acids (MCFA)^{29 31} and fatty dicarboxylic acids³². To the best of our knowledge, there are currently no experimental studies reporting on the role of peroxisomes in any of the deficiencies of mitochondrial dehydrogenases (SCADD, MCADD and VLCADD).

The goal of this study was to establish and characterize an iPSC-derived hepatobiliary organoid system for the study of MCADD. iPSCs derived from fibroblasts of symptomatic MCADD patients with the classical c.985A>G (p.K329E) mutation were differentiated into hepatic organoids and compared to organoids from healthy controls. Here we demonstrate that MCADD organoids recapitulate typical diagnostic MCADD markers. Moreover, mature organoids upregulate peroxisomal markers, making them a suitable system to study patient-specific differences in peroxisomal metabolism. Finally, we report a minor regulation of peroxisomal CoA metabolism, already in these organoids of symptomatic MCADD patients.

RESULTS

Generating induced pluripotent stem cells from control and MCADD patient fibroblasts

Control and MCADD fibroblasts were reprogrammed into iPSCs following a previously published protocol³³. Immunofluorescence confirmed the expression of NANOG, OCT4, SOX2, SSEA-4, Tra-1-60 and Tra-1-81 indicating the pluripotency of the iPSCs (**Supplementary figure 1**).

Generating expandable hepatic organoids (EHOs) from control and MCADD iPSCs

In order to differentiate iPSCs into hepatic organoids, a previously published protocol³⁴ was slightly adapted (**Figure 1a**): to supplement Wnt3a and hRspn1, conditioned medium was used instead of recombinant proteins. At day 8 the cells were transferred from 2D culture and embedded into BME domes and cultured in expansion medium (EM) for at least 10 days. Morphological changes in the cells were observed at the different stages of the differentiation (**Figure 1b**). While most of the organoids were cystic and contained clear lumina, more complex structures could also be observed. Some organoids formed “lobule-like” structures emerging from a central structure (**Figure 1b**). At this stage, expandable hepatic organoids (EHO) could be cryopreserved and - after thawing - expanded in culture for several passages without any clear morphological changes.

In order to assess cell identity at the different stages of differentiation, the gene expression profile of the organoids was characterized (**Figure 1c-e**). We defined different developmental stages including iPSCs, definite endoderm (DE), hepatoblasts (HB), and EHOs (**Figure 1a and b**), and compared them to human liver biopsies. Endoderm-specific markers *SOX17*, *FOXA2*, *GATA4*, and *GATA6* were all induced at DE stage. *FOXA2*, *GATA4*, and *GATA6* stayed higher than in the iPSCs at all stages, while *SOX17* declined in EHOs, resembling the liver reference (**Figure 1c**). Early hepatic specification markers *TBX3* and *HNF4-α* were already observed in the DE stage but peaked in the EHOs. For alpha-fetoprotein (*AFP*), a fetal hepatocyte marker, we observed a peak in expression at the stage of EHOs and barely any presence in the earlier stages, nor in liver tissue. The hepatic marker albumin was not observed until later stages of the differentiation (HB) and showed its maximal expression in the EHOs. Interestingly, the albumin expression was very high in the EHOs and almost comparable to that in human liver (**Figure 1d**). Finally, the expression of early biliary markers *CK19* and *SOX19* (**Figure 1e**) illustrates the presence of more than one cell type in the organoids. Together, these results

highlight that the differentiation protocol from iPSCs into EHOs recapitulates the early stages of hepatic development.

Different functional assays as well as immunostainings were performed in the EHOs to determine their “liver-like” state. Immunostainings of the EHOs in culture revealed the expression of more mature hepatic markers *ALB* and *HNF4- α* (**Figure 1f**). Finally, the functionality of EHOs was confirmed by the secretion of albumin and urea into the supernatant (**Figure 1g**).

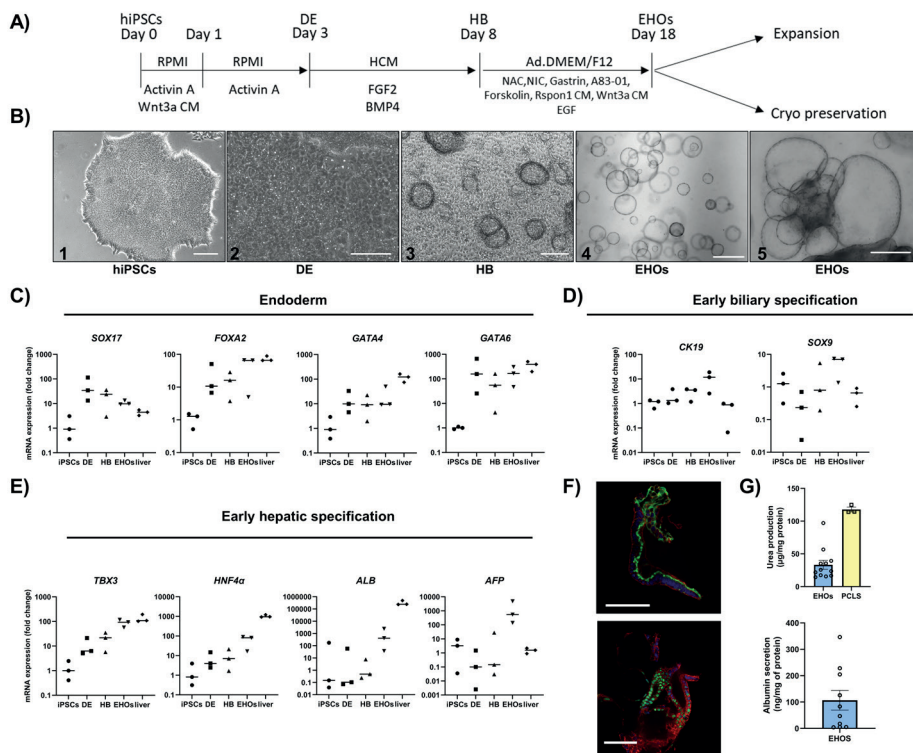


Figure 1. Protocol for the generation of human expandable hepatic organoids (EHOs) from iPSCs. (A) Schematic depiction of the differentiation protocol from iPSCs to hepatobiliary organoids. (B) Representative images depicting morphological changes at different stages of the differentiation. From left to right: iPSCs, DE, HB, cystic EHOs and “lobule-like” EHOs. Scale bars, 200 μ m for B1-3 and 500 μ m for B4-5. (C) Relative gene expression at different stages of the differentiation of endoderm markers, (D) early hepatocyte markers and (E) early biliary specification. Data represents 3 biological replicates from independent control donors. For C-E, human liver samples were included in the analysis. (F) Immunofluorescent staining of EHOs using albumin (green) on top and HNF4 (green) bottom, with nuclei in blue and cell membrane in red. Scale bar = 100 μ m. (G) Upper graph: Urea released in supernatant by organoids (blue) and human precision-cut liver slices (PCLS) (yellow) in 24 hours. Lower graph: Albumin released in supernatant by organoids (blue) in 24 hours. Data represents 10 biological replicates for the organoids and 3 biological replicates for the PCLS from independent experiments. All graphs: error bars indicate SEM.

Next, we assessed the carnitine profile of the organoids to confirm the accumulation of medium-chain acyl-carnitines, characteristic of MCADD patients. Control and MCADD organoids were incubated with palmitate and L-carnitine for 24 hours and the acyl-carnitine profile was assessed both intracellularly and in the supernatant. While no changes were observed in short- and long-chain acyl-carnitines (**Suppl Figure 2**), MCADD organoids accumulated medium-chain acyl-carnitines with 6 to 10 carbon atoms (C6, C8, and C10 in **Figure 2cd**). Moreover, intracellularly the C8/C10 ratio, an important diagnostic biomarker of MCADD in clinical practice¹, was strongly upregulated in MCADD organoids (from 11 to 20) (**Figure 2d**). The same pattern was observed in the supernatant where the C8/10 ratio was upregulated from 6 to 8 (**Figure 2d**). The values are in the same range as those observed in the plasma of severe MCADD patients (median 13.1), whereas mild MCADD patients ($\geq 10\%$ residual MCAD activity) had a median C8/10 ratio of 3.10 and healthy controls 0.8¹.

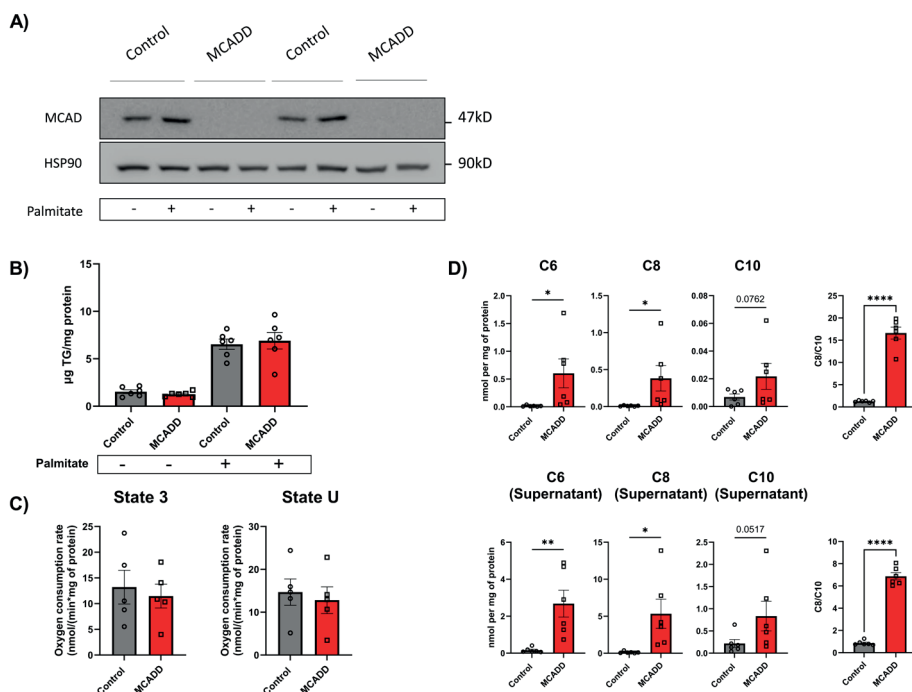


Figure 2. MCADD EHO organoids display an MCADD-characteristic phenotype in culture. (A) Representative immunoblot images illustrating the lack of MCAD protein in MCADD organoids; data represents 2 MCADD lines and 2 control lines. (B) Intracellular triglyceride levels in control and MCADD organoids. On the left organoids were stimulated with bovine serum albumin (BSA). The graph on the right depicts the values after treating the organoids with 0.5mM of BSA-Palmitate; data represents the mean of 6 biological replicates \pm SEM (Unpaired two-tailed t-test) (C) Oxygen consumption rate in organoids measured at state 3 (stimulated with ADP, octanoyl carnitine and malate) and uncoupled (state U); Data represents the mean of 5 biological replicates \pm SEM (Unpaired two-tailed t-test). (D) Upper panel: medium chain acyl-carnitines measured in the organoids incubated with palmitate and L-carnitine for 24 hours (C6, C8 and C10) and C8/C10 ratio; data represents 6 biological replicates from independent cultures \pm SEM. Lower panel: Medium-chain acylcarnitine measured in supernatant (C6, C8 and C10) and C8/C10 ratio. Data represents 6 biological replicates from independent cultures \pm SEM. (* $P < 0.05$, ** $P < 0.01$, *** $P < 0.001$, **** $P < 0.0001$ one-tailed unpaired t test).

Maturation of EHOs into Mat-EHOs increases peroxisome abundance

Although peroxisomes are specialized in their ability to oxidize very-long-chain, branched and dicarboxylic fatty acids, they are also capable of oxidizing

medium-chain acyl-CoA. Given the indications of higher number of peroxisomes in hepatic cells³⁶, we decided to first further differentiate the EHOs into mature EHOs (Mat-EHOs) in order to stimulate peroxisome proliferation.

EHOs were kept in expansion medium (EM) for 4-5 days after passage and then transferred to maturation medium (MM) (**Figure 3a**). Maturation medium contains different cytokines that allow the EHOs to mature into a more hepatocyte-like state. EHOs in MM underwent morphological changes, shrinking in size and developing thicker outer edges. (**Figure 3b**). Maturation was confirmed by upregulation of mature hepatocyte markers *HNF4- α* , *AFP*, Albumin and *CYP2C9*. Matured organoids also showed lower expression of cholangiocyte markers *TBX3* and *CK19*. Moreover, genes coding for enzymes involved in peroxisomal fatty-acid oxidation (*ABCD1*, *ACOX1*, and *CROT*) were significantly upregulated (**Figure 3c**). Finally, Mat-EHOs secreted higher levels of albumin into the supernatant than EHOs, in line with a more hepatocyte-like phenotype (**Figure 3d**).

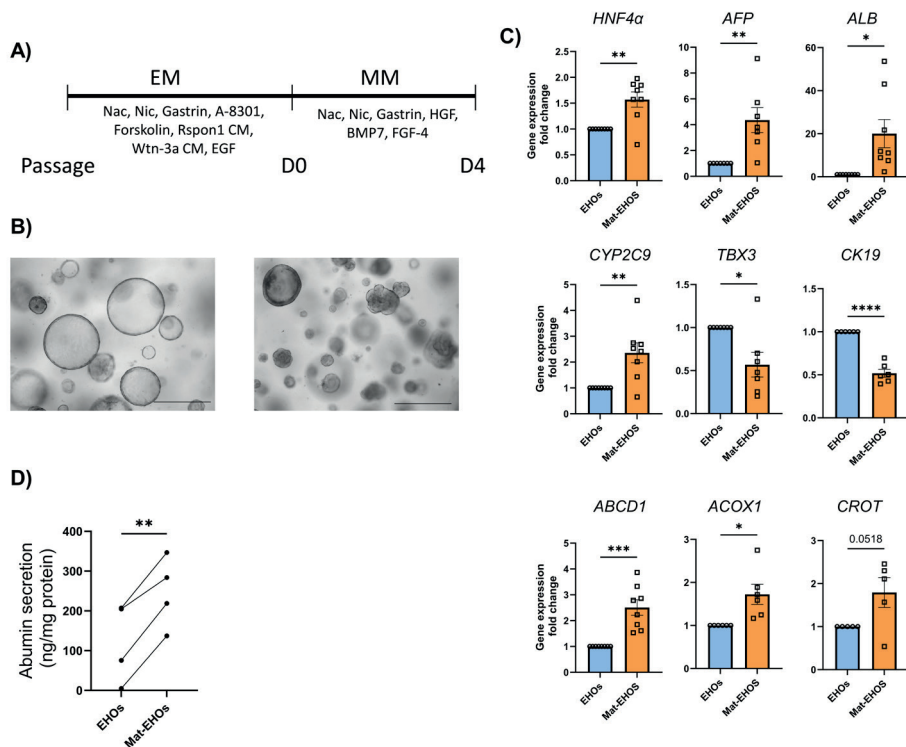


Figure 3. Maturation of EHOs into Mat-EHOs. (A) Schematic depiction of the maturation protocol (B) Representative brightfield images of EHOs and Mat-EHOs. Scale bar = 500 μ m. (C) Relative gene expression of mature hepatic markers and peroxisomal markers in EHOs and Mat-EHOs. Data represents 8 biological replicates from independent experiments \pm SEM. (* P <0.05, ** P <0.01, *** P <0.001, **** P <0.0001 two-tailed unpaired t test). (D) Albumin secreted into the supernatant after 24 hours in EHOs and Mat-EHOs. Data represents 4 biological replicates \pm SEM. (* P <0.05, ** P <0.01, two-tailed unpaired t test).

Peroxisomal adaptation in MCADD

Subsequently, we investigated if mitochondrial and peroxisomal fatty-acid oxidation pathways (**Figure 4a**) were regulated in response to loss of MCAD protein. In order to mimic the fasting conditions, which often trigger symptoms in patients, we exposed the Mat-EHO organoids to glucose-free medium in the presence of BSA-palmitate and carnitine. Again similar to the clinical phenotype, medium-chain acyl-carnitines accumulated in MCADD and the ratio C8/C10 was strongly elevated (**Figure 4b-c**). Interestingly, and unlike in

the EHOs, in Mat-EHOs short-chain acyl-carnitine (C2) and long-chain myristoyl-carnitine (C14) were downregulated (**Figure 4b**).

Interestingly, we observed that several genes encoding mitochondrial β -oxidation enzymes were downregulated in the MCADD Mat-EHOs relative to controls, including medium-chain ketoacyl-CoA thiolase (MCKAT) (encoded by *ACAA2*), hydroxyacyl-coenzyme A dehydrogenase (M/SCHAD) (encoded by *HADH*) and carnitine/acylcarnitine carrier protein (CACT) (encoded by *SLC25A20*) (**Figure 4d**). Given the ability of peroxisomes to oxidize MCFA, it has been hypothesized that in the absence of MCAD, excess medium-chain acyl-CoAs can also be channeled to peroxisomes, where they undergo further β -oxidation until C6-acyl-CoA, which may be shuttled back into the mitochondria to be oxidized by SCAD²⁹ (**Figure 4a**). For the peroxisomal β -oxidation, the genes encoding for the transporters ABCD1 and ABCD3 (ATP binding cassette transporter subfamily D; *ABCD1* and *ABCD3*), the oxidase ACOX1 (acyl-CoA oxidase 1; *ACOX1*), DBP and LBP (D-bifunctional protein and L-bifunctional protein; *HSD17B4* and *EHHDAH*, respectively) and the thiolases ACAA1 and SCPx (*ACAA1* and *SCP2*, respectively) were evaluated (**Figure 4e**). Apart from a non-significant decline in *ACOX1* expression, other measured genes were not regulated in MCADD organoids.

In conclusion, all the observed adaptations showed downregulation, rather than upregulation of putative compensatory pathways.

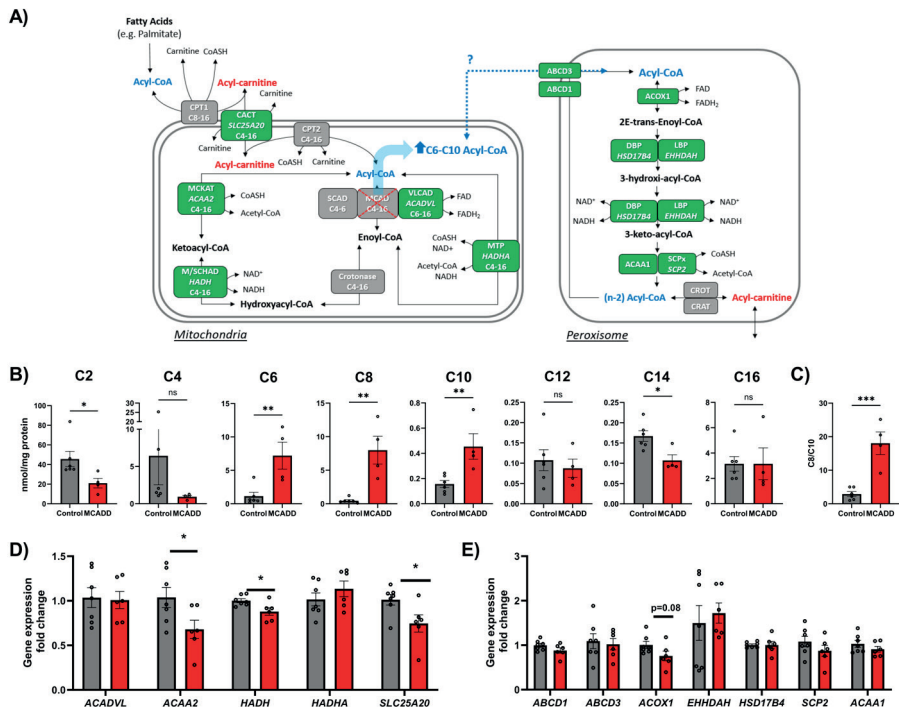


Figure 4. Adaptations of mitochondrial and peroxisomal β -oxidation in MCADD in Mat-EHOs. (A) Schematic depiction of the hypothesized interplay between mitochondria and peroxisomes in the β -oxidation of medium chain fatty acids. In green, the targets analyzed in D-E. (B) Acyl-carnitines measured in supernatant collected after 24 hours in glucose-free medium supplemented with BSA-palmitate and L-carnitine. (C) C8/C10 ratio; For B-C, data represents 6 biological replicates for control and 4 for MCADD \pm SEM (* P <0.05, ** P <0.01 two-tailed unpaired t-test). (D) Relative gene expression of genes involved in the mitochondrial β -oxidation. (E) Relative gene expression of genes involved in the peroxisomal β -oxidation. For E and D, organoids were grown in glucose-free medium supplemented with BSA and L-carnitine. Data represents 6-7 biological replicates for control and 5-6 for MCADD \pm SEM. (* P <0.05, ** P <0.01, two-tailed unpaired t test). Control (grey) and MCADD (red).

In agreement with the changes observed in the acyl-carnitine profile (**Figure 4b**), a recent in silico study, based on a detailed kinetic model of human fatty acid oxidation, predicted decreased levels of short-chain and C12-14 acyl-CoA and acyl-carnitines in MCADD²⁸. Such decrease has been suggested to be associated with a concomitant depletion in the free coenzyme A (CoA) levels and, consequently, reduced entry of long-chain fatty acids into the pathway^{28,37}. CoA is an essential intracellular cofactor involved in several metabolic pathways

and its level is dynamically regulated to adjust to the metabolic state through biosynthesis and turnover (**Figure 5a**)³⁸.

Next, we measured the relative gene expression of different genes involved in coenzyme A biosynthesis and total CoA levels (**Figure 5b-c**). This process occurs partly in the cytosol and partly in the mitochondria (**Figure 5a**). *PANK2*, encoding the mitochondrial pantothenate kinase, was slightly, but significantly downregulated in the MCADD organoids (**Figure 5c**). In addition to CoA biosynthesis, carnitine acyl-transferases and acyl-thioesterases (ACOT) also modulate the size of the CoA and acyl-CoA pools in different intracellular compartments. Peroxisomes also contain several enzymes involved in CoA recycling (**Figure 5a**), among them two carnitine acyl-transferases: carnitine octanoyl-transferase (CROT) and carnitine acetyl-transferase (CRAT), in charge of converting Acyl-CoAs into their respective acyl-carnitine form, with the concomitant release of free CoA. MCADD organoids showed substantially lower *CROT* and *CRAT* expression than healthy controls (**Figure 5d**). *NUDT7*, a gene that encodes a peroxisomal Nudix hydrolase, which hydrolyzes CoA and acyl-CoA species into 4'pantotheine and acyl-4'-pantotheine^{39,40} and also plays a role in the metabolism of dicarboxylic acids^{41,42} was clearly upregulated in MCADD organoids (**Figure 5d**). The total CoA pool (free CoA plus acyl-CoA) did not differ between MCADD and control Mat-EHOs (**Figure 5b**). Taken together, we observe a regulation of some genes involved in CoA metabolism, but an obvious compensatory response could not be identified.

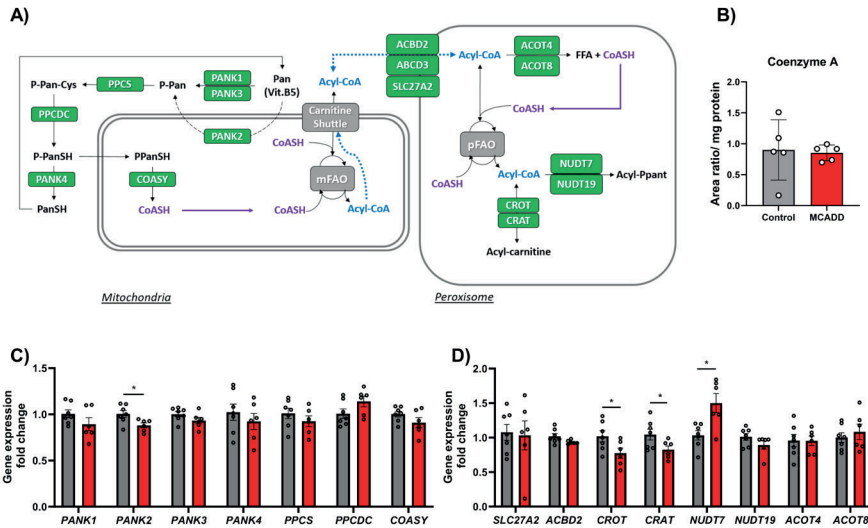


Figure 5. CoA biosynthesis and metabolism in Mat-EHOs. (A) Schematic depiction of the hypothesized effect of MCADD on CoA pools and compensatory mechanism from peroxisomes. In green, the targets analyzed in C-D. (B) Total coenzyme A pools in control (grey) and MCADD (red) organoids. Organoids were grown in glucose-free medium supplemented with BSA-palmitate and L-carnitine. Data represents 5 biological replicates \pm SEM. (C) Relative gene expression of genes involved in CoA biosynthesis. Data represents 7 biological replicates for the control group and 5 for MCADD \pm SEM. (* P <0.05, ** P <0.01, two-tailed unpaired t test). (D) Relative gene expression of genes involved in CoA metabolism. For C and D, organoids were grown in glucose-free medium supplemented with BSA and L-carnitine. Data represents 7 biological replicates for the control group and 5 for MCADD \pm SEM. (* P <0.05, ** P <0.01, two-tailed unpaired t test).

DISCUSSION

In this paper we have established a patient-specific iPSC-derived hepatic organoid system for the study of MCADD. These organoids recapitulated the metabolic profile with high levels of medium-chain acyl-carnitines and an elevated C8/C10 ratio that is typical of severe MCADD patients. Furthermore, the Mat-EHOs expressed pathways that are relevant for future studies of the pathophysiology of the disease. It may not be surprising that we observed only minor adaptations in putative compensatory pathways, since the MCADD organoids were derived from symptomatic patients. Compensatory pathways would rather be expected to be more pronounced in asymptomatic patients. Nevertheless, we observed some conspicuous differences between MCADD organoids and controls in respect of CoA metabolism, evidenced by reduced levels of C14-acyl-carnitine and upregulation of *NUDT7* in MCADD.

Studying metabolic functions in iPSC-derived hepatobiliary MCADD organoids

Discovery of organoids in 2009¹⁶, revolutionized the field of biomedical research, providing an alternative to traditional primary hepatocytes. Recent work has focused on the development of organoids from iPSCs. iPSC-derived hepatobiliary organoids have often been described as closer to fetal tissue²⁵, and advancing their maturity levels to that of liver tissue remains a challenge. Here we compared different maturation stages of the organoids for the study of MCADD. While the original protocol uses a 3-step procedure which relies on spontaneous aggregation of hepatic single cells²⁰, we found that this step was hard to reproduce and did not yield enough biomass for metabolic readouts. Therefore, for the purpose of our study, EHOs were matured to Mat-EHOs (equivalent of “pre-maturation” stage in the reference paper²⁰). At this stage, Mat-EHOs were found to already exhibit liver-like phenotypes such as typical hepatocyte mRNA markers, albumin and urea secretion, and the presence of functional mitochondria and peroxisomes.

Importantly, both MCADD EHOs and Mat-EHOs showed accumulation of medium-chain acyl-carnitines (C6-C10), recapitulating a major clinical phenotype. Interestingly, only MCADD Mat-EHO organoids presented reduced levels of short- and long-chain acyl-carnitine relative to their control counterparts. These changes are in alignment with a recent *in silico* study from our group, based on a detailed computational model of the fatty-acid oxidation, which predicted reduced levels of short- and long-chain acyl-CoAs and their corresponding acyl-carnitines in MCADD²⁸. Decreased short-chain

acyl-CoA or acyl-carnitine levels are not surprising, since they are downstream of the deficient MCAD enzyme. C14, however, is upstream of MCAD, and at first sight it might therefore be expected to be elevated or unchanged. In the computational model the reduced C14-acyl-CoA could be attributed to a limitation of free CoA availability. Free CoA was sequestered into medium-chain acyl-CoAs, which strongly accumulated in MCADD. The decrease of free CoA, in turn limited the entry of new long-chain fatty acids into the mFAO pathway^{28,37} and thereby led to a reduced C14-acyl-CoA. Thus, our data provides experimental validation of this non-intuitive computational prediction.

Together these data suggest that the maturation step into Mat-EHO organoids, accompanied by peroxisome and mitochondrial enrichment and a representative acylcarnitine profile, is a relevant step to study the pathophysiological mechanisms of MCADD.

Adaptations of mitochondrial and peroxisomal β -oxidation and CoA metabolism in MCADD

While peroxisomes have been reported to oxidize MCFAs²⁹, we did not observe any regulation of peroxisomal enzymes involved in the import and oxidation of fatty acids in MCADD organoids, which suggests this pathway was not further activated.

In addition to the oxidation of fatty acids, peroxisomes play a central role in the oxidation of dicarboxylic fatty acids (DCA)⁴³. Under high fatty acid (FA) supply, such as fasting and mFAO disorders, excess FAs are channeled to DCA via ω -oxidation^{44,45}. DCA accumulation in the liver can be toxic, causing inflammation, fibrosis and death⁴⁶. In MCADD, patients in metabolic crisis have been reported to exhibit accumulation of medium-chain dicarboxylic fatty acids (MC-DCA) and high excretion in urine^{47,48}. Excess DCAs can be metabolized by the peroxisomal β -oxidation^{43,49} or via the activity of nudix hydrolase 7 (NUDT7)^{41,42}. The expression of peroxisomal ABCD3 transporter and LBP, both playing a major roles in DCA oxidation⁵⁰, was not regulated in the MCADD organoids. Recent animal studies suggest that Nudt7 contributes to the regulation of dicarboxylic fatty acid metabolism in the liver^{41,42}. Male mice lacking Nudt7 (Nudt7 $-/-$) exposed to high fat diet showed accumulation of MC-DCA⁴¹. The authors proposed a major role of NUDT7 in the regulation of the levels of MC-DCA. The upregulation NUDT7 expression in the MCADD organoids may therefore play a role in preventing excessive accumulation of MC-DCA that otherwise could be toxic⁴⁶.

Conclusion and Outlook

In conclusion, the Mat-EHO organoids derived from iPSCs of severe MCADD patients show a phenotype that is characteristic for these patients and provide a good basis for future studies into patient-to-patient variability. For instance, they can be used to assess the phenotype of genetic variants of the *ACADM* gene that give rise to different residual activities. More interestingly, they can be used to study putative compensatory pathways in asymptomatic patients with a classical c.985A>G and zero residual MCAD activity. Furthermore, nutritional interventions and different stressors can be modulated in vitro, to study liver-specific aspects of MCADD pathophysiology and potential therapeutic interventions.

METHODS

Human fibroblasts

Fibroblasts from patients without documented heritable metabolic diseases (n=2) and also from symptomatic patients with MCADD carrying the classical c.985A>G missense mutation (n=2) were obtained from the Department of Genetics of the University Medical Center Groningen. Patients 5 and 8, previously described in the literature²⁸, were chosen for this study because of their classical mutation, symptomatology and normal growth of fibroblasts. Control fibroblasts from C104 and C105 were also described in the literature²⁸. All patients were born prior to the implementation of the neonatal MCADD screening in the Netherlands (2007). Both MCADD patients were symptomatic, suffered at least one recorded metabolic crisis, resulting in hospitalization with hypoglycaemia (<2.6 mmol/L), coma, and/or seizures.

Fibroblasts were cultured in Ham's F-10 Nutrient Mix (Thermo Fisher Scientific 11550043), supplemented with 10% FCS (Gibco) and 1% penicillin/streptomycin (Gibco).

Generation and culture of iPSCs from patient fibroblasts

Human fibroblasts were reprogrammed into induced pluripotent stem cells following the previously published protocol³³. iPSCs were cultured in Matrigel (Corning)-coated plates in mTeSR™ Plus medium (STEMCELL Technologies). Cells were passaged every 4-6 days and medium was changed every other day.

Generation of EHOs from iPSCs

iPSCs were differentiated into expandable hepatic organoids (EHOs) following the previously published protocols for hESCs^{51,52} with some adaptations. iPSC cells were cultured in Matrigel-coated plates and placed in RPMI1640 medium supplemented with 1X B27-Supplement (Invitrogen), 100ng/ml Activin A (Peprotech), and 30% Wnt3a-conditioned medium (kindly provided by Hans Clevers). Wnt3aCM was removed after 24 hours and cells were kept in the same medium supplemented with 100ng/ml Activin A and 2X B27-supplement for 48 hours. The cells were then transferred to Hepatocyte Culture Medium (HCM) (Lonza, CC-3198) without EGF and supplemented with 20ng/ml BMP4 and 10ng/ml FGF2 (both Peprotech) for the next 5 days. After 5 days, the cells were dissociated using 0.25% Trypsin-EDTA and embedded in BME domes (5000-10000 cells per 50 μ L dome) in Corning 24-well plates. The cells were cultured in an expansion medium (expansion medium) containing Ad. DMEM/F12 (Gibco) supplemented with 1X Glutamax, 1X HEPES, P/S (all Gibco), 1X B-27 Supplement, 1X N-2 Supplement (all Invitrogen), 10mM Nicotinamide (Sigma Aldrich), 1.25mM N-acetylcysteine (Sigma Aldrich), 50ng/ml EGF (Peprotech), 10 μ M Forskolin (TOCRIS), 10nM Iso-leu gastrin (Sigma Aldrich), 30% Rspan1-CM (Kindly provided by Calvin J. Kuo) and 10% Wnt-3a CM.

Medium was changed every 2-3 days. Organoids were passaged every 7-9 days by manually disrupting the BME domes and split in a ratio 1:8-1:10 depending on the line and supplemented with 10 μ M Y 27632 dihydrochloride (Axon Medchem) for 2 days after passaging.

Maturation of EHOs into Mat-EHOs

Expandable hepatic organoids were matured into hepatocyte-like EHOs (Mat-EHOs) following the previously published protocol⁵¹. Organoids were kept in expansion medium for 4-6 days after passage, and then placed in maturation medium (MM) containing Ad. DMEM/F12 supplemented with 1X Glutamax, 1X HEPES, P/S, 1X B-27 Supplement, 1X N-2 Supplement, 10mM Nicotinamide, 1.25mM N-acetylcysteine, 10nM Iso-leu gastrin, 50 ng/ml HGF, 25 ng/ml BMP7 and 25 ng/ml FGF4 (all growth factors from Peprotech). Organoids were kept in maturation medium for 4 days prior to collection for downstream analysis.

Organoid imaging and immunofluorescence

For brightfield imaging, organoids were imaged using an AxioObserver Z1 compound microscope (Carl Zeiss), 2.5× and 5× objectives and an AxioCam MRm3 CCD camera (Carl Zeiss).

For immunofluorescence images, organoids were processed following the previously published protocol⁵³. After collection with ice-cold Ad. DMEM/F12 the organoids were kept on ice for 10 minutes to ensure BME degradation. After centrifugation at 80G at 4°C, the organoids were reconstituted in 4% PFA and kept at 4C for 45 minutes. After fixation, organoids were permeabilized using PBS containing 0.1% Tween 20 and kept in that buffer for 2 days. Primary and secondary antibody incubations were performed in PBS containing 0.1% Tween 20 and 0.2% BSA. Primary and secondary antibodies are listed on supplementary table 2. Organoids were imaged using an ImageXpress Micro Confocal High-Content Imaging System (Molecular devices) with a 20X water-immersion objective (molecular devices). 50 slices with 2µm step size were acquired for each wavelength. Image processing was performed using Fiji v1.8.0.

RNA isolation, reverse transcription and quantitative real-time qPCR

RNA was isolated from the organoids using RNase easy Kit (Qiagen) as described by the manufacturer. NanoDrop (NanoDrop Technologies) was used to assess the quality and yield of total RNA. M-MLV Reverse Transcriptase (200U/µl) (Invitrogen) was used to perform reverse transcription as established by the manufacturer. qPCR was performed in 384 well format in duplicates (5 -10 ng per well) using FastStart Universal SYBR Green Master (Rox) (Sigma Aldrich) using QuantStudio 7 Flex (Thermo Fischer Scientific). All primer (Integrated DNA technologies Inc) sequences are listed in supplementary table 1. β-actin served as endogenous control, and was used for normalization.

Hepatocyte functional assays

For albumin measurements, the supernatant was collected after 24 hours. Levels of albumin in the supernatant were measured with the human albumin ELISA kit (Abcam) as described by the manufacturer using the Synergy H4 Hybrid Microplate Reader (BioTek Instruments Inc).

Urea secretion was assessed in the organoids supernatant using the QuantiChrom™ Urea kit as described by the manufacturer.

All results were normalized to protein content.

Immunoblotting

The protocol followed for immunoblotting was slightly modified from a previously published paper⁵⁴. Organoids were collected using ice-cold Ad. DMEM/F12 and kept on ice for 10 minutes to degrade the BME. Organoids were then centrifuged at 290g for 5 minutes at 4°C and washed with cold PBS prior to another centrifugation step. After the second centrifugation, the organoids were reconstituted in radio immunoprecipitation assay (RIPA) buffer containing 1% IGEPAL CA-630, 0.1 % SDS, and 0.5 % sodium deoxycholate in PBS. RIPA buffer was supplemented with Phosphatase Inhibitor Cocktail 2 (Cat. No. P5726) and Cocktail 3 (Cat. No. P0044) and Complete Protease Inhibitor Cocktail (Cat. No. 1186145001) (All Sigma Aldrich). Sonics Vibra cell VCX130 (Sonics & Materials Inc.) was used to sonicate organoid lysates using 4 pulses of 10 second on, 30 seconds off at an amplitude of 30%. Lysates were then centrifuged at 12000 rcf for 10 minutes at 4°C to ensure the precipitation of cell debris. Protein content was determined using Pierce BCA Protein Assay Kit (ThermoScientific) and all samples were adjusted to the lowest concentration value. Lysates were adjusted with Laemmli loading buffer (5X: 60 mM Tris-Cl pH 6.8, 10% glycerol, 1% SDS, 0.05% Bromophenol Blue, 1% beta-mercaptoethanol). Protein separation was done in SDS-PAGE 10-14% using a Mini PROTEAN Tetra Vertical Electrophoresis Cell system (Bio-Rad, 1658029FC). For western blot, proteins were transferred to a polyvinylidene difluoride membrane (Immobilon®-P, Millipore).

Fat isolation and triglyceride quantification

Organoids were collected in 1x TBS (137 mM NaCl, 2.7 mM KCl, 66 mM Tris, pH 7.4) in MiliQ water. Fat was extracted in chloroform: methanol in a ratio 2:1. The levels of hepatic triglycerides were quantitatively determined using the DiaSys Triglyceride FS kit (Holzheim). Results were normalized to protein content.

High resolution respirometry

Organoids were collected at day 8-10 using ice-cold Ad. DMEM/12 and kept on ice for 10 minutes. Organoids were then centrifuged at 290 g at 4°C for 5 minutes and washed with 2mL of MiR05 buffer, followed by another spin and finally reconstituted in 600uL of MiR05 buffer, containing 110 mM sucrose, 60 mM potassium lactobionate, 20 mM taurine, 20 mM HEPES, 0.5 mM EGTA, 10 mM KH₂PO₄, 3 mM MgCl₂, and 1 mg/ml bovine serum albumin, at pH 7.1.

Oxygen consumption rate was measured in the organoids using a two-channel high-resolution Oroboros Oxygraph-2 k (Oroboros). Organoids were first permeabilized by addition of digitonin (0.02 mg/ml). The maximal coupled respiration was measured in the presence of 1mM ADP, 25 μ M octanoyl-carnitine and 2mM malate (state 3). Basal respiration was determined by the subsequent addition of 0.002 mg/ml of oligomycin to block ATP synthase (state 4). Finally, uncoupled respiration (state U) was measured after subsequent administration of 1.5 μ M carbonyl cyanide p-(trifluoromethoxy) phenylhydrazone (FCCP). Oxygen consumption rates were normalized to protein concentration.

Acylcarnitines measurements

EHO organoids were incubated with 0.5mM BSA-conjugated palmitate (Sigma-Aldrich, P9767) and 2 mM l-carnitine (Sigma Aldrich) for 24 h prior to collection in PBS. Acylcarnitines were measured both in supernatant and intracellularly following the published protocol⁵⁵.

Total CoA measurements using HILIC-MS/MS analysis

Mat-EHO organoids were incubated in glucose-free maturation medium supplemented with 0.5mM BSA-conjugated palmitate and 2 mM l-carnitine for 24 h. Organoids were collected in ice-cold medium and washed 2X in ice-cold PBS. Samples were prepared as described elsewhere⁵⁶. Briefly, the pellet was reconstituted in 600 μ L MilliQ H₂O and the lysate was sonicated using a Sonics Vibra cell VCX130 (25 seconds, 50% amplitude, 2 times). Lysates were centrifuged at 14000 rpm for 15 minutes at 4°C. In a new tube, 80 μ L Tris (2-carboxyethyl)phosphine hydrochloride (10 mM) was added to 400 μ L supernatant and, incubated for 15 minutes at room temperature. Next, samples were spun down (14000 rpm, 15 minutes, 4°C). In a new tube, 40 μ L ammonia solution was added to 400 μ L supernatant (1.25% v/v) and, incubated shaking at 500 rpm at 60°C for 60 minutes. Lastly, samples were dried using a SpeedVac (Eppendorf) and reconstituted in 100 μ L ice-cold 80% methanol.

Coenzyme A was extracted by a two-step protocol using chloroform/methanol/water based on the Bligh and Dyer approach⁵⁷. The detailed sample preparation and HILIC-MS/MS protocol are described in detailed in the literature⁵⁸.

Human Precision-Cut Liver Slices (hPCLS)

PCLS with approximately 250–300 μM thickness were prepared using a Krumdieck Tissue Slicer (Alabama Research and Development), as described elsewhere. Individual slices were kept in culture for 24h in Williams E medium (WE), containing 25 mM glucose, 0.5% BSA, 1 mM l-carnitine, and gentamycin (Invitrogen). The plates were kept under a continuous supply of 80% O_2 /5% CO_2 , shaking at 70 rpm.

Human liver tissue was collected from a transplantation donor at the University Medical Center Groningen (UMCG, Netherlands). The liver was used for research purposes after being rejected for transplantation with the approval of the Research Ethics Committee of UMCG.

Statistical Analyses

All results are expressed as mean \pm standard error of the mean (SEM). Analyses were performed using GraphPad Prism Software Version 9.02 (Graphpad Software). Statistical significance was determined as *P value < 0.5 , **P value < 0.01 and ***P value < 0.001 ; no indication means no significant changes (ns). For iPSC work, biological replicates are considered individual donors. For organoid work, due to low number of patients, biological replicates are considered organoids coming from the two same patients or healthy controls that were at least one passage apart.

Informed consent

The use of historical patient fibroblasts was approved by the Medical Ethical Committee of the University Medical Center Groningen and confirmed according to the Dutch law.

FUNDING

This work was supported by the European Union's Horizon 2020 research and innovation programme under the Marie Skłodowska-Curie Actions Grant Agreement PeriCo No 812968 and PoLiMeR, No 812616; the Stichting De Cock-Hadders and the Stichting Beatrix Kinderziekenhuis.

ACKNOWLEDGMENTS

We would like to thank Emmalie Jager for providing the fibroblasts, Christoff Odendaal for insightful discussions on CoA metabolism and MCADD, and Peter Olinga for kindly providing the human precision-cut liver slices. We would like to thank Isabel Tamargo Rubio for the different CYP primers and the nice insights into the Cytochrome P450. We would also like to acknowledge Hans Clevers and Calvin J. Kuo for kindly providing the conditioned medium. BMB and JMHN have received funding from the European Union's Horizon 2020 research and innovation programme under the Marie Skłodowska-Curie grant agreement No 81296. BMB and LAK have received funding from the European Union's Horizon 2020 research and innovation programme under the Marie Skłodowska-Curie grant agreement No 812616

REFERENCES

1. Jager, E. A. *et al.* A nationwide retrospective observational study of population newborn screening for medium-chain acyl-CoA dehydrogenase (MCAD) deficiency in the Netherlands. *J Inherit Metab Dis* 42, 890–897 (2019).
2. Touw, C. M. *et al.* In vitro and in vivo consequences of variant medium-chain acyl-CoA dehydrogenase genotypes. *Orphanet J Rare Dis* 8, (2013).
3. Derks, T. G. J. *et al.* The natural history of medium-chain acyl CoA dehydrogenase deficiency in the Netherlands: Clinical presentation and outcome. *Journal of Pediatrics* 148, (2006).
4. Touw, C. M. L. *et al.* Risk stratification by residual enzyme activity after newborn screening for medium-chain acyl-CoA dehydrogenase deficiency: Data from a cohort study. *Orphanet J Rare Dis* 7, (2012).
5. Wilson, C. J., Champion, M. P., Collins, J. E., Clayton, P. T. & Leonard, J. V. Outcome of medium chain acyl-CoA dehydrogenase deficiency after diagnosis. *Arch Dis Child* 80, 459–462 (1999).
6. Mason, E., Hindmarch, C. C. T. & Dunham-Snary, K. J. Medium-chain Acyl-COA dehydrogenase deficiency: Pathogenesis, diagnosis, and treatment. *Endocrinol Diabetes Metab* 6, (2023).
7. Smith, E. H. *et al.* Allelic diversity in MCAD deficiency: The biochemical classification of 54 variants identified during 5 years of ACADM sequencing. *Mol Genet Metab* 100, 241–250 (2010).
8. Arnold, G. L. *et al.* Lack of genotype-phenotype correlations and outcome in MCAD deficiency diagnosed by newborn screening in New York State. *Mol Genet Metab* 99, 263–268 (2010).
9. Arghmann, C. A., Houten, S. M., Zhu, J. & Schadt, E. E. A Next Generation Multiscale View of Inborn Errors of Metabolism. *Cell Metab* 23, 13–26 (2016).
10. Martines, A. C. M. F. *et al.* Transcriptome analysis suggests a compensatory role of the cofactors coenzyme A and NAD⁺ in medium-chain acyl-CoA dehydrogenase knockout mice. *Sci Rep* 9, (2019).
11. Tolwani, R. J. *et al.* Medium-chain acyl-CoA dehydrogenase deficiency in gene-targeted mice. *PLoS Genet* 1, 0205–0212 (2005).
12. Karunanidhi, A. *et al.* Heptanoic and medium branched-chain fatty acids as anaplerotic treatment for medium chain acyl-CoA dehydrogenase deficiency. *Mol Genet Metab* 140, (2023).
13. Chegary, M. *et al.* Mitochondrial long chain fatty acid β -oxidation in man and mouse. *Biochim Biophys Acta Mol Cell Biol Lipids* 1791, 806–815 (2009).
14. Kretzschmar, K. & Clevers, H. Organoids: Modeling Development and the Stem Cell Niche in a Dish. *Developmental Cell* vol. 38 590–600 Preprint at <https://doi.org/10.1016/j.devcel.2016.08.014> (2016).
15. Huch, M. *et al.* Long-term culture of genome-stable bipotent stem cells from adult human liver. *Cell* 160, 299–312 (2015).
16. Sato, T. *et al.* Single Lgr5 stem cells build crypt-villus structures in vitro without a mesenchymal niche. *Nature* 459, 262–265 (2009).

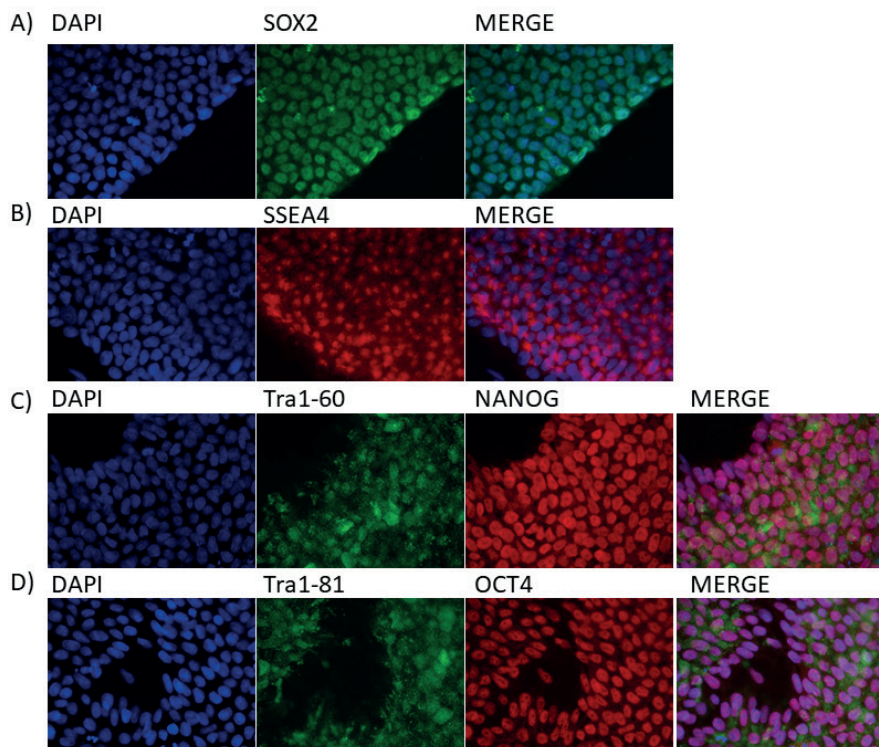
17. Lancaster, M. A. & Knoblich, J. A. Organogenesis in a dish: Modeling development and disease using organoid technologies. *Science* (1979) 345, (2014).
18. Schutgens, F. & Clevers, H. Human Organoids: Tools for Understanding Biology and Treating Diseases. (2019) doi:10.1146/annurev-pathmechdis.
19. Lee, J., Mun, S. J., Shin, Y., Lee, S. & Son, M. J. Advances in liver organoids: model systems for liver disease. *Archives of Pharmacal Research* vol. 45 390–400 Preprint at <https://doi.org/10.1007/s12272-022-01390-6> (2022).
20. Wang, S. *et al.* Human ESC-derived expandable hepatic organoids enable therapeutic liver repopulation and pathophysiological modeling of alcoholic liver injury. *Cell Res* 29, 1009–1026 (2019).
21. Sampaziotis, F. *et al.* Cholangiocytes derived from human induced pluripotent stem cells for disease modeling and drug validation. *Nat Biotechnol* 33, 845–852 (2015).
22. Wu, D. *et al.* Production of Functional Hepatobiliary Organoids from Human Pluripotent Stem Cells. *Int J Stem Cells* 14, 119–126 (2021).
23. Guan, Y. *et al.* Human hepatic organoids for the analysis of human genetic diseases. *JCI Insight* 2, (2017).
24. González, F., Boué, S. & Belmonte, J. C. I. Methods for making induced pluripotent stem cells: Reprogramming à la carte. *Nat Rev Genet* 12, 231–242 (2011).
25. Baxter, M. *et al.* Phenotypic and functional analyses show stem cell-derived hepatocyte-like cells better mimic fetal rather than adult hepatocytes. *J Hepatol* 62, 581–589 (2015).
26. Harrison, S. P. *et al.* Liver Organoids: Recent Developments, Limitations and Potential. *Frontiers in Medicine* vol. 8 Preprint at <https://doi.org/10.3389/fmed.2021.574047> (2021).
27. Chang, M., Bogacheva, M. S. & Lou, Y. R. Challenges for the Applications of Human Pluripotent Stem Cell-Derived Liver Organoids. *Frontiers in Cell and Developmental Biology* vol. 9 Preprint at <https://doi.org/10.3389/fcell.2021.748576> (2021).
28. Odendaal, C. *et al.* Personalised modelling of clinical heterogeneity between medium-chain acyl-CoA dehydrogenase patients. *BMC Biol* 21, 184 (2023).
29. Violante, S. *et al.* Peroxisomes contribute to the acylcarnitine production when the carnitine shuttle is deficient. *Biochim Biophys Acta Mol Cell Biol Lipids* 1831, 1467–1474 (2013).
30. Wanders, R. J. A. & Waterham, H. R. Biochemistry of mammalian peroxisomes revisited. *Annual Review of Biochemistry* vol. 75 295–332 Preprint at <https://doi.org/10.1146/annurev.biochem.74.082803.133329> (2006).
31. Violante, S. *et al.* Peroxisomes can oxidize medium- and long-chain fatty acids through a pathway involving ABCD3 and HSD17B4. *FASEB Journal* 33, 4355–4364 (2019).
32. Vickers, S. D. *et al.* NUDT7 regulates total hepatic CoA levels and the composition of the intestinal bile acid pool in male mice fed a Western diet. *Journal of Biological Chemistry* 299, 102745 (2023).
33. Okita, K. *et al.* A more efficient method to generate integration-free human iPS cells. *Nat Methods* 409–412 (2011) doi:10.1038/nmeth.1591.

34. Wang, S. *et al.* Human ESC-derived expandable hepatic organoids enable therapeutic liver repopulation and pathophysiological modeling of alcoholic liver injury. *Cell Res* 29, 1009–1026 (2019).
35. Maier, E. M. *et al.* Protein misfolding is the molecular mechanism underlying MCADD identified in newborn screening. *Hum Mol Genet* 18, 1612–1623 (2009).
36. Horcas-Nieto, J. M. *et al.* Organoids as a model to study intestinal and liver dysfunction in severe malnutrition. *Biochim Biophys Acta Mol Basis Dis* 1869, (2023).
37. Martines, A. C. M. F., van Eunen, K., Reijngoud, D. J. & Bakker, B. M. The promiscuous enzyme medium-chain 3-keto-acyl-CoA thiolase triggers a vicious cycle in fatty-acid beta-oxidation. *PLoS Comput Biol* 13, (2017).
38. Naquet, P., Kerr, E. W., Vickers, S. D. & Leonardi, R. Regulation of coenzyme A levels by degradation: the 'Ins and Outs'. *Prog Lipid Res* 78, (2020).
39. Gasmi, L. & McLennan, A. G. The mouse Nudt7 gene encodes a peroxisomal nudix hydrolase specific for coenzyme A and its derivatives. *Biochem. J* 357, 33–38 (2001).
40. Reilly, S. J., Tillander, V., Ofman, R., Alexson, S. E. H. & Hunt, M. C. The nudix hydrolase 7 is an acyl-CoA diphosphatase involved in regulating peroxisomal coenzyme A homeostasis. *J Biochem* 144, 655–663 (2008).
41. Vickers, S. D. *et al.* NUDT7 regulates total hepatic CoA levels and the composition of the intestinal bile acid pool in male mice fed a Western diet. *Journal of Biological Chemistry* 299, (2023).
42. Shumar, S. A., Kerr, E. W., Fagone, P., Infante, A. M. & Leonardi, R. Overexpression of Nudt7 decreases bile acid levels and peroxisomal fatty acid oxidation in the liver. *J Lipid Res* 60, 1005–1019 (2019).
43. Suzuki, H., Yamada, J., Watanabe, T. & Suga, T. Compartmentation of dicarboxylic acid β -oxidation in rat liver: importance of peroxisomes in the metabolism of dicarboxylic acids. *Biochim Biophys Acta Gen Subj* 990, 25–30 (1989).
44. Wanders, R. J. A., Komen, J. & Kemp, S. Fatty acid omega-oxidation as a rescue pathway for fatty acid oxidation disorders in humans. *FEBS Journal* 278, 182–194 (2011).
45. Preiss, B. & Bloch, K. Omega-Oxidation of Long Chain Fatty Acids in Rat Liver. *J Bio Chem* 239, (1964).
46. Ding, J. *et al.* The Peroxisomal Enzyme L-PBE Is Required to Prevent the Dietary Toxicity of Medium-Chain Fatty Acids. *Cell Rep* 5, 248–258 (2013).
47. Tserng, K.-Y., Jin, S.-J., Kerr, D. S. & Hoppel, C. L. Abnormal urinary excretion of unsaturated dicarboxylic acids in patients with medium-chain acyl-CoA dehydrogenase deficiency. *J Lipid Res.* 31, 763–771 (1990).
48. Kølvrå, S., Gregersen, N., Christensen, E. & Hobolth, N. In vitro fibroblast studies in a patient with C6-C1- dicarboxylic aciduria: evidence for a defect in general acyl-CoA dehydrogenase. *Clin Chim Acta.* 126, 53–67 (1982).
49. Zhang, X. *et al.* Fasting induces hepatic lipid accumulation by stimulating peroxisomal dicarboxylic acid oxidation. *Journal of Biological Chemistry* 296, (2021).
50. Ranea-Robles, P. *et al.* The peroxisomal transporter ABCD3 plays a major role in hepatic dicarboxylic fatty acid metabolism and lipid homeostasis. *J Inherit Metab Dis* 44, 1419–1433 (2021).

51. Wang, S. *et al.* Human ESC-derived expandable hepatic organoids enable therapeutic liver repopulation and pathophysiological modeling of alcoholic liver injury. *Cell Res* 29, 1009–1026 (2019).
52. Rashidi, H. *et al.* 3D human liver tissue from pluripotent stem cells displays stable phenotype in vitro and supports compromised liver function in vivo. *Arch Toxicol* 92, 3117–3129 (2018).
53. Dekkers, J. F. *et al.* High-resolution 3D imaging of fixed and cleared organoids. *Nat Protoc* 14, 1756–1771 (2019).
54. Heberle, A. M. *et al.* The PI3K and MAPK/p38 pathways control stress granule assembly in a hierarchical manner. *Life Sci Alliance* 2, (2019).
55. Evers, B. *et al.* Simultaneous quantification of the concentration and carbon isotopologue distribution of polar metabolites in a single analysis by gas chromatography and mass spectrometry. *Anal Chem* 93, 8248–8256 (2021).
56. Srinivasan, B. *et al.* Extracellular 4'-phosphopantetheine is a source for intracellular coenzyme A synthesis. *Nat Chem Biol* 11, 784–792 (2015).
57. Wu, H., Southam, A. D., Hines, A. & Viant, M. R. High-throughput tissue extraction protocol for NMR- and MS-based metabolomics. *Anal Biochem* 372, 204–212 (2008).
58. Singh, M., Akemi Kiyuna, L., Odendaal, C., Bakker, B. M. & Hankemeier, T. Development of HILIC-MS/MS method for acyl-CoAs covering short-to long-chain species in a single analytical run. *ChemRxiv. Cambridge: Cambridge Open Engage. This content is a preprint and has not been peer-reviewed* (2023) doi:10.26434/chemrxiv-2023-h0w52.

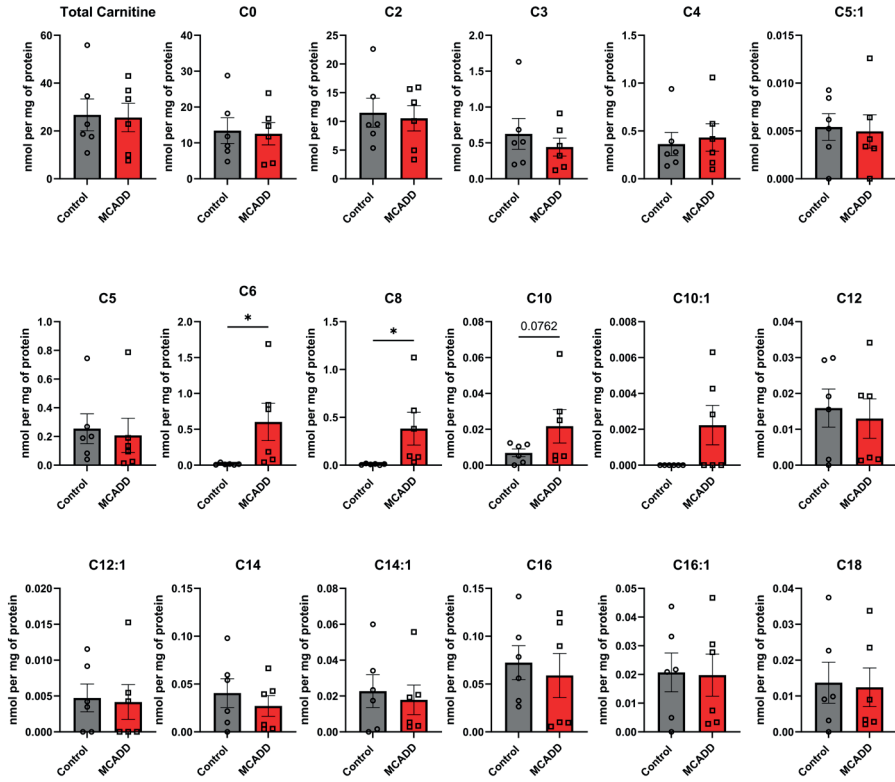
SUPPLEMENTARY FILES

Supplementary Figure 1. Expression of iPSC markers in iPSC control line.



Immunofluorescent staining of DAPI (blue) and (A) SOX2 (green), (B), SSEA4 (red), (C) Tra1-60 (green) and NANOG (red) and (D) Tra1-81 (green) and OCT4 (red).

Supplementary Figure 2. Intracellular acyl-carnitine profile of control and MCADD EHOs.



Control organoids in grey and MCADD organoids in red. Data represents 6 biological replicates \pm SEM. (* $P < 0.05$ one-tailed unpaired t-test).

Supplementary Table 1. List of primer sequences used in RT-qPCR

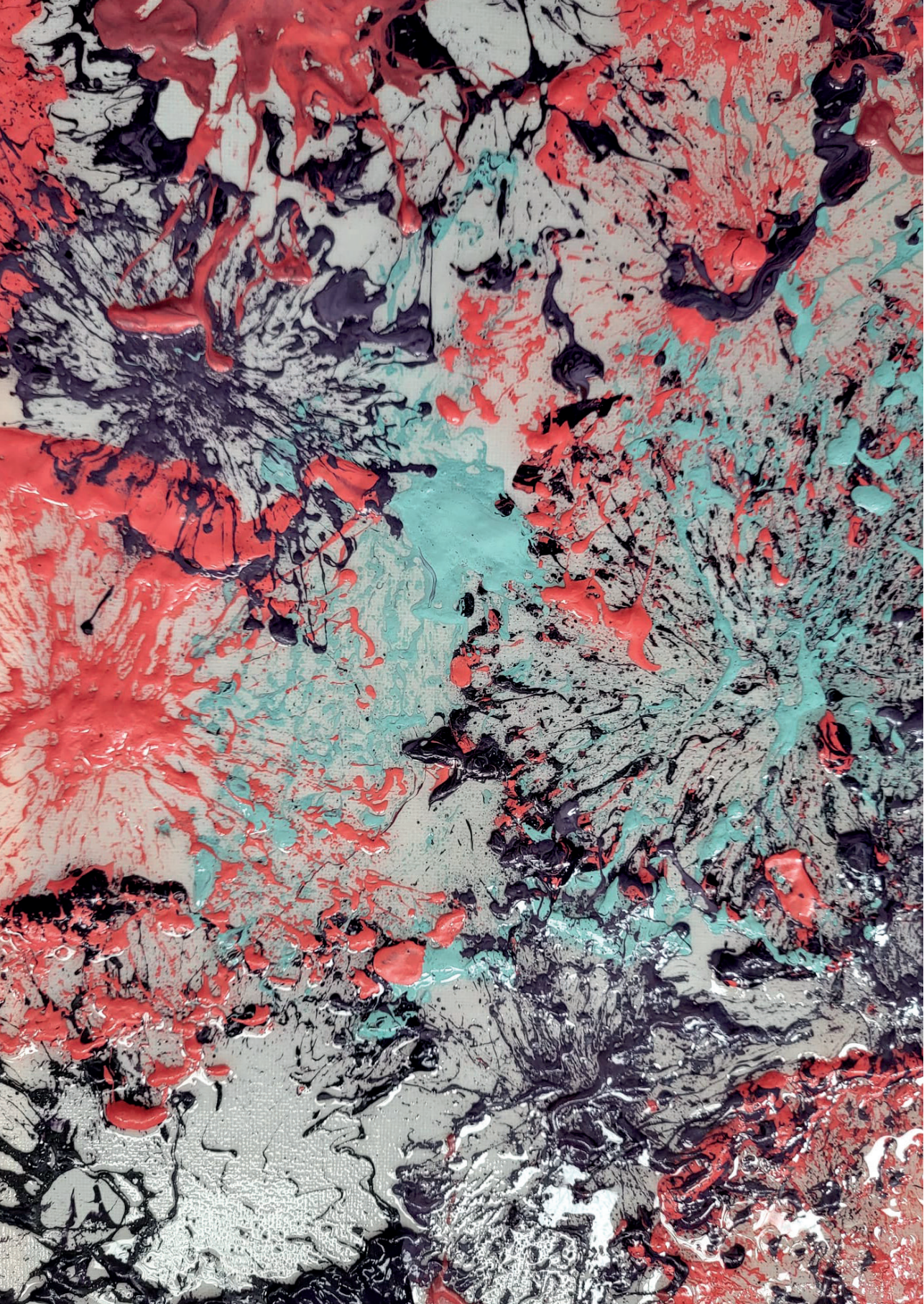
Gene Name	Forward and reverse primer sequence (5'- 3')
<i>SOX17</i>	Fwd: CGCACGGAATTTGAACAGTA Rev: GGATCAGGGACCTGTACACAC
<i>FOXA2</i>	Fwd: ACTACCCCGGCTACGGTTC Rev: AGGCCCGTTTTGTTCGTGA
<i>GATA4</i>	Fwd: CCTCTTTCTCAGCAGAGCTGTA Rev: CTCTGCTACAGCCAGTAGGATT
<i>GATA6</i>	Fwd: CCCACAACACAACCTACAGC Rev: GCGAGACTGACGCCTATGTA
<i>TBX3</i>	Fwd: TTTACAAATTCTCGGTGGATGGTGGC Rev: ACGACTTTGGACATGCACTGTTCC
<i>HNF4a</i>	Fwd: ACTACATCAACGACCGCCAGT Rev: ATCTGCTCGATCATCTGCCAG
<i>Albumin</i>	Fwd: GAGACCAGAGTTGATGTGATG Rev: AGTTCCGGGGCATAAAAAGTAAG
<i>AFP</i>	Fwd: CTTTGGGCTGCTCGCTATGA Rev: GCATGTTGATTTAACAAGCTGCT
<i>CK19</i>	Fwd: ACGACCATCCAGGACCTGCGG Rev: TCCCACTTGGCCCTCAGCGTA
<i>SOX9</i>	Fwd: ACTTGCAACAACGCCGAG Rev: CTGGTACTTGTAATCCGGGTG
<i>ABCD1</i>	Fwd: CTTCTGGAACGCCTGTGGTAT Rev: TTCCAAGGCTGCCTTCTTCAG
<i>ABCD3</i>	Fwd: GTTCCTTTAGCAACGCCAAATGG Rev: CTCTTTCCGACCCATTGGAC
<i>NUDT7</i>	Fwd: CTCGTCCTTTTGCCATTGGTG Rev: TGTCTGTAGGGTCACGCTTACC
<i>NUDT19</i>	Fwd: GCACCACTCGCCGCTTTGACA Rev: GTTGCCTCTGATGGAGATGACC
<i>SLC27A2</i>	Fwd: GTGGAGAAAGATGAACCTGTCCG Rev: CTGAGCCTTTGCTCCAGCATAG
<i>ACBD2</i>	Fwd: GCTGCCAGCAAGGATGACTCAA Rev: GCTTTCTCCTCTACTCCACCAG
<i>ACOT4</i>	Fwd: CTTTGCCACGTTGGCTCTAGCT Rev: CCTAGAGAAATGCCAAAAGCCC
<i>ACOT8</i>	Fwd: GCTGACCACTGGATGCTCTATG Rev: AGGTCACAGCTAGGACTCCATC
<i>ACOX1</i>	Fwd: GGCGCATACATGAAGGAGACCT Rev: AGGTGAAAGCCTTCACTCCAGC
<i>EHHADH</i>	Fwd: CGGAGCATCGTGAAAACAGCA Rev: CCGAGTCTACAGCAATCACAGG
<i>SCP2</i>	Fwd: GACAAGGTGCAACGCTGGTTGA Rev: CCAGCAGAGTTCTGCACACTGA

<i>ACAA1</i>	Fwd: GACAGGTCATCACGCTGCTCAA Rev: CCAGGGTATTCAAAGACGGCAG
<i>HSD17B4</i>	Fwd: GAGAATGCCAGCAAGCCTCAGA Rev: GCTGTAGACGTTGCACGACTAG
<i>ACADS</i>	Fwd: CACGCCTTTCCACAGTGGTGAC Rev: CACGCCTTTCCACAGTGGTGAC
<i>ACADVL</i>	Fwd: TAGGAGAGGCAGGCAAACAGCT Rev: CACAGTGCCAAACTGCTCCAGA
<i>ACAA2</i>	Fwd: GGCCTGAAGAAAGCAGGACTG Rev: GTGACCCAAAGCAATGGCTCCT
<i>HADH</i>	Fwd: TCCGTTGTCCACAGCACAGACT Rev: GGAGGAAGTGTGCTGGCAAAG
<i>HADHA</i>	Fwd: GCCGACATGGTGATTGAAGCTG Rev: GGAGAGCAGATGTGTTACTGGC
<i>SLC25A20</i>	Fwd: ACCGAGTTTGCCTGGACAACCT Rev: CCCAAAGAAGCACACGGCAAAC
<i>CROT</i>	Fwd: CTAGTGAGGAGCGAACTCGATG Rev: CCTCTGGTGTTACATGTGGACTG
<i>CRAT</i>	Fwd: CCTACAGACCAACAAGGAGCCT Rev: TGCATCTAGGCACACGGTGAAG
<i>CYP2C9</i>	Fwd: GACATGAACAACCTCAGGACTTT Rev: TGCTTGTCTCTCTGTCCCA
<i>PANK1</i>	Fwd: AGGTGTCAGCATTCTAGCCGTG Rev: GGTCTCACAAACCAGTCAGCAAG
<i>PANK2</i>	Fwd: CGTGAGATAGCACCAAAGTGG Rev: CAGGTCCTCTTTACTGACAGCC
<i>PANK3</i>	Fwd: TTGCCAGGTTGGGCTGTAGCAT Rev: GCACACATTCGTGCCACAGAAC
<i>PANK4</i>	Fwd: TCGTGGATTCTACAGCGAGTG Rev: CTGTCCCTCTAAGGAGTAGCTC
<i>PPCS</i>	Fwd: TCCTGGCAGTAGAGTTCACCAC Rev: GGCATTTCCAGAGACAGGAACATAG
<i>PPCDC</i>	Fwd: CAAGAAGCTGGTGTGCGGAGAT Rev: GTCAACTCTGCTGGAAGCCACT
<i>COASY</i>	Fwd: TGAGGTGTGGACTGCTGTCATC Rev: TGGCTCTGTCCACAAGCTGCT

Fwd, forward primer; Rev, reverse primer.

Supplementary Table 2. List of primary and secondary antibodies used in immunoblotting.

Name	Company	Catalogue number	Dilution
ACOX1	Abcam	Ab184032	WB 1:1000
B-actin	Sigma-Aldrich	A5441	WB 1:1000
PMP70	Sigma-Aldrich	P0497	WB 1:1000
Albumin	R&D systems	MAB1455	IF 1:100
MCAD	Abcam	AB92461	IF 1:100
CK19	Cell Signaling	4558	IF 1:200
Epcam	Invitrogen	17-5791-82	IF 1:200
HNF4- α	Cell Signaling	3113	IF 1:1000
Hoechst 33342	Life Technologies	H3570	2.5 μ M
Alexa Fluor 555 Phalloidin	Cell Signaling	8953S	IF 1:50
Alexa Fluor 488 goat anti-mouse IgG (H+L)	Invitrogen	A11029	IF 1:300
Alexa Fluor 488 goat anti-rabbit IgG (H+L)	Invitrogen	A11034	IF 1:300



Chapter

General Discussion



This thesis focuses on the development of new in vitro and in silico translational models to study two diseases affecting fatty acid metabolism. Liver and intestinal organoids are presented as suitable tools to study malnutrition and medium-chain acyl-CoA dehydrogenase deficiency (MCADD). Moreover, I also present two in silico models that helped compliment the findings of the in vitro systems as well as to predict metabolic responses. During the thesis, I also focused on the effects of both diseases on peroxisomal and mitochondrial homeostasis and their interplay.

In this chapter, I focus on (i) a general discussion about different aspects related to these new translational models and (ii) the importance of the peroxisomal-mitochondrial interplay in health and disease.

PART 1. ESTABLISHING TRANSLATIONAL IN VITRO AND IN SILICO MODELS FOR THE STUDY OF MALNUTRITION AND MCADD

In this thesis, I established two in vitro organoid models to study malnutrition and medium chain acyl-CoA dehydrogenase deficiency. I have also focused on the development of two in silico models. First, I developed a detailed kinetic model to study fluxes and metabolite concentrations of the peroxisomal β -oxidation. Secondly, I contributed to the development of a deep learning (DL) model to measure and track organoid size. This was done by providing data, defining requirements and validating the outcomes. In this section, I discuss about the establishment of these models for the study of the above-mentioned diseases and how to tailor them to metabolic research. Next, I highlight the limitations of these models and focus on the potential approaches and optimizations needed to overcome these limitations.

Applications and advantages of translational models for metabolic research

In **chapter 2**, I focused on the development of two in vitro models to study malnutrition. These models were established using primary tissue from murine liver and intestine to set up hepatic and intestinal organoids respectively. To the best of our knowledge, these are the first hepatic and intestinal organoid models of malnutrition described. A variation of the intestinal model was recently described in the literature to understand the role of mitochondrial homeostasis and intestinal barrier function¹. More recently, human intestinal organoids have also been established for the study of malnutrition in vitro².

However, this study focused on removal of not only amino acids but also proteins and carbohydrates. Moreover, they studied intestinal permeability of the organoids but did not characterize metabolic (mitochondrial or peroxisomal) function.

Organoids are three-dimensional cell structures that recapitulate multiple functions of the organ of origin whilst continuing to proliferate in culture³. Since their discovery⁴, tens of different organoid models have been described, including the pancreas⁵, stomach⁶, lungs⁷, and brain⁸. Organoids have been used for a wide range of purposes such as developmental studies^{3,9}, modeling genetic diseases¹⁰, and drug screening¹¹. Here, I demonstrated that hepatic and intestinal organoids make suitable models to study malnutrition in vitro. In order to mimic low protein diets (LPD), used in in vivo models to induce malnutrition¹²⁻¹⁴, organoids were grown in culture medium without any amino acids. However, CG-MS analysis of the organoid supernatant revealed that all amino acids were present, probably coming from the hydrogel or from the degradation of the growth factors in the medium, yet in much lower levels than in the control cultures. These in vitro systems present a wide range of advantages and new possibilities when compared to in vivo studies¹⁵. One main point of interest is the possibility to study one specific organ at a time¹⁶. This allowed us to study the effects of amino-acid restriction on the liver and the intestine in an isolated system without a systemic response. A key example highlighting the importance of organ-specific studies is discussed in **chapter 4**. Here I reported that, opposite to what was expected from in vivo studies¹²⁻¹⁴, the autophagic flux was clearly upregulated in hepatic and intestinal organoids upon amino-acid restriction. While these results might seem contradictory, it is not uncommon to see different responses between in vivo and in vitro models. Moreover, this organ-specific approach paves the way for characterizing and studying different organ-specific-pathophysiological processes which can provide great insight into the disease of interest.

Another advantage of these translational in vitro models is the possibility to pre-screen large numbers of drugs prior to in vivo testing^{17,18}. In **chapter 2**, to illustrate the potential of the models, I tested the effects of fenofibrate and rapamycin in the liver and the intestine, respectively, as a proof of principle. These compounds showed a similar response as to that observed in vivo¹⁴. Moreover, in **chapter 4** I focused on a more extensive drug screening to prevent peroxisomal loss in the hepatic malnutrition model. In this chapter I evaluated the potential of different PPAR- α activators including synthetic and naturally occurring compounds. These studies led us to the findings that docosahexaenoic acid (DHA), an omega-3 fatty acid, could prevent the loss

of multiple peroxisomal and mitochondrial proteins in amino-acid restricted organoids. While these results are promising, they should be interpreted as a first step into the characterization of the biological effect of such compound and this should be further tested and validated *in vivo*.

Another *in vitro* model developed during this thesis is introduced in **chapter 6**. Together with my colleague Ligia Kiyuna, we developed an iPSC-derived hepatobiliary model to study MCADD. To the best of our knowledge, this is the first patient-specific liver organoid model for the study of MCAD deficiency. Similar to primary organoids, iPSC-derived organoids allow us to understand different pathophysiological processes within a given disease. Moreover, they present a very valuable advantage as they are derived from patient tissue^{19,20}. This offers the opportunity to understand the effect of different mutations on different factors such as development, cell fate, or cell metabolism.

In the case of MCADD, it is not uncommon to see patients who are asymptomatic even if they carry the same mutations as other symptomatic patient^{21,22}. In this first study, we have only used fibroblasts coming from patients with the classical mutation c.985A>G. However, the model offers the opportunity to generate organoids from fibroblasts from patients with different mutations to understand and determine the differences between symptomatic and asymptomatic patients.

I developed two *in silico* models applied to the study of malnutrition *in vitro* and *in vivo*. In **chapter 3**, together with my colleague Asmaa Haja from the Perico ITN consortium, I contributed to the development of an automated tool to measure and track organoid size and morphology in brightfield images. As my contribution, I provided data to train the algorithm, defined the requirements of the system and validated the results. The need for this tool stemmed from the demand to quantify large sets of images containing, at times, hundreds of organoids. This deep-learning model was developed to speed up the quantification and characterization of the organoid work done in **chapter 2**, and to be applied for future experiments. In addition to minimizing the workload, another reason to develop this model was to reduce the intrinsic variability associated to organoid measuring and counting. The goal was to identify as many organoids as possible per image and track their individual growth rate in time. During the data analysis phase, distribution profiles were generated, avoiding solely relying on the average of all the data points. This model represents one of the many applications of artificial intelligence to *in vitro* research.

In **chapter 5**, I focused on the development of another *in silico* model, aimed to provide insight into the effects of amino-acid restriction on the peroxisomal β -oxidation of fatty acids. This model relies on kinetic information of the enzymes involved, including rate equations describing the kinetic behavior of the enzymes, kinetic parameters such as V_{\max} and K_{ms} , and ordinary differential equations. Kinetic models have been used to understand multiple metabolic pathways as well as to provide insight into the regulation of the pathway, for instance by understanding what enzyme or enzymes have the most control on the flux. One very interesting application of these models, is the combination with proteomics data from *in vitro* or *in vivo* studies to approximate it to physiological conditions^{23,24}. The use of proteomics data also leads to the development of personalized models, very important tools in the case of rare diseases²⁵. Moreover, these models can provide information on the effects of different drugs to the pathway and predict potential accumulations of toxic metabolites. While the model of peroxisomal β -oxidation presented in this thesis is a first approximation which needs further optimization, the long-term goal is to characterize the effects of amino-acid restriction on the peroxisomal β -oxidation of fatty acids and combine it with our previously established mitochondrial counterpart. We believe that this combination of both models might shed some light into the metabolism of fatty acids in the liver not only in malnutrition but also in all diseases where FAO is implicated. Moreover, I have performed metabolic control analysis²⁶ under different conditions. The results from these studies pointed towards ACOX1 as the enzyme with the highest control on the pathway, in line with previous studies describing the enzyme as the rate limiting step of the pathway^{27,28}. Moreover, I have used proteomics data from the *in vitro* hepatic model to understand the effects of amino-acid restriction on the flux control of the different enzymes of the pathway.

Limitations of new translational models and future perspectives

Although it is undeniable that the discovery of organoids has transformed the field of biomedical research, it is crucial to be aware of their limitations. Most of the early work on organoids focused on the study of developmental biology, recapitulation of the organ of origin, and disease modelling. Some studies have highlighted some limitations of these *in vitro* models, such as lack of different cell populations or failure to recapitulate some functions of the organ of origin^{29,30}.

During the course of the PhD, I have encountered multiple challenges in the establishment and application of metabolic techniques onto organoid cultures. Most of these issues stemmed from either low reproducibility between organoid cultures, low number of cells, or the presence of hydrogels such as Matrigel or BME (**Figure 1**).

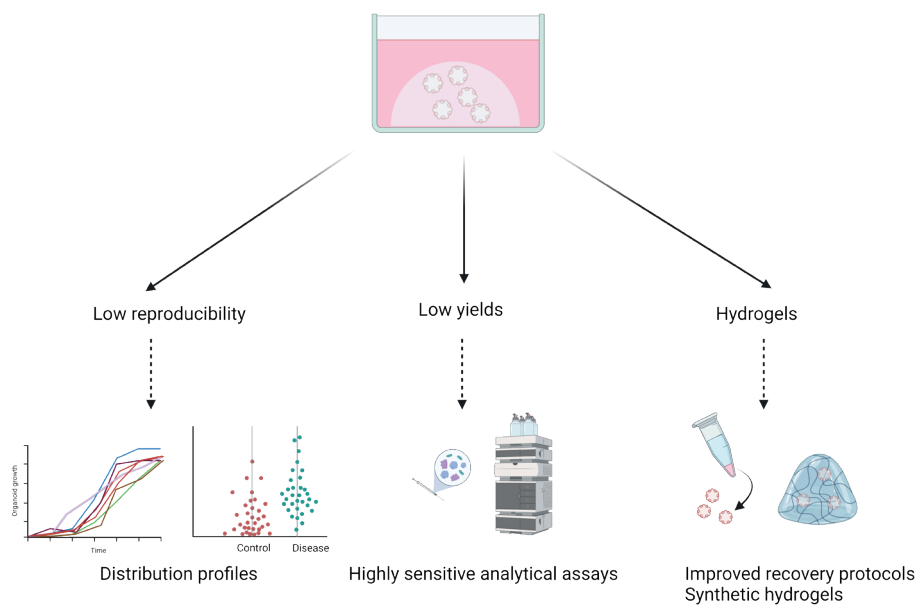


Figure 1. Technical limitations of organoids cultures in metabolic research and proposed approaches to overcome them. Created with BioRender.com

One relevant point to discuss is the high variability observed between organoid cultures. It is well known that organoids are highly heterogenous, displaying variability between cells within the same organoid (intra-organoid heterogeneity), between organoids within the same plate and between organoids from different patients (inter-organoid heterogeneity)¹⁶. While this heterogeneity is crucial to capture differences between patients, and therefore for personalized-medicine purposes, it is also a setback in reproducibility^{16,31}. While inter-organoid heterogeneity is not a problem, inter-organoid variability can minimize reproducibility in many downstream analyses. When working on metabolic profiling of these organoids, it is common to observe disparate absolute values of metabolites within different organoid cultures when they

are derived from the same patient. This heterogeneity between organoids highlights the need for standardized procedures and protocols³². This is particularly important in the field of metabolism which requires precise quantitation.

In order to avoid data misinterpretation, correct analysis and interpretation are crucial. In some cases, it may be considered to normalize the data of each individual organoid line to its own control prior to processing with the other biological replicates. This approach could help identify trends in responses to different treatments or as a result of different insults. A second approach to this issue is the use of distribution profiles of individual organoids instead of averages. In that instance, observational studies of each organoid in the culture could help reduce the risk of losing individual responses based on the averaged trend. One example on how to prevent this, is illustrated in **chapter 3**. OrganelX is able to track individual organoids in time, allowing us to get individual growth rates of all the organoids in a culture. The data for each individual organoid can be used to obtain an average response but also allows to identify individual responses. While this approach could help optimize the interpretation of data, it does not prevent the above-mentioned heterogeneity.

Another limitation of the organoid work is the number of cells and biomass obtained for downstream assays. While organoids are composed of thousands of cells, traditional organoid work is done in 24-well plates containing 50 μ L domes. Upon collection, the average number of cells obtained from a 50 μ L dome containing hepatic organoids can range from $3 \cdot 10^4$ to $5 \cdot 10^5$ cells. In contrast, the average number of HEPG2 cells in a 10 cm^2 dish used for metabolic assays ranges between $4 \cdot 10^6$ and $8 \cdot 10^6$. While two domes of 50 μ L can provide enough material to perform qPCR or immunofluorescence, this would not be sufficient for most metabolic assays. For some metabolic techniques performed in this thesis, pooling of 3-4 wells was required, which in some cases still did not yield enough material for reliable quantification. Moreover, the high number of organoids needed also increased the costs of the experiment.

One straightforward approach is to increase the number of organoids, and therefore cells, by upscaling the cultures or optimizing the culture procedures³³. This would allow us to obtain more reliable readouts that depend on cell number. However, this can also increase costs associated with the amount of media needed, cytokines and consumables. An alternative solution is to increase the sensitivity of the bioanalytical assays performed in metabolomic studies. Several groups are focused on the profiling of different metabolites in small quantities using small numbers of cells with microscale analytical

techniques such as capillary electrophoresis-mass spectrometry (CE-MS).^{34,35} These new techniques could allow for reliable and reproducible metabolic profiles of organoid samples with limited biomass.

Another important and limiting factor of organoid work is the use of hydrogels. Hydrogels, are extracellular matrix (ECM) proteins that work as a scaffold, allowing organoids to grow in three dimensions³⁶. These matrices are commonly from tumor origin and present high batch-to-batch variability³⁷. Alternatively to animal-derived undefined matrixes, the biomaterials field is currently moving towards alternatives including decellularized extracellular matrix, synthetic hydrogels and gel-forming recombinant proteins³⁸. It is important to mention that biological hydrogels contain high concentrations of proteins and their presence might interfere with downstream analysis, particularly in proteomics analysis. During the work for this thesis, I observed how correct degradation and removal of the hydrogel prior to downstream analysis is essential to obtain reliable proteomics results. This could be caused by the amount of hydrogel left after removal, which can also impact total protein concentrations and cause variations in normalization. Therefore, it is important to establish robust and standardized protocols for the complete removal of matrixes and to avoid issues derived from the hydrogels.

Finally, I would also like to bring the attention to a commonly overlooked limitation of organoid work, namely the economic costs. Organoid culture medium often requires expensive growth factors and cytokines, which are used in large quantities. Moreover, the hydrogels needed to grow organoids in three dimensions are also costly and needed in large amounts. Because of these high costs, the organoid technology is not yet accessible to all research groups. Surprisingly, little information has been published on this topic. While the organoid technology slowly becomes a daily practice in more and more labs, it is still far from being accessible to everyone. There is a clear need for companies and academic labs to work together, towards the development and commercialization of robust, well-defined and inexpensive matrixes to standardize biological research.

Regarding the *in silico* models presented in this thesis, some aspects require further attention. These models are presented as tools to predict *in vitro*/*in vivo* responses or behaviors. However, in order to build biologically accurate models, we rely on kinetic parameters from the enzymes in the model. While working on **chapter 5**, I found that there is a lack of standardized and reliable kinetic parameters of the enzymes involved in the peroxisomal β -oxidation. Most of the studies describing kinetics of the enzymes date back to the 80s

and 90s of the twentieth century and lack information on oxidation of very-long-chain fatty acids or branched-chain fatty acids³⁹. This was due to the insoluble nature of these compounds making it challenging to work with them. Moreover, very little information on kinetic parameters of the transporters is available. In order to perform kinetic studies, transporters are often reconstituted in liposomes to perform transport assays which can be affected by lipid membrane dynamics⁴⁰. As a solution, I propose to re-visit the early kinetic studies making use of the current technology to fully characterize the mechanism and kinetic parameters of the enzymes of interest, making for new and more detailed kinetic models.

PART 2. THE IMPORTANCE OF PEROXISOMES AND MITOCHONDRIAL IN FATTY ACID METABOLISM AND THEIR INTERPLAY IN HEALTH AND DISEASE

The main aim of the thesis was to develop *in vitro* and *in silico* models to study two diseases affecting fatty acid metabolism. In both diseases, peroxisomes and mitochondria are involved, highlighting the importance and interplay of these two metabolic organelles. While mitochondria have been extensively studied and characterized, we have an incomplete overview of the many peroxisomal functions that are still being discovered. Recent studies have described peroxisomes to be involved in different processes such as aging⁴¹, immunometabolism⁴², etc.

Peroxisomes and mitochondria in Severe Malnutrition

In **chapter 2**, I focused on the effects of malnutrition on peroxisomes and mitochondria both in the liver and the intestine and the mechanisms regulating the balance between biosynthesis and degradation of both organelles. As a proxy to malnutrition, I exposed the organoids to amino-acid restricted media for different periods of time. The amino-acid restricted conditions in our studies mimic the effects of low protein diets, leading to a reduction in peroxisomal and mitochondrial mass and function. In the case of the liver, mitochondrial loss is described to follow peroxisomal degradation while this time dependence was not observed in the intestinal organoids. However, while the loss of peroxisomes and mitochondria in the hepatic organoids recapitulates the findings of the *in vivo* models¹⁴, the loss of peroxisomes observed in the malnourished intestinal organoids has not yet been investigated *in vivo*. In **chapter 4**, I discussed whether the reduction in peroxisomal number in the

hepatic organoids is caused by increased degradation or reduced biosynthesis. While impaired biogenesis could be a potential explanation, little information is available on the topic. Only one *in vivo* study using rats on an LPD reported no changes in the expression of any peroxins (PEX) involved in peroxisomal biogenesis and maintenance¹⁴. During this chapter I showed how amino-acid restricted organoids showed regulation of several PEX genes. This differential regulation indicates, that although it is hard to determine whether biogenesis is up- or downregulated, it is clearly affected by amino acid restriction. In the case of PEX5, linked to pexopathy in nutrient starvation⁴³, we observed a clear upregulation under the amino-acid restricted conditions. Further studies should be done in order to fully understand the effect of amino-acid restriction on peroxisomal biogenesis.

In contrast, several groups have focused on the effects of LPD on autophagic degradation in rodents. It is important to emphasize that different experimental conditions lead to different results, and in some cases comparison between models might be misleading. Low protein diets have been shown to induce peroxisomal and mitochondrial loss as well as dysfunctional mitochondria both in children and laboratory animals^{13,14,44}. Most of the *in vivo* work on malnutrition has reported that long exposure to LPD leads to an impairment in autophagic turnover^{12,13}. However, the results found in this thesis, using *in vitro* models, opposed those found in *in vivo* studies. In **chapter 4**, I reported that amino-acid restriction leads to a clear upregulation of autophagic degradation, as measured with an autophagic probe. An interesting aspect of this model is the use of amino-acid restriction instead of a complete amino-acid starvation. While it has been previously described that complete amino-acid starvations induce autophagy *in vitro*^{45,46}, there is no information of the effect of long periods of time of amino-acid restriction. If we try to compare our results with the *in vivo* models, they are more in line with what was observed in the liver of rats fed a LPD for 1 week¹⁴. However, in that same study, the authors reported a block in autophagy after 4 weeks of LPD. These results, together with those of the mouse models which used 2 weeks of LDP, might indicate that autophagy is differentially regulated according to the time of exposure to LPD. On that note, in **chapter 4**, I also reported a different regulation of autophagy in organoids deprived of amino acids for 48 h and 96 h. These results also point towards a differential regulation based on time. However, in the case of the amino-acid restricted hepatic organoid model, amino-acid restrictions of longer than 4 days were hard to recapitulate using the organoids due to technical limitations. On this note, it is important to emphasize the challenges of translating time length from organoid work to animal models.

During the work on this thesis, I also illustrated the potential of 3D in vitro models to test different therapeutic approaches to prevent peroxisomal and mitochondrial loss in the context of amino-acid restriction. In **chapter 2**, I briefly focused on the therapeutic effects of fenofibrate and rapamycin in the liver and the intestine, respectively. Fenofibrate prevented the loss of peroxisomal markers in 48h amino-acid restricted hepatic organoids, but failed to prevent loss of peroxisomal function. In **chapter 4** I tested the effects of different PPAR- α agonists on preventing peroxisomal and mitochondrial loss during longer amino-acid restrictions (96h). When comparing the effects of docosahexaenoic acid (DHA) supplementation with other PPAR- α agonists we observed disparate results. DHA supplementation prevented the loss of multiple peroxisomal and mitochondrial proteins, whilst the rest of the compounds showed little to no effect. Interestingly, the results were different from those of fenofibrate in **chapter 2**. However, it is not possible to compare these results directly as the amino-acid restriction time was different between experiments in the two chapters. Given the differences between DHA and the other agonists, we hypothesized a PPAR- α -independent effect of DHA leading to the prevention of peroxisomal and mitochondrial loss. While in this chapter I only focused on a small panel of compounds, this platform is suitable for larger screenings of other compounds to either stimulate peroxisomal biogenesis or to prevent their degradation. The use of targeted proteomics could be applied to larger screenings of compounds, assessing their effect on prevention of peroxisomal loss in the context of amino-acid restriction. Optimization of the number of organoids needed for the protocol would greatly benefit the upscaling process and minimize associated costs.

Potential roles of peroxisomes in MCADD

Finally, in **chapter 6**, I focused on the study of medium chain acyl-CoA dehydrogenase deficiency. This inherited disease affects the metabolism of medium chain acyl-CoA leading to accumulation of medium-chain fatty acids and fatty-acid esters under different circumstances. One interesting point of discussion raised in chapter 6 is the heterogeneity in symptomatology observed amongst MCADD patients^{21,22,47}. While the main aim of this chapter was to develop an in vitro model to study and characterize the disease, we also explored a potential compensatory role of peroxisomes. Here, we hypothesized that different compensatory mechanisms involving peroxisomes could explain the differences in adaptation to conditions such as fasting or illness. In this chapter we observed no regulation of the peroxisomal β -oxidation of fatty acids in MCADD organoids. However, we identified a clear regulation of several genes

coding for enzymes involved the metabolism of CoA, both in the peroxisome and mitochondria. These results point towards a peroxisomal contribution to MCADD and emphasize the need to further characterize the interplay of both organelles in the disease. For this study, and to set up the model, we purposefully selected fibroblast from symptomatic patients. For that reason, we believe that differentiation of fibroblast from a larger number of patients, including symptomatic and asymptomatic, will provide broader view of the adaption mechanisms of peroxisomes in the disease.

PART 3. CONCLUDING REMARKS AND FUTURE DIRECTIONS

In conclusion, this work illustrates the potential of new translational models to understand and characterize disorders affecting mitochondrial and peroxisomal fatty-acid metabolism. I present two in vitro and two in silico models for the study of malnutrition and MCADD and introduce them as tools for the study of the pathophysiology of the diseases and discovery of therapeutic approaches.

As an proof-of-principle, the intestinal model has already been used to test the effect of amino-acid restriction on mitochondrial homeostasis and intestinal permeability¹. Moreover, as shown in chapter 2 and 4, the organoid models can be used to test different therapeutic and pharmacological interventions. Future studies, including higher number of compounds should be performed to find the best approach to minimize peroxisomal and mitochondrial defects in malnutrition.

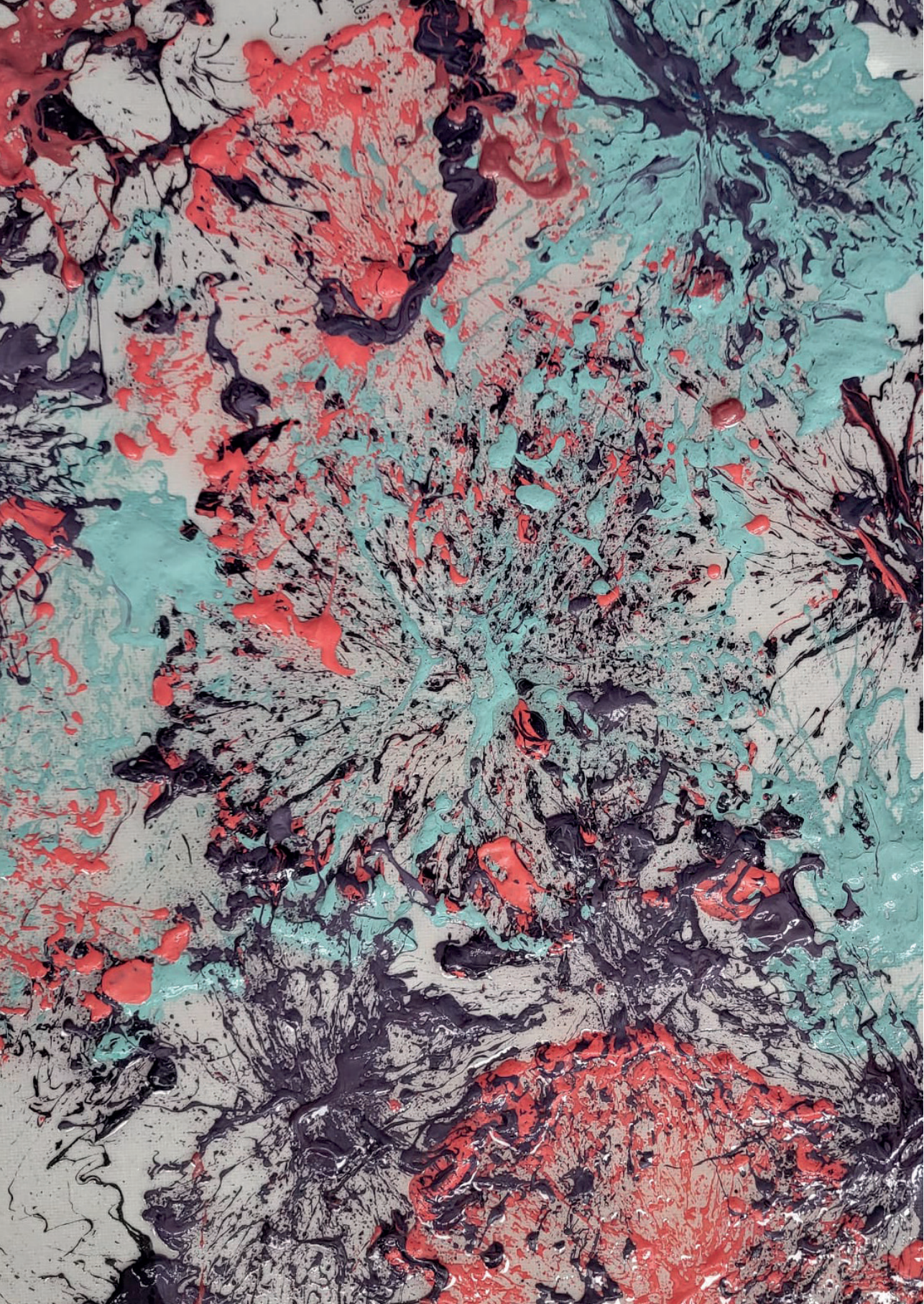
In the case of MCADD, we aim to perform further studies including RNAseq and untargeted proteomics to understand the differences between MCADD and control organoids. Furthermore, we intend to establish organoids from asymptomatic patients in order to compare them to the symptomatic ones. We believe that this approach will help us uncover and understand potential adaptation mechanisms in MCADD.

REFERENCES

1. Ling, C. *et al.* Rebalancing of mitochondrial homeostasis through an NAD⁺-SIRT1 pathway preserves intestinal barrier function in severe malnutrition. *EBioMedicine* 96, (2023).
2. Perlman, M., Senger, S., Verma, S., Carey, J. & Faherty, C. S. A foundational approach to culture and analyze malnourished organoids. *Gut Microbes* 15, (2023).
3. Kretzschmar, K. & Clevers, H. Organoids: Modeling Development and the Stem Cell Niche in a Dish. *Developmental Cell* vol. 38 590–600 Preprint at <https://doi.org/10.1016/j.devcel.2016.08.014> (2016).
4. Sato, T. *et al.* Single Lgr5 stem cells build crypt-villus structures in vitro without a mesenchymal niche. *Nature* 459, 262–265 (2009).
5. Casamitjana, J., Espinet, E. & Rovira, M. Pancreatic Organoids for Regenerative Medicine and Cancer Research. *Front Cell Dev Biol* 10, (2022).
6. Barker, N. *et al.* Lgr5+ve Stem Cells Drive Self-Renewal in the Stomach and Build Long-Lived Gastric Units In Vitro. *Cell Stem Cell* 6, 25–36 (2010).
7. Barkauskas, C. E. *et al.* Lung organoids: Current uses and future promise. *Development (Cambridge)* 144, 986–997 (2017).
8. Lancaster, M. A. *et al.* Cerebral organoids model human brain development and microcephaly. *Nature* 501, 373–379 (2013).
9. Lancaster, M. A. & Knoblich, J. A. Organogenesis in a dish: Modeling development and disease using organoid technologies. *Science (1979)* 345, (2014).
10. Perez-Lanzon, M., Kroemer, G. & Maiuri, M. C. Organoids for Modeling Genetic Diseases. in *International Review of Cell and Molecular Biology* vol. 337 49–81 (Elsevier Inc., 2018).
11. Hu, W. & Lazar, M. A. Modelling metabolic diseases and drug response using stem cells and organoids. *Nature Reviews Endocrinology* vol. 18 744–759 Preprint at <https://doi.org/10.1038/s41574-022-00733-z> (2022).
12. Arvidsson Kvissberg, M. E. *et al.* Inhibition of mTOR improves malnutrition induced hepatic metabolic dysfunction. *Sci Rep* 12, (2022).
13. Hu, G. *et al.* The role of the tryptophan-NAD⁺ pathway in a mouse model of severe malnutrition induced liver dysfunction. *Nat Commun* 13, (2022).
14. van Zutphen, T. *et al.* Malnutrition-associated liver steatosis and ATP depletion is caused by peroxisomal and mitochondrial dysfunction. *J Hepatol* 65, 1198–1208 (2016).
15. Sugimoto, S. & Sato, T. Organoid vs In Vivo Mouse Model: Which is Better Research Tool to Understand the Biologic Mechanisms of Intestinal Epithelium? *CMGH* 13, 195–197 (2022).
16. Zhao, Z. *et al.* Organoids. *Nature Reviews Methods Primers* 2, (2022).
17. Hirt, C. K. *et al.* Drug screening and genome editing in human pancreatic cancer organoids identifies drug-gene interactions and candidates for off-label therapy. *Cell Genomics* 2, (2022).
18. Zhang, S. *et al.* Integration of organoids in peptide drug discovery: Rise of the high-throughput screening. *VIEW* (2023) doi:10.1002/VIW.20230010.

19. Chitrangi, S., Vaity, P., Jamdar, A. & Bhatt, S. Patient-derived organoids for precision oncology: a platform to facilitate clinical decision making. *BMC Cancer* 23, (2023).
20. Turhan, A. G. *et al.* iPSC-Derived Organoids as Therapeutic Models in Regenerative Medicine and Oncology. *Front Med (Lausanne)* 8, (2021).
21. Touw, C. M. *et al.* In vitro and in vivo consequences of variant medium-chain acyl-CoA dehydrogenase genotypes. *Orphanet J Rare Dis* 8, (2013).
22. Touw, C. M. L. *et al.* Risk stratification by residual enzyme activity after newborn screening for medium-chain acyl-CoA dehydrogenase deficiency: Data from a cohort study. *Orphanet J Rare Dis* 7, (2012).
23. Bordbar, A. *et al.* Personalized Whole-Cell Kinetic Models of Metabolism for Discovery in Genomics and Pharmacodynamics. *Cell Syst* 1, 283–292 (2015).
24. Saa, P. A. & Nielsen, L. K. Formulation, construction and analysis of kinetic models of metabolism: A review of modelling frameworks. *Biotechnol Adv* 35, 981–1003 (2017).
25. Odendaal, C. *et al.* Personalised modelling of clinical heterogeneity between medium-chain acyl-CoA dehydrogenase patients. *BMC Biol* 21, 184 (2023).
26. Moreno-Sánchez, R., Saavedra, E., Rodríguez-Enríquez, S. & Olín-Sandoval, V. Metabolic Control Analysis: A tool for designing strategies to manipulate metabolic pathways. *J Biomed Biotechnol* 2008, (2008).
27. Osumi, T., Hashimoto, T. & Ui, N. Purification and Properties of Acyl-CoA Oxidase from Rat Liver 1. *J Biochem* 87, 1735–1746 (1980).
28. Inestrosa, N. C., Bronfman, M. & Leighton, F. Detection of Peroxisomal Fatty Acyl-Coenzyme A Oxidase Activity. *Biochem. J* 182, 779–788 (1979).
29. Kim, J., Koo, B. K. & Knoblich, J. A. Human organoids: model systems for human biology and medicine. *Nature Reviews Molecular Cell Biology* vol. 21 571–584 Preprint at <https://doi.org/10.1038/s41580-020-0259-3> (2020).
30. Jensen, K. B. & Little, M. H. Organoids are not organs: Sources of variation and misinformation in organoid biology. *Stem Cell Reports* 18, 1255–1270 (2023).
31. Li, Y., Tang, P., Cai, S., Peng, J. & Hua, G. Organoid based personalized medicine: from bench to bedside. *Cell Regeneration* 9, (2020).
32. Bose, S., Clevers, H. & Shen, X. Promises and challenges of organoid-guided precision medicine. *Med* 2, 1011–1026 (2021).
33. Brandenberg, N. *et al.* High-throughput automated organoid culture via stem-cell aggregation in microcavity arrays. *Nat Biomed Eng* 4, 863–874 (2020).
34. van Mever, M. *et al.* Profiling acidic metabolites by capillary electrophoresis-mass spectrometry in low numbers of mammalian cells using a novel chemical derivatization approach. *Analytical Science Advances* 3, 3–13 (2022).
35. He, B. *et al.* Analytical techniques for biomass-restricted metabolomics: An overview of the state-of-the-art. *Microchemical Journal* vol. 171 Preprint at <https://doi.org/10.1016/j.microc.2021.106794> (2021).
36. Kasai, R. D. *et al.* A review on hydrogels classification and recent developments in biomedical applications. *International Journal of Polymeric Materials and Polymeric Biomaterials* (2022) doi:10.1080/00914037.2022.2075872.

37. Gan, Z., Qin, X., Liu, H., Liu, J. & Qin, J. Recent advances in defined hydrogels in organoid research. *Bioact Mater* 28, 386–401 (2023).
38. Kozłowski, M. T., Crook, C. J. & Ku, H. T. Towards organoid culture without Matrigel. *Commun Biol* 4, (2021).
39. Kamp, F., Zakim, D., Zhang, F., Noy, N. & James Hamilton, and A. *Fatty Acid Flip-Flop in Phospholipid Bilayers is Extremely Fast*. *Biochemistry* vol. 34 <https://pubs.acs.org/sharingguidelines> (1192).
40. Fitzgerald, G. A., Mulligan, C. & Mindell, J. A. A general method for determining secondary active transporter substrate stoichiometry. *Elife* 6, (2017).
41. Deori, N. M., Kale, A., Maurya, P. K. & Nagotu, S. Peroxisomes: role in cellular ageing and age related disorders. *Biogerontology* vol. 19 303–324 Preprint at <https://doi.org/10.1007/s10522-018-9761-9> (2018).
42. Di Cara, F., Savary, S., Kovacs, W. J., Kim, P. & Rachubinski, R. A. The peroxisome: an up-and-coming organelle in immunometabolism. *Trends in Cell Biology* vol. 33 70–86 Preprint at <https://doi.org/10.1016/j.tcb.2022.06.001> (2023).
43. Eun, S. Y. *et al.* PEX5 regulates autophagy via the mTORC1-TFEB axis during starvation. *Exp Mol Med* 50, (2018).
44. Doherty, J. F., Golden, M. H. & Brooks, S. E. Peroxisomes and the fatty liver of malnutrition: an hypothesis. *Am J Clin Nutr* 54, 674–681 (1991).
45. Ghislat, G. & Knecht, E. Regulation of Autophagy by Amino Acid Starvation Involving Ca²⁺. in *Autophagy: Cancer, Other Pathologies, Inflammation, Immunity, Infection, and Aging* vol. 6 69–79 (Elsevier Inc., 2015).
46. Chen, R. *et al.* The general amino acid control pathway regulates mTOR and autophagy during serum/glutamine starvation. *Journal of Cell Biology* 206, 173–182 (2014).
47. Derks, T. G. J. *et al.* The natural history of medium-chain acyl CoA dehydrogenase deficiency in the Netherlands: Clinical presentation and outcome. *Journal of Pediatrics* 148, (2006).





Appendices

Summary

Samenvatting

Resumen para público no científico

Acknowledgements

List of publications

Curriculum vitae

SUMMARY

Overview of the thesis for the general public

The main aim of this thesis is to establish different *in vitro* and *in silico* models for the study of malnutrition and medium chain acyl-CoA dehydrogenase deficiency (MCADD).

Biomedical research has traditionally relied on *in vivo* models which depend on the use of animals to test different hypotheses and study biological processes. Animal models not only present ethical issues, but also translational challenges due to differences with humans. This emphasizes the need for appropriate *in vitro* and *in silico* models.

Two emerging fields aim to shift the focus away from *in vivo* biology, striving to minimize the amount of work done in animal models. These are developmental and regenerative biology, focusing on *in vitro* models, and systems biology, focusing on *in silico* models. *In vitro* models are studied outside the living organism of interest, using an environment that mimics the natural conditions of the organism. These models can recapitulate multiple organs (liver, intestine, pancreas, etc.) and can be used to study different biological processes, specific diseases or screen for drugs amongst many other applications. In this thesis, I focus on the use of organoids or “mini organs”. The discovery of organoids in 2009 revolutionized the field of *in vitro* research in biomedicine. Organoids are three dimensional structures that resemble the organ of origin. They have the ability to proliferate in culture, as well as to maintain some of the functions of the organ of origin. Organoids can be derived either from primary tissue (biopsies obtained directly from different organs) or from induced pluripotent stem cells (iPSCs). On the other hand, *in silico* models are mathematical representations that allow to simulated a biological system of interest. These models rely on mathematical formulas and algorithms that describe the behaviour of certain pathways or biological processes. *In silico* models can be complemented with data obtained from other models (including *in vitro* and *in vivo*) to understand multiple biological processes. Deep learning has emerged as an efficient tool within the field of *in silico* modelling for biological purposes and can be applied to a wide range of models. Detailed kinetic models are computational tools that can be used for the study of metabolic pathways and rely on kinetic equations to describe the behaviour of the different enzymes. These models allow us to understand the importance of metabolic pathways and how these are regulated in health and disease.

In this thesis, I have focused on the establishment of *in vitro* and *in silico* models for the study of two diseases affecting fatty acid metabolism. The first disease, central to this thesis, is severe malnutrition. Malnutrition refers to an imbalance or deficit in the intake of energy and/or nutrients necessary to maintain cellular homeostasis. Malnutrition can be caused by a deficiency or excess of nutrients, undernutrition and overnutrition respectively. In this thesis the term malnutrition is used to refer to undernutrition. Severe malnutrition is known as the most severe form of macronutrient deficiency, such as that of proteins or lipids. Long exposures to low protein diets result in low number of peroxisomes in the liver. Peroxisomes are small, single-membrane organelles, present in most eukaryotic cells, with a wide range of functions including metabolism of fatty acids (long, very-long, and branched-chain fatty acids). In the case of children, severe malnutrition hinders optimal growth and development. Current approaches for the study of malnutrition are primarily based on the use of animal models, including primates, rats, and most frequently, mice on low protein diets (LPD). These models have proven extremely valuable to understand the pathophysiology of malnutrition in the liver and intestine and are able to recapitulate specific disease phenotypes (e.g., hepatic steatosis or barrier dysfunction). Moreover, they allow for a whole-body characterization and study of the interplay between the organs. Although physiologically relevant, they are also limited by blood and tissue sampling, the large numbers of animals required per study and translational discrepancies between humans and rodents.

The second disease discussed in this thesis is medium chain acyl-CoA dehydrogenase deficiency (MCADD). Medium chain acyl-CoA dehydrogenase (MCAD) is a mitochondrial enzyme in charge of metabolizing medium chain fatty acids. MCADD is a genetic disorder that affects the body's ability to process medium-chain fatty acids. This can lead to energy deficits during fasting, long bouts of exercise or intercurrent illness. In the case of MCADD, mitochondria (a subcellular organelle with a central role in the Gibbs energy supply to the cell) are affected. While the effects of malnutrition on peroxisomes have been widely described, little is known about the effects of MCADD on said organelle. Similar to the first disease, conventional approaches for the study of MCADD involve the use of animal models in which the disease is induced. One very important limitation of rodent models for MCADD is the presence of an extra enzyme (with similar functions to MCAD) not present in humans.

Chapter overview

The aim of this thesis was to establish new *in vitro* and *in silico* models to study the role of peroxisomes in malnutrition and medium chain acyl-CoA dehydrogenase deficiency and to gain biological insights of both diseases. The thesis includes a general introduction, presented in **chapter 1**, in which *in vitro* and *in silico* models are introduced as well as the different organelles and diseases described in this thesis. **Chapter 1** also introduces the different types of *in vitro* and *in silico* models and compares the different approaches available at the moment.

In **chapter 2** of the thesis, I described how I have developed, together with a collaborator, two *in vitro* models (using primary-tissue derived organoids) of malnutrition in the liver and intestine. These models recapitulated important characteristic events of malnutrition, including the loss of peroxisomes, loss of intestinal barrier function and accumulation of fat in the liver. At the end of the chapter, we demonstrated how loss of peroxisomes could be prevented by co-treatment with fenofibrate (a pharmacological PPAR- α agonist) in the liver and rapamycin (an autophagy inducer) in the intestine. The hepatic organoid model was then further optimized and applied in **chapter 4**. In this chapter I focused on the degradation of peroxisomes, in a low-amino acid environment, via autophagy, and tried to find different compounds to activate the synthesis of new peroxisomes. I found that DHA (docosahexaenoic acid) (a polyunsaturated fatty acid) prevented the loss of peroxisomes in low-amino acid conditions. While I observed a minor blockage in peroxisomal degradation, I could not fully elucidate the mechanism of action of DHA. Further work is proposed to understand the mechanism of DHA and its role preventing peroxisomal degradation.

Chapters 3 and **5** focus on the development of two *in silico* models.

In **chapter 3**, I supplied data for and validated a deep-learning tool to track and measure organoids in brightfield images. This tool was developed by a colleague from the European PerlCo consortium. This tool was applied to the *in vitro* hepatic malnutrition model to assess the effects of amino acid deprivation on organoid size and number. The deep learning model was able to replicate the manual counting and measuring of organoids presented in chapter 2. Overall, I demonstrated that hepatic organoids exposed to low amino acids were smaller in size (depending on their developmental stage) while intestinal organoids exhibited shorter crypts (key structures in the intestine that play a crucial role in intestinal regeneration).

Chapter 5 describes another *in silico* model, in this case using detailed kinetics. This model integrates the behavior of the enzymes involved in the peroxisomal β -oxidation of straight-chain fatty acids. Making use of data generated in **chapter 4**, as well as from the literature, I predicted the behavior of the pathway under amino acid deprivation as well as in the presence of DHA. Further work is required to expand the model to also recapitulate the metabolism of branched-chain fatty acids.

In **chapter 6**, I established an iPSC-derived hepatic organoid model to study MCADD. To do so, iPSCs from MCADD patients were differentiated to organoids and compared with healthy controls. Expandable hepatic organoids (EHOs) have the ability to proliferate and to further develop into mature EHOs (mat-EHOs) which recapitulate many liver functions. MCADD EHOs accumulated medium chain acyl-carnitines (esterified form of fatty acids), which are known biomarkers of the disease. Interestingly, MCADD and healthy organoids exhibited some differences in peroxisomal coenzyme A metabolism. This *in vitro* model is a promising tool to further study the role of peroxisomes, as well as the interaction between peroxisomes and mitochondria, in MCADD and to link the different symptomatology of the disease with the different mutations of the donors.

Finally, **chapter 7** presents a general discussion on the use of *in vitro* and *in silico* models to study malnutrition and MCADD. In this chapter I also discussed how these new models can help understand the pathophysiology of different diseases prior to referring to *in vivo* models, while mentioning some of the limitations and proposed approaches to overcome such limitations. This chapter also focuses on discussing the importance of peroxisomes and mitochondria in health and disease and their potential interplay in both malnutrition and MCADD.

Final remarks

In this thesis I have demonstrated that *in vitro* and *in silico* models are suitable tools for the study of malnutrition and medium chain acyl-CoA dehydrogenase. These models have proven valuable to gain biological insights into both diseases and understand different pathophysiological processes. Moreover, these results can potentially be extrapolated into other diseases. Although the use of animal models remains an essential tool in the field of biology, the emergence of new methodologies should be regarded as a significant step towards a future with reduced reliance on animal experimentation.

SAMENVATTING

Overzicht van het proefschrift voor het algemene publiek

Van oudsher worden in biomedisch onderzoek in vivo modellen (dieren, mensen) gebruikt om ziekten te bestuderen, medicijnen te screenen en biologische processen te karakteriseren. Diermodellen roepen niet alleen ethische kwesties op, maar hebben ook biologische verschillen met mensen. In vitro- en in silico-systemen bieden de mogelijkheid om het gebruik van diermodellen te minimaliseren en onderzoek te doen dat beter toepasbaar is op mensen. In vitro-modellen worden bestudeerd buiten het levende organisme en in een omgeving die de natuurlijke omstandigheden van het organisme nabootst. Deze modellen kunnen meerdere organen nabootsen en kunnen worden gebruikt om verschillende biologische processen, specifieke ziekten of de werking van medicijnen te bestuderen. In dit proefschrift richt ik me op het gebruik van organoïden of "mini-organen". De ontdekking van organoïden in 2009 heeft het veld van in vitro onderzoek in de biogeneeskunde gerevolutioneerd. Organoïden zijn driedimensionale structuren die lijken op het oorspronkelijke orgaan. Ze kunnen groeien en zich vermeerderen in kweek, en behouden gedeeltelijk de functies van het oorspronkelijke orgaan. Organoïden kunnen worden afgeleid van primair weefsel (biopten verkregen direct uit verschillende organen) of van geïnduceerde pluripotente stamcellen (iPSC's). In silico-modellen zijn wiskundige beschrijvingen van een biologisch systeem. Deze modellen zijn gebaseerd op wiskundige formules en algoritmen die de biochemische reacties uit stofwisselingsroutes of biologische processen beschrijven. Ze bevatten verschillende parameters zoals reactiesnelheden, reactiemechanismen en thermodynamische parameters. In silico-modellen kunnen worden aangevuld met gegevens verkregen uit andere modellen (inclusief in vitro en in vivo) om verschillende biologische processen te begrijpen. In dit proefschrift ontwikkel ik twee soorten in silico-modellen: een 'deep learning'-model, gebaseerd op kunstmatige intelligentie, en een gedetailleerd kinetisch model. 'Deep learning' is efficiënt instrument binnen het veld van in silico-modellering voor biologische doeleinden en kan heeft een breed toepassingsgebied. Gedetailleerde kinetische modellen zijn gebaseerd op snelheidsvergelijkingen om het gedrag van de verschillende enzymen te beschrijven, en kunnen worden gebruikt de studie van de stofwisseling. Gezamenlijk stellen de verschillende soorten in silico modellen ons in staat om de werking van metabole paden te begrijpen en hoe deze worden gereguleerd in gezondheid en ziekte.

In dit proefschrift heb ik me gericht op het opzetten van in vitro- en in silico-modellen voor de studie van twee ziekten waarin de afbraak van vetzuren betrokken is. De eerste ziekte die centraal staat in dit proefschrift, is ernstige ondervoeding. Ondervoeding verwijst naar een tekort in de inname van energie en/of voedingsstoffen die nodig zijn om de cellulaire homeostase te handhaven. Ernstige ondervoeding staat bekend als de meest extreme vorm van macronutriëntdeficiëntie, zoals een tekort aan eiwitten en vetten. Langdurige blootstelling aan diëten met een laag eiwitgehalte is direct gekoppeld aan een laag aantal peroxisomen in de lever. Peroxisomen zijn kleine, enkelwandige organellen die aanwezig zijn in de meeste eukaryote cellen, met een breed scala aan functies, waaronder de afbraak van vetzuren (lange, zeer lange en vertakte ketenvetzuren), synthese van lipiden, synthese van galzuren en cholesterol en metabolisme van reactieve zuurstofmoleculen.

Bij kinderen belemmert ondervoeding optimale groei en ontwikkeling. Huidige benaderingen voor de studie van ondervoeding zijn voornamelijk gebaseerd op het gebruik van diermodellen, waaronder ratten en vooral muizen op diëten met een laag eiwitgehalte. Deze modellen hebben zich uiterst waardevol getoond om de pathofysiologie van ondervoeding in de lever en darm te begrijpen en kunnen specifieke ziektefenotypen repliceren (o.a. leververvetting, barrière-dysfunctie). Bovendien stellen deze in vivo-modellen ons in staat om het hele lichaam te bestuderen binnen dit ziektebeeld, in plaats van slechts één orgaan. Hoewel fysiologisch relevant, zijn deze modellen beperkt in de afname van bloed- en weefselmonsters, de grote aantallen dieren die nodig zijn per onderzoek en de discrepanties tussen mensen en knaagdieren.

De tweede ziekte die in dit proefschrift wordt besproken, is medium-chain acyl-CoA-dehydrogenasedeficiëntie (MCADD). MCADD is een genetische aandoening die de verwerking van middellange ketenvetzuren aantast. Dit wordt veroorzaakt door het ontbreken van het enzym medium-chain acyl-CoA-dehydrogenase (MCAD) (een mitochondriaal enzym verantwoordelijk voor het omzetten van middellange-keten vetzuren). Dit kan leiden tot energietekorten tijdens vasten, langdurige inspanning of ziekte. In het geval van MCADD zijn mitochondria (subcellulaire organellen met meerdere functies zoals ATP-productie, calciummetabolisme, ontgiftingsprocessen) aangetast. Terwijl de effecten van ondervoeding op peroxisomen uitgebreid zijn beschreven, is er weinig bekend over de effecten van MCADD op dit organel. Net als bij de eerste ziekte omvatten conventionele benaderingen voor de studie van MCADD het gebruik van diermodellen waarin de ziekte wordt geïnduceerd. Een zeer belangrijke beperking van knaagdiermodellen voor MCADD is de aanwezigheid van een extra enzym (met vergelijkbare functies als MCAD) dat niet aanwezig

is bij mensen. Momenteel zijn er slecht een beperkt aantal in vitro- of in silico-modellen beschikbaar om MCADD te bestuderen.

Hoofdstukoverzicht

Het doel van dit proefschrift was het opzetten van nieuwe in vitro- en in silico-modellen om de rol van peroxisomen te bestuderen bij (1) ondervoeding en (2) medium-chain acyl-CoA-dehydrogenasedeficiëntie. In hoofdstuk 1 worden in vitro- en in silico-modellen geïntroduceerd, evenals de verschillende organellen en ziekten die in dit proefschrift worden beschreven. Hoofdstuk 1 introduceert ook de verschillende soorten in vitro- en in silico-modellen en vergelijkt de beschikbare benaderingen.

In hoofdstuk 2 van het proefschrift beschrijf ik hoe we twee in vitro-modellen hebben ontwikkeld van ondervoeding in de lever en darm, met behulp van organoïden. Deze modellen bootsen enkele van de karakteristieke gevolgen van ondervoeding na, zoals verlies van peroxisomen en ophoping van vet in de lever. In het geval van de darm hebben we ook afname van de barrièrefunctie waargenomen. We hebben aangetoond hoe verlies van peroxisomen kan worden voorkomen door behandeling met fenofibraat (een farmacologische PPAR- α -agonist) in de lever of rapamycine (een autophagy-inductor) in de darm.

In hoofdstuk 3 heb ik data aangeleverd voor de ontwikkeling en validatie van een deep learning-tool om organoïden te volgen en hun omvang meten met behulp van microscopie. Deze deep-learning tool was ontwikkeld door een collega uit het PerlCo consortium. Deze methodiek heb ik vervolgens toegepast op ons in vitro-model van ondervoeding om de effecten van aminozuurdeprivatie op de grootte en het aantal organoïden te kwantificeren. De resultaten waren hetzelfde als bij handmatig tellen en meten van organoïden, maar de methode was veel minder arbeidsintensief. Biologisch hebben we aangetoond dat leverorganoïden blootgesteld aan minder aminozuren kleiner van omvang waren (afhankelijk van hun ontwikkelingsstadium).

Het leverorganoïdemodel wordt vervolgens verder besproken en toegepast in hoofdstuk 4. In dit hoofdstuk richt ik me op de afbraak van peroxisomen in een omgeving met weinig aminozuren en onderzoek ik verschillende farmaceutische stoffen om de synthese van nieuwe peroxisomen te activeren. Hier heb ik aangetoond dat DHA (docosahexaeenzuur) (een meervoudig onverzadigd vetzuur) het verlies van peroxisomen in omstandigheden met weinig aminozuren voorkomt. Hoewel ik een gedeeltelijke blokkade in de afbraak van peroxisomen heb waargenomen, kon ik het volledige werkingsmechanisme

van DHA niet ophelderen. Verder onderzoek is nodig om het mechanisme van DHA en de rol ervan bij het voorkomen van peroxisomale afbraak te begrijpen.

Hoofdstuk 5 behandelt een nieuw in silico-model gebaseerd op gedetailleerde enzymkinetiek. Dit model beschrijft het gedrag van de peroxisomale β -oxidatie van rechte-keten vetzuren, gebaseerd op de kinetiek van de belangrijkste enzymen. Met behulp van gegevens gegenereerd in hoofdstuk 4, evenals uit de literatuur, kunnen we het gedrag van het pad voorspellen onder aminozuurdeprivatie en in aanwezigheid van DHA. Een vervolgstap is om het model uit te breiden om ook het metabolisme van andere vetzuren die vaak worden omgezet door peroxisomen, te repliceren.

In hoofdstuk 6 heb ik een op iPSC gebaseerd leverorganoïdemodel opgezet om MCADD te bestuderen. Hiertoe werden iPSC's van MCADD-patiënten gedifferentieerd tot organoïden en vergeleken met die van gezonde proefpersonen. Deze leverorganoïden (EHO's) hebben het vermogen om zich te delen en zich verder te ontwikkelen tot volwassen EHO's (mat-EHO's) die veel leverfuncties nabootsen. Zoals verwacht, hoopten carnitine-esters van middellange-keten vetzuren zich op in MCADD EHO's. Dit zijn bekende biomerkers voor MCADD. Het was opvallend dat er verschillen waren in het peroxisomale metabolisme van Coenzym A tussen MCADD en gezonde organoïden, zoals de upregulatie van NUDT7. We presenteren dit in vitro-model als een instrument om verder onderzoek te doen naar de rol van peroxisomen, evenals de interactie tussen peroxisomen en mitochondriën, in MCADD. Daarnaast kan dit model gebruikt worden om de verschillende fenotypes van de ziekte te koppelen aan de verschillende mutaties van de donoren.

Tot slot bediscussieer ik in hoofdstuk 7 het gebruik van in vitro- en in silico-modellen om ondervoeding en MCADD te bestuderen. In dit hoofdstuk bespreek ik ook hoe deze nieuwe modellen kunnen helpen bij het begrijpen van de pathofysiologie van verschillende ziektebeelden voordat gebruikt wordt gemaakt van in vivo-modellen. Hierbij worden ook enkele van de beperkingen en voorgestelde benaderingen om deze beperkingen te overwinnen besproken. Dit hoofdstuk richt zich ook op het belang van peroxisomen en mitochondriën in gezondheid en ziekte en hun onderlinge interactie in zowel ondervoeding als MCADD.

Tot slot

In dit proefschrift heb ik aangetoond dat in vitro- en in silico-modellen geschikte instrumenten zijn voor de studie van ondervoeding en medium-chain acyl-CoA-dehydrogenase-deficiëntie. Bovendien kunnen deze resultaten mogelijk worden geëxtrapoleerd naar andere ziekten. Hoewel het gebruik van diermodellen soms noodzakelijk blijft binnen de biologie, is opkomst van nieuwe methodologieën een belangrijke stap naar een toekomst waarin we minder afhankelijk worden van dierproeven.

RESUMEN PARA PÚBLICO NO CIENTÍFICO

Objetivos de la tesis y tema principal

El objetivo principal de esta tesis es establecer diferentes modelos *in vitro* e *in silico* para la caracterización y estudio de dos enfermedades que afectan a los peroxisomas (malnutrición y deficiencia de la acil-coenzima A deshidrogenasa de cadena media (MCADD, por sus siglas en inglés)).

La célula y los peroxisomas

Las células eucariotas (aquellas que se encuentran en humanos, animales y plantas) están compuestas por diferentes compartimentos. Estos pueden separarse, a grandes rasgos, en núcleo, citoplasma y orgánulos. Cada una de estas partes de la célula tiene funciones indispensables para su supervivencia y función. Se sabe que existen diferentes enfermedades que afectan a distintas partes de la célula, impidiendo su funcionamiento y/o supervivencia. En esta tesis, me centro en un orgánulo conocido como peroxisoma. Los peroxisomas se encuentran en la mayoría de las células eucariotas y presentan un gran rango de funciones entre las que se incluyen el metabolismo de especies reactivas de oxígeno (ROS) y nitrógeno (RNS), síntesis de plasminógeno, síntesis de ácidos biliares y metabolismo de ácidos grasos de cadena larga, muy larga y ramificada. En esta tesis, me he centrado principalmente en estudiar el metabolismo de ácidos grasos.

Modelos *in vitro* e *in silico*

Antes de continuar, es indispensable familiarizarse con los términos *in vitro* e *in silico* y cómo interpretarlos en el ámbito de la biología.

Los modelos *in vitro*, son aquellos que se realizan fuera del organismo vivo, pero utilizando un entorno que imita las condiciones de la naturaleza como, por ejemplo, el uso de células en cultivo. Para ello, las células se mantienen a 37°C en presencia de factores de crecimiento, proteínas y nutrientes indispensables para su crecimiento. Estos modelos de células (de hígado, intestino, cáncer, etc.) son comúnmente denominados como modelos *in vitro*. Estos modelos celulares se pueden utilizar para estudiar diferentes enfermedades o exposición a fármacos. En esta tesis, he desarrollado, en colaboración con otros científicos, dos modelos *in vitro*; uno para estudiar la malnutrición, y otro para estudiar la deficiencia de acil-coenzima A deshidrogenasa de cadena media (MCADD). Nuestros modelos *in vitro* están basados en el uso de organoides, que son

estructuras tridimensionales que se asemejan a un órgano en miniatura y se forman en el laboratorio a partir de células madre (células capaces de replicarse y diferenciarse a otro tipo de células). Para el modelo celular de malnutrición, hemos utilizado organoides derivados de ratón, mientras que para el modelo de MCADD, hemos utilizado organoides hepáticos diferenciados a partir de células madre pluripotentes reprogramadas, obtenidas de fibroblastos de pacientes.

Por otro lado, *in silico* se refiere al uso de modelos y simulaciones de ordenador, que se utilizan para predecir el comportamiento de un sistema biológico. Para el desarrollo de sistemas *in silico*, se combinan datos de diferentes experimentos con el conocimiento teórico del sistema de estudio. En el caso de esta tesis, hemos desarrollado un modelo de inteligencia artificial capaz de localizar organoides en cultivo y medir su tamaño. Además, hemos creado un modelo *in silico* empleando cinética de enzimas para explicar el proceso de oxidación de ácidos grasos de cadena larga en el peroxisoma. Este modelo ha sido aplicado al contexto de la malnutrición, utilizando datos obtenidos del modelo *in vitro* mencionado anteriormente.

Malnutrición y deficiencia de acil-coenzima A deshidrogenasa de cadena media

La primera enfermedad, central en esta tesis, es la malnutrición severa (SM). La malnutrición se refiere a un desequilibrio o déficit en la ingesta de energía y nutrientes necesarios para mantener el equilibrio celular. La malnutrición puede ser causada por una deficiencia o un exceso de nutrientes, desnutrición y sobrenutrición, respectivamente. En esta tesis se utiliza el término malnutrición para referirse a la desnutrición. La malnutrición severa se conoce como la forma más grave de deficiencia de macronutrientes (proteínas, lípidos, etc.) que, en el caso de niños, puede obstaculizar un crecimiento y desarrollo óptimo. Hay diferentes tipos de desnutrición, como el retraso del crecimiento, emaciación, peso insuficiente y deficiencias de vitaminas y minerales. El retraso del crecimiento se refiere a niños que son demasiado bajos para su edad y la emaciación se utiliza para describir a los niños que son demasiado delgados para su altura. Por último, el término desnutrición abarca tanto el retraso del crecimiento como la emaciación. La desnutrición grave es un problema de salud mundial: en 2023, aproximadamente 45 millones de niños padecían emaciación, de los cuales 13,7 millones padecían emaciación grave. La malnutrición severa es común en los países de bajos ingresos, donde las dietas suelen ser ricas en carbohidratos y bajas en proteína.

Los niños que sufren malnutrición presentan un amplio espectro de síntomas que afectan al hígado y al intestino, entre otros órganos. En casos de malnutrición grave, es común observar disfunciones intestinales, como diarrea y aumento de la permeabilidad de la barrera intestinal. Estos factores pueden contribuir a un mayor riesgo de deshidratación y sepsis, respectivamente. En cuanto a los efectos de la desnutrición en el hígado, la acumulación de grasa, la hipoalbuminemia y la hipoglucemia son algunos de los problemas comunes observados en niños desnutridos. De manera notable, se ha observado que el número de peroxisomas en las células del hígado de niños malnutridos es mucho más bajo que el de niños sanos, lo que podría estar relacionado con la acumulación de grasa en el hígado anteriormente mencionada.

Los enfoques actuales para el estudio de la desnutrición se basan principalmente en el uso de modelos animales, incluidos primates, ratas, y más frecuentemente, ratones con dietas bajas en proteínas (LPD). Estos modelos han arrojado algo de luz sobre la fisiopatología de la desnutrición en el hígado y el intestino y son capaces de recapitular los fenotipos específicos de la enfermedad (por ejemplo, esteatosis hepática, disfunción de la barrera, etc.). Aunque estos modelos son fisiológicamente relevantes y permiten una caracterización de la enfermedad en el organismo completo, también están limitados por el muestreo de sangre y tejido y requieren el sacrificio de una gran cantidad de animales.

Estas limitaciones enfatizan la necesidad de crear modelos de malnutrición *in vitro* relevantes para estudiar la enfermedad en diferentes órganos y elucidar el rol de los peroxisomas. Como se ha mencionado anteriormente, el objetivo de esta tesis es demostrar que los modelos *in vitro* e *in silico* son adecuados para el estudio de la malnutrición, contribuyendo a reducir el sacrificio animal y a resolver las diferencias entre humanos y ratones.

Por otro lado, la segunda enfermedad presentada en esta tesis es la deficiencia de acil-coenzima A deshidrogenasa de cadena media (MCADD). MCADD es un trastorno genético que afecta la capacidad del cuerpo para procesar las grasas de cadena media, lo que puede conllevar problemas de energía durante el ayuno. Un dato curioso de esta enfermedad es que pacientes con la misma mutación pueden presentar sintomatologías completamente diferentes. Mientras un paciente puede desarrollar síntomas e incluso morir, otro paciente con la misma mutación puede vivir una vida sana y sin ningún tipo de síntoma. Al igual que ocurre con la malnutrición, la forma convencional de investigar la MCADD implica el uso de modelos animales, lo que conlleva el sacrificio de un gran número de ratones. Debido a la gran variabilidad en sintomatología

observada entre pacientes, el uso de material extraído directamente de los pacientes es crucial para entender la enfermedad.

El **capítulo 1** de esta tesis, es una introducción general a los diferentes temas tratados durante el texto. Aquí, presento las dos enfermedades de estudio en profundidad y analizo los diferentes tipos de modelos (in vivo, in vitro e in silico) y sus usos dentro del estudio de la biomedicina y biología de sistemas.

En el **capítulo 2** de la tesis, describo como hemos desarrollado dos modelos in vitro, utilizando organoides, para estudiar la malnutrición en el hígado y el intestino. Estos modelos demuestran ser capaces de reproducir algunos de los eventos característicos de la malnutrición, incluyendo la pérdida de peroxisomas en las células. Al final del capítulo, demostramos como la activación farmacológica de la síntesis de nuevos peroxisomas puede ayudar a paliar los efectos de la enfermedad.

En el **capítulo 3**, hemos desarrollado un modelo in silico basado en la inteligencia artificial que nos permite localizar, medir y estudiar el crecimiento de imágenes de organoides. Esto, nos facilita tanto el estudio de la enfermedad como la automatización del proceso.

El **capítulo 4** se centra en la aplicación del modelo in vitro de hígado descrito en el capítulo 2. En este capítulo me centro en dos aspectos: entender cómo se produce la degradación de los peroxisomas y explorar diferentes estrategias para estimular la síntesis de nuevos peroxisomas. En este capítulo demostramos, por primera vez, que la suplementación de ácido docosahexaenoico (DHA) (un ácido graso de cadena larga poliinsaturado) es capaz de incrementar el número de peroxisomas en la célula en condiciones restricción de amino ácidos. Curiosamente, no hemos logrado confirmar que esto sea debido a un incremento en la síntesis, aunque parece haber un cierto bloqueo en la degradación. Las razones definitivas de este incremento en peroxisomas en las células tratadas con DHA deben ser estudiadas más en detalle en el futuro.

En el **capítulo 5**, me enfoco en el establecimiento de un nuevo modelo in silico aplicado a la malnutrición. En este caso describo el establecimiento de un modelo cinético que describe el comportamiento de diferentes enzimas. Este modelo, es combinado con datos biológicos obtenidos de nuestros modelos in vitro y nos permite predecir el efecto de la malnutrición y el subsecuente tratamiento con DHA en el metabolismo de ácidos grasos en los peroxisomas.

Finalmente, en el **capítulo 6** me centro en la segunda enfermedad descrita en esta tesis, la deficiencia de acil-coenzima A deshidrogenasa de cadena media

(MCADD). En este capítulo describo como hemos desarrollado un modelo in vitro de la enfermedad a través de material biológico obtenido de diferentes pacientes. A diferencia del modelo descrito en el capítulo 2, este modelo está desarrollado a partir de células madre pluripotentes reprogramadas de fibroblastos de pacientes. Es decir, las células de la piel de pacientes fueron convertidas a células madre que luego fueron diferenciadas a células hepáticas. Una vez en cultivo, estas células son utilizadas para entender el papel de los peroxisomas en la enfermedad y determinar si estos son capaces de realizar algunas de las funciones que la mitocondria (donde la enzima deficiente reside) no puede realizar.

Conclusiones finales

Con esta tesis, hemos demostrado la validez de diversos modelos in vitro e in silico como herramientas fundamentales para investigar distintos aspectos de la malnutrición y del MCADD. En el caso de la malnutrición, nuestro modelo in vitro supone una gran plataforma para estudiar el efecto de diferentes fármacos y nutrientes en la síntesis de peroxisomas antes de continuar su estudio en modelos superiores (como animales).

En el caso de MCADD, hemos logrado establecer un modelo que nos permitirá entender por qué pacientes con la misma mutación pueden desarrollar síntomas diferentes. Además, nos permitirá explorar el crucial papel que los peroxisomas pueden desempeñar en esta enfermedad.

ACKNOWLEDGMENTS

The following pages are dedicated to acknowledge every person who has helped me along the way and who made it possible, in one way or another, for me to complete this thesis. These pages are not enough to express my deep gratitude.

To start, I would like to thank my supervisor Prof. **Barbara M Bakker** and **Prof. Robert Bandsma**. Dear **Barbara**, I cannot think of the words to express how grateful I am to you. From the very beginning, you have believed in me and encouraged me to learn and enjoy what I do. Since I started the PhD, you have motivated me to be a better scientist and not only do what I already know but also to learn and take with me as much as possible. You have always motivated me to be a better scientist, to ask the right questions and to always find the links; not only between words, but also between ideas. After every meeting I felt like no problem was big enough that it couldn't be solved. I am grateful I could share my professional and personal journey with someone who finds such joy in what they do. I hope you continue to guide and inspire as many people as possible in the future. And for me, I only hope I can, one day, inspire someone the way you inspired me.

Dear **Robert**, thank for all the help and support throughout the PhD. Although I could not pop into your office as easily as with Barbara, I am extremely grateful for your help and support. I truly admire your scientific drive and how easy it is for you to have a global vision of science and integrate the smallest details into the bigger picture. I am extremely thankful for the opportunity to spend 3 months at Sickkids working with you and your team. This was one of the most enriching experiences of my PhD, not only academically but also personally. I admire your work in the field of malnutrition and I hope I can read more research coming from the Bandsma lab in the future.

I would also like to thank the members of my PhD committee **Prof. Ronald Wanders**, **Prof. Amalia Dolga**, **Prof. Klaas Nico Faber**, **Prof. Ida van der Klei**, **Prof. Hans Jonkers**, **Prof. Adélaïde Raguin** and **Dr. Dorota Kurek**, for taking the time to read my thesis and evaluate my scientific contribution.

Next, I would like to thank all my coauthors and collaborators for your help and contribution to the different manuscripts in this thesis. Also, I would like to thank the funding institutions that allowed this work to take place.

I would also like to thank the European Union's Horizon 2020 research and innovation programme under the Marie Skłodowska-Curie grant agreement No 812968; and all the Perico members. **Tjaša** thank you for the help with the

peroxins analysis, **Asmaa** thank you for the contribution to our paper and the great work done in the development of the algorithm for chapter 2. **Serhii**, thank you very much for the nice collaboration in chapter 4 and the very nice comments. Thank you to all the PIs and researchers involved in **PeRico** for the great science and good times we had together.

Queridos paraninfos, probablemente necesite dos tesis más para agradecerlos lo muchísimo que significáis para mí.

Alejandro, creo que sobran las palabras para decirte lo importante que eres para mí. Desde el primer momento en que nos conocimos en la fiesta de Laura, has sido mi apoyo más importante en Groningen y en gran parte de mi vida. No soy capaz de encontrar las palabras para decirte lo muchísimo que le has dado forma a mi vida. De un amigo a un hermano. Contigo no tengo que fingir ser quien no soy, contigo puedo ser yo, que ya es bastante. Estos últimos cuatro años han sido maravillosos y eres la primera persona a la que tengo que darle gracias por ello. Todas las aventuras que he vivido siempre has estado ahí y estoy seguro que también lo estarás en las futuras. Sin ti, mi vida no sería lo increíble que es hoy ni conocería a la multitud de amigos maravillosos que ahora tengo. Espero algún día poder devolvarte todo lo que me has dado.

Dear **Sara**, my beloved friend. Thank for you taking the task to be my paranymp and a true friend. I cannot express how glad I am I got to meet you and share so much with you during the past years. Since we met, I have always felt at home with you. Your kindness, your happiness and easiness make life a sunnier place (even in cloudy Groningen). I truly hope you move down south and get to spend even more time together. Regardless of what happens I know you will be in my heart.

Ara, ¿qué decirte que ya no sepas? Desde el primer día que nos conocimos en clase hasta ahora siempre has estado presente. Los cuatro años de carrera me hicieron ver lo increíble que eres. Siempre he admirado (y un poco envidiado) esa actitud tan positiva y luchadora que tienes, ante todo. Nada puede pararte y lo has demostrado día a día. Sin ti, mi experiencia en el extranjero hubiera durado una semana y hubiera vuelta a casa llorando sin lograrlo después de compartir casa con más de un “homeless”. Ese año en Leeds fue una de las aventuras más locas y maravillosas de mi vida, y cada historia que tengo, tú siempre estás ahí. Todas las bromas que la vida nos ha presentado, múltiples compañeros de piso, una ambulancia en casa la noche de navidad, una casa sin suelo, un sótano satánico, cubatas más largos que un día sin pan, brazos de gitano en las escalera y miles de fiestas. Desde que partimos caminos me falta un pedacito, pero lo tengo clarísimo que en el futuro tenemos muchísimas

más historias y aventuras por vivir juntos. Muchísimas gracias por todo Araceli, te quiero. (¡Me has criado!)

Dear Systems Medicine group. Dear Barbies, I am extremely thankfully and honored to have grown and learnt with you. I cannot believe how lucky I got with our research team. **Melany**, desde la primera vez que nos conocimos has sido una gran mentora, compañera y amiga. Estoy super agradecido por todo el apoyo, ayuda y (gentle) bullying durante la tesis. Esta chucha ha sido genial! Dear **Bernard**, it was truly nice to work together and have someone so kind in the group. I will never forget how much you swear in Spanish! **Christoff**, I am extremely thankful that we got to work together and get to know each other. Thank you for all the help and putting up with my stupid questions about modeling but mostly, thank you for being a friend. **Karen**, thank you very much for all the help and advice during the past 4 years. **Emmalie**, although we didn't work side by side, we did boulder side by side! It was great getting to know you! Dear **Chris**, thank you so much for all the great times we had together in the lab. Since day 1 until you finished it was the two of us vs the world (or at least vs the organoids). It was a pleasure working together with you and accompanying you during your final stages and being your paranymp. I am extremely happy I now get to call you friend, and super excited we get to live so close to each other again! Can't wait to continue exploring Leiden together. **Ligia**, thank you very much for everything. I don't think I can express with words how nice it was to work with you and become your friend. You are such a kind and nice person. I loved every single trip together (specially Norway!) and working together in our super fun project. I am thankful to you for all the help and support during the last days and I am happy we got to share the "pain" of the last stage. **Marcelito** de mi vida y de mi corazón. Muchísimas gracias por todo. Por acogerme, por tratarme tan bien y por ser tan increíble persona. Desde que llegue al grupo siempre fuiste la persona a la que podía acudir por cualquier problema, duda o celebración. Te estoy infinitamente agradecido y soy super feliz que hayamos acabado tan cerca. ¡Espero seguir viendo Rupaul's Drag Race Season 98 cuando seamos viejitos! **Kishore**, thank you for everything. Although not officially a Barbie I feel like you were always one of us. It was great working with you, and having you so close I could ask you anything. I wish you the best in the future. **Romy**, thank you for your help and contribution to my work. It was a pleasure having you in our group during your internship.

Candelas, ha sido un placer trabajar contigo, aunque haya sido poco. Mucha suerte con tu próximo capítulo!

Dear **Miriam**, thank you very much for all the help during the past 4 years. Without you, I would not be where I am right now. You are such a diligent, dedicated and resourceful person. It was a pleasure working together and I am extremely thankful for all the support with the culturing and the endless western blots! Dear **Alberto**, thank you for being such an important figure during the PhD. Your support and help go a long way. It was a pleasure working with you and learning from you. I will miss both of you greatly.

I would also like to thank everyone in the **Pediatrics Department of the UMCG** for all the scientific help, input and support during my PhD. Thank you for everyone in the molecular genetics team who helped me during my time in ERIBA. **Alfredo**, muchísimas gracias por todo. La ayuda, los buenos ratos, el apoyo y la compañía. Me ha encantado aprender contigo de autophagy y FACS y todo lo que sabes. Me llevo un amigo. **Ankia**, it was great having you on board. Although we never worked together, I feel like we had enough coffees (and gossip) to consider you a friend. I wish you all the best! **Manolis**, thank you for so much fun in the lab! It was a blast seeing you play Venetia! Dear **Hans**, thank you for the help with the autophagy paper and the nice discussions about PPAR. **Niels**, thank you so much for all the help and nice attitude in the lab! **Nicolette** and **Marieke** thank you for all the support and help in the lab for the past 4 years. **Karin Wolters**, thank you very much for all the help and guidance with the proteomics work. **Maikee**, thank you very much for your great scientific input during our group meetings. It was great learning from someone so passionate.

Venetia, I will never forget the time we spent together in the lab. I was great having someone so open minded and fun around. I am extremely happy we became so close and I can now call you a friend. You are the prove that “negativity is basically laziness”. I can’t wait to have more trips like Berlin and share many more fun moments together.

Also, I would like to take a moment to thank all the people and friends I made during my time at the UMCG and Groningen.

Nadka, thank you so much for everything. Since day 1 you have proven to be such an amazing and wonderful person. Your attitude and enthusiasm are contagious and I couldn’t be happier about that. You are a truly kind human being and I am very thankful we met during our time in Groningen. It was so much fun doing so much together. I cannot wait to see what more adventures we have ahead of us!

Tiago, thank you so much for all these amazing years of shenanigans. It was a great adventure. I wish you all the best in the future and I hope I get to see more Tiago in my life. My dear **Siobhan**, thank you so much for all the help these years. I cannot think of a kinder, gentler human being. I am eternally thankful we got to spend time together in Groningen and I hope I get to visit you in Greece very often. **Erika**, I am so very glad I got to meet you during my time in Groningen. Thank you for everything and all the good times! I will miss you very much! **Miguelito**, mucho obrigado for being such a good friend! I can't wait to have you down south! **Sem, Carli, and Tegan**, I am super glad we got to travel to Mexico together! It was such a fun experience! I can't wait for the next one!

Kim, Prajit, Takuya, Audrey, thank you so much for all these years of fun and good times!

Manu! Muchas gracias por estos meses viviendo juntos, me alegro muchísimo tenerte en esta nueva aventura en Leiden!

My beloved **Katie**. Ever since we met, I feel like you truly understand me and share (part of) my vision of the world: fears, joys and intrigues. The two years we lived together were such a fun part of life, even in dull, flat Cambridge. Thank you for taking care of me and listening to me when needed. I am truly grateful for all the time we spend together and the fact that I can now call you one of my closest friends. I can't wait to see what's next for you!

También me gustaría darle las gracias a tantos y tantos amigos que he tenido la suerte de conocer.

Quiero darle las gracias a mis "chochis" por hacer la vida un poco menos difícil. Muchas gracias por seguir ahí, al pie del cañón incluso después de tantos años. Me alegro muchísimo de haberme leído esa obra de arte escrita desde la perspectiva de Edward y haber podido entablar una primera conversación contigo, **Marta** (claramente siempre hemos tenido el mejor gusto en el grupo). **Celia**, muchísimas gracias por todos los buenos momentos desde el cole hasta Edimburgo, ¡Valencia y hasta Polonia! ¡Mi **chufi** favorita! ¡Muchísimas gracias por todo, por esa maravillosa aventura juntos en Edimburgo y por acogerme en Madrid y por básicamente todo! Querida **Menchu**, nos quedan menos de 9 años para hacerlo oficial. ¡Voy a ir buscando un traje ya! ¡Muchas gracias por todo, eres super importante para mí y ojalá el futuro nos tenga un poco más cerca! Gracias a todas, por tanto. Desde ese maravilloso volcán que hicimos (básicamente los cinco) pasando por esa mega llorada en casa de Mercedes (hace ya algunos años) hasta todas las tarde buenas que devotamente cumplimos, es un tremendo placer teneros a todas en mi vida.

Carmen Cerrato, muchas gracias por todo. Hace ya tanto tiempo que coincidimos en natación y aquí seguimos. Desde novios falsos a mejores amigos del mundo mundial. Gracias por todo.

¡Querida **María** (Mero)! Muchas gracias por todo. Desde que (por suerte para ti) acabamos en la misma clase en el bachillerato siento que gran parte de este camino tú has estado presente. Ha sido genial pasar tanto tiempo y juntos y te echo muchísimo de menos. Junto con mi amor **Peña**, echo de menos todo el tiempo que hemos pasado juntos los tres. Tantas comilonas, y rayadas en el coche de peña y tantas veces a punto de morir por conducción temeraria. Os quiero muchísimo a los dos y espero que en un futuro no muy lejano estemos mucho más cerca de lo que estamos ahora. Muchas gracias **Achi** por tanto tiempo juntos, tanto apoyo y por compartir conmigo el comienzo de mi carrera científica en ese laboratorio de química analítica durante todo un verano.

Bea, muchas gracias por tantísima ayuda. Gracias por enseñarme a entenderme y a confiar en mi mismo.

Y, por último, querida familia: aunque no seamos muy sentimentales me gustaría dedicaros unas palabras.

Tata, muchas gracias, por tanto. Todos estos años en los que me has acompañado y querido. Gracias por aceptarme tal y como soy. ¡Y gracias por montarte en un avión por mí!

Belén, muchas gracias por hacer de terapeuta aparte de hermana. Obviamente no podría haberlo hecho sin ti. Mitad de esta tesis es tuya, al menos en carga emocional.

Mamá y Papá, gracias por todo. Por el apoyo, el cariño y por aceptarme como soy. Gracias por darme todo lo que me ha llevado a ser quién soy.

Sobra decir que no estaría donde estoy si no fuera por vosotros. Os quiero.

También me gustaría dar las gracias al resto de las personas que de una forma u otra ya no están presentes. A todas y cada una de las personas que han dado forma a quién soy. Gracias.

CURRICULUM VITAE

José Manuel Horcas Nieto was born on April 10th 1993 in Córdoba, Andalucía, Spain. He lived in Córdoba for 22 years during which he attended the Universidad de Córdoba (UCO) to pursue a bachelor's degree in Biochemistry in 2011. After two years he became a voluntary intern at the department of Molecular Biology and Biochemistry under the supervision of Prof. Juan Jurado. During his final year internship, he focused on the establishment of High-Performance Liquid Chromatography for the separation of casein proteins under the supervision of Prof. Maria de la Paz Aguilar Caballos.

After graduating, José pursued an MSc in Drug Chemistry at Newcastle University (Newcastle, UK) from 2016 to 2017. Following the completion of his master's degree, José commenced his professional career at STEMCELL Technologies (Cambridge, UK) where he was first introduced to the field of in vitro modeling and organoids.

Two years later, driven by the motivation to advance his education, José was awarded a Marie Curie Innovations ITN PhD to conduct his research at the University Medical Center Groningen (Groningen, The Netherlands). Under the guidance of Prof. Dr. Barbara M. Bakker, he focused on the implementation of in vitro and in silico models for the study of malnutrition and MCADD. In 2022 José continued his research at the SickKids Hospital (Toronto, Canada) under the supervision of Dr. Robert Bandsma.

José was awarded several grants including the De Cock-Hadders grant for financial support of scientific research and the Boehringer Ingelheim Fonds Travel Grant. Additionally, in collaboration with his research partner Ligia Kiyuna, José secured a BKZ grant to initiate the establishment of iPSC-derived organoids from MCADD patients.

Following his PhD, José continues his scientific career in the field of in vitro modeling at Toxys B.V (Leiden, The Netherlands), where he focuses on the establishment of in vitro models to examine toxicity of different commercial drugs.

LIST OF PUBLICATIONS

Original article

Organoids as a model to study intestinal and liver dysfunction in severe malnutrition

Horcas-Nieto JM*, Versloot CJ*, Langelaar-Makkinje M, Gerding A, Blokzijl T, Koster MH, Baanstra M, Martini IA, Coppes RP, Bourdon C, van Ijzendoorn S, Kim P, Bandsma RHJ, Bakker BM. *Biochim Biophys Acta Mol Basis Dis.* 2023;1869(3). doi:10.1016/j.bbadis.2022.166635 (**Chapter 2**)

*These authors contributed equally

Towards automatization of organoid analysis: A deep learning approach to localize and quantify organoid images

Haja A*, **Horcas-Nieto JM***, Bakker BM, Schomaker L. *Computer Methods and Programs in Biomedicine Update.* 2023; 100101(3). doi.org/10.1016/j.cmpbup.2023.100101 (**Chapter 3**)

*These authors contributed equally

Rebalancing of mitochondrial homeostasis through an NAD⁺-SIRT1 pathway preserves intestinal barrier function in severe malnutrition

Ling C, Versloot CJ, Arvidsson Kvissberg ME, Hu G, Swain N, **Horcas-Nieto JM**, Miraglia E, Thind MK, Farooqui A, Gerding A, van Eunen K, Koster MH, Kloosterhuis NJ, Chi L, ChenMi Y, Langelaar-Makkinje M, Bourdon C, Swann J, Smit M, de Bruin A, Youssef SA, Feenstra M, van Dijk TH, Thedieck K, Jonker JW, Kim PK, Bakker BM & Bandsma RHJ. *EBioMedicine*, vol. 96, 104809. doi.org/10.1016/j.ebiom.2023.104809

